Investigations on Dye-Doped PMMA based Optical Waveguides for Photonic Applications

Ph. D. Thesis submitted to

Cochin University of Science and Technology

In partial fulfilment of the requirements for the award of the Degree of

Doctor of Philosophy

Jaison Peter

Reg. No: 4066

International School of Photonics
Faculty of Technology
Cochin University of Science and Technology
Cochin -682022, Kerala, India

August 2016

Investigations on Dye-Doped PMMA based Optical Waveguides for Photonic Applications

Ph D thesis in the field of Photonics

Author:

Jaison Peter
Research Fellow
International School of Photonics
Cochin University of Science & Technology
Cochin -682022, Kerala, India
jaison.peter@gmail.com

Research Advisor:

Dr. M. Kailasnath
Professor
International School of Photonics
Cochin University of Science & Technology
Cochin -682022, Kerala, India
mkailasnath@gmail.com

International School of Photonics
Cochin University of Science & Technology
Cochin -682022, Kerala, India
www.photonics.cusat.edu

August 2016

Cover image: ***Polymer optical fibers***

INTERNATIONAL SCHOOL OF PHOTONICS
COCHIN UNIVERSITY OF SCIENCE AND TECHNOLOGY
COCHIN -682022, KERALA, INDIA

Certificate

This is to certify that the thesis entitled **"Investigations on Dye-Doped PMMA based Optical Waveguides for Photonic Applications"** submitted by **Mr. Jaison Peter**, is an authentic record of research work carried out by him under my guidance and supervision in partial fulfilment of the requirement of the degree of Doctor of Philosophy of Cochin University of Science and Technology, under the Faculty of Technology and has not been included in any other thesis submitted previously for the award of any degree.

Kochi-682022
08 - 08 - 2016

Dr. M. Kailasnath
(Supervising guide)

Phone: +91 484 2575848 Fax: 0091-484-2576714.
Email: mkailasnath@gmail.com

INTERNATIONAL SCHOOL OF PHOTONICS
COCHIN UNIVERSITY OF SCIENCE AND TECHNOLOGY
COCHIN -682022, KERALA, INDIA

Certificate

This is to certify that the thesis entitled **"Investigations on Dye-Doped PMMA based Optical Waveguides for Photonic Applications"** submitted by **Mr. Jaison Peter**, has incorporated all the relevant corrections and modifications suggested by the audience during the pre-synopsis seminar and recommended by the Doctoral Committee.

Kochi-682022
08 - 08 - 2016

Dr. M. Kailasnath
(Supervising guide)

Phone: +91 484 2575848 Fax: 0091-484-2576714.
Email: mkailasnath@gmail.com

Declaration

I, Jaison Peter, do hereby declare that the thesis entitled **"Investigations on Dye-Doped PMMA based Optical Waveguides for Photonic Applications"** is a genuine record of research work done by me under the supervision of Dr. M. Kailasnath, Professor, International School of Photonics, Cochin University of Science and Technology, Kochi–22, India and it has not been included in any other thesis submitted previously for the award of any degree.

Kochi- 682022
08 - 08 - 2016

Jaison Peter

Dedicated to God Almighty,
my wife, parents, brother,
teachers and all
well-wishers

Acknowledgements

I am indebted to many individuals who have provided assistance and support during the period of this research.

First and foremost, I would like to express my sincere gratitude to my supervisor Dr. M. Kailasnath, Professor, International School of Photonics (ISP), for giving me an opportunity to work under his guidance. His inspiration, encouragement, constant support and valuable suggestions have gone a long way in the completion of my work. His extraordinary attention to detail and endless efforts in reviewing this thesis and many manuscripts are highly appreciated.

I would like to thank Prof. V. P. N. Nampoori, Professor Emeritus, International School of Photonics, for his encouragement and constructive remarks in the course of my Ph D studies. His inspiration, encouragement, constant support and valuable suggestions have gone a long way in the completion of my work.

I express my deep and sincere thanks to Prof. P. Radhakrishnan, Professor Emeritus, International School of Photonics, for unselfishly providing time and energy by giving valuable suggestions to the work.

I am extremely indebted to Prof. C. P. G. Vallabhan, Professor Emeritus, International School of Photonics, for his wholehearted support and advice during the work.

I greatly acknowledge, Prof. A. Mujeeb, Director, International School of Photonics, for his valuable support, suggestions, love, caring and encouragement to carry out my Ph. D.

I gratefully thank Prof. V. M. Nandakumaran, Prof. Pramod Gopinath, Dr. Sheenu Thomas, Dr. Reethama Thomas, Dr. Priya, Dr. Saji, Dr. Manu, Mr. Rishad, Mrs. Sreekumari and all other teachers of both ISP and Centre of Excellence in Lasers and Optoelectronic Sciences (CELOS) for the support provided during the years of my Ph D.

Sincere thanks to Dr. Jomon George, Dr. Mothi and Dr. Mahesh Kumar for helpful discussion and technical support.

My special and sincere thanks to Prof. Radhakrishna Prabhu, Professor, Robert Gorden University, Aberdeen, UK, for helping me in doing my work at Scotland and also for his loving concern extended throughout my work at UK.

Sincere thanks go to my colleagues Boni Samuel, Anand V. R., Adrine Correya and students Rasool Saleem and Ananthu Sebastian for the support and encouragement that they have provided in all my activities.

I would like to acknowledge other co-scholars of the ISP, in particular, Mr. Retheesh Raj, Vivek Viswambharan, Pradeep Chandran, Bini Pathrose, Jessy Simon, Vijesh K.R., Remya M, Aleena Kuriakose, Roopa Venkitaraj, Sony Udayan, Raj Shah, Ajina C., Anupama V., Priyamvada V.C., Pooja Gitty, Linslal, Bobby Mathews, Bejoy Varghese, Nideep T K, Dr. Divya Sasi, Dr. Libish T.M, Dr. Aparna Subhash, Dr. Sr. Rosmin, Dr. Indu Sebastian, Dr. Suneetha Sebastian, Dr. Sithara, Dr. Mathew and for all their support and for creating a very vibrant environment. The group has been a source of friendship as well as good advice and collaboration.

Special thanks to all Lab, library, administrative staff, M.Sc and M.Tech students of the ISP for the assistance extended during the tenure.

I would also like to thank my Pappikunju, Antappan, Saji aliyan, Reji, Biju, Jomon chettan, Jaison, Mini, Jija, Jaya, Jeenamol chechi, Jaimy, Johnson chettan, Reena chechi, Dona mol, Unnikuttan, Prince chettan, Jipsy chechi and all my friends and relatives for their support and love during this time.

I am also grateful to my beloved pappa, mom, Eldhose chettayi, Cinta Chechi, Evin kuttan whose love and encouragement during my Ph.D time.

Sincere thanks to my ever loving wife Princy for her unfailing support and encouragement to complete this research program.

Thanks to the Almighty God

Jaison Peter

"God is light and in him is no darkness at all."

1 John 1:5 (The Holy Bible)

Preface

Photonics deals with the generation, emission, transmission, modulation, signal processing, switching, amplification, detection and sensing of light. The application and potential advantages of optics and photonics have been the enabling factor in the shift of modern information technology era from the Electronics age to Photonics age. In the last few years, interest in polymer optical fibers (POFs) has increased significantly because of its ease of handling, flexibility and potential low cost. Availability of inexpensive sources in the visible region has increased the utilization of POF in data communication.

However, the higher loss factor is a major handicap for POF. Recently developed techniques for decreasing losses in poly (methyl methacrylate) (PMMA)-based POF have raised much interest in different fields such as short distance communication, lasing and sensing applications. One of the important advantages of the PMMA compared to the traditional optical materials is that it is possible to introduce organic dyes or other compounds that can play the role of active components into the polymers, which appreciably changes the characteristics of the polymer matrix. Laser dyes, which act as highly efficient media for amplification and lasing have a wide range of tunability in the visible region. The main advantage of incorporating laser dyes in solid matrices such as POF is that it is easier and safer to handle them than when they are in liquid form. Rhodamine dyes are the best known of all laser dyes, which have been frequently investigated in solid-state dye lasers in a variety of hosts, on account of their high fluorescence quantum yield, low intersystem crossing rate and low excited state absorption at both pump and lasing wavelengths.

The thesis presented in seven chapter's deals with the work carried out on different types of dye doped polymer optical fiber and dye doped polymer coated waveguides.

Chapter 1 gives an overview of guided Polymer Optical Fibers (POFs). Historical developments of polymer waveguides/fibers and commonly used polymer materials together with their applications have been covered in this chapter. It also deals with the potential advantages of POFs over silica fiber.

Chapter 2 provides useful information on the photophysical properties of Rhodamine B (Rh B) dye in different solvents with theoretical support. The structural geometries, UV-vis absorption spectra and emission intensities of Rh B in various solvents have been determined for different excited states by density functional theory (DFT) and time-dependent (TD) with polarizable continuum model (PCM) methodologies. This chapter also demonstrates the pulsed, photo-pumped multimode laser emission in the visible spectral range from Rh B dye dissolved in various solvents. The cavity lasing spectral structure and the number of longitudinal modes are easily controlled by changing the solvents. A shift in the emission spectra observed by changing the solvent allows a limited range of tuning of laser emission wavelength. The gain coefficients, stimulated emission cross-section and life time for the Rh B dye dissolved liquid laser system are also determined in this chapter.

Chapter 3 discusses in detail about the various fabrication techniques of Rhodamine 6G (Rh6G) doped polymer optical fibers, such as step index, graded index and hollow fiber. This chapter also gives the details of the optical characterization of different types of dye doped POFs drawn under different initial conditions like, draw rate, feed rate and temperature. Cut back method and Side Illumination Fluorescence (SIF) technique have been employed to

characterize the drawn fiber. Detailed measurements were made to understand the amplified spontaneous emission (ASE) and photo degradation phenomena in these POF systems. Measurements of peak emission wavelength, optimum length, line-width and half-life of Rh6G doped hollow, GI and SI POFs are included in this chapter.

In chapter 4, we report the observation of multimode laser emission at wavelengths corresponding to whispering gallery modes (WGMs) from a free-standing micro-ring cavity based on Rh6G dye doped hollow polymer optical fiber (DDHPOF). Theoretical modelling of WGM resonator has also been realized using COMSOL Multiphysics software package. Cylindrical microcavities with different diameters were fabricated and their performances have been evaluated. Resonant modes of the microring laser are excited inside the gain medium which is strongly confined along the radial direction so that the spacing of lasing modes is controlled by the diameter of the cylindrical microcavity. A reduction in the free spectral range of WGM spectra along with a red-shift is observed with an increase in the diameter of DDHPOFs. In the second part of this chapter, we discuss two different types of pumping schemes to characterize the DDHPOF; 1) stripe illumination and 2) spot illumination. As the pump power is increased, stripe illumination shows a blue-shift and spot illumination shows a red-shift for the emission spectra. By using spot illumination, the slope efficiency of system is enhanced by more than three times than that of stripe illumination. However, due to higher power density, spot illumination will lead to quicker degradation of dye molecules as compared to stripe illumination.

Chapter 5 describes multimode laser emission from symmetric (SRC) as well as asymmetric resonant cylindrical (ARC) microcavity based on a Rh B dye doped hollow polymer optical fiber by transverse pumping. An SRC can provide a circularly symmetric whispering gallery mode (WGM)-like laser emission from its surface with a quality factor (Q) of ~1.2×10^4, while an ARC supports a

strongly chaotic internal ray dynamics, which will in turn lead to an anisotropic emission with a lower Q of ~8×10^2 with a far field divergence of about 20° in the plane of the cavity. An ARC can be fabricated by a controlled deformation of SRC, which enables dumping out the stored light effectively with minimum loss. Such deformed free-standing cylindrical polymer microcavities also provide a stable and constant laser emission in a desired direction, which can effectively utilized in the design of highly sensitive fiber laser sensor and low threshold micro-lasers for organic optoelectronic integrated devices. We also observed two different sets of resonant laser modes: namely, fundamental whispering gallery high Q modes (HQMs) and leaky unidirectional low Q modes (LQMs) from an asymmetric hollow polymer optical fiber. It is found that the far-field emission pattern of LQM shows a good directionality with a narrow divergence angle when compared with HQM. Numerical results for asymmetric resonant cavity (ARC) with suitably positioned air hole can support LQM with highly directional emission. It has also been found that the emission directionality can be tuned by adjusting the deformity of the microcavity.

In Chapter 6, we demonstrates pulsed, photo-pumped multimode laser emission in the visible spectral range from cylindrical microcavities of dye doped thin polymer film deposited on silica core optical fiber. The laser emission is characterised by two different sets of resonant modes viz; waveguided modes (WMs) and whispering gallery modes (WGMs). Simultaneous occurrence of the WGM and WMs will lead to a resonant modulation in the laser emission spectrum. In the second part of this chapter, a detailed study of amplified spontaneous emission from a polymer thin film doped with Rh6G is presented. The emission spectrum of the dye-doped polymer thin film on a glass substrate exhibits high directionality, narrow linewidth and presence of soft threshold behavior. Performance of a compact solid-state laser based on leaky mode

propagation from dye-doped polymer free-standing film waveguide is also discussed. The partial reflections from the broad lateral surfaces of the free-standing films provided the optical feedback for the laser emission.

Chapter 7 deals with the fabrication and characterisation of Rh B doped microring resonator embedded in the inner walls of the silica capillary. Strongly modulated multimode laser emission has been observed from such microresonators by transverse pumping. We have studied the lasing behavior of different thickness microring cavities with enhanced mode selection and particularly almost single mode lasing with a side mode suppression ratio of up to 10.2 dB is obtained from a very thin microring cavity. The lasing modes inside such cavities can be easily collected from one end due to its very good propagation characteristics.

Chapter 8 deals with the main conclusions of the work presented in this thesis. A brief sketch of future research prospects is also mentioned in this chapter.

List of Publications

Journal Papers

- **Jaison Peter**, Mahesh Kumar, V. R. Anand, Rasool Saleem, Ananthu Sebastian, P. Radhakrishnan, V. P. N. Nampoori, C. P. G. Vallabhan, Radhakrishna Prabhu, and M. Kailasnath "Solvent effects on lasing characteristics for Rh B laser dye", Journal of Luminescence, Volume 169, Part A, pp.227-232, January 2016.
- **Jaison Peter**, Radhakrishna Prabhu, P. Radhakrishnan, C. P. G. Vallabhan, V. P. N. Nampoori and M. Kailasnath "Angular dependent light emission from planar waveguides". J. Appl. Phys. 117, 015301 (2015).
- **Jaison Peter**, C. P. G. Vallabhan, P. Radhakrishnan, V. P. N. Nampoori, & M. Kailasnath, "ASE and photostability measurements in dye doped step index, graded index and hollow polymer optical fiber". Optics & Laser Technology, 63, 34-38 (2014).
- **Jaison Peter**, P. Radhakrishnan, V. P. N. Nampoori, & M. Kailasnath, "Multimode Laser Emission from Free-standing Cylindrical Microcavities". Journal of Luminescence 05/2014; 149:204-207 (2014).
- **Jaison Peter**, Rasool Saleem, Ananthu Sebastian, , P. Radhakrishnan, V. P. N. Nampoori, C. P. G. Vallabhan & M. Kailasnath. "Pumping scheme dependent multimode laser emission from free-standing cylindrical microcavity". Optics Communications 01/2014; 320:125–128 (2014).
- **Jaison Peter**, C. P. G. Vallabhan, V. P. N. Nampoori, P. Radhakrishnan, & M. Kailasnath. "Characteristics of Whispering Gallery Mode Laser Emission from Free-standing Cylindrical Microcavity", OPEN JOURNAL OF MODERN PHYSICS ISSN (Print): 2372-627X ISSN (Online): 2372-6288 VOLUME 1, NUMBER 2, JUNE 2014.

- **Jaison Peter**, C. P. G. Vallabhan, P. Radhakrishnan, V. P. N. Nampoori, & M. Kailasnath,. "Microring lasing from a dye-doped polymer-coated silica fiber". Laser Physics, 23(11), 115104(2013).
- C. L. Linslal, **Jaison Peter**, S. Mathews, and M. Kailasnath, "Multimode laser emission from dye-doped hollow polymer optical fibre", Pramana Journal of Physics, Vol 82, No. 2, p.p 233-236, February 2014.

Publications in Conference Proceedings

- **Jaison Peter**, Boni Samuel, V. R. Anand, Retheesh Raj, Adrine Antony Correya, T. K. Nideep, Bejoy Varghese, C. Bobby Mathews, P. Radhakrishnan, C. P. G. Vallabhan, V. P. N. Nampoori and M. Kailasnath, "Directional multimode laser emission from deformed polymer cylindrical microcavity", Advances in Applied Mathematics, Materials Science and Nanotechnology for Engineering and Industrial Applications (IC-AMMN-2K16), 7-9 January 2016, Federal Institute of Science and Technology, Hormis Nagar, Angamaly-683 577, Kerala.
- **Jaison Peter**, Mahesh Kumar, V. R. Anand, Boni Samuel, Adrine Antony Correya and M. Kailasnath, "Photophysical studies and modeling of Rhodamine B as calculated by TDDFT/ PCM method" , National Laser Symposium (NLS-24), RRCAT, Indore, 2-5 Dec, 2015 NLS-24.
- Rasool Saleem.U, Ananthu Sebastian, **Jaison Peter**, P Radhakrishnan, G Radhakrishna Prabhu, and M. Kailasnath. "Solvent Effects on Lasing Characteristics for Rh B Laser Dye". International Conference on Fibre Optics and Photonics. December 13-16, 2014.
- **Jaison Peter**, Radhakrishna Prabhu, P. Radhakrishnan, C. P. G. Vallabhan and M. Kailasnath. "Characteristics of the cutoff and guided modes in planar waveguides". Photon 14, 1-4 Sept. Imperial College London, U.K, 2014.
- K. C. Sreechandralijith, **Jaison Peter**, Aparna Thankappan, V. P. N. Nampoori and P. Radhakrishnan, "Random lasing and coherent back scattering study

in rhodamine 6G doped polymer optical fiber (POF) particles" AIP Conf. Proc. 1620, 521 (2014).

- C. S. Sarika, **Jaison Peter**, C. L. Linslal & M. Kailasnath "Fabrication and Characterisation of Rhodamine B Doped Polymer Optical Fiber with Multiple Holes", NLS 21; 02/2013.
- C. L. Linslal, **Jaison Peter**, S. Mathew & M. Kailasnath, "Multimode laser emission from dye doped hollow polymer optical fiber", NLS 21; 02/2013.
- **Jaison Peter**, C. L. Linslal & M. Kailasnath, "Pumping angle dependence of multimode lasing from doped hollow optical fiber". NLS 21; 02/2013.
- Suneetha Sebastian, S. Sooraj, A. Aaryan, **Jaison Peter**, V. P. N. Namboori, C. P. G.Vallaban, & M. Kailasnath, Impact of laser ablated gold nanoparticles on absorption and fluorescence of Rhodamine 6G in Methyl Methacrylate. In Optical Engineering (ICOE), International Conference on IEEE, pp. 1-5, (July, 2012).
- **Jaison Peter**, C. L. Linslal & M. Kailasnath, "Characterization of Dye Doped Step Index and Graded Index Polymer Optical Fiber by Side Illumination Fluorescence Technique". 27th annual convention of IAPT and seminar on Recent Trends in Photonics. IAPT 11/2012.

Contents

xxx

List of figures

List of tables

Chapter 1
Polymer Optical Waveguides: An overview

"Your word is a lamp to my feet and a light to my path"

Psalms 119:105

Abstract

This chapter gives an overview of guided Polymer Optical Fibers (POFs). Historical developments of polymer waveguides/fibers and commonly used polymer materials together with their applications have been covered in this chapter. It also deals with the potential advantages of POFs over silica fiber.

1.1 Introduction

The advances in the field of fiber optics communication and integrated opto-electronics have increased the interest in guided wave optics, in which optical waveguides and optical fibres play a central role. Photonics and related applications have an extremely large information capacity (due to broad bandwidth), high immunity to internal noise, cross talk, electrical noise, ringing, echoes or electromagnetic interferences, immunity to lightning and thus unaffected by lightning caused hazards. The transmitted signal through the fibers does not radiate and photons do not interact linearly when multiple wavelengths propagate in an optical medium and thus allow parallel processing of different wavelengths. Further the signal cannot be tapped from a fiber in an easy manner. Therefore optical fiber communication provides hundred percent signal security. Fiber optic cables are developed with small radii, and they are flexible, compact and lightweight. The fiber cables can be For twisted without damage. Further the optical fiber cables are superior to the copper cables in terms of storage, handling, installation and transportation, maintaining comparable strength and durability, low risk of fire, explosion and ignition. Due to the recent advancement in optical fiber technology the fabrication costs of optical fibers are coming down drastically. Even though the initial cost of installation is very high when compared to electrical communication cables, it has very low maintenance cost.

Polymer waveguide technology has a great potential for economic mass production of complex planar photonic circuits and polymer optical fibers. The low cost prospect arises from the availability of a wide range of inexpensive optical polymers and the simplicity of fabricating waveguides from them. A significant subset of optical polymer materials has shown excellent optical, chemical and mechanical characteristics that are very attractive for wide range

of applications such as optical communication devices, physical and chemical sensors and illuminators.

Polymer optical fibers (POFs) are the most promising solution for “last 100 m” in data communication. Polymer waveguide technology has a great potential for economic mass production of complex planar photonic circuits and POFs. In photonic applications, they offer advantages over optical glass; they weigh less, have flexibility, ease of handling, low cost, relatively high resistance to fracture and high geometrical versatility (they can be easily molded into spherical, aspheric and symmetric shapes).

POF was introduced by Dupont in the mid-1960s at approximately the same time when glass optical fiber (GOF) was suggested as a transmission medium for optical communications. Dupont’s product was a step index fiber with a poly methyl methacrylate (PMMA) core and fluoropolymer cladding. Despite the fascinating ability to guide light, POF had very large attenuation, limited applicability and negligible commercial value as far as the field of long distance communication was concerned. Due to the incomplete purification of the monomer materials used and the attenuation in excess of 1000 dB/km made their use in long haul optical communication impractical. Now various types of POF products including Graded index (GI) type POF, single mode POF, fluorescent POF, non-linear POF, etc. have been developed which are widely used in the fields of light and image transmitting, sensing, and information transmission over short distance.

As we have already mentioned, POFs present some important advantages over their glass counterparts. Specifically their large diameter (typically 0.25 - 1 mm) allows low precision plastic connectors to be used, which reduce the total cost of the system. In addition, POFs stand out for their greater flexibility and resistance to impacts and vibrations, as well as for the greater coupling of light from the light source to the fiber. Because of these merits, various

applications with POFs have been developed and commercialized from their use as a simple light transmission guide in displays to their utilization as sensors and telecommunication cables.

1.2 Optical waveguide structures

In guided wave optics, light travel using the phenomena of total internal reflections (TIR), in which light gets confined in the optical waveguide. Generally in an optical waveguide a thin-film is deposited over a glass or quartz slide or a filament of dielectric material is coated on a cylindrical structure. Depending on the various possible patterns of propagating or standing electromagnetic fields, there are single or multimode optical waveguides.

1.2.1 Planar waveguide structure

After the invention of the laser and development of coherent optics, the need for long distance propagation medium and other guiding structures to build optical components and connect them to other opto-electronic circuits arose. Planar waveguide structure is a promising and efficient guiding structure to interconnect other electronic circuits at all frequencies up to the microwave range. Rectangular dielectric waveguides were first studied theoretically by Schlosser in 1964. The film waveguides as well as other planar components and circuitry for applications in the infra-red range were constructed by Anderson in 1965. Planar waveguide integrated optics involves the manipulation of stripe beams that are confined in the waveguide. The confined wave can propagate in a direction parallel to the surface of high-index guiding layer. Figure 1.1 shows the light confinement in an asymmetric and free-standing planar waveguide structure.

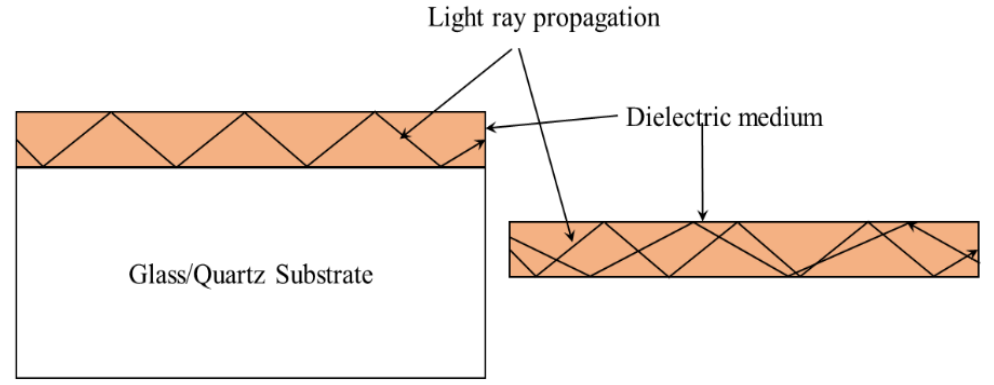

(a. Asymmetric planar waveguide structure) (b. Free-standing planar waveguide structure)

Figure 1.1 Light propagation through an asymmetric and free-standing planar waveguide structure.

The different techniques for the fabrication of planar waveguides are listed below

- Ion etching of polyimides
- Ion irradiation
- Photo-structuring (Mask aligner, laser writing)
- Induced diffusion of doped polymers
- Injection molding
- Molecular orientation of the doping
- Phot-bleaching
- Electron beam structuring (photoresist)
- Sol-gel technology
- Casting technique
- Spin coating

One of the most important advantages of polymer waveguide is the low processing temperature and the possibility of casting into any shape, which is particularly important for mass production.

1.2.2 POF Structure

POFs used for optical communications are highly flexible cylindrical waveguides composed of nearly transparent dielectric materials. The cross-section of these fibers is circular and generally divisible into three layers as shown in figure 1.2. The structure of POFs consists of a core surrounded by a cladding layer, both of which are made of dielectric materials. To confine the light in the core, the Refractive Index (RI) of the core must be greater than of the cladding. In practical fibers, the cladding is usually coated with another protective layer, generally referred to as Jacket.

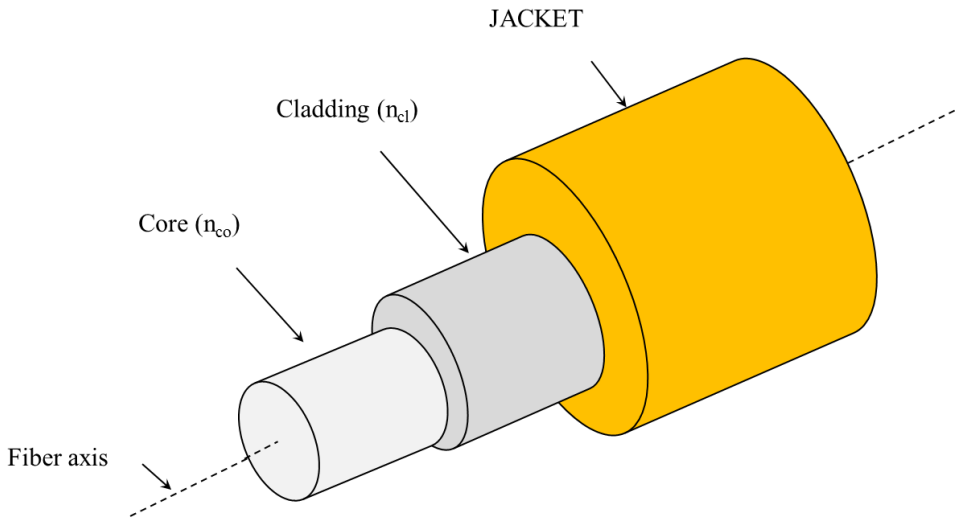

Figure 1.2 Structure of POF

1.3 Optical fiber fabrication techniques

1.3.1 Glass fibers

Glass fibers are normally produced using preform method. The desired refractive index profile is usually produced by doping with small amounts of materials such as germanium and boron. The most important doping method is

based on vapour deposition, in which layers of the desired materials are successively deposited and oxidised by a flame.

1.3.2 Polymer fibers

In polymers, there is no equivalent to vapour deposition and it is difficult to control the refractive index profile precisely. Some of the approaches tried include co-extrusion of materials with slightly different composition, centrifuging during polymerisation and interfacial gel polymerisation. Co-extrusion comes closest to vapour deposition technique in terms of its versatility, as it allows multiple steps in refractive index to be achieved. In all cases however, considerable optimisation of the process is required to obtain the required profile. The use of two different materials generally produces much larger difference in refractive index than doping. Polymer optical fiber, which usually has a high contrast between core and cladding, possesses a relatively high Numerical Aperture (NA). The fabrication techniques of different types of POF have been well explained in the chapter 3.

1.4 Polymer fiber optics

Silica glass fibers have enabled the modern Information Superhighway, but POFs are of great commercial interest because they can maintain flexibility at thicker fiber sizes making them easier to handle and install when the communication systems make their way from the local loop (premise networks and local area networks) and Fiber to the Home (FTTH). POF may also be an important building block for devices used in future ultrafast all optical communication systems because it has many attractive properties that silica optical fiber lacks. An important one is its low processing temperature (typically less than 200°C). This allows organic nonlinear optical materials to be incorporated into the POF, which is otherwise impossible in silica-based fiber because of its high process temperature (typically 1800°C to 2000°C).

Many useful devices such as optical switches may be constructed based on fibers with fast response and high nonlinearity.

1.5 Advantages of POF over silica fibers

In general the polymers have certain advantages which make thus a suitable candidate for easier optical fiber fabrication. Their advantages as follows:

- POF is very elastic in contrast to silica fiber, which is very brittle. This property is important for the fiber interface within the optoelectronic systems where space is usually limited [1].
- Commercial POF has a typical diameter of 1mm with no cladding or only a thin cladding, making it a multimode fiber. The large core diameter and flexibility allow ease of handling, large alignment tolerance and connection cost.
- Low processing temperature (200°C to 250°C) of POF allows organic nonlinear optical materials to be incorporated into the POF which is otherwise impossible in silica fibers because of its high processing temperature (1000°C to I500°C).
- The transmission windows of POF are distributed throughout the visible wavelength range. The availability of inexpensive sources in the visible region has increased the utilization of POF in data communication over local area network (LAN) systems.
- Silica fibers have very small non-linear coefficient requiring a large amount of optical power or very long fiber length to induce sufficient non-linear phase change. Polymer fibers can be made non-linear by appropriate doping material. POFs doped with laser dyes or rare-earth elements are potential candidates for optical amplifier working in the visible region.

But some of the problems are:

• Poor dimensional stability

• Poor scratch resistance

So far, highly purified inorganic glass core materials are still unsurpassed in their low transmission loss or low attenuation. However, fibers made of glass need to have very small diameters to obtain flexibility due to its high Young's modulus. Furthermore, glass fibers are very brittle and very sensitive to damage to the surface. This implies that connecting glass optical fibers is a time consuming process that require high precision tools and skilled workers.

Unfortunately the main disadvantage of POF is their very high loss, in comparison with the silica fibers. Losses in all optical fiber are dominated at short wavelengths by Rayleigh scattering, but in polymers absorption due to the harmonics of the C-H vibration becomes very significant at wavelengths longer than about 600 nm. One approach to reduce this has been to shift the harmonics to longer wavelength by replacing hydrogen with some heavier, such as deuterium or fluorine. The use of fluorination has substantially improved the transmission of polymer fibers, not just by reducing the loss but also by extending their transmission window into infrared. This is particularly interesting because it allows the use of low-cost components such as sources and detectors previously developed for use with silica fibers. Later Kaino *et al.* successfully fabricated POF using deuterated PMMA core with a lowest loss achieved of 20 dB/km at 680 nm [2].

1.6 Materials used for POF

History of the development of POFs can be found in Zubia and Arrue [3]. A variety of optical polymers are used in the fabrication of POFs including

- PMMA
- Amorphous fluorinated polymer (CYTOP)
- Polystyrene (PS) and

- Polycarbonate (PC).

Most PMMA-based or PS-based POFs cannot withstand temperature higher than 90°. However, it is desirable to increase the temperature working of POFs. POFs based on PC shows high thermal resistance and can be used at a temperature as high as 150°. The commonly used polymers for waveguide fabrication are poly methyl methacrylate, polystyrene, poly vinyl alcohol (PVA), poly acrylic acid (PA), poly carbonates. As noted earlier, polymer waveguides have a great potential to create all-optical devices, which can be realized by the incorporation of various functional materials such as organic dyes in the polymer host matrix. The basic requirements imposed on a polymeric host for lasing dye molecules are good optical transparency at both pump and lasing wavelengths, good solubility of the dye in the material and resistance to pump laser radiation. The most commonly used material for the production of POF is PMMA, which is better known as Plexiglas®. PMMA has been the most frequently used host for lasing dyes due to its excellent optical transparency in the visible and its relatively high laser-damage resistance. The matrix viscoelastic properties of polymers determine the optical damage resistance. The external plasticization of the polymer by adding low molecular weight dopants improves significantly the laser resistance. For example, by the copolymerization of methyl methacrylate (MMA) with 2-hydroxyethyl methacrylate (HEMA), the plasticity of the material can be internally increased. The presence of HEMA as co-monomer not only increases the plasticity of the material while maintaining the good transparency in the near-ultraviolet and visible spectral ranges, but also ensures good solubility of dyes such as Rhodamine 6G due to the polar character of HEMA.

1.6.1 PMMA

The higher loss factor is a major handicap for POF. However, recently developed techniques for decreasing losses in PMMA based POF have raised much interest in the field of short distance communications. In order to obtain POFs with the proper optical characteristics, it is necessary to prepare specific preform of PMMA produced by the controlled polymerization of methyl methacrylate. From the beginning of 80's the available POF were found to have an attenuation of around 150 dB/km. PMMA-SI-POF has a theoretical minimum attenuation of 106 dB/km at 650nm which is due to the Rayleigh scattering and absorption of C-H bonds. In addition there are losses resulting from waveguide structure particularly when taking into account the attenuation resulting from cladding. PMMA is produced from ethylene hydrocyanic acid and methyl alcohol [4-6]. It is resistant to water, diluted acids, petrol, mineral oil and turpentine oil. PMMA is an organic compound forming long chains with typical molecular weight around 10^5. PMMA is amorphous in nature when polymerized and has a very good optical transparency. The density of PMMA is 1.18 g/cm^3. Its tensile strength is approximately 7-8 kN/cm^2 [7]. The refractive index of PMMA is 1.492 and glass transition temperature T_g lies between +95°C and +125°C. At room temperature and 50% relative humidity the material can absorb upto 1.5% water, which also affects the attenuation characteristics. MMA monomer has eight C-H bonds. Typical properties of PMMA are presented in table 1.1.

Table 1.1 Properties of PMMA

Parameter	**Unit**	**Value**
Refractive Index (RI)	--	1.492
Density	g/cm^3	1.18
Tensile strength	KN/cm^2	7-8
T_g	°C	+95 to +125
Molecular weight	--	10^5

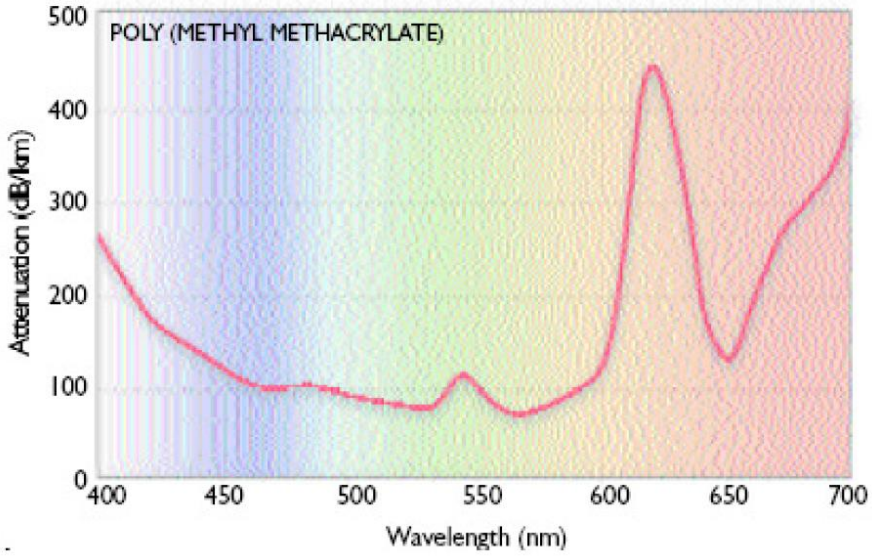

Figure 1.3 Loss spectrum of PMMA fiber

Figure 1.3 illustrates the absorption spectrum of PMMA fabricated at Southampton university [8]. It is evident that the absorption is mainly caused by the overtone due to the stretching vibration of the C-H bond. Between the overtone absorption from stretching vibration there are some minor absorption from a combination of stretching and bending vibrations.

1.6.1.1 Properties of PMMA

(a) Optical behavior

The two loss properties that define the transmission quality of an optical fiber are attenuation and dispersion. The attenuation coefficient, 'α' is a measure of the power loss of lightwave propagating through the optical fiber per unit distance and is defined as,

$$\boldsymbol{P(z) = P_{(0)} 10^{-\alpha z/10}} \qquad \textbf{1.1}$$

where z is the distance along the optical fiber axis, $P_{(0)}$ is the input power of the light wave and $P(z)$ is the output power at a distance z. The source of attenuation in optical fibers can be divided into two types, intrinsic and extrinsic [1]. Intrinsic losses are inherent to the material (e.g. material absorption, Rayleigh scattering), whereas extrinsic losses are introduced during the fabrication of fibers (e.g. structured imperfections, microbends etc.). Kuzyk *et al.* [9] first fabricated polymer optical fiber (PMMA) with a doped core that was single mode at an operating wavelength of λ=1300 nm. These fibers demonstrated attenuation levels of approximately 0.3 dB/cm which is close to the intrinsic material attenuation for PMMA at that wavelength.

(b) Refractive index (RI)

The RI of MMA is about 1.41. When it polymerized the index of refraction will increase up to 1.49 due to volume reduction during liquid to solid phase transition. These indices are close to those of silica material. It is also possible to make the RI of polymer to match perfectly with that of silica by adding other methacrylates.

During the fabrication of polymer fiber preform, the controlling and tuning of the index are important. The difference between the RI profile of the core-cladding region is controlled by adding trifluro-ethyl methacrylate to the

cladding or by adding benzyl-methacrylate to the core. Copolymerization with trifluro-ethyl methacrylate may reduce the index to the range of 1.45 to 1.48. Alternatively, copolymerization with benzyl-methacrylate may rise the index by about 0.08.

(c) Mechanical behavior

The mechanical properties of POFs depend strongly upon the fiber drawing process including the drawing ratio (ratio of preform diameter to fiber daimeter) temperature and speed [10-11]. An important factor in the fiber mechanical behaviour is the annealing process to remove internal stress during the drawing process. The polymer molecules align in the axial direction during the drawing process, creating anisotropic material properties. In addition to changing the mechanical properties, anisotropy in the optical fiber creates birefringence in the fiber cross-section which reduces the lightwave transmission through the optical fiber. This stress relaxation also causes small cracks to appear in the radial direction [12]. This effect is enhanced at elevated draw temperature. Jiang *et al.* [11] annealed polymer bulk material above the glass transition temperature for one week before drawing to ensure that they were isotropic.

Aging due to high temperature or humidity environments is an important challenge for some POF sensor applications [13]. The maximum operating temperature for POFs are typically in the range of 80-100°C [1]. However, elevated temperatures below the maximum operating temperature can cause the POF to become brittle and disintegrate over time. In addition to weakening the POF, these changes increase the attenuation in the POF and can affect the dopant properties, changing the RI profile in the cross-section [13]. Humidity is another important concern affecting the long term stability of POFs and is further emphasized at elevated temperatures. Ziemann [14] provides detailed results of extended temperature and humidity testing of POFs. He

demonstrated that low or elevated temperature environments accelerate in bending of POF.

(d) Strain and temperature sensitivity

To measure the strain sensitivity of an optical fiber for sensing devices, the fiber is subjected to a pure axial strain. The strain sensitivity can be measured by the phase change in a lightwave propagating through the optical fiber/unit length of elongation. Based on the Pockel's constants for bulk PMMA the strain sensitivity of PMMA-POF is theoretically predicted to be 132.6×10^5 rads/m [15]. This is about 15 % larger than the strain sensitivity of bulk silica, which is 115×10^5 rads/m.

Most PMMA based POF cannot withstand temperature higher than 90˚C, which is almost the glass transition temperature (T_g). At temperature higher than T_g, the optical properties of POF deteriorates quickly. Likewise the thermal sensitivity is measured by the phase shift in a light-wave propagating through the optical fiber per unit change in temperature per unit length of the fiber. For bulk PMMA, the thermal sensitivity is calculated to be -154.3 rad m^1 k^{-1}. This is not only larger in magnitude compared to that of silica (98.8 rad m^1 k^{-1}), but also of the opposite sign. This -ve thermo-optic coefficient, which is the case for some polymers, will present new possibilities for temperature compensation in strain sensors.

(e) Bandwidth

One of the major advantage of SI-POF is its large numerical aperture (NA) compared with that of silica based fiber. High NA (ranges from 0.3 to 0.6) which corresponding to acceptance angle between 35 to 74˚ provides the ability to accept and guide much more optical power than silica fibers. However, large NA will lead to pulse broadening due to intermodal dispersion in multimode fibers, which in turn reduce the total bandwidth of the optical fiber. Typical bandwidth for a SI-POF is in the order of 5 MHz/Km. Later

researchers from NEC and Keio university have demonstrated a 100m POF system with transmission rates as high as 2.5 GHz/s which is equivalent to 400 channels of compressed video signals [8].

1.7 Application of Polymer Waveguides

The flexibility of POF is very much higher than that of silica fibers and therefore it can withstand much higher strains, which enables applications of POFs as elongation sensors in a strain range unattainable for silica fibers [16]. Polymer materials have a much lower modulus than inorganic glass and therefore can possess much larger diameter and still retain their flexibility. Optical polymer materials can exist in a broad refractive index range from 1.29 to 1.7. Polymer optical fibers also possess a higher NA. As a result, the acceptance angle or the light gathering capacity is large compared to glass optical fibers. What is more, no expensive lens systems are required to couple the light into the fiber due to the high numerical aperture. This makes POFs a suitable candidate in short distance data communications and optical integrated circuits. POF systems are found in local area network, fiber to home applications, fiber optic sensor, the automotive [17] and aviation [18] industry. Polymer fibers may show better parameters than fibers made of silica in a variety of applications. One of the key advantage is the biological compatibility, which opens the possibility for medical applications.

In the field of sensors, numerous types of products based on POFs have been commercialized [19], for example scanning heads, shape-defect detectors used in bottling plants, and liquid-level detectors. In addition, by using conventional POFs, it is possible to make sensors measure distance, position, shape, color, brightness, opacity, density, turbidity, etc. [20-21]. These sensors can serve to control the various manufacturing parameters in automated production processes with robots. On the other hand, the development of fluorescent POFs has enabled sophisticated sensors such as those utilized for

particle tracking to be made [22]. In the field of data transmission, POFs are especially suitable for short-haul communications links requiring a large number of connections, as usually happens in cars and trains inside the buildings of some companies or in local area networks. Because of their large diameter, POFs are easier to install and align than their glass counterparts [23-24].

In recent years, polymer optical fibers (POFs) are becoming increasingly attractive for sensing applications, particularly in biomedical and in large strain measurement for health monitoring of civil infrastructure. This is because unlike silica optical fibers, POFs are rugged, biocompatible and do not produce shards when broken.

1.7.1 High speed data transmission

POF has been called the "consumer" optical fiber because the fiber and associated optical links, connectors and installation are all inexpensive. Due to the attenuation and distortion characteristics of the traditional PMMA fibers they are commonly used for low-speed, short-distance (up to 100 meters) applications in digital home appliances, home networks, industrial networks (PROFIBUS, PROFINET) and car networks (MOST). The perfluorinated polymer fibers are commonly used for much higher-speed applications such as data center wiring and building LAN wiring. They provide data transmission up to 400 Mbits/s over 50 meters and are used in consumer electronics and industrial electronics as well as the automotive industry.

1.7.2 Sensing

The ability to detect and measure physical parameters such as strain, stress, load, temperature, displacement and pressure makes POF suitable for structural health monitoring applications. In addition to being cheaper than their glass-counterpart, polymer fibers offer better fracture resistance and flexibility. They also offer ease of termination, safe disposability and ease of

handling. Moreover, POFs have a much larger elastic limit and can withstand larger strains; this makes POF particularly attractive in large strain measurement [25]. On the other hand, POF based optical sensors eliminate the risk of electric sparks in explosive environments. It can be also used for measuring liquid levels in harsh environments such as oil/petrol tanks or bio-mass boilers to be used in condominiums and buildings.

Nowadays, Fiber Bragg Grating (FBG) based optical devices are very commonly used in sensors and communication systems [26]. Polymer based FBG sensors have exhibited more than 10 times sensitivity than silica FBGs sensors [27]. Fiber Bragg grating in single-mode POF have been reported since 1999 and many studies have been carried out on the temperature and strain characteristics together with the associated applications. However, there is little work done on the polymeric FBG-based biomedical applications.

Muto *et al.* have realized a dye doped POF based sensor to measure the moisture level [28]. In their work, they fabricated moisture sensitive POFs using PMMA doped with phenol red dye. This device also operating as an excellent humidity sensor with fast response time.

Over the past few years, the advancement of microstructured polymer optical fiber (mPOF) leads to many applications in the field of communication and sensing. Argyros *et al.* have reported the first demonstration of mPOF based amplifier with a high gain of 30 dB [29]. Recently mPOFs are widely used in bio-medical related applications. For example, it is possible to selectively or locally detect antibodies in mPOFs [30], because sensor layers of bio-molecules can be immobilized inside the air holes of the mPOF and localized sensor layers may be activated on the inner side of the air holes in a predetermined section of the mPOF. By doping the mPOF with fluorescence dye an optical pH sensor is also possible [31]. Further study should be carried

out on biomedical applications using POFs and mPOFs with FBGs written in them.

The use of POF based sensors are more economic, especially in situation like throw away sensors are to be used. In recent years several planar optical waveguide sensors have been suggested for biological applications due to its biocompatibility.

1.7.3 Illumination and displays

A growing market however is being explored for side scattering POF for stripe lighting. They are produced by incorporation of scattering particles in the polymer and can be used at lengths upto 5 meter, usually in conjunction with an LED source. Illumination optics is the single largest application of POF and certainly one that exploit its advantages. Because of the very large cores, high light gathering capacity and flexibility, POF is very suitable for illumination purpose. Historically most illumination applications have used POF as point sources, for example as highly localised spot lights in buildings or areas where there is a limited space.

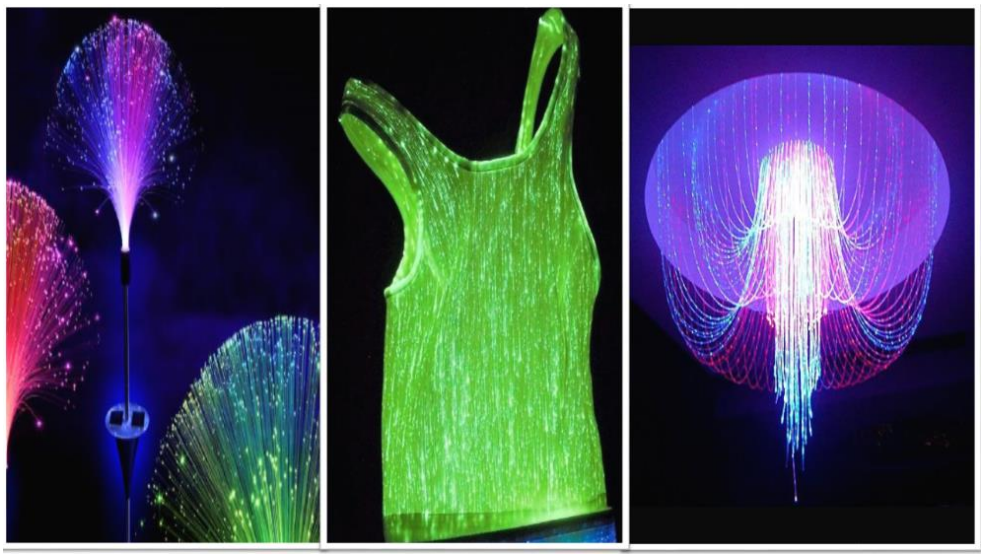

Figure 1.4 Illuminations using POF

POF can be woven like any other textile to form a light-guiding cloth. The flexibility and light weight of POFs along with the inexpensive technique of fabrication making them ideal for such products. Generally the red-green and blue-emitting PMMA fibers run parallel to each other and are illuminated with LEDs. Different patterns are etched into the cladding by making a series of pits. Each pit is a pixel and scatters light out from the fiber. Commercially pits are made by micro-imperfection of POF by chemical treatment with a solvent. In this method, the image is permanent. However, multiple images can be made and interlaced within a system. In this way, one of several images may be selected by illuminating the appropriate set of fibers.

1.7.4 Automotive applications

Perhaps one of the most interesting developments has been the use of POFs in automotive applications, taking advantage of their being light in weight and showing simplicity of connections and interconnection. Increasing data volumes add more and more complexity to control systems in the automotive field and make these technologies particularly useful for instrumentation and control. However, POF does have to meet a number of demanding constraints for use in automotive applications, including resistance to chemical, mechanical and thermal stress as well as being available with high optical quality fiber end. In particular, work is continuing in the development of simple and reliable terminations for these devices for these types of applications.

The biggest hurdle to using polymers in active device applications is the photostability. Given the fast pace of improvements in polymeric materials and highly stable laser dyes to photo degradation, the polymer active systems may one day be the material of choice for photonic applications.

1.8 Dye doped polymer waveguides

A large number of optical devices such as switches and tunable wavelength filters are constructed based on the non-linear effect in the fiber. Generally silica fibers have a very small non-linear coefficient and hence requiring a large amount of optical power or very long fiber length to induce a sufficient non-linear phase change. But in POF, we can easily dope with organic dyes, which is having a very large non-linear coefficient resulting in optical switching at a fraction of a mW optical power.

The increased demand for compact visible laser has accelerated the research in the field of dye-doped polymer waveguides. Due to long gain length and optical confinement, waveguide structures can reduce the lasing threshold which is a requirement for efficient lasing. Due to extremely low lasing threshold, the device can be optically pumped for a long time without damage. Polymer waveguide doped with laser dyes exhibited enhanced amplification of light guided through it.

In the past two decades, waveguide lasers are largely attributed to the geometry of the gain medium, which provides the possibility to store optical energy on very small dimension in the form of optical mode. This will allow the realization of optical source with enhanced optical gain, low lasing threshold and high quality factors. This type of micron sized dye doped polymer waveguides will open up exciting possibilities in the area of integrated optics by facilitating their on-chip integration with different functionalities and highly compact photonic circuits.

In the beginning of 21st century, optically pumped solid-state dye lasers with high optical quality was realized in the form of cylindrical and planar waveguide structures. The merits of the waveguide geometry and the associated optical confinement have been first highlighted for the fabrication of the same. Among them fiber structure is most suitable for the realization of

highly efficient amplifier and laser sources owing to the unrivalled low loss performance. However, the planar geometry has the potential for integration with different functions to photonic circuits and the possibility to convert into both nonlinear and dispersion waveguides by suitably choosing their design.

1.8.1 Dye doped POF as light amplifier

Short distance communication and network designs such as LANs have brought amplifiers and repeaters using polymer optical fibers to the forefront of research and development activities. The possibility of a large bandwidth available in visible wavelength-based data communication has encouraged studies exploring the possibility of using dye-doped POFs as optical amplifiers [32-33]. Laser dyes, which act as highly efficient media for lasing and amplification, have a wide range of tunability in the visible region. In the recent years, the incorporation of dyes into solid-state material has enabled development of various opto-electronic devices ranging from tunable lasers and amplifiers to non-linear devices such as switches and modulators.

The tremendous interest in the field of waveguide lasers in the past two decades is largely attributed to the geometry of the gain medium, which provides the possibility to store optical energy on a very small dimension in the form of an optical mode. Given the great flexibility in controlling the optical properties of a dye-doped polymer, it is possible to make polymer fiber sources that act over a broad range of colours. This allows the realization of sources with enhanced optical gain, low lasing threshold and small footprint which opens up exciting possibilities in the area of integrated optics by facilitating their on-chip integration with different functionalities and highly compact photonic circuits. Waveguide structures provide long gain length and optical confinement, which offer reduction of lasing thresholds, a requirement for efficient lasing. Polymer optical fibers are attractive as waveguide

structures because of their symmetric output beam profile and adaptability to optical fiber based communication systems.

Availability of inexpensive sources in the visible region has increased the utilization of POF in data communication in the visible region necessitating the development of suitable optical amplifiers working in this region [34-36]. POF doped with dyes or rare-earth elements are potential candidates for this purpose. The availability of different organic dyes makes light amplification possible in the above region [37].

In dye-doped polymer matrix systems, the dye molecules like – rhodamines, coumarins, pyrromethanes etc- are dispersed in solid host media. Polymeric matrices offer several advantages such as wide spectral coverage by chemical tailoring of structures, ease of processibility that permits fabrication of the devices of virtually any shape and potentially very low cost. They also show better optical transparency, homogeneity of refractive index and good compatibility with organic dyes.

With low intensity illumination, not many molecules in a material are excited so that stimulated emission is not likely. Under this condition, only a fluorescence (broad emission) spectrum is observed. As the intensity turned up, stimulated emission begins. Since many more photons are created at a wavelength corresponding to the fluorescence peak than at any other wavelength and more of the inverted population corresponds to this energy. This wavelength will be favoured for stimulated emission and amplification. The wavelength at which a sample will emit ASE is therefore determined from the competition between the material absorption spectrum and fluorescence spectrum.

In an optically amplified medium, not only amplification of photons created by stimulated emission can occur but also amplification of spontaneously emitted photons. This phenomenon is called Amplified

Spontaneous Emission (ASE). The optical amplification scheme is the same as for laser light but here a spontaneously emitted photon is amplified i.e. the spontaneous decay of an excited molecule sets off an avalanche effect of optical amplification and many exact copies of original photons are produced without the use of a cavity.

In 1995, A. Tagaya [32] and co-workers demonstrated the first optical amplification in the visible wavelength using dye doped POFs. In their experiment, a gain of 27 dB was achieved at 591 nm wavelength with a pump power of 11 kW [38] using a dye doped graded index POF. The bandwidth of the GI POFA was estimated to be several hundred megahertz per kilometer at 3 dB. Subsequently, Peng *et al.* have reported high gain and high efficiency optical amplification in Rh B doped POF with a low pump power of 1 kW [33]. The gain of a dye doped POF amplifier mainly depends on the doping concentration and diameter. The gain of such POFs varies as quadratic function of pump power. However, the endurance of dye doped POF amplifier is purely depends on the pump power. Hence the pump power has to be limited below a certain level to improve the photostability of POF amplifier. High power amplification with an output power of several hundred watts was achieved in POFA with a short fiber length (less than 0.5 m) because of the fibers large core diameter (250-500 μm) and large emission cross-section. Such a high power amplification was never realized in conventional Er^{3+} doped silica fiber amplifiers due to dielectric breakdown in a very small core diameter (<10 μm). Therefore POFA have interesting applications as an amplifier in the optical fiber local area network and a booster for a laser diode in the visible region.

1.8.2 Dye doped fiber laser

A fiber amplifier can be converted into a laser by placing it inside a cavity to provide optical feedback; such lasers are so called fiber lasers. Soffer and

McFarland first demonstrated a solid-state dye laser using a PMMA sample containing Rh 6G dye [39]. Dye doped polymer microcavities provide an excellent coupling of spontaneous emission into lasing modes. These cavities are found to be an ideal candidate as a laser resonator due to their high quality factors (Q) and low lasing threshold.

Generally the ASE process can deplete the population of the upper laser level, thereby diminishing the amplification of a possible subsequent incoming laser signal. ASE radiation can possess spatial coherence but lacks temporal coherence compared to laser light. The lack of temporal coherence is understandable since the choice of spontaneously emitted photon to amplify is coincidental. External feedback is necessary to obtain laser emission. In the case of fibers there are no external mirrors to give feedback to the gain medium. The optical feedback for the gain medium is provided by the cylindrical surface of the optical fiber, which exhibits microcavity-like behavior due to Fabry-perot effects. Generally a laser device is constructed by the combination of the laser medium and an optical feedback structure.

Optical amplifiers and lasers made of dye doped fiber require much less pump power than in bulk material because of the effective confinement and long interaction length available in the fiber [40]. These microcavities confine light into an interior region close to the surface of the resonator by resonant circulation due to total internal reflection at the boundary. Resonators having diameters from a few tens to several hundreds of micrometers can have a very large free spectral range of several nanometers. Generally a microring cavity is realized by making a coating of few micron thick conducting polymers [41] or dye doped transparent polymer over a glass fiber [42]. The most important parameter for a solid-state dye laser system is the rate of dye photo-degradation. In all applications of a laser dye, the main concern is the photostability of the dye under irradiation by the pump light. The bleaching of

dye molecules could be assumed mainly due to the thermal effect. Also the thin and long geometry of the fiber is ideal for good thermal relaxation to minimize the thermally induced photo-bleaching as well.

1.9 Outline of the thesis

The main objective of the research work is the design of compact polymer based devices for various applications. Different types of dye doped polymer optical waveguides were chosen to be the suitable candidate for the realization of the same. The thesis focused on the design, fabrication and characterization of different types of dye doped polymer optical waveguides as a light amplifier and laser resonator. The photo-physical properties of Rh B laser dye along with its theoretical studies in details for a good number of solvent environments have been discussed in chapter 2. Subsequently the gain coefficient, stimulated emission cross-section and life time for rhodamine B dye dissolved in various solvents are determined. The third chapter deals with the fabrication and optical characterization of different types of dye doped polymer fibers. Observation of Whispering gallery mode (WGM) lasing from dye doped hollow polymer optical fiber (DDHPOF) and its characteristics are presented in chapter 4. Important parameters such as free spectral range, mode volume, Q-factor and finesse in WGM resonators are presented. The characterizations of laser emission from an asymmetric ring-type cylindrical cavity (ARC) with the help of theoretical studies are described in chapter 5. A detailed observation of ASE and different mode propagation in an asymmetric planar waveguide are presented in chapter 6. In this chapter we also discuss the multimode laser emission from free-standing dye doped polymer film and dye doped polymer coated silica fiber. Chapter 7 deals with the fabrication and characterization of different thickness microring embedded cylindrical microcavities. Conclusion and future prospects are discussed in the last chapter.

1.10 Conclusions

This chapter briefly presents an overview of polymer optical waveguide systems, historical development of polymer optical fibers, types of polymer optical waveguide structures and the different properties of poly methyl methacrylate (PMMA). This chapter also deals with the potential advantages of polymer optical fibers over their silica counterparts and its application in different fields. The last section of the chapter discusses the outline of the presented thesis.

References

1 G. D. Peng, P. L. Chu, X. Lou and R. A. Chaplin, "Fabrication and characterisation of polymer optical fibers", Journal of Electrical and Electronics Engineering, Australia, IF Aust and The IEEE society Vol. 15, No. (1995).

2 T. Kaino, K. Jinguji and S. Nara, "Low loss poly-methyl methacrylate core optical fibers", Appl. Phys. Lett. 42, 567-569 (1983).

3 J. Zubia and J. Arrue, "Plastic optical fibers: an introduction to their technological processes and applications", Opt. Fiber Technol 7, 101-40 (2001).

4 Bruno Vollmert, "Polymer chemistry", Springer (2000).

5 Marvin J. Weber, Weber J, "Handbook of optical materials", CRC Press (2003).

6 Marc J. Madou, "Fundamentals of microfabrication", CRC Press (2002).

7 Olagoke Olabisi, "Handbook of Thermoplastics", Marcel Dekker (1997).

8 C. Emslie, "Review-Polymer Optical Fibers", J. Mat. Sci., Vol 23, No.8, 2281 (1988).

9 M. G. Kuzyk, U. C. Paek, and C. W. Dirk, "Guest-host polymer fibers for nonlinear optics", Appl. Phys. Lett. 59, 902-904 (1991).

10 D. Bosc and C. Toinen, "Tensile mechanical properties and reduced internal stress of polymer fiber", Polym. Conpos. 14, 410-413 (1993).

11 C. Jiang, M. G. Kuzyk, J. L. Ding, W. E. Johns, and D. J. Welker, "Fabrication and mechanical behaviour of dye doped polymer optical fiber", J. Appl. Phys. 92, 4-12 (2002).

12 J. Duges and G. Maurel, "Mode coupling processes in polymethyl methacrylate-core opticl fibers", Appl. Opt. 31, 5069-5079 (1992).

13 O. Ziemann, J. Krauser, P. E. Zamzow and W. Daun, "POF Handbook (Berlin:Springer)" Chapter 9 (2008).

14 O. Ziemann, W. Daun, A. Brauer, J. Schlick and W. Frank, “Result of a German 6000h accelerated aging test of PMMA POF and consequences for the practical use of POF”, Proc. POF (Boston), 133-137 (2000).

15 M. Silva-Lopez, A. Fonder, W. N. MacPherson, J. S. Barton, J. D> C. Jones, D. Zhao, H. Dobb, D. J. Webb, L. Zhang and I Bennion, “Strain and temperature sensitivity of a single-mode polymer optical fiber”, Opt. Lett., 30, 3129-3131 (2005).

16 D. Webb and K. Kalli, “Polymer fiber bragg gratings” in Fiber Bragg Grating Sensors Recent Advancement, Industrial applications and Market Exploitation, A. Cutolo, and J. Albert, Eds. Sharjab (Bentham Science Publishers), pp. 292-312 (2011).

17 T. Kibler, S. Poferl, G. Bock, H. P. Huber, E. Zceb, “Optical data buses for automotive applications”, J. Lightwave Tech., 22 (2004).

18 K. R. Cooper, J. Elaster, M. Jones, R. G. Kelly, “Optical fiber based corrosion sensor systems for health monitoring of aging aircraft”, AUTOTESTCON proceedings IEEE systems Readiness Technology Conference (2001).

19 U. Steiger, ‘‘Sensor properties and applications of POFs,’’ in Proc. Seventh International Conference on Plastic Optical Fibres and Applications-POF98, Berlin Ž Germany., pp. 171_177, 1998; H. Poisel, K. F. Klein, V. Levin, and G. Lohr, ‘‘Progress with the Fiber Optic Slipring,’’ in Proc. Sixth International Conference on Plastic Optical Fibres and Applications-POF97, Kauai HI, pp. 22-25, (1997).

20 Club des Fibres Optiques Plastiques, Plastic Optical Fibres: Practical Applications, Wiley, New York, (1997).

21 R. J. Bartlett, S. L. Caulder, R. P. Chandy, D. F. Merchant, R. Morgan, and P. Scully, ‘‘Plastic optical fibers sensors and devices’’, in Proc. Seventh International Conference on Plastic Optical Fibres and Applications-POF 98, Berlin Ž Germany., pp. 245-246, (1998).

22 A. J. Schilk and T. W. Bowyer, ‘‘The use of scintillating plastic optical fibers for the detection of radioactive contamination,’’ in Proc. Fourth International Conference on Plastic Optical Fibres and Applications-POF 95, Boston MA, pp. 171-176, (1995).

23 T. Kaino, ‘‘Polymer optical fibers,’’ in Polymers for Lightwave and Integrated Optics. Dekker, NewYork, 1992; E. Nihei, T. Ishigure, N. Tanio, and Y. Koike ‘‘Present prospect of graded index plastic optical fiber in telecommunications,’’ IEICE Trans. Electron., vol. E-80-c, 117-122, (1997).

24 High performance plastic fiber optics, ESKA, Mitsubishi Rayon Co. Ltd.

25 K. S. C. Kaung, S. T. Quek, M. Maalej, Meas. Sci. Technol., 15, 2133-2141 (2004).

26 H. Y. Liu, G. D. Peng, P. L. Chu, IEEE Photon. Technol. Lett. 14, 935-937 (2002).

27 H. B. Liu, H. Y. Liu, G. D. Peng, P. L. Chu, Opt. Commun. 219, 139-142 (2003).

28 S. Muto, A. Fukasawa, T. Ogawa, M. Morisawa, H. Ito, Jap. J. Appl. Phys. 29 (6), 1023-1025 (1990).

29 A. Argyros, M. A. Van, Eijkienborg, S. D. Jackson, and R. P. Mildren, " Microstructured polymer fiber laser", Opt. Lett- 29, 1882-1884 (2004).

30 J. B. Jenson, P. E. Hoiby, L. H. Pederson and A Bjarklev, "Selective detection of antibodies in microstructured polymer optical fibers", Opt. Express 13, 5883-5889 (2005).

31 X. H. Yang, and L. L. Wang, "Fluorescence pH probe based on microstructured polymer optical fiber", Opt. Express, 15, 25, 16478-16483 (2007).

32 A. Tagaya, S. Teramoto, E. Nihei, K. Sasaki, and Y. Koike, "High-power and high-gain organic dye-doped polymer optical fiber amplifiers: novel techniques for preparation and spectral investigation", Appl. Opt. 36, 572-578 (1997).

33 G. D. Peng, P. K. Chu, Z. Xiong, T. W. Whitbread, R. P. Chaplin, "Dye-doped step-index polymer optical fiber foe broad band optical amplification", J. Lightwave Technol. 14, 2215-2223 (1996).

34 A. Tagaya, S. Teramoto, T. Yamamoto, K. Fujii. E. Nehei, Y. Koike, K. Sasaki. "Theoretical and experimental investigation of rhodamine B-doped polymer optical amplifier", IEEE J. Quant. Elect. 31, 2215-2220 (1995).

35 C. Koeppen, S. Yamada, G. Jiang, A. F. Garito, L. R. Dalton, "Rare-earth organic complexes for amplification in polymer optical fibers and waveguides", J. Opt. Soc. Am. B. 14, 155 (1997).

36 T. Yamamoto, K. Fujii, S. Teramoto, A. Tagaya, E. Nihei, T. Kinoshita, Y. Koike, K. Sasaki, "High-power polymer optical fiber amplifiers and there applications", Proceedings of SPIE, 2289, 142-152 (1994).

37 M. Saito, H. Ishiguro, "Anisotropic fluorescence emission of a dye doped fiber ring that is pumped by a ring laser beam", J. Opt. A: Pure Appl. Opt. 8, 208-213 (2006).

38 A. Tagaya, Y. Koike, T. Kinoshita, E. Nihei, T. Yamamoto and K. Sasaki, "Polymer optical fiber amplifier", Appl. Phys. Lett. 63, 883-884 (1993).

39 B. H. Soffer and B. B. McFarland, "Continuously tunable, narrow band organic dye lasers", Appl. Phys. Lett. 10, 266-267 (1967).

40 M. Kailasnath, T. S. Sreejaya, R. Kumar, C. P. G. Vallabhan, V. P. N. Nampoori, P. Radhakrishnan, Opt. Laser Technol. 40, 687-691 (2008).

41 N. Tessler, G. J. Denton, R. H. Friend, "Lasing from conjugated polymer microcavities", Nature 382, 695-697 (1996).

42 J. Peter, C. P. G. Vallabham, P. Radhakrishnan, V. P. N. Nampoori and M. Kailasanath “Microring lasing from a dye doped polymer coated silica fibre”, Laser Phys. 23, 115104 (2013).

Chapter 2
Photophysical and lasing properties of Rhodamine B laser dye

"Anyone who has never made a mistake has never tried anything new"
Albert Einstein

Abstract

This chapter provides useful information on the photophysical properties of Rh B dye in different solvents with theoretical support. The structural geometries, UV-vis absorption spectra and emission intensities of rhodamine B (Rh B) in various solvents have been determined for different excited states by density functional theory (DFT) and time-dependent (TD) with polarizable continuum model (PCM) methodologies. This chapter also demonstrates the pulsed, photo-pumped multimode laser emission in the visible spectral range from rhodamine B dye dissolved in various solvents. The cavity lasing spectral structure and the number of longitudinal modes are easily controlled by changing the solvents. A shift in the emission spectra observed by changing the solvent allows a limited range of tuning of laser emission wavelength. The gain coefficients, stimulated emission cross-section and life time for the Rh B dye dissolved liquid laser system are also determined in this chapter.

The major contents of this chapter has been published in ***Journal of Luminescence****, Volume 169, Part A, pp.227-232, January 2016.*

2.1 Introduction

The first laser was built in 1960 by Maiman [1], 44 years after Einstein's suggestion of stimulated emission. Six years after, the first dye laser was realized by Sorokin and Lankard [2]. Organic dyes of Rhodamine family have been extensively used for a laser medium for tunable lasers because of its large absorption and emission cross-sections, high internal quantum efficiency and their good solubility in different solvents. These dyes are also used as a sensor [3], non-linear optical material [4], photosensitizer [5], optical amplifier and material protease label [6]. The ultrawide wavelength tuning range and the ability to generate both narrow linewidth continuous wave output and ultra-short pulses (<100 fs) make dye lasers an ideal coherent source for spectroscopy [7]. The liquid dye lasers can be easily cooled, bleached molecules can be exchanged and the cost of the gain medium is relatively low compared to crystals, typically used for solid-state lasers [8]. However, conventional liquid dye laser is generally referred to as "user unfriendly system" due to their bulky and complex liquid-handling systems and hazards of toxic dyes. Therefore, conventional dye laser systems cannot be used in many applications.

Liquid dye lasers are the first material systems used to study the laser action and other optical processes in microcavities. In liquid dye lasers, tuning of the laser wavelength is performed either by changing the concentration of the dye, ***concentration tuning,*** or by changing the optical path length in the cavity. To change the optical path of the cavity, the solvent of the dye can be changed, thereby changing the refractive index in the cavity. This method is so called ***solvent tuning***. One should keep in mind that by changing the solvent, other properties of the fluid which can affect the laser wavelength may be changed due to the interaction between dye molecules and the solvent molecules.

2.2 Photophysical properties of laser dye

Generally, laser dyes are complex organic molecules containing long chains of conjugated double bonds. The complex molecular structure will lead to many vibrational and rotational energy levels within a single electronic state. Therefore, laser dyes often have strong and wide absorption bands in the UV and visible region [9-10]. For the sake of simplicity, we confine our attention to S_0 and S_1 level, and ignore the influence of other electronic and triplet levels. In figure 2.1 we show an energy level diagram in which dye molecules have been excited from the ground level (S_0) to the first excited singlet level (S_1). Before absorption of a photon, almost all the molecules are in the zero vibrational level (ν=0) of the S_0 state, because the spacing between vibrational levels is much larger than thermal energy.

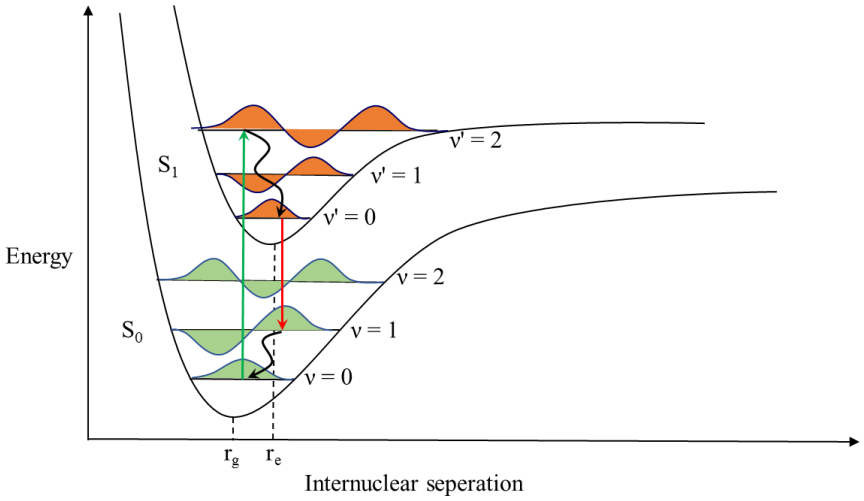

Figure 2.1 Energy level diagram of a typical organic dye molecule

The quantum mechanical Franck-Condon principle states that the probability of each transition is determined by the extent of overlap between the ground and excited state vibrational wave function. From figure 2.1, one could observe that the overlap of wave function between the S_0 (ν=0) and S_1 (ν=2) is very high. Under optical excitation, dye molecules are pumped from

the ground state S_0 (v=0) to some vibrational-rotational sublevel (v=2) in the first excited singlet state S_1 as marked by green line in figure 2.1. The dye molecule in this level will quickly relax by a non-radiative decay process to the bottom of S_1 (v=0) (the lowest rotational-vibrational sublevel) within a few picoseconds or less. From this level, dye molecules can undergo either spontaneous emission or stimulated emission (marked as red line in figure 2.1) to a sublevel (v=1) in the ground state S_0, where the probability of transition is higher due to the extent of overlap wave function between these levels. Due to the non-radiative decay process, the emitted photon has always a lower energy (higher wavelength) than the absorbed photon. After the emission of a photon, rapid thermalization takes place to the bottom of the ground state in a pico second time scale.

Organic laser dyes typically show a large fluorescence yield ranging from about 0.6 to near the optimum 1. Figure 2.2 shows the absorption spectra of Rh B with a concentration of 5×10^{-4} mol/dm^3, which is dissolved in methanol, ethanol, ethylene glycol and glycerol respectively. These spectra were recorded using a quartz cuvette in a UV-VIS spectrophotometer (Jasco V570). The absorption spectra exhibit a solvatochromic shifts after exchange between one solvent to another. Due to the electron redistribution within the solvent molecules, the energy difference between the ground state and excited states will vary.

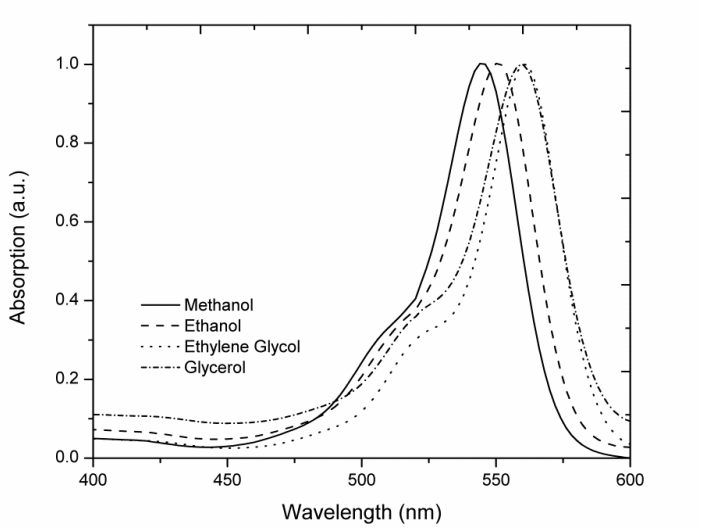

Figure 2.2 Absorption spectra of Rh B dye (5 X 10^{-4} mol/dm^3) dissolved in various solvents.

When the properties of the solvent such as refractive index (n) and dielectric constant (ε) changes, the ground and excited state of the dye gets stabilized instantaneously by movements of electron within the solvent molecules. This electron redistribution results in a change in energy difference between the ground and excited states. The stokes shift is related to the orientation polarizability term Δf, which is also known as solvent polarity function. The value of Δf can be measured by,

$$\boldsymbol{\Delta f} = \left(\frac{\boldsymbol{\varepsilon-1}}{\boldsymbol{2\varepsilon+1}} - \frac{\boldsymbol{n^2-1}}{\boldsymbol{2n^2+1}}\right) \qquad \textbf{2.1}$$

The difference in the two terms (first term depends on the polarizability and second term depends on the RI) accounts for the spectral shifts due to re-orientation of the solvent molecules. Hence the energy state difference between the excited state and the ground state of the dye is sensitive to the different properties of the solvents.

2.3 Theoretical Methodology

Theoretical studies can not only provide valuable information on the photophysical and spectroscopic properties of dyes but also play a key role in

growing a number of disciplines from nano-biotechnology to photonics and opto-electronics with improved performance [4,9]. The optimized structure of Rhodamine B with labelling of atoms in gaseous phase is shown in figure 2.3. The molecular structure of Rhodamine B (Rh B) dye is constituted by a diameno-xanthene ring with a pendant carboxy-phenyl substituent. The highest occupied molecular orbital (HOMO) and lowest unoccupied molecular orbital (LUMO) of the molecule in gas phase was calculated using B3LYP exchange correlation functional and 6-31+ G (d) basis set implemented in Gaussian 09 suite of codes [11-13].

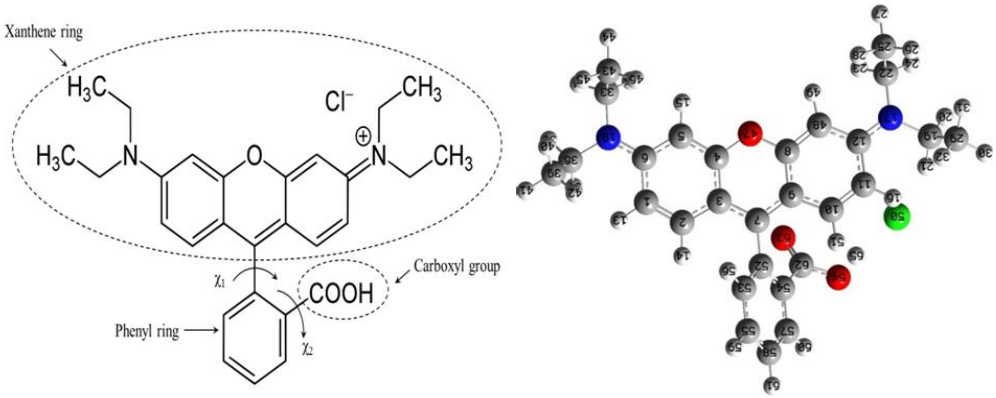

Figure 2.3 Molecular formula and optimized structure of Rhodamine B with labeling of atoms in gaseous phase

The stationary points are characterized by frequency analysis and the excited state properties of the molecule are predicted by TD-DFT method. Solvation model is also included in the TD-DFT calculation.

2.4 Computational modelling

Diameno-xanthene systems are characterized by a π HOMO with a non-bonding character located on the xanthene ring and to some extent on the amino substituents as shown in the figure 2.4. The π^* LUMO, is mainly located on the xanthene ring and can be partially located on the phenyl ring.

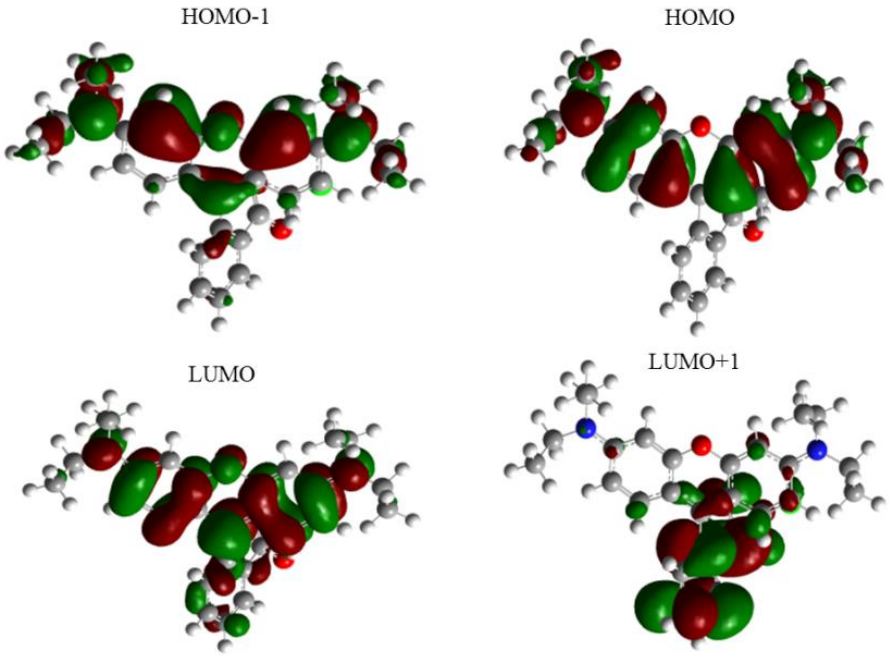

Figure 2.4 Kohn-Sham Frontier molecular orbitals of Rhodamine B

Rh B molecules in the Franck-Condon region are characterized by the presence of two closely lying states: a bright locally excited state, centered on the xanthene moiety and a dark charge transfer state corresponding to a transition from the carboxy-phenyl to the xanthene group. The first transition is the most intense (with an oscillation strength of 0.9) and corresponds to a π to π^* transition between HOMO and LUMO orbitals. This will lead to a bright locally excited state which is responsible for a strong absorption band in the visible domain with its maximum around 530 nm. The second transition corresponds to a n to π^* transition between HOMO-1 to LUMO orbitals. This transition is mainly due to intramolecular PeT (Photo-induced electron Transfer), which takes place from phenyl (electron donar moiety) to xanthene ring (electron withdrawn group). This type of intramolecular PeT will lead to dark state, which is responsible for non-radiative decay (with oscillation strength of 0.08) with a weak absorption around 420 nm.

Table 2.1 Vertical excitation data of Rhodamine B in different solvent

Solvent	State	Main character	Wavelength (nm)	Oscillator strength (f)
Ethanol	State 1	H ⟶ L	538.65	1.1666
	State 2	H-1 ⟶ L	426.94	0.0466
	State 3	H-2 ⟶ L	373.58	0.0165
Methanol	State 1	H ⟶ L	539.84	1.1725
	State 2	H-1 ⟶ L	427.24	0.0464
	State 3	H-2 ⟶ L	369.54	0.0623
Butanol	State 1	H ⟶ L	536.54	1.1558
	State 2	H-1 ⟶ L	426.44	0.0469
	State 3	H-2 ⟶ L	381.60	0.0048

The vertical excitation results using the computational method will give some accurate data of the photophysical properties in different environments, which are listed in table 2.1. On comparing the TDDFT/ PCM calculated data with experimental results we have demonstrated the accuracy of the TDDFT/ PCM approach for calculating vertical transition energy. The solvent effects were included by Conductor-like Polarizable Continuum Model (C-PCM) [14-15] solvation model.

The relative energies of these two states depend on the relative orientation of the two subgroups present in the molecules, which actually depends on the χ_1 and χ_2 torsions. Dihedral angle χ_1 represents the relative orientation of the phenyl and xanthene rings, whereas angle χ_2 describes the rotation of the carboxyl group with respect to the phenyl ring.

Table 2.2 χ1 and χ2 dihedral angles (degree) of the Rh B dye in different solvents in the ground and excited state at the DFT/TD-DFT – B3LYP/6-31 G (d) and C-PCM solvation model.

Energy state	Solvent	Xanthene ring to Phenyl ring (χ1)	Phenyl ring to carboxyl group (χ2)
Ground	Methanol	-92.93°	-0.00152°
	Ethanol	-92.95°	-0.005°
	Butanol	-92.99°	-0.0034°
Excited	Methanol	-67.34°	-15.347°
	Ethanol	-67.315°	-15.3569°
	Butanol	-67.237°	-15.41°

From the theoretical approach, it is observed that, for the various solvents the xanthene to phenyl planes is almost perpendicular and the carboxyl group lying in the phenyl plane, at the ground state. The χ_1 and χ_2 torsion angles vary in the excited state geometries and are listed in table 2.2.

When the dye is dissolved in various solvents, new electronic distribution of the dye will happen during the electronic transition due to the electronic reorganization of the surrounding enviornments. This will lead to a solvatochromic shift to the vertical excitation profile. The effect of the different solvent on the geometries, oscillating frequency strength (f) and corresponding vertical excitation wavelengths were calculated at the TD-DFT level within the adiabatic approximation with the same functional and basis set along with the integral equation formalism of the PCM. The vertical excitation resulting from the computational method will give some accurate data of the photophysical properties in different environments. The good agreement with experimental data makes our approach suitable to study and monitor the interaction of dye molecules in different environment systems.

2.5 Concentration tuning

Figure 2.5 shows the tuning of emission wavelength peak with variation in the dye concentration in methanol. The peak emission wavelength of Rh B dye with 1 $\times 10^{-4}$ mol/dm^3 concentration is found to be at 589 nm. By increasing the concentration of Rh B, the peak wavelength shows a clear redshift and at 5 $\times$ 10^{-3} mol/dm^3 concentration the emission peak is at 624 nm.

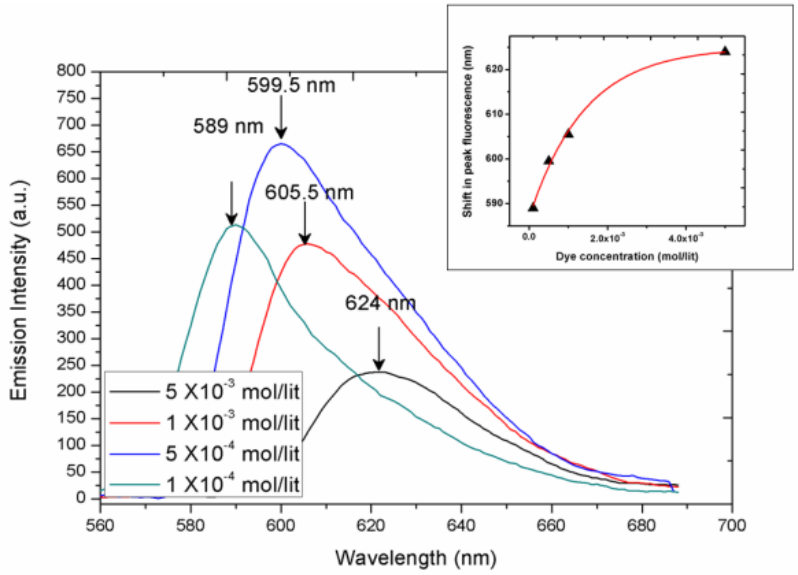

Figure 2.5 Florescence spectra of Rh B dye dissolved in methanol at different concentrations. Inset shows red-shift of peak fluorescence with the concentration of Rh B.

Due to Stokes shift, the shorter wavelength of emission spectrum is absorbed by Rh B molecule and re-emit at the higher wavelength. The increase in concentration will increase the interaction between the dye molecules and the fluorescence light which will result in the shifting of the emitted fluorescence peak towards the longer wavelength region. This type of concentration dependent red-shift was also reported by F. P Schafer [16]. These types of tuning of the emission wavelength by changing the concentration of the dye are generally known as *concentration tuning*. The

inset of figure 2.5 shows the redshift of emission spectra as a function of dye concentration. From this, it is clear that the lasing wavelength is tunable over a wide range (589-624 nm) due to the overlap of absorption and emission spectra of Rh B dye. However, after a particular dye concentration, the shift tends to exhibit saturation behavior.

2.6 Life time measurements

Fluorescence life time measurement is one of the important tool for understanding several aspects of excited state dynamics and interaction between molecules. The fluorescent life time of Rh B dye were performed with standard time-correlated single photon counting (TCSPC) method. The dye is dissolved in various solvents with a fixed concentration of 5×10^{-6} mol/dm^3 were used for life time studies. The typical emission decay curve of Rh B in methanol is shown in figure 2.6.

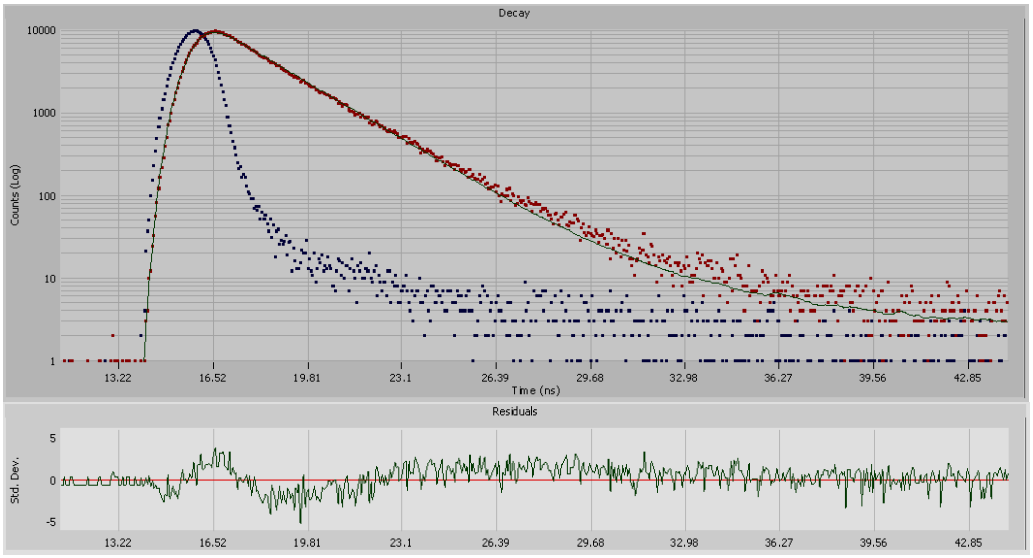

Figure 2.6 Fluorescence decay curve, instrument response (IR) curve, fitting line and fitting residue of Rh B in methanol. Excitation: 379 nm laser (0.1 mW, 69ps); emission 590 nm.

Table 2.3 Photophysical and chemical properties of Rh B dye in different solvents.

Solvent	Chemical formula	Life time (ns)	Boiling Point (°C)	RI (n)	Dielectric constant	Polarity
Water	H-O-H	1.44	100	1.333	78.54	10.2
Methanol	CH_3-OH	2.05	64.7	1.34	32.7	5.1
Ethanol	CH_3-CH_2-OH	2.71	78.29	1.36	24.5	5.2
Propanol	CH_3-CH_2-CH_2-OH	2.36	97.2	1.38	20.1	4.0
Butanol	CH_3-CH_2-CH_2-CH_2-OH	2.7	117.6	1.399	17.84	5.4
Ethylene Glycol	C_2-H_6-O_2	2.6	197.3	1.43	37	8.0

Table 2.3 summarizes the different photophysical and chemical properties of Rh B dye in different solvents.

2.7 Lasing studies

2.7.1 Experimental setup

To observe lasing from the different dye solutions, we used the second harmonic output of a Q-switched Nd:YAG laser that emits pulses of 8 ns duration at a repetition rate of 10 Hz as the excitation source. The pump power was adjusted with neutral density filters, and focused by a cylindrical lens into a 0.2 mm × 4 mm stripe transverse to a quartz cuvette of 1 cm inner length that contained dye solution. The schematic of the experimental setup is shown in figure 2.7 (a). This optical setup induces amplified spontaneous emission (ASE) along with the gain guiding and laser emission. The parallel windows of the quartz cuvette will provide the optical feedback, which is necessary for laser action. The emissions guided along the excitation stripe were collected from the side of the cuvette using a collecting fiber, and were then spectrally

analyzed using a spectrometer and a charge coupled device. All the investigations were done in Rh B dye solutions with a constant dye concentration of 5×10^{-4} mol/dm^3 in different solvents, while all the experimental conditions such as pump power, ambient temperature, excitation length of the gain medium and mode of collection remained the same.

2.7.2 Laser emission

In our study, Rh B dye is dissolved in different solvents such as ethanol, methanol, butanol, ethylene glycol and glycerol, which are pumped transverse with short light pulses of several energies [17-18]. Apart from its particularly large cross section, it has high photochemical stability, which is important in practice to withstand multiple excitation cycles with a pulsed pump laser.

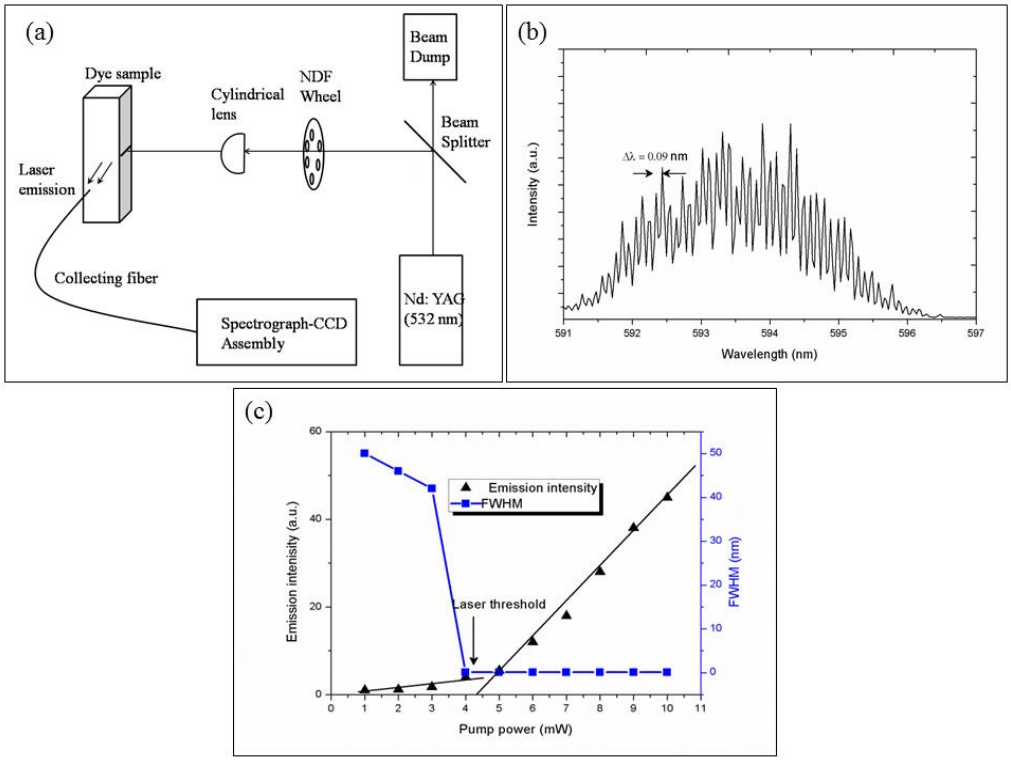

Figure 2.7 (a) Shows the schematic of experimental setup. (b) Lasing spectrum of Rh B solution in Butanol at a pump power of 15 mW and (c) shows the emission intensity and FWHM of emission band versus pump power.

To study the emission characteristics from the dye dissolved in butanol, the emission spectra were recorded for various pump powers. When the pump power was increased, the amplified spontaneous emission spectrum collapsed into multiple narrow lines as shown in figure 2.7 (b). In the laser spectrum, each emission line had a linewidth less than 0.1 nm. Such a spectral narrowing cannot be found in ordinal ASE in which the linewidth gradually decreases to several nanometers [19]. A clear threshold behavior in the emission versus excitation intensities plot and a second decrease in the linewidth at higher excitation intensity indicated the onset of laser action as shown in figure 2.7 (c). The strongly modulated laser spectrum with numerous evenly spaced peaks clearly indicates the resonant modes. Above the threshold, the total emission intensity increased much more rapidly with the excitation pump power. As the pump power is increased, the lasing action occurred in the direction of the highest gain parallel to the excitation stripe. For increasing pump powers, the absorption decreases and the fluorescence grow due to the increased population inversion, which increase the gain. Due to Stokes shift, the gain maximum grows and moves towards the higher energy side (smaller wavelengths). The gain maximum is very important since it has a big influence on the spectral position of the laser mode. Ideally, if all cavity modes have the same loss, the laser mode is the cavity mode which is positioned closest to the gain maximum. Similar blue-shift with the pump power has also been observed in various dye laser systems [20-21].

The resonant modes are centered at the maximum of optical gain which in turn corresponds to the photoluminescent spectrum peak [22]. A large number of sharp lines can be seen within the fluorescent emission profile. The lasing modes are spectrally narrow with an FWHM of 0.05 nm at a pump power of $P_{th}\times4$ (~ 15 mW), where P_{th} is the lasing threshold pump power. When the pump power is higher than the lasing threshold ($P_{th}\times1.2$) lasing modes appear

in the longer wavelength range (593–596 nm) of the photo-luminescence spectra of the gain medium. When the pump power is further increased, the lasing modes with high intensities start to develop on the shorter wavelength region of the spectra. The number of lasing modes and the resonant mode intensities increase with pump power as can be clearly seen in figure 2.8. The blue-shift as a function of pump power is attributable to the transfer of mode energy to that of the shorter wavelength side, which has got a large gain coefficient. However, the magnitude of this transition of energy gets saturated after a particular pump power.

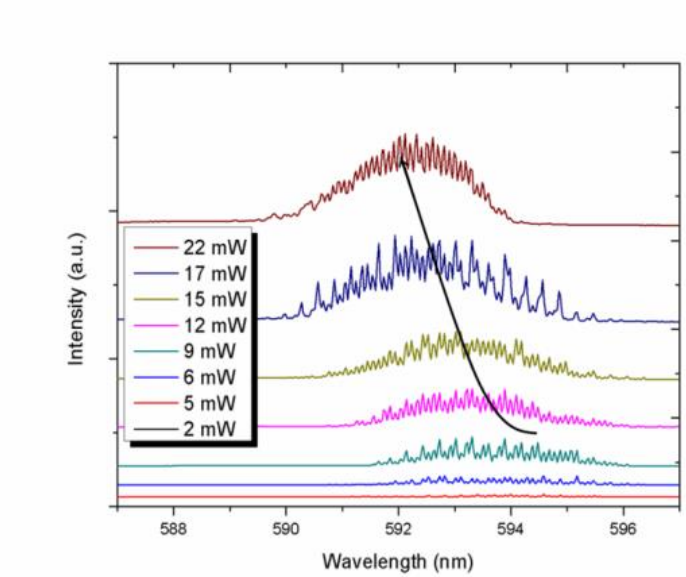

Figure 2.8 The graph illustrates the lasing intensities of Rh B dye (5 X 10^{-4} mol/dm^3) dissolved in butanol at different pump powers. The spectrum moves towards shorter wavelengths with growing pump power.

2.7.3 Resonant condition

In our lasing experiment, external feedback at the cuvette sides might have encouraged the lasing action. It was expected that both the stimulated emission along with the gain guiding and the external feedback at the cuvette sides would induce a high gain for the laser action. The occurrence of mode structure in the emission from dye solution was also reported by Guang *et al.*,

where the laser emission was attributed to the Fresnel reflection feedback from the two parallel optical windows of the cuvette [23]. Thus the partial reflectance from the window of the cuvette produces the effect of a Fabry-Perot etalon and provides the optical feedback necessary for laser emission. In this case four subcavities are involved for cavity lasing; the cavity lasing wavelength should fulfil the following resonant conditions

$$\left.\begin{aligned} \mathbf{2[nL + n'(l_1 + l_2)] = K_1\lambda}, \\ \mathbf{2nL = K_2\lambda}, \\ \mathbf{2(nL + n'l_2) = K_3\lambda}, \\ \boldsymbol{2(nL + n'l_1) = K_4\lambda}, \end{aligned}\right\} \qquad \mathbf{2.2}$$

where L is the length of the medium, n' is the refractive index (RI) of quartz, l_1 and l_2 are the thickness of the cuvette, n is the RI of the gain medium and K_1, K_2, K_3 and K_4 are arbitrary integers. The schematic of quartz with its possible resonant condition is shown in fig 2.9.

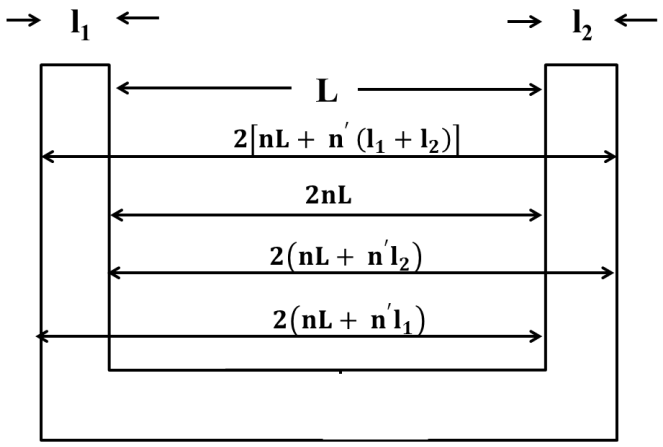

Figure 2.9 Schematic of quartz cuvette with its resonant condition.

The resonance condition providing the shortest spectral periodicity is obtained by the subtraction of the condition 1 and 3 of equation 2.2, which results

$$\boldsymbol{2n'l_1 = K\lambda}, \qquad \mathbf{2.2}$$

where K = K_1-K_3.The above equation is equivalent to the maximum transmission condition of the a Fabry-Perot etalon with an equivalent optical

thickness of $n'l_1$. This implies that the cavity lasing spectrum will be modulated by this equivalent Fabry–Perot etalon which provides the optical feedback necessary for laser emission. For the lasing spectrum the wavelength spacing between two adjacent modes is given by

$$\Delta\lambda = {\lambda^2}/{2n'l_1} \qquad 2.4$$

where λ is the average lasing wavelength. Substituting for refractive index of quartz, n' as 1.46, the average lasing wavelength λ as 593 nm and the Δλ obtained from our studies with a cuvette of 1 cm path length is 0.09 nm. The thickness of the first parallel window is measured as ~1.1 ± 0.03 mm. The estimated value of l_1 is found to be 1.15 mm at different position of the cuvette, which is in close agreement with the observed value.

2.7.4 Tuning of laser emission

The dye medium is found to be sensitive to the polarity and refractive index (RI) of the solvent in its nature of laser emission. The interaction between the solvents and the dye molecules affects the energy difference between the ground state and excited states. This energy difference is described by the Lippert equation. Most of the laser dyes are polar in nature and excitation into their low lying excited singlet state will be accompanied by an increase in the dipole moment. Hence the solvent polarity has a decisive role in shifting the laser wavelengths. In most of the cases, increasing the solvent polarity will shift the gain curve towards the longer wavelength side which is known as Stokes shift [24]. The emission spectra are recorded for different solvents such as Ethanol, Butanol, and Glycerol at a fixed dye concentration of 5×10^{-4} mol/dm^3 and are shown in figure 2.9. All the experimental conditions remained the same throughout the investigations at an ambient temperature of 21° C. The result shows a correlation between the physical characteristics such as RI, polarity of the different solvents and the

multimode laser emission from the cavity. From the figure 2.9 one could observe that the change in solvents introduces a corresponding shift in emission spectra. From ethanol to butanol the shift is approximately 4 nm, and from ethanol to glycerol the shift is approximately 6 nm. These types of shift in the emission spectrum with change in the solvent will allow a limited range of tuning of emission wavelengths. However, the spectral width and spacing between the adjacent lasing modes does not depend on the nature of the solvents but it mainly depends on the structure of the cavity.

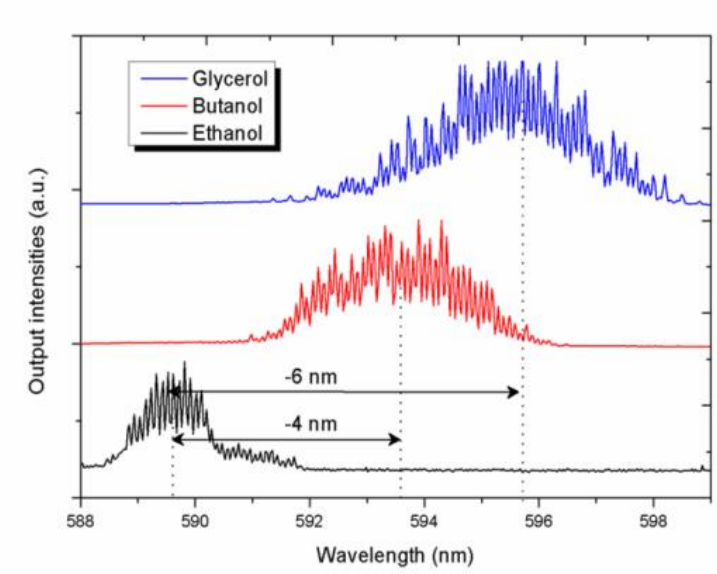

Figure 2.10 Three measured laser spectra using Rh B dissolved (5 X 10^{-4} mol/dm^3) in ethanol, butanol and glycerol as the active gain medium at a pump power of 15 mW. The change of solvent introduces an over-all shift of the output spectra due to a shift of the gain-spectrum of the dissolved laser dye.

For a detailed analysis of the effect of solvent in the lasing characteristics of Rh B laser dye, the dye is also dissolved in different solvents such as methanol, toluene and ethylene glycol at a fixed dye concentration of 5 X 10^{-4} mol/dm^3. Interesting results were obtained and these showed that the shift in emission spectrum not only depends upon the value of RI and polarity of solvents but also on the lower threshold population inversion [10] given by the

solvent molecules. For the non-polar solvents like toluene, a deviation is observed from the polar and dipole aprotic solvents. This is due to the fact that toluene has a comparatively lower quantum yield as compared to other solvents and also the high RI, which is almost higher than the quartz cuvette. Hence the reflection coefficient of the surface is also important for the lasing characteristics. Table 2.4 summarizes peak wavelength and number of lasing modes of Rh B dye dissolved in various solvents. From the table the laser emission is observed to be red-shifted in Ethylene Glycol solution which is less polar and has lower RI as compared to Glycerol. This may be attributed to the more viscous nature of Glycerol, which may reduce the molecule interaction between dye and solvent molecules. The increased interaction between the dye molecules and the fluorescent light will result the shifting of emission wavelength toward the longer wavelength region. From this we can also conclude that the laser emission from the dye solution not only depends on the RI and polarity of the solvent but also on the other nature of solvents such as viscosity and higher quantum efficiency or lower cavity loss of the solvents.

Table 2.4. Comparison of emission peak and number of longitudinal resonant modes for different solvents.

Solvent name	Emission peak (nm)	Number of lasing modes
Methanol	590	26
Ethanol	591	24
Butanol	594	42
Ethylene Glycol	598	46
Glycerol	596	62
Toluene	585	(Only ASE)

2.7.5 Modulation of lasing

A typical lasing spectrum from Rh B dissolved in methanol is shown in figure 2.10. The lasing peaks were considerably modulated as a clustered pattern. The resonance condition providing the widest spectral periodicity is obtained by the subtraction of the last two conditions of equation 2.2, which results,

$$\boldsymbol{2n'\,(l_2 - l_1) = K\lambda,} \qquad \textbf{2.5}$$

where K = (K_3 –K_4). From equation 2.6 the modulation period can be determined by,

$$\boldsymbol{\delta\lambda = \frac{\lambda^2}{2n'(l_2 - l_1)}}, \qquad \textbf{2.6}$$

From the equation we can observe that the modulation period is inversely proportional to the difference in the wall thickness $(l_2 - l_1)$ of the cuvette. The measured mode spacing $\delta\lambda$ is ~ 1.2 nm which is in good agreement with the calculated value of mode spacing (~ 1.19 nm), where $(l_2 - l_1)$ is estimated as 100 µm.

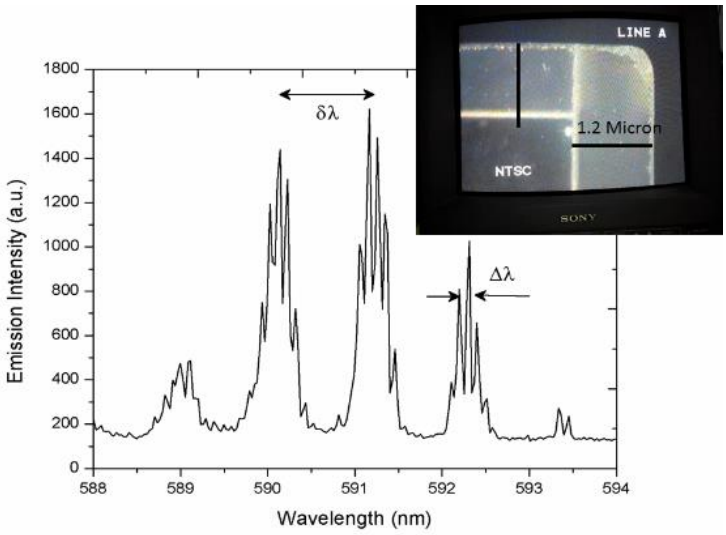

Figure 2.11 Resonant modulation of laser modes of Rh B dye dissolved in methanol at a pump power of 15 mW. Inset shows the enlarged view of the variation in the thickness of the two walls of the cuvette.

The photograph of the CCD image taken for two walls of a cuvette is given in figure 2.10 inset, which clearly indicates the change in thickness of the different walls of the cuvette. The obtained laser emission spectra are modulated by the superposition of the laser modes due to optical thickness of $n'l_1$ and difference in the wall thickness $n'(l_2 - l_1)$ as shown in figure 2.10. We therefore attribute the appearance of emission spectra to a resonant modulation of the two type of laser resonant modes within the cavity.

2.8 Gain Coefficient

The net gain of the dye doped laser system was generally measured by the variable stripe length (VSL) method. An adjustable slit was used to select the central portion and vary the width of the pump beam. The output intensity is given by,

$$\boldsymbol{I(\lambda) = \frac{\eta g'(\lambda)}{g(\lambda)} \left(e^{g(\lambda)l} - 1\right)} \qquad \textbf{2.7}$$

where g(λ) (=g'(λ)-α, α is the loss coefficient) is the net gain coefficient, g'(λ) is the internal gain coefficient due to stimulated emission process and l is the length of the pumped stripe. The value of the gain can be determined by plotting the emission intensity as a function of pumped stripe length and fitting the resulting curve to the expected dependence given by the equation 2.7. The systematic measurements of the intensity of the emitted light as a function of stripe length for three different pump powers 3 mW, 15 mW and 20 mW have been shown in figure 2.11.

The black line in figure 2.11 is a fit to the data given by equation 2.7, which yields a net gain of 7.2 cm^{-1} at a pump power of 3 mW (<P_{th}). Above P_{th}, the measured gain is 34 cm^{-1} and 42.1 cm^{-1} by fitting the data using blue and red line for 15 and 20 mW respectively. In the equation 2.7, we have not considered the gain saturation and thus the net gain coefficient represents the subsets of data for which gain saturation is not evident.

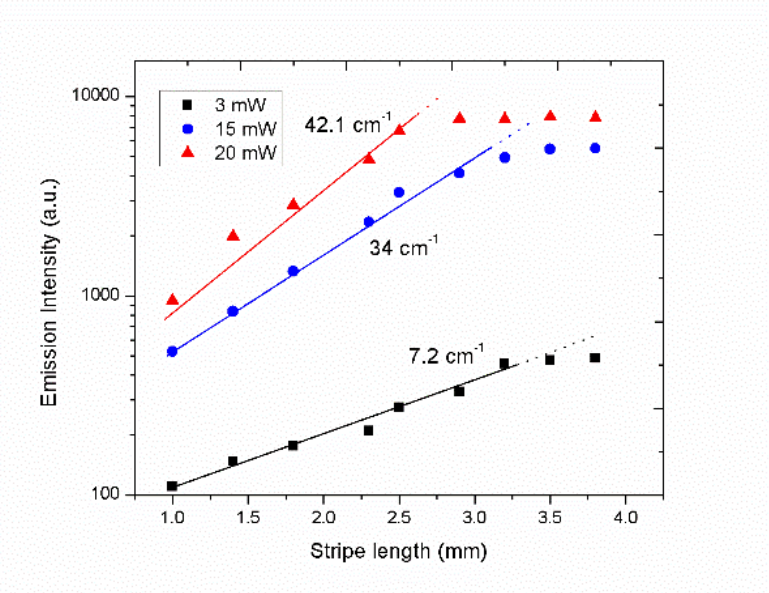

Figure 2.12. Dependence of the emission intensity on stripe length at three different pump powers (3, 5, 20 mW) for dye dissolved in butanol. The solid lines are fits to the data using equation 2.7.

2.9 Stimulated emission cross-section

Another important optical quantity used to characterize a laser medium is stimulated emission cross-section (σ_e). The value of σ_e can be derived from the emission spectrum E(λ), which is by

$$\boldsymbol{\sigma_e = \frac{\lambda^4 E(\lambda)}{8\pi c \tau m^4}} \qquad \textbf{2.8}$$

where c is the speed of light in free space, m is the refractive index of the medium (solvent), τ is the fluorescent life time and it is assumed to be 2 ns. From the equation 2.8, we could obtain the value of $\sigma_e \sim 8 \times 10^{-18}$ cm^{-1}.

2.10 Conclusions

In this chapter we provide a detailed discussion of the photophysical and lasing studies of Rhodamine B laser dye dissolved in various solvents. Changing solvent will allow a shift in the emission wavelength which will in turn provides a limited range of tuning of emission wavelength. The amount of shift in emission wavelength depends on the different physical property of the

solvents, such as polarity, refractive index, viscosity etc. The solvatochromic and Stokes-shift of Rh B in various solvents were successfully compared to experimental data with computational data using DFT/TD-DFT/PCM methodologies. Upon optical excitation, the laser modes are found to originate from the subcavities formed by the plane parallel walls of the cuvette containing the gain medium. In our study we also determined the gain coefficient and stimulated emission cross-section of the Rh B dye laser system. The dye dissolved in methanol solution also provides a modulated laser emission due to two sets of laser resonance achieved by the difference in the wall thickness of the cuvette.

References

1. Frank L. Pedrotti and Leno S. Pedrotti. “Introduction to Optics”. Patience Hall International, Second edition, (1996).
2. F. P. Schafer (Editor). “Dye Lasers”. Springer-Verlag, (1973).
3. P. Boutin, J. Ow and U. Wiesner, “Fluorescent core–shell silica nanoparticles: towards “Lab on a Particle” architectures for nanobiotechnology”, Chem. Soc. Rev., 35, 1028, (2006).
4. E. Rampazzo, S. Bonacchi, M. Montalti, L. Prodi and N. Zaccheroni, “Self-Organizing Core−Shell Nanostructures: Spontaneous Accumulation of Dye in the Core of Doped Silica Nanoparticles”, J. Am. Chem. Soc., 129, 14251-14256, (2007).
5. A. Burns, J. Vider, H. Ow, E. Herz, O. Penate-Medina, M. Baugmgart, S. M. Larson, U. Wiesner and M. Bradbury, “Fluorescent Silica Nanoparticles with Efficient Urinary Excretion for Nanomedicine”, Nano Lett., 9, 442-448, (2009).
6. J. E. Fuller, G. T. Zugates, L. S. Ferreira, H. S. Ow, N. N. Nguyen, U. B. Wiesner and R. S. Langer, “Intracellular delivery of core–shell fluorescent silica nanoparticles”, Biomaterials, 29, 1526-1532, (2008).
7. F. P. Schafer, “Dye lasers”, Springer, Volume 1 of series Topics in applied physics, p.p 1-89, (1990).
8. Marika Savarese, Anna Aliberti, Ilaria De Santo, Edmndo Battista, Filippo Causa, Paolo A. Netti and Nadia Rega, “Fluorescent Lifetimes and Quantum Yields of Rhodamine Derivarives: New Insights from Theory and Experiment”, J. Phys. Chem. A, 116, 7491-7497 (2012).

9. M. Gersborg-Hansen, S. Balslev, N. A. Mortensen, A. Kristensen, "A coupled cavity micro-fluidic dye ring laser", Microelectronic Engineering 78-79, 185-189, (2005).

10. O. G Pereson, J. P.Webb, and W.C. Mc Colgin, "Organic dye laser threshold", J. Appl. Phys. 42 (5); 1917-1928, (1971).

11. Gaussian 09, Revision **D.01**, Frisch, M. J.; Trucks, G. W.; Schlegel, H. B.; Scuseria, G. E.; Robb, M. A.; Cheeseman, J. R.; Scalmani, G.; Barone, V.; Mennucci, B.; Petersson, G. A.; Nakatsuji, H.; Caricato, M.; Li, X.; Hratchian, H. P.; Izmaylov, A. F.; Bloino, J.; Zheng, G.; Sonnenberg, J. L.; Hada, M.; Ehara, M.; Toyota, K.; Fukuda, R.; Hasegawa, J.; Ishida, M.; Nakajima, T.; Honda, Y.; Kitao, O.; Nakai, H.; Vreven, T.; Montgomery, J. A., Jr.; Peralta, J. E.; Ogliaro, F.; Bearpark, M.; Heyd, J. J.; Brothers, E.; Kudin, K. N.; Staroverov, V. N.; Kobayashi, R.; Normand, J.; Raghavachari, K.; Rendell, A.; Burant, J. C.; Iyengar, S. S.; Tomasi, J.; Cossi, M.; Rega, N.; Millam, J. M.; Klene, M.; Knox, J. E.; Cross, J. B.; Bakken, V.; Adamo, C.; Jaramillo, J.; Gomperts, R.; Stratmann, R. E.; Yazyev, O.; Austin, A. J.; Cammi, R.; Pomelli, C.; Ochterski, J. W.; Martin, R. L.; Morokuma, K.; Zakrzewski, V. G.; Voth, G. A.; Salvador, P.; Dannenberg, J. J.; Dapprich, S.; Daniels, A. D.; Farkas, Ö.; Foresman, J. B.; Ortiz, J. V.; Cioslowski, J.; Fox, D. J. Gaussian, Inc., Wallingford CT, (2009).

12. R. G. Parr and W. Yang, "Density-functional theory of atoms and molecules", Oxford Univ. Press, Oxford, (1989).

13. A. D. Becke, "Density-functional thermochemistry. III. The role of exact exchange", J. Chem. Phys. 98, 5648−5652, (1993).

14. P. J. Stephens, F. J. Devlin, C. F Chabalowski, M. J. Frisch, "Ab initio calculation of vibrational absorption and circular dichroism spectra using density functional force fields", J. Phys. Chem. 98, 11623−11627, (1994).

15. V. Barone and M. Cossi, "Quantum calculation of molecular energies and energy gradients in solution by a conductor solvent model," J. Phys. Chem. A, 102, 1995-2001 (1998).

16. F. P Schafer.; "Dye lasers; topics in applied physics 1", 3rd Edn. Springer, Heidelberg (1990).

17. G. D. Peng, Z. Xiong, P. L. Chu, "Fluorescence decay and recovery in organic dye-doped polymer optical fibers", Journal of Lightwave Technol. 16, 2365-2372, (1998).

18. A. Tagaya, Y. Koike, E. Nichei, S. Teramoto, K. Fujii, T. Yamamoto, K. Sasaki, "Basic performance of an organic dye-doped polymer optical fiber amplifier", Appl. Opt., 34, 988-992, (1995).

19. D. S. Weirsma, M. P. Van Albada, and A. Lagendijk, "Random laser?", Nature (London) 373, 203, (1995).

20. Jaison Peter, Rasool Saleem, Ananthu Sebastian, P. Radhakrishnan, V. P. N. Nampoori, C. P. Girijavallabhan, M. Kailasnath, "Pumping scheme dependent

multimode laser emission from free-standing cylindrical microcavity", Optics Communications 320, 125-128 (2014).

21. Jaison Peter, C P G Vallabhan, P Radhakrishnan, V P N Nampoori and M Kailasnath, "Microring lasing from a dye-doped polymer-coated silica fiber", Laser Phys. 23 115104 (3pp), (2013).
22. Jaison Peter, P. Radhakrishnan, V. P. N. Nampoori, M. Kailasnath, "Multimode laser emission from free standing cylindrical microcavity", Journal of Luminescence 149, 204-207 (2014).
23. Guang S. He, Raffaella Signorini, and Paras N. Prasad, "Two-photon-pumped frequency-upconverted blue lasing in Coumarin dye solution", Appl. Opt. Vol. 37, No. 24, 20 August (1998).
24. Ritty J. Nedumpara, Thomas K. J., Jayasree V. K., C. P. Girijavallabhan, V. P. N. Nampoori and P. Radhakrishnan, "Study of solvent effect in laser emission from Coumarin 540 dye solution", Appl. Opt. Vol. 46, No. 21, (2007).

Supporting information from the computational data

Ethanol

Excited State 1: Singlet-A 2.3018 eV 538.65 nm f=1.1666 <S**2>=0.000
127 ->128 0.70556
This state for optimization and/or second-order correction.
Total Energy, E(TD-HF/TD-KS) = -1881.06720673
Copying the excited state density for this state as the 1-particle RhoCI density.
Excited State 2: Singlet-A 2.9040 eV 426.94 nm f=0.0466 <S**2>=0.000
122 ->128 -0.15299
126 ->128 0.67817
Excited State 3: Singlet-A 3.3188 eV 373.58 nm f=0.0165 <S**2>=0.000
123 ->128 0.11108
125 ->128 0.69264

Methanol

Excited State 1: Singlet-A 2.2967 eV 539.84 nm f=1.1725 <S**2>=0.000
127 ->128 0.70557
This state for optimization and/or second-order correction.
Total Energy, E(TD-HF/TD-KS) = -1881.06825969
Copying the excited state density for this state as the 1-particle RhoCI density.
Excited State 2: Singlet-A 2.9020 eV 427.24 nm f=0.0464 <S**2>=0.000
122 ->128 -0.13151
123 ->128 -0.12255
126 ->128 0.67846
Excited State 3: Singlet-A 3.3551 eV 369.54 nm f=0.0623 <S**2>=0.000
122 ->128 -0.10262
123 ->128 -0.22352
124 ->128 0.11430
125 ->128 0.64617

Butanol

Excitation energies and oscillator strengths:
Excited State 1: Singlet-A 2.3108 eV 536.54 nm f=1.1558 <S**2>=0.000
127 ->128 0.70555
This state for optimization and/or second-order correction.
Total Energy, E(TD-HF/TD-KS) = -1881.06530285
Copying the excited state density for this state as the 1-particle RhoCI density.
Excited State 2: Singlet-A 2.9074 eV 426.44 nm f=0.0469 <S**2>=0.000
122 ->128 -0.16965
126 ->128 0.67760
Excited State 3: Singlet-A 3.2491 eV 381.60 nm f=0.0048 <S**2>=0.000
125 ->128 0.70233

Chapter 3
Fabrication and Characterization of Different types of Dye doped Polymer optical fibers

"Discovery consists of seeing what everybody has been seen and thinking what nobody has thought"

Albert von Szent-Gyorgy

Abstract

This chapter discusses in detail about the various fabrication techniques of dye doped polymer optical fibers, such as step index, graded index and hollow fiber. This chapter also gives the details of the optical characterization of different types of dye doped POFs drawn under different initial conditions like, draw rate, feed rate and temperature. Cut back method and Side Illumination Fluorescence (SIF) technique have been employed to characterize the drawn fiber. Detailed measurements were made to understand the amplified spontaneous emission (ASE) and photo degradation phenomena in these POF systems. Measurements of peak emission wavelength, optimum length, line-width and half-life of Rh6G doped hollow, GI and SI POFs are included in this chapter.

---

*The major content of this chapter has been published in the journal "**Optics and Laser Technology**, 63, 34-38 (2014).*

3.1 Introduction

Liquid dye lasers are coherent sources of radiation with advantages such as wide tuning range, high output power, high pulse energy and wide choice of pumping sources [1]. The first solid-state dye laser were reported by Soffer and Mcfarland [2] and then Peterson and Snavely [3] in the late 1960s. From the early days of development of dye lasers, attempts were made to overcome the problems posed by organic solvents by incorporating the dye molecules into solid matrices [1]. They demonstrated stimulated emission from polymeric matrices doped with organic dyes. Solid-state dye lasers avoid the problems of toxicity [4-8], volatile and flammability, present a low cost gain medium, and are compact and easy to operate and maintain [4]. Their application range over spectroscopy, communications, atmospheric sensing, medical treatment and so on. Various classes of materials like porous glasses, organically modified silicates, sol-gel materials and polymers were extensively studied as host materials for laser dyes because of their optical properties and commercial viability [9]. In addition to low cost and tunability, the configurability and potential for minimal size of solid-state dye doped material would be advantageous in integrated optics application [10].

Polymer optical fibers (POFs) have attracted much attention during the past two decades for short distance communication because of their unique characteristics, such as flexibility, ease of handling, and relative low costs in coupling [11]. POFs have the potential to be used in optical logic-devices such as optical switches and amplifiers because of fiber waveguide geometry, which is compatible with silica glass fiber; low production cost and wide range of available materials that can be incorporated into the fiber core [12]. Properties like attenuation due to microbends, sensitivity to temperature and humidity of POFs can be effectively utilized for sensor applications [13].

Polymeric matrices have some advantages over other hosts materials because they have better chemical compatibility with organic dyes and inexpensive and simple fabrication technique, although they suffer from relatively poor thermal conductivities as well as lower laser radiational damage thresholds [10]. PMMA is one of the most commonly used polymeric hosts, which shows higher optical homogeneity and transparency in the visible region of electromagnetic spectra [1]. The high optical homogeneity of this active medium is extremely important for narrow linewidth oscillators and for single mode generation [14]. Most of the work on solid-state dye lasers have been elaborated with dyes emitting in the yellow and red region of the spectrum, such as the well-known Rhodamine 6G (Rh6G). Rh6G, the best known of all laser dyes, has been frequently investigated in solid-state dye lasers in a variety of solid hosts, on account of its high fluorescence quantum yield, low intersystem crossing rate and low excited state absorption at both pump and lasing wavelength [15]. Organic luminescent dyes dissolved in polymers as potential source of light amplifying media are still very attractive materials for fabrication of tunable lasers with high gain and lifetime due to easy processing, low cost and wide spectral range [16].

This chapter deals with the fabrication of different types of dye doped polymer fibers as well as their characterization. The properties of dye doped polymer fibers should be clearly known before they are used for all optical devices. Improvement in the performance of this device requires a thorough knowledge of the optical absorption and emission characteristics. The loss characterisation was done by cut-back method and non- destructive side illumination fluorescence technique.

3.2 Fabrication techniques for different types of POFs

3.2.1 Purification of the monomer

The base material used for the fabrication of polymer fiber is methyl methacrylate (MMA), which is a monomer. Purification of the monomers is an important step in the fabrication of preforms. The impurities present in the monomers can cause high loss for the fiber. The more pure the polymer, better light guidance through the fiber.

(a) Removing Inhibitor

Usually, the monomer can contain impurities like metal ions, solvents etc. which can be purified through distillation. Moreover the received monomers contain 'hydroquinone derivatives' as inhibitors to prevent polymerization during transport and storage.

To remove the inhibitor from the monomer, the liquid monomer is washed with 5% sodium hydroxide (NaOH) solution taking both in equal volumes. The pure MMA and the inhibitor reacted with NaOH forms two separate layers and the monomer can be separated. This process was repeated seven times. Then the purified monomer was also washed seven times with distilled water to remove the remaining NaOH contents from it. Then, calcium chloride ($CaCl_2$) is added to MMA and kept for one day in order to remove the water content (OH^- impurity). Then the monomer is purified by vacuum distillation under reduced pressure.

(b) Monomer distillation

Figure 3.1 shows the distillation set up. The distillation is done under modest vacuum conditions in order to lower the boiling temperature of the solution to safer levels. The boiling point scales with the pressure, so less heat is required for high vacuum. The boiling point of MMA is 101 °C. The vacuum pump used to create the vacuum conditions is a standard oil sealed

rotary pump. High vacuum conditions such as the highest attainable with the pump used are actually undesirable, as much of the volatile MMA would simply evaporate and be sucked into the vacuum lines. Even under low vacuum conditions, a cold trap should be placed between the distillation apparatus and the vacuum pump. The condenser allows cold water to flow through an outer region which is adjacent to the inner distillation region. The flowing water cools the vapour more quickly than air. Finally the distilled MMA is collected in a glass flask.

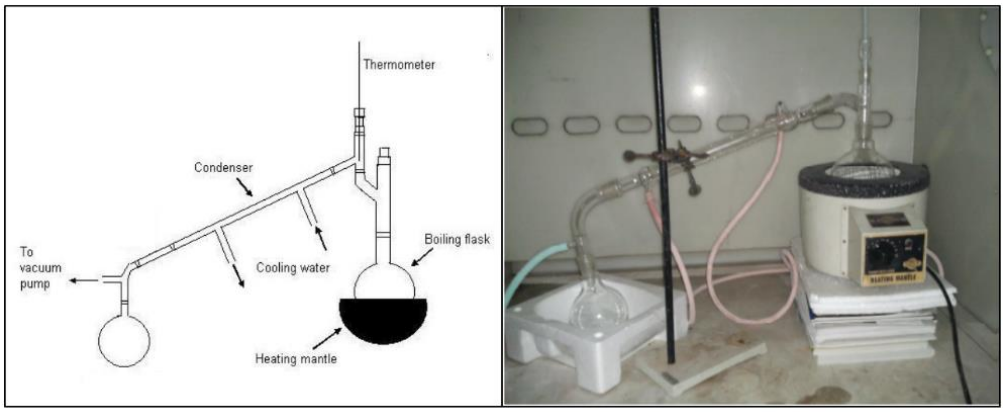

Figure 3.1 Schematic and photograph of MMA distillation set up

3.2.2 Polymerisation process

Polymerisation requires an initiator (which starts the polymerisation process) and a chain transfer agent (which limits the chain lengths of the polymer formed) to be added to the monomer. In this work, we are using benzoyl peroxide (BPO) (C4H10O14) as the initiator and n-butyl mercaptan (C4H10S) as the chain transfer agent. The bond between the two oxygens in the peroxide is very weak and benzoyl peroxide readily undergoes homolysis (symmetrical scission), forming free radicals whose half-life decreases with increase in temperature. The half-life is 1 hour at 92 °C and 1 minute at 131 °C.

$$[C_6H_5C(O)]_2O_2 \rightarrow 2C_6H_5CO_2{}^*$$

The symbol * indicates that the products are radicals, i.e., they contain at least one unpaired electron. Such species are highly reactive. The homolysis is usually induced by heating. Since the two radicals of the peroxide are highly chemically active, each one bonds to one side of a monomer molecule and opens a chemically active site on the other side of the monomer molecule. This site then bonds to a second monomer molecule to begin chain formation and is followed by sequential chain growth until the process is terminated by encountering a molecule of the chain transfer agent. The growing polymer chain end radical abstracts the H atom from the mercaptan along with one of the electrons in the S-H bond of the mercaptan. This terminates the growing chain with a hydrogen atom as shown in figure 3.2. Therefore, the average chain length of the polymer is determined by the chain transfer agent concentration. For the polymer to have the molecular weight suitable for drawing, it is important to control the average chain length during polymerisation. If the chain length is too short, the resulting fiber is brittle and cracks upon handling. If the chain length is too long, the polymer does not flow even at temperature beyond the polymer melting temperature.

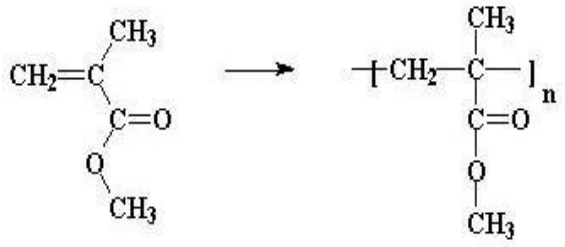

Figure 3.2 Polymerisation of methyl methacrylate to get poly-methyl methacrylate.

About 15 ml of monomer is taken in the test tube and 0.01% weight of BPO and 0.06M mercaptan are added, which were placed in an ultrasonic bath in order to mix the BPO and CTA in MMA. The test tube containing the monomer, initiator and chain transfer agent is put in oil bath (filled with

silicone oil) at 70° C for 3 days as shown in figure 3.3. Silicone oil is a water clear silicone fluid in a wide viscosity range. The following properties make silicone oil a suitable candidate for its use in oil bath.

- Little change in physical properties over a wide temperature range.
- The fluid can be used from -400 °C to 2800 °C.
- Excellent water repellences.
- Low toxicity.
- Inertness.

Figure 3.3 Photograph of oil bath

After polymerisation, the test tube is taken, allowed to cool and broken in order to get the preform. Then it is placed in an oven at 110 °C for 24 hours for the complete polymerization.

3.2.3 Optimization of PMMA composition

There are many factors which affect the processability of a polymer. The molecular weight and molecular weight distribution play an important role in this regard. It has already been proved by researchers that, for the good drawability of a preform, a molecular weight (Mw) between 60,000 to 1,00,000 is preferred and the molecular weight distribution should be narrow.

The chemistry of polymer synthesis, including the amount and type of initiator and chain transfer agent, can control the molecular weight and molecular weight distribution of the polymer formed. Thus, the initial trials were focused on the determination of a definite composition of MMA/initiator/chain transfer agent for the better drawability of preforms.

In this work, a peroxide type initiator (BPO) and chain transfer agents (CTA) were used in different amounts. The CTA were mercaptan (thiols), 1-butane thiol and dodecane thiol, as the mercaptans have a better chain transfer constant for MMA polymerization than any other chemical species.

3.2.4 Step index fibers

A step index (SI) fiber has a simple structure owing to its simpler fabrication techniques. The monomer mixed with the initiator, dye, and chain transfer agent is poured into a glass test tube of the required diameter and length. The uniform mixing of the dye-monomer mixture was ensured by stirring well with a magnetic stirrer and filtered using filter paper to ensure that no undissolved part remained. This was then kept in a constant temperature bath at 70 °C for 48 h, at 90 °C for 18 h, and at 105°C in an air furnace for 8 h. These steps led to a high quality polymer preform that could be used for drawing the fiber. The detailed fabrication technique of SI fiber has been furnished by Rajesh *et al.* [17].

3.2.5 Hollow Fiber

"Teflon technique" [18-20] is the most successful technique for the fabrication of the preform. In this technique a thin Teflon string is properly fixed at the centre of a glass tube. The thermal polymerization of the filled tube is carried out in a temperature controlled oil bath. After the monomers are fully polymerized and heat treated, the Teflon string is removed and we obtain a polymer tube (polymer rod with a small hole at its centre).

The advantages of using the Teflon technique in the fabrication of polymer preform are: a) its non-sticking property allows the string to be easily removed b) it has a very good chemical and thermal stability c) it gives smooth finish for the inner surface of the polymer tube. d) It gives good core-cladding interface and hence reduces the losses due to scattering.

3.2.6 Graded index fiber

To date, several methods have been suggested for the manufacture of GI-POFs. Although continuous extrusion is the dominant method for the manufacture of GI-POF as in the case of SI-POF, the preform method appears to be the preferred approach due to its versatility.

(a) Photo-copolymerization

The first GI POF was fabricated by Ohtsuka and Hatanaka in [21-22] 1976 by heat drawing graded index plastic rods. Graded index plastic rods were also made by two- step co-polymerization and photo- copolymerization techniques [23-27]. In two step co-polymerization, a polymerized rod is prepared and immersed into a co-monomer that has a lower refractive index. The co-monomer then diffuses into the rod to form a concentration gradient in the radial direction. This is subsequently fixed by further polymerization. To prevent the immersed rod from dissolving too much while allowing the co-monomer to diffuse inward, the pre-polymerised rod has a cross linked network structure. Conversely, a GI rod made by photo-copolymerization does not have a network structure, and can be heat drawn into POF.

Figure 3.4 shows schematic of the photo-co-polymerization apparatus by Ohtsuka *et al.* [25]. A 2.9 mm diameter glass tube reactor was positioned vertically in a constant temperature chamber and rotated about its vertical axis while being irradiated by UV radiation. The UV radiation quickly induces polymerization reaction forming a gel phase. Since the UV intensity was

higher near the wall of the glass tube, the gel phase formed first on the inner wall of the glass tube and grew inward towards the centre of the tube.

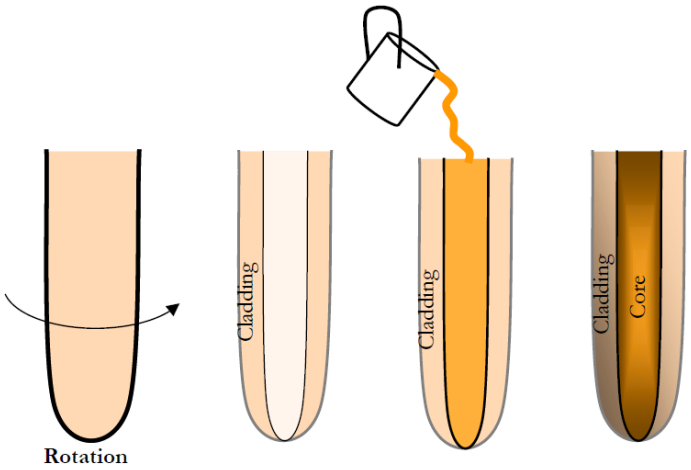

Figure 3.4 The steps involved in photo-copolymerization technique

(b) Interfacial gel polymerization

The best known method for the fabrication of GIPOF is the interfacial gel polymerization method which was pioneered by Koike and his co-workers [28-29]. At first, this method was applied to the co-polymerization of the monomer mixture with different reactivity ratios and different refractive indices. Later it was applied to mixtures of a monomer and a non-reacting organic dopant. In this method a transparent polymeric tube (e.g. PMMA) is prepared and this tube is then filled with a mixture of two monomers (e.g. methyl methacrylate and vinyl benzoate) that is polymerized thermally while the tube is rotated. The inner wall of the tube is swollen by the monomer mixture as it forms a thin gel phase. Due to "gel effect" the polymerization reaction is faster inside the gel phase than in the monomer bulk phase. Consequently, the reaction occurs preferentially on the inner surface of the tube and the co-polymer phase extends inward towards the centre of the tube

as reaction proceeds. Due to the difference in the reactivity ratios the composition of the copolymer changes gradually in the radial direction. If the monomer with higher reactivity ratio has a smaller refractive index than the other monomer, the preform will have a gradually increasing refractive index towards the centre. The refractive index profile obtained by this method depends on the relative ratios of monomer mixture.

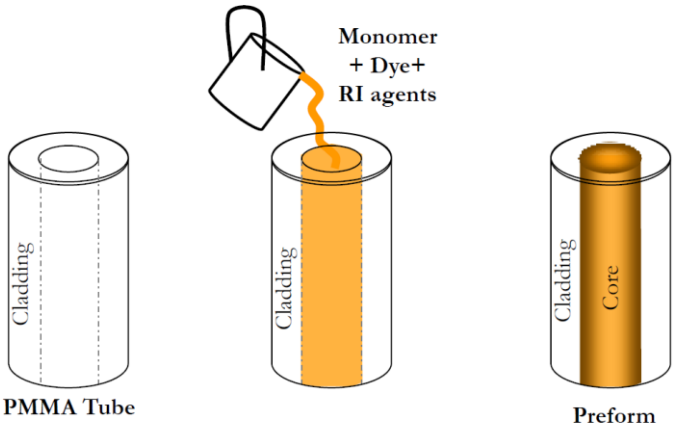

Figure 3.5 The different steps involved in the interfacial gel polymerization technique

3.2.7 Heat drawing process

The heat drawing process is shown schematically in figure 3.6. The tower is about 2.5 m high. There is a preform holder attached to the top of the tower. A stepper motor feeds the preform into the heating furnace. The heating furnace used here, has IR lamps for heating the preform. There are three IR lamps (Philips) 250W each, which can swing 180° in the clockwise and anticlockwise directions so that uniform heating of the preform is achieved. Figure 3.7 shows the heating furnace of the drawing tower.

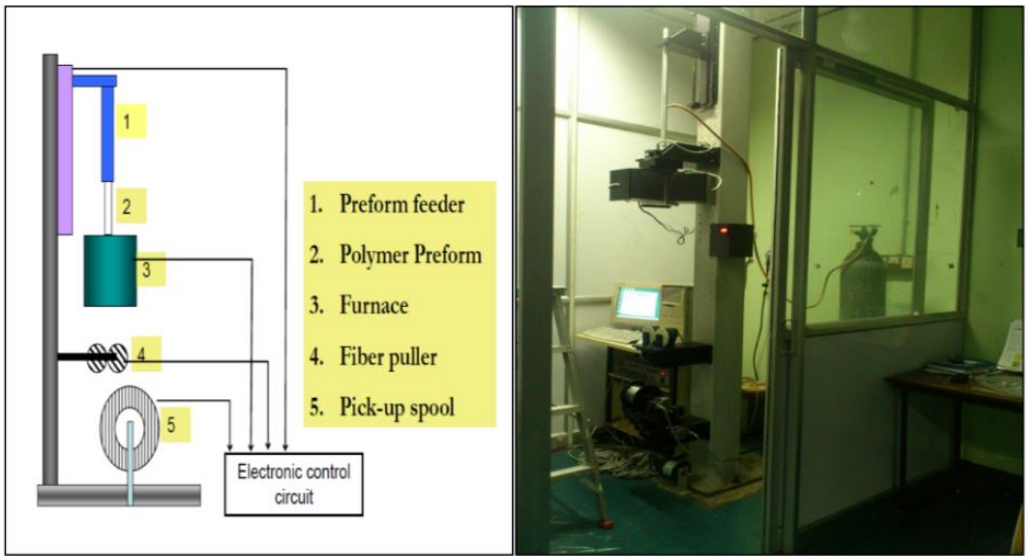

Figure 3.6 Schematic diagram and setup of heat drawing workstation

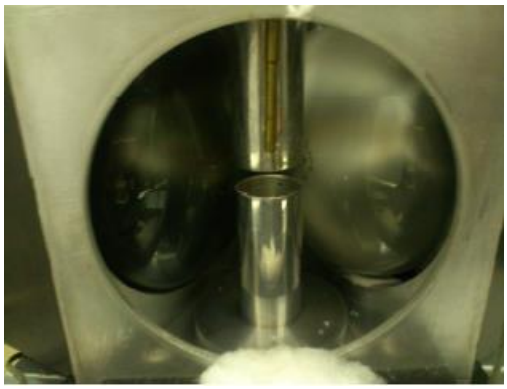

Figure 3.7 IR Lamp heating furnace

The heater temperature is controlled by means of a temperature controller which senses the temperature inside the furnace and compares it with the temperature set. The set temperature is maintained by continuously turning on and off the IR lamps by the temperature controller. The preform forms a neck-down region that starts at the hottest point in the preform and comes down due to gravity. There is a drawing capstan for pulling the fiber, which is controlled

by another stepper motor. Finally, the fiber is wound on a take up spool. The winding drum is moved in x and y directions by using two stepper motors so that the fiber is properly and evenly wound on it. The diameter of the fiber is controlled by varying the ratio of the feed rate of the preform and draw rate of the fiber. The diameter is calculated from mass conservation equation 3.1

$$\frac{D^2}{d^2} /= \frac{V_d}{V_f} \qquad \textbf{3.1}$$

where D is the diameter of the preform, d is the diameter of the fiber drawn, V_f is the preform feed rate and V_d is the fiber draw rate. The drawn fibers can be taken in a take up spool which is also controlled by an electronic circuit. The table 3.1 shows the results of final fiber diameter, which was drawn at different conditions.

Table 3.1 Result obtained under various drawing conditions

Preform type	**Temp (°C)**	**Feed rate (µ/s)**	**Draw rate (µ/s)**	**Heater rotaion speed (°/s)**	**Cal. Dia (µm)**	**Exp. Dia (µm)**
Solid (dia = 5 mm)	205	10	10000	6	500	557
Solid (dia = 5 mm)	210	5	10000	6	340	420
Hollow (ID=6 mm, OD=12 mm)	190	8	10000	5	520	500
Hollow (ID=6 mm, OD=12 mm)	185	6	10000	8	550	520

3.3 Fiber attenuation Measurement

Fiber attenuation measurement techniques have been developed in order to determine the total fiber attenuation and this is contributed by both absorption losses and scattering losses. The overall fiber attenuation is of great interest to the system designer but the relative magnitude of the different loss mechanisms is important in the development and fabrication of low loss fibers. Different methods can be employed for measuring attenuation: the insertion

loss method (non destructive) ,the substitution method (non destructive) and the cut –back method (destructive) . A commonly used standard technique for determining the total fiber attenuation per unit length is the cut- back or the differential method.

3.3.1 Cut back method

The cut- back method provides more accurate results than the insertion and substitution method. The advantage of this method lies in the fact that launching conditions remain unchanged. A schematic diagram of a typical experimental set up is shown in figure 3.8.

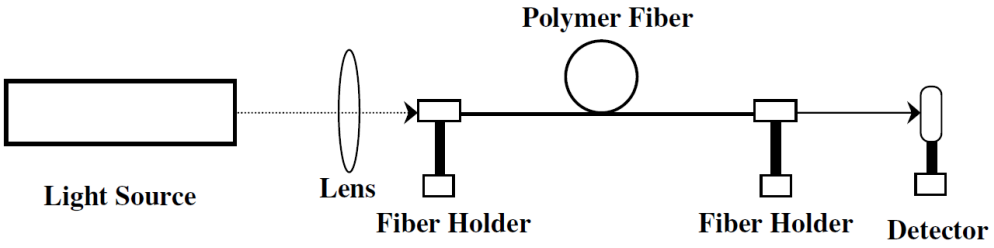

Figure 3.8 Fiber attenuation measurement using cutback method

Light beam from a DPSS laser (10 mW, 532 nm) is launched into the fiber with the help of a lens. After polishing the fiber end faces, the fiber is firmly held in a suitable holder such that only a small length projects outside with V groove made on a small horizontal steel platform. The incident beam is adjusted at the input end of the fiber so that maximum output power is obtained at the output end. The output power is measured with the help of a photo detector and let it be $P(L_1)$, where L_1 is the length of the test fiber. Without disturbing the launching conditions, a short length of the fiber from the output end is cut and polished. The output power is again measured and let it be $P(L_2)$ where L_2 is the cut back length of the fiber. The cutting, polishing

and measuring process is repeated several times. From these measurements the attenuation can be measured using the equation

$$\alpha_{dB} = \frac{10\, log(P(L_2)/P(L_1))}{(L_1 - L_2)} \qquad \textbf{3.2}$$

where L_1 and L_2 are the original and cut back fiber lengths respectively, and $P(L_1)$ and $P(L_2)$ are the corresponding output optical power from the original and cut back fiber lengths. The attenuation is usually expressed in decibel (dB). In this method incident intensity need not be measured. One of the important issues is that, it is almost impossible to measure with certainity how much light actually couples in to the fiber. First the input side of the fiber is left untouched during the whole measurement process so that the intensity coupled in to the fiber does not change between the two measurements. The best method for protecting the input coupler side is to use a long length of fiber so that the cutting and polishing process is as far away from the input end as possible. The loss spectrum of a typical poly (methyl methacrylate) fiber is given in figure 1.3 which shows that, the maximum attenuation occurs at 632 nm wavelength and minimum loss at 530, 570 and 650 nm, all in the visible range. Since loss is minimum around 532 nm, we have used a diode pumped solid state laser (DPSSL, 532nm) as light source for attenuation measurements.

Figure 3.9 Light propagation through drawn fiber

3.4 Side Illumination Fluorescence (SIF) Technique

Usually the propagation losses in fibers and planar waveguide structures are measured by the cut-back technique [30-31] which consists in comparing the transmittance of several fibers with different lengths at a specific wavelength. The disadvantage of the cut-back technique is that it is a destructive method. As an alternative to the above mentioned technique, a non-destructive side illumination fluorescence technique for measuring the optical attenuation in dye doped fibers has been developed by Kruhlak *et al.* [32-33].

3.4.1 Experimental setup

The main component of the experimental setup is the Rh6G (10^{-5} mol/litre) doped SI and GI and hollow POFs with a diameter of 500 micron, Nd: YAG laser (Quanta Ray DCRll) and a monochromator-CCD. The optical emission from the dye doped fiber was excited using 532 nm radiation from a frequency doubled pulsed Nd: YAG laser. The transverse pumping was done with the pump beam profile as a stripe obtained by employing a cylindrical

lens of appropriate focal length [32-34].The spectral emission characteristics and the gain studies were carried out by collecting the fluorescence from the doped fiber using a detector fiber coupled to a monochromator-CCD system. Figure 3.10 illustrates the experimental set up for side Illumination fluorescence technique.

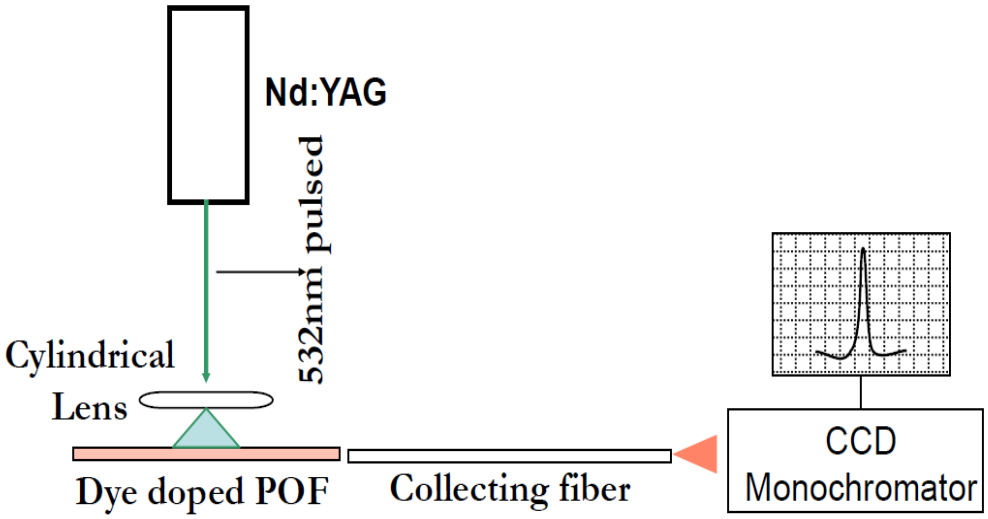

Figure 3.10 Experimental setup of SIF technique

Using interfacial-gel-polymerization technique, a dye doped graded index polymer fiber preform was fabricated. The photograph of different types of dye doped PMMA preforms are shown in figure 3.11. Figure 3.12 shows an enlarged cross sectional view of a hollow fiber using a CCD camera and the preform after the fiber drawn. The refractive index (RI) profile for different types of dye doped fibers is shown in figure 3.13.

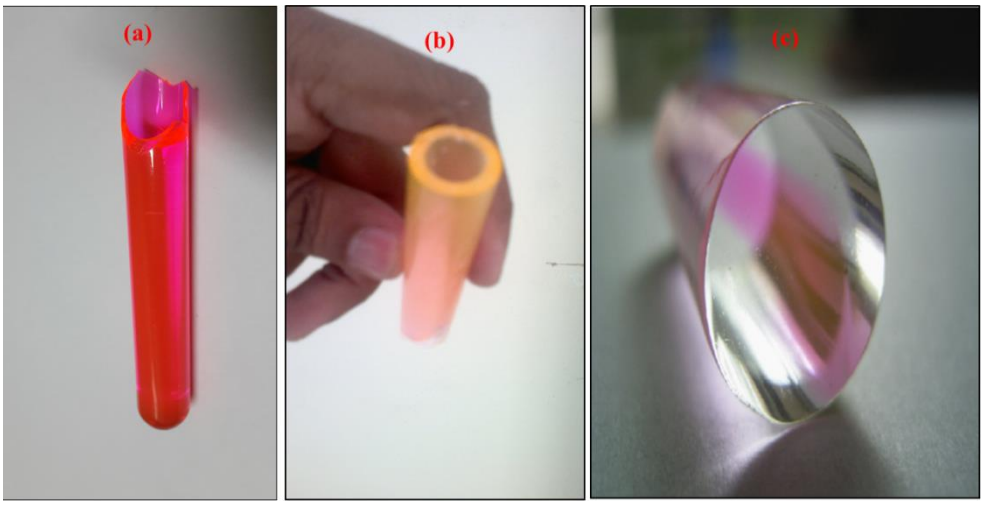

Figure 3.11 Different types of dye doped PMMA preforms (a) SI, (b) hollow and (c) GI respectively.

Figure 3.12 Dye doped PMMA preform after the fiber is drawn and enlarged cross sectional view of Rh6G-hollow POF using a CCD camera

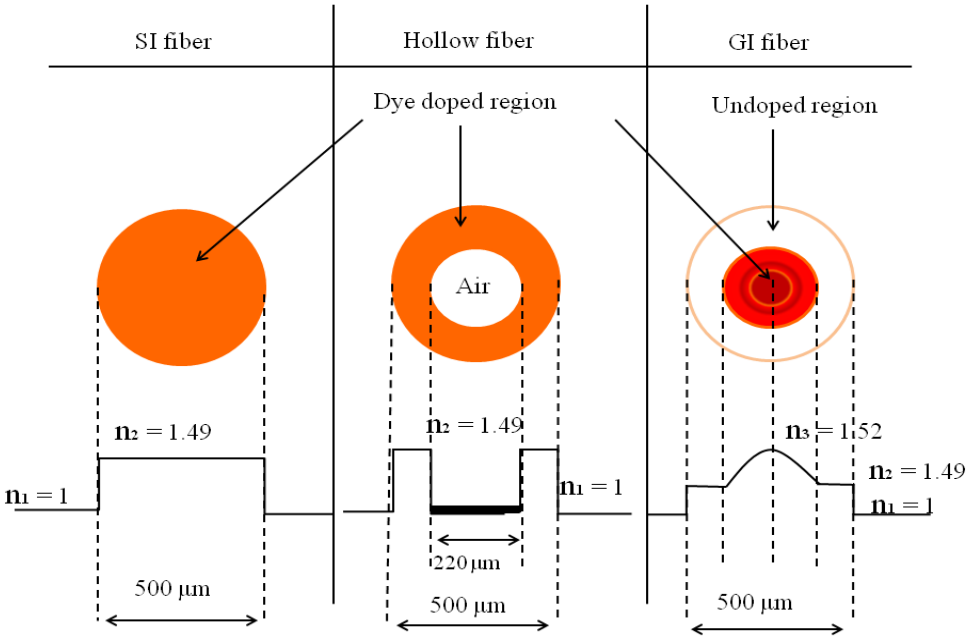

Figure 3.13 Refractive index of the different types of dye doped fibers

3.4.2 ASE and line narrowing

Fluorescence of dye doped POF is due to the absorption and re-emission mechanism taking place in the dye molecules [35]. Fluorescence emission spectra from Rh6G doped hollow POFs at various pump powers are depicted in figure 3.14. At low pump power (<10 mW), only fluorescence spectrum was observed. A clear line narrowing from 42 to 5 nm has been observed from 5 mW to 30 mW above which no further line sharpening was observed. Similar line narrowing has also been observed in dye doped SI and GI fiber. Spectral line narrowing as a function of pump power is the signature of light amplification.

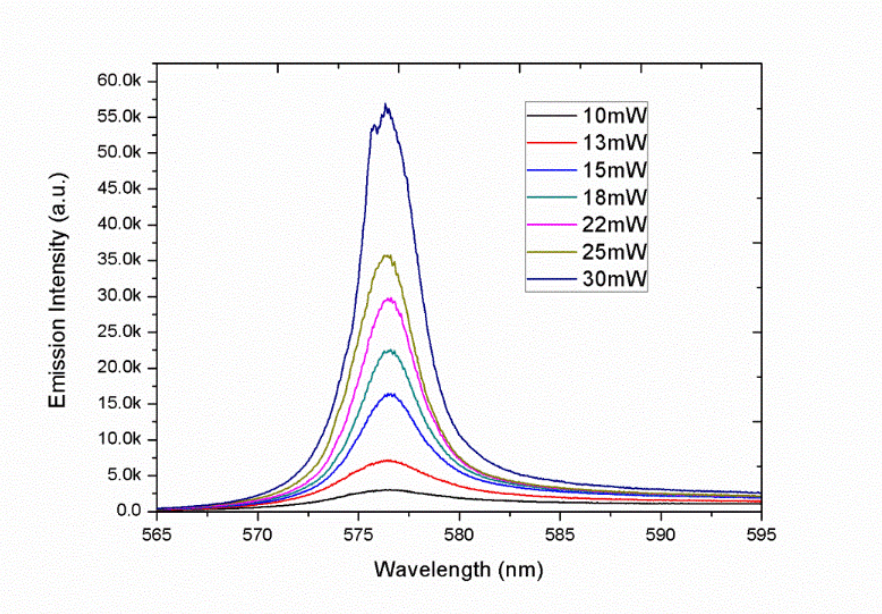

Figure 3.14 Fluorescent emission from Rh6G-hollow-POF at different pump power

There is a narrowing coupled with a blue shift in the fluorescence emission spectra as pump power is increased in Rh6G doped hollow POFs. This blue shift is due to the selective excitation of those modes which have sufficient gain for amplification [15].

There is a blue-shift in the peak fluorescence emission for Rh6G doped SI to hollow and to GI POFs as shown in figure 3.15. From SI to GI doped POFs, the shift is approximately 10 nm and from SI to hollow doped POFs the shift is 6 nm. The shift is attributed to the variation of dye concentration in the different types of POFs.

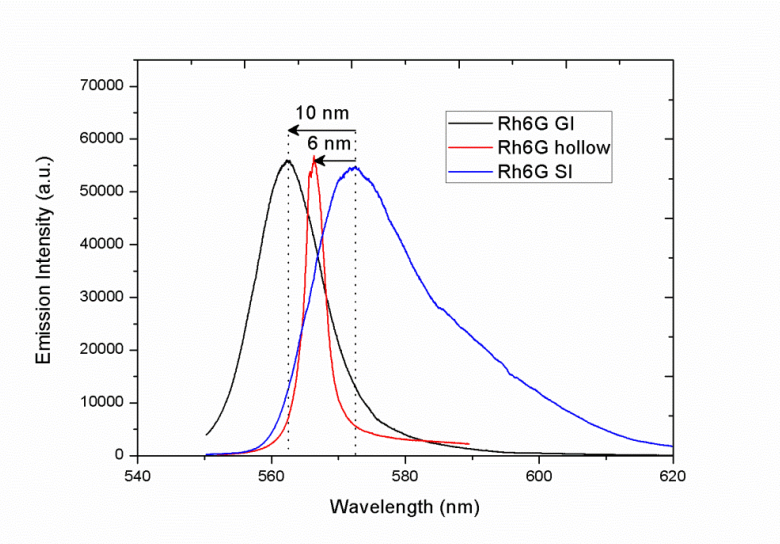

Figure 3.15 Comparison of fluorescence emission from Rh6G doped hollow, GI and SI POFs at a pump power of 30 mW.

From the figure 3.16 we observe that, at given dye concentration, dye doped hollow fiber shows maximum line narrowing at a given pump power. This is due to the fact that net concentration of dye molecule is lower in the case of hollow fiber as compared to SI. Previous experimental studies [36] already shown that at higher dye molecule concentration the line width should be higher. This phenomenon has been explained in the basis of enhanced reabsorption and emission process of dye molecules. When the concentration increases, more dye molecules will participate in the absorption and emission process, this will lead a reduction in the light intensity. Also the hollow fiber has an annular structure; that can dissipate more heat to air. Increase in temperature inside the fiber will reduce the fluorescent intensity due to reduction of quantum yield of dye molecules [37].

It can also be observed that the ASE from the dye doped POF was increased as a function of increasing the pump power. At high intensities, the ASE peak grows and narrows until most of the energy from the sample is emitted within the ASE peak. Fluorescence in a fiber can enhance the effect

due to transverse confinement, making it possible to build efficient optical amplifiers, light sources and lasers.

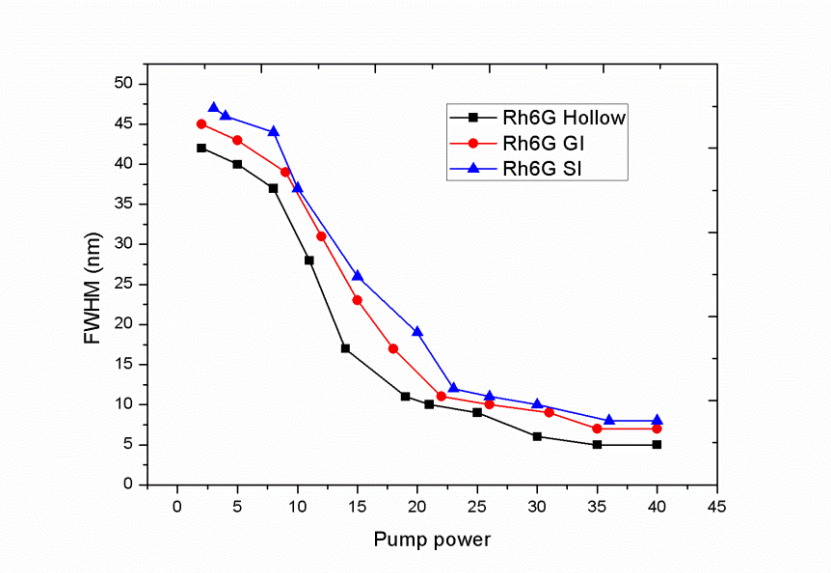

Figure 3.16 FWHM of the spectral emission from Rh6G doped hollow, GI and SI POF as a function of pump power

The fluorescence emission is measured from various positions of the fiber starting from a position closer to the pumping region and then progressing towards the other end of the fiber. The optical loss coefficients for shorter and longer distances of propagation through the dye doped fiber are different. Figure 3.17 shows the variation of output intensity and shift in peak wavelength with the length of Rh6G doped SI, GI and hollow POF at a pump power of 30 mW. The optimum length for maximum output intensity from different types of fiber is different. As the propagation distance increases, the magnitude of the output intensity increases up to a length of 2 cm for SI, 4 cm for hollow and 7 cm for GI POF. Further increase in length will reduce the intensity due to various loss mechanisms such as absorption and scattering of fluorescence. The optimum length of fiber samples also depends on the dye concentration and input pump power because a longer length of inverted medium can be achieved by a higher pump power [38].

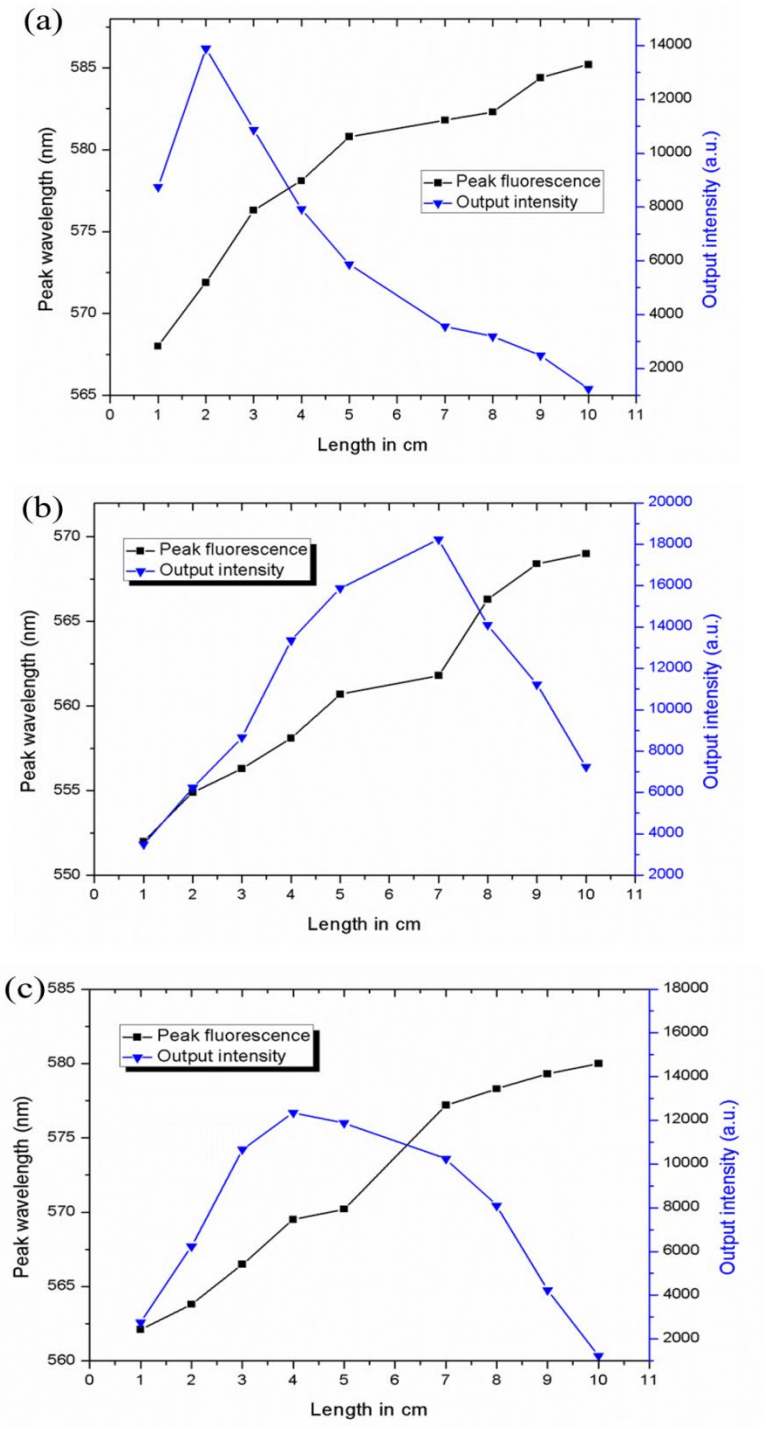

Figure 3.17 Variation of emission peak and output intensity with length of Rh6G doped SI-POF (a), GI-POF (b) and Hollow POF (c) at a pump power of 30 mW.

The red shift of the fluorescence signal is fiber length dependent, and is produced by the self-absorption and re-emission effects of the laser dye. Due to this self-absorption and re-emission process, the peak emission wavelength shows a redshift with an increase in concentration [39]. Increasing the path length through the dye doped sample is somewhat similar to an increment in dye concentration. The experimental results of the red shift of the fluorescence peak when the fiber length is increased for different types of doped fiber have been shown in figure 3.17. This red shift in fluorescence can be attributed to the gain achieved as the radiation is propagated through the amplifying medium as well as to the reemission from the interacting dye molecules at longer wavelengths. These types of red-shift in peak fluorescence with propagation length will allow a limited range of tuning of emission wavelength from the different types of dye doped fibers.

3.5 Photostability

An important parameter, determining potential application of the solid-state dye laser system in which the ASE phenomenon can be observed, is the rate of dye photo-degradation during the prolonged exposure to pulsed excitation by laser light. Hence photostability is one of the main concerns in solid-state gain media. In most organic laser dye systems, luminescence efficiency decreases after thousands of excitation pulses and photo-bleaching is observed [16].

Optical amplifiers and lasers made of dye doped fiber require much less pump power than in bulk material, because of the effective confinement and long interaction length available in fiber geometry [20]. Since photo-bleaching increases with the exposure intensity, low pump power would increase the life time of gain medium. Also, the thin and long geometry of the fiber is ideal for good thermal relaxation to minimize the thermally induced photo-bleaching as well [40].

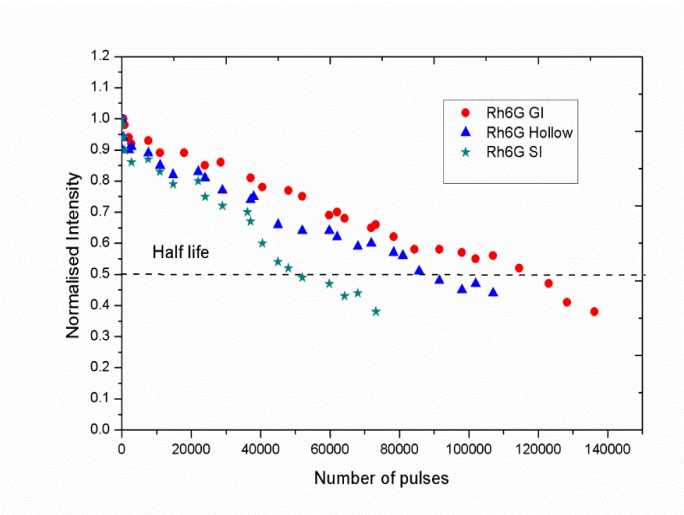

Figure 3.18 Normalized output intensity as a function of number of pump pulses for Rh6G doped different type of POFs at a pump power of 30 mW.

Therefore solid-state dye doped gain media usually have limited life time. There are also other factors that could contribute to the optical bleaching of organic dyes. Thermal effect from optically absorbing impurities is another important source. Figure 3.18 shows an evolution of normalized output intensity as a function of number of pump pulses for Rh6G doped GI, SI and hollow POFs. The half-life of different types of dye doped POF has been compared. From the figure it is observed that Rh6G doped GI-POF has the highest life time as compared to other types of POFs. For a pump power of 30 mW, the output intensity remains at 50% of initial value after 150,000 shots (excitation pulses). From the study, we also conclude that the photo-degradation is particularly fast for step index type fiber, moderate in hollow type and slower in graded index fiber for a given pump power.

Generally bleaching can happen due to thermal effects as well as excited state absorption [21]. In our case bleaching of dye molecules takes place mainly due to thermal effects. Bleaching of dye molecules due to thermal effects cause permanent and irreversible photo degradation and they no longer

cause any emission hence the bleaching in our case does not happen due to excited state absorption.

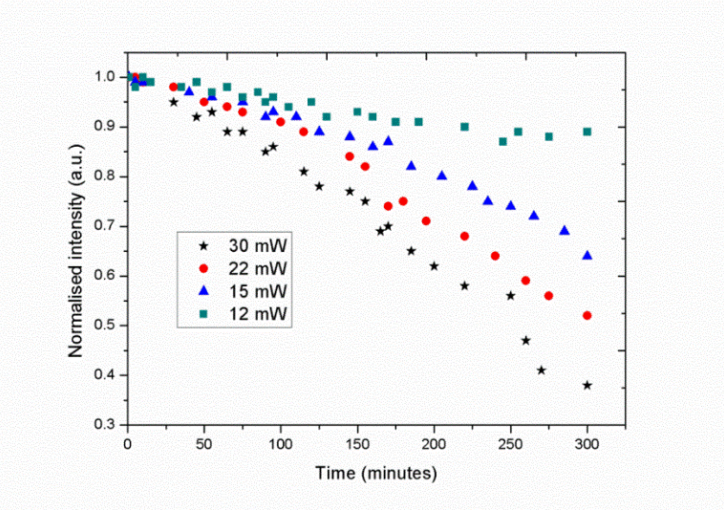

Figure 3.19 Normalized emission intensity for Rh6G-hollow fiber at different pump power versus the exposure time

Figure 3.19 shows the normalized output intensity as a function of exposure time for Rh6G doped hollow POF at different pump powers. The higher pump intensity could cause quicker degradation of dye molecules. From the figure it is observed that the photo-bleaching increases with the increase of the exposure intensity, low pump intensity would increase the lifetime of the gain medium [20].

Table 3.2 Summarize emission characteristics of Rh6G doped Hollow, GI and SI POFs

Fiber type	Peak wavelength (nm)	Optimum length (cm)	FWHM (nm)	Half life (shot)
Hollow	562	4	5	95,000
GI	585	7	7	1,20,000
SI	572	2	8	50,000

Table 3.2 summarizes peak wavelength, optimum length, line-width and half-life of Rh6G doped hollow, GI and POFs investigated in the present study. The experiment was carried out at 10 Hz repetition rate with a pump power of 30 mW.

3.6 Conclusions

In this chapter we have discussed the fabrication techniques for different types of polymer optical fibers (POF) such as SI, hollow and GI. Laser pump power dependence of fluorescence emitted from Rh6G doped SI, GI and hollow POFs were studied and compared. It has been observed that the ASE of dye doped POFs has been increased by increasing the pump power and Rh6G doped hollow POF shows the highest spectral narrowing for a given pump power compared to GI and SI POFs. With the increase in propagation length through the fiber, the emission peak shows a red shift due to self-absorption and reemission by the dye molecules. Thus we could tune the ASE wavelength by adjusting the propagation distance through the fiber. The capability to tune the fluorescence peak position gives the capability to tune the spectral gain of the doped POFs. The peak wavelength, optimum length, line-width and half-life of Rh6G hollow, GI, and SI POFs were compared. From our study, we also concluded that the photo-degradation is particularly fast in step index fiber, moderate in hollow type and slower in graded index fiber for a given pump power.

References

1. D. Y. Chen, Y. G. Jiang, R. W. Fan, E. B. Jia, Y. Q. Xia, and Y. Yao, “Highly Photo-stable Solid-State Dye Lasers Based on Mixed Pyrromethene 567 and Coumerin 500” Laser Physics, Vol. 19, No. 9, pp. 1877-1881 (2009).
2. B. H. Soffer, B. B. McFarland “Laser Second-Harmonic-Induced Stimulated Emission of Organic Dyes” Applied Physics Letter 10, 266-267 (1967).
3. O. G. Peterson and B. B. Snavely “Stimulated Emission from Flashlamp-Excited Organic Dyes in Polymethyl Methacrylate” Applied Physics Letter 12, 238 (1968).

4. A. Costela, I. García-Moreno and R. Sastre "Polymeric solid-state dye lasers: Recent developments", Phys. Chem. Chem. Phys., 5, 4745-4763 (2003).

5. T. Susdorf, D. del Agua, A. Tyagi, A. Penzkofer, O. García, R. Sastre, A. Costela, I. García-Moreno, "Photophysical characterization of pyrromethene 597 laser dye in silicon-containing organic matrices", Applied Physics B, Volume 86, Issue 3, pp 537-545 (2007).

6. A. Costela, , I. Garcia-Moreno, J.M. Figuera, F. Amat-Guerri, J. Barroso, R. Sastre, "Solid-state dye laser based on Coumarin 540A-doped polymeric matrices", Optics Communications, Volume 130, Issues 1–3, Pages 44–50 (1996).

7. R. Bornemann, U. Lemmer, and E. Thiel, "Continuous-wave solid-state dye laser", Optics Letters Vol. 31, Issue 11, pp. 1669-1671 (2006).

8. Søren Balslev, Andrej Mironov, Daniel Nilsson, and Anders Kristensen, "Micro-fabricated single mode polymer dye laser", Optics Express Vol. 14, Issue 6, pp. 2170-2177 (2006).

9. A. Costela, I. Garcia-Moreno, H. Tian, J. Sub, K. Chen, F. Amat-Guerri, M. Carrascoso, J. Barroso, R. Sastre, "Internal photostabilization of polymeric solid-state dye lasers based on trichromophoric rhodamine 6G molecules", Chemical Physics Letters,Volume 277, Issue 4, Pages 392–398 (1997).

10. Mark D. Rahn and Terence A. King, "Comparison of laser performance of dye molecules in sol-gel, polycom, ormosil, and poly(methyl methacrylate) host media", Applied Optics Vol. 34, Issue 36, pp. 8260-8271 (1995).

11. Changhong Jiang, Mark G. Kuzyk, Jow-Lian Ding, William E. Johns and David J. Welker, "Fabrication and mechanical behavior of dye-doped polymer optical fiber", J. Appl. Phys. 92, 4 (2002).

12. B. Chiron, In: Proceedings of SPIE on plastic optical fibers, Boston, MA, 1592, P. 86-95 (1991).

13. S. Muto, Sato and T. Hosaka, In: Proceedings of the third international conference on plastic optical fibers and applications- POF, Yokohama, Japan, P. 46-48 (1994).

14. Jaison Peter, P. Radhakrishnan, V.P.N. Nampoori, M. Kailasnath, "Multimode laser emission from free-standing cylindrical microcavities", Journal of Luminescence, Volume 149, Pages 204–207 (2014).

15. K Geetha, M Rajesh, V P N Nampoori, C P G Vallabhanand P Radhakrishnan, "Laser emission from transversely pumped dye-doped free-standing polymer film", J. Opt. A: Pure Appl. Opt. 8, 189 (2006).

16. L. Sznitko, J. Mysliwiec, K. Parafiniuk, A. Szukalski, K. Palewska, S. Bartkiewicz, A. Miniewicz, "Amplified spontaneous emission in polymethyl methacrylate doped with 3-(1,1-dicyanoethenyl)-1-phenyl-4,5-dihydro-1H-

pyrazole (DCNP)", Chemical Physics Letters, Volume 512, Issues 4–6, Pages 247–250 (2011).

17. M. Rajesh, "Fabrication and characterization of polymer optical fibers for smart sensing and optical amplification", P.hD Thesis, July 2006.
18. M. Kailasnath, V. P. N. Nampoori, P. Radhakrishnan, "A microring multimode laser using hollow polymer optical fibre", Volume 75, Issue 5, pp 923-927 (2010).
19. Gang Ding Peng, Chu, P.L. Zhengjun Xiong, Whitbread, T.W., Chaplin, R.P. "Dye-doped step-index polymer optical fiber for broadband optical amplification", Journal of Lightwave Technology, Volume:14 Issue:10 (1996).
20. M. Kailasnath, T.S. Sreejaya, Rajesh Kumar, C.P.G. Vallabhan, V.P.N. Nampoori, P. Radhakrishnan, "Fluorescence characterization and gain studies on a dye-doped graded index polymer optical-fiber preform", Optics & Laser Technology, Volume 40, Issue 5, Pages 687–691 (2008).
21. Y. Ohtsuka and Y. Hatanaka, "Preparation of light-focusing plastic fiber by heat-drawing process", Appl. Phys. Lett., 29,735 (1976).
22. Y. Ohtsuka and I. Nakamoto, "Light-focusing plastic rod prepared by photo copolymerization of methacrylic esters with vinyl benzoates", Appl. Phys. Lett., 29,559 (1976).
23. M.J. Niknam Jahromi, Jui-Hsiang Liu, "Gel effects on the fabrication of gradient refractive index plastic rods via energy-controlled polymerization", Journal of the Taiwan Institute of Chemical Engineers, Volume 43, Issue 2, Pages 301–305 (2012).
24. Dong Min Sim, Min-Jae Choi, Yoon Hyung Hur, Boae Nam, Geesung Chae, Jong Hyun Park andYeon Sik Jung, "Ultra-High Optical Transparency of Robust, Graded-Index, and Anti-Fogging Silica Coating Derived from Si-Containing Block Copolymers", Advanced Optical Materials Volume 1, Issue 6, pages 428–433, (2013).
25. Yasuji Ohtsuka and Yukiko Terao, "Studies on the light-focusing plastic rod. IX. Chemical composition of the copolymer rod-diethylene glycol bis(allyl carbonate) with 2,2,3,3-tetrafluoropropyl methacrylate", Journal of Applied Polymer Science,Volume 26, Issue 9, pages 2907–2915, (1981).
26. Yasuji Ohtsuka and Yasuhiro Koike, "Determination of the refractive-index profile of light-focusing rods: accuracy of a method using Interphako interference microscopy", Applied Optics Vol. 19, Issue 16, pp. 2866-2872 (1980).
27. Fan Zhang, Xinghua Wang, Qijin Zhang, "Refractive index distribution of graded poly(methyl methacrylate) preform described by self-diffusion approaches of free-volume theory in a ternary system", Volume 41, Issue 26, Pages 9155–9161 (2000).

28. Y. Koike, T. Ishigure, Nihei, Eisuke, "High-bandwidth graded-index polymer optical fiber", Journal of Lightwave Technology, Volume:13 Issue:7 (1980).

29. Yasuhiro Koike, Eisuke Nihei, Norihisa Tanio, and Yasuji Ohtsuka, "Graded-index plastic optical fiber composed of methyl methacrylate and vinyl phenylacetate copolymers", Applied Optics Vol. 29, Issue 18, pp. 2686-2691 (1990).

30. D. W. Garvey, K. Zimmerman, P. Young, J. Tostenrude, J. S. Townsend, Z. Zhou, M. Lobel, M. Dayton, R. Wittorf, M. G. Kuzyk, J. Sounick, and Carl W. Dirk, "Single-mode nonlinear-optical polymer fibers", Journal of the Optical Society of America B Vol. 13, Issue 9, pp. 2017-2023 (1996).

31. Toshikuni Kaino, "Waveguide fabrication using organic nonlinear optical materials", J. Opt. A: Pure Appl. Opt. 2 (2000).

32. R. J. Kruhlak and M. G. Kuzyk, "Side-illumination fluorescence spectroscopy. I. Principles", Journal of the Optical Society of America B Vol. 16, Issue 10, pp. 1749-1755 (1999).

33. R. J. Kruhlak and M. G. Kuzyk, "Side-illumination fluorescence spectroscopy. II. Applications to squaraine-dye-doped polymer optical fibers", Journal of the Optical Society of America B Vol. 16, Issue 10, pp. 1756-1767 (1999).

34. Jaison Peter, C P G Vallabhan, P Radhakrishnan, V P N Nampoori and M Kailasnath, "Microring lasing from a dye-doped polymer-coated silica fiber", Laser Phys. 23 115104 (2013).

35. C. V. Shank, "Physics of dye lasers", Rev. Mod. Phys. 47, 649 (1975).

36. Shiyoshi Yokoyama, Akira Otomo, and Shinro Mashiko, "Laser emission from high-gain media of dye-doped dendrimer", Appl. Phys. Lett. 80, 7 (2002).

37. David Ross, Michael Gaitan, and Laurie E. Locasio, "Temperature measurement in Microfluidic Systems using a temperature dependent fluorescent dye", Anal. Chem. 73, 4117-4123 (2001).

38. M. Sheeba, M. Rajesh, V. P. N. Nampoori, and P. Radhakrishnan, "Fabrication and characterization of dye mixture doped polymer optical fiber as a broad wavelength optical amplifier", Applied Optics Vol. 47, Issue 11, pp. 1907-1912 (2008).

39. F. P. Schafer, "Dye laser", Topics in applied physics, Volume 1, Chapter 1 (1990).

40. J. S. Vrentas, C. M. Vrentas, "Solvent Self-Diffusion in Glassy Polymer-Solvent Systems" Macromolecules, 27 (20), pp 5570–5576 (1994).

Chapter 4
Dye Doped Hollow Polymer Optical Fiber (DDHPOFs) as Microring Resonator

"Creativity is not the finding of a thing, but the making something out of it after it is found"

James Russell Lowell

Abstract

In this chapter we discuss the observation of multimode laser emission at wavelengths corresponding to whispering gallery modes (WGM) from a free-standing micro-ring cavity based on Rhodamine 6G dye doped hollow polymer optical fiber (DDHPOF). Theoretical modelling of WGM resonator has also been realized using COMSOL Multiphysics software package. Cylindrical microcavities with different diameters were fabricated and their performances have been evaluated.

In the second part of this chapter, we discuss two different types of pumping schemes to characterize the DDHPOF namely 1) stripe illumination and 2) spot illumination. As the pump power is increased, stripe illumination shows a blue-shift and spot illumination shows a red-shift for the emission spectra. By using spot illumination, the slope efficiency of system is enhanced by more than three times than that of stripe illumination.

---

*The major content of this chapter has been published in the journal "**Journal of Luminescence** 05/2014; 149:204-207 (2014) and **Optics Communications**" 01/2014; 320:125–128 (2014).*

4.1 Introduction

Lasers have the unique property that they emit light at a single frequency, which is not the case for classical light sources. However, any real laser has some finite spread in frequency. Stable narrow-linewidth lasers are indispensable in many scientific and technological fields such as telecommunications, sensing, interferometric measurements, gas detection and frequency metrology.

In 1917 Albert Einstein proposed the ingenious idea of stimulated emission in atoms [1]. The first experimental observation followed about ten years later by Ladenburg [2]. A few decades later, in the 1950's, the first device was theoretically described and built which made use of this idea by amplifying the stimulated emission (SE) of microwave radiations to create the first masers [3-4]. Efforts were made in the search for possibilities of devices with shorter wavelengths, and Schawlow and Townes theoretically described the concepts of infrared and optical maser [5]. Finally in 1960 Maiman succeeded in inducing the first stimulated optical output in Ruby crystals [6], which marked as the birth of LASER (Light Amplification by Stimulated Emission of Radiation). Subsequently research groups all over the world focused on using multitude gain media in their lasers, which included the invention of helium-neon lasers [7], semiconductor lasers [8], carbon-dioxide lasers [9], dye lasers [10-11] and later excimer lasers [12].

Incredible new uses of lasers were discovered in the last 50 years, primarily due to their unique properties such as their directionality, monochromaticity, and spatial coherence

Therefore, the customized usage of the term laser is generally associated with the stricter criteria of

(i) Spectral of narrow line emission coinciding with resonant cavity modes.

(ii) Spatial coherence

(iii) Strongly polarized output and

(iv) Lasing threshold

Similarly, phenomena such as line narrowing [7–9], mirrorless lasing [10] or laser-like emission do exhibit some light output properties that match those of lasing behaviour to a certain extent. This is a consequence of the fact that these high optical gain effects result from large SE cross-sections. There are also so-called modeless lasers providing high-quality output in terms of emission stability, linewidth and coherence that are built by travelling wave amplification without any feedback structure [11].

Generally, a laser device is constructed by the combination of the laser medium and an optical feedback structure. The high gain medium that serves as the active material is energetically pumped by either optical excitation or electrical excitation. By virtue of the feedback structure the buildup of the laser oscillation is restricted to a few resonant modes. In the conventional approach this resonator structure is formed by two end mirrors that form the resonator cavity; however, there are many alternative feedback designs which can be employed: e.g., ring microstructures, Distributed Feedback (DFB) structures.

Much effort has been put into the development of materials incorporating the organic dyes into solid host matrices. During recent years new and optimized approaches have led to significant advances in these systems with respect to laser efficiency and damage threshold. In the dye-doped matrix systems the dye molecules (rhodamines, coumarins or pyrromethenes etc.) are dispersed in the solid host media which are either chosen to be sol–gel materials or polymers.

Another important point with regard to the feasibility of employing these new materials in highly emissive devices is their photo-stability and photo-chemical stability. This is not only important for the long lifetime performance

of light emitting diodes, but also for organic solid-state lasers. The main reasons for material degradation in devices under operation are local heating effects and the role of photochemical processes, like photo-assisted oxidation. Even for high-gain materials with large SE cross-sections, intense pumping is required to accomplish lasing and for continuous operation the laser active media must be capable to undergo a large number of excitation cycles. So, evidently, photothermal and photo-oxidative stability is one of the most important issues to be addressed, together with the intrinsic emissive properties of polymeric laser materials.

4.2 Microcavity resonator

Optical resonator/cavity represents a key component or platform in nonlinear optics, light emitting diodes, low-threshold micro-sized lasing, enhanced light-matter interaction and in miniaturized photonic circuit [13-14].The microcavity resonators have shown several advantageous properties, such as high Q factor, narrow resonance line-width, compact size and strong optical field enhancement inside cavities. With these unique characteristics, microcavity resonators have demonstrated lots of applications in high resolution spectroscopy, optical filters, frequency stabilization and all optical switching [15-17]. Current WGM research includes biological sensing [18], optomechanics [19-20], macroscopical ground state cooling [21], cavity quantum electrodynamics [22], light storage [23], microcavity lasers [24-25], thresholdless lasers [26], on-chip frequency comb generation [27] and ultra narrow filtering techniques [28].

The design of a microcavity provides one possibility for a compact light-emitting device structure. The microcavity devices consist of the luminescent material placed within a Fabry–Perot resonator with a length of the order of the wavelength of emitted light. In this way the light emission is coupled to the cavity mode(s) and characteristically the light output is spectrally narrowed

and directed. Microcavity designs are important to modify spontaneous emission properties in electro and photoluminescent devices and a few are attractive as resonators for laser emission. Optical microcavities are mainly classified as,

- Fabry- Perot (FP) type
- Dielectric optical microcavity

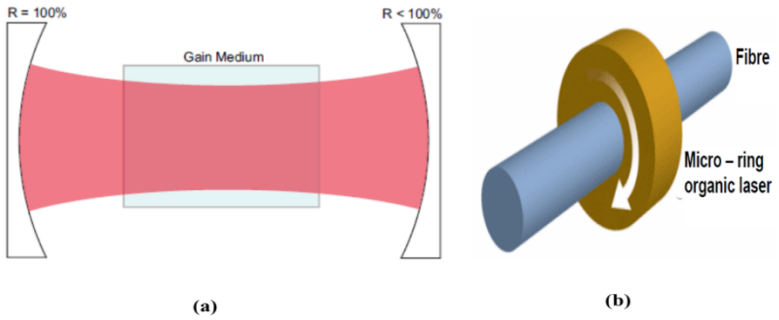

Figure 4.1 Illustration of a (a) Fabry-Perot laser and (b) a ring laser respectively

The first one is the conventional Fabry-Perot (FP)-type cavities (as shown in figure 4.1(a)) comprising of an optical gain media is placed between two concave dielectric or metal mirrors facing each other at a distance of the order of a few 100 μm. FP-type optical cavities are widely utilized in all branches of modern optics, including lasing feedback, optical parametric oscillators, and in some interferometers. The second type is the dielectric optical microcavities with circular/cylindrical shapes as shown in figure 4.1 (b), referred to as WGM resonators. In these resonators, light propagates along the resonators boundary via total internal reflection with the guided modes known as whispering gallery modes.

Lasing at low-power thresholds can be achieved by virtue of the strong optical confinement due to the high contrast of the refractive index between the active medium and the surrounding. This provides light guiding into closed optical paths (ring modes) and coupling of these high refractive modes. Laser

action will then occur along these circumferences for which the gain exceeds the round trip losses. Whispering-gallery microlasers were demonstrated for dye doped polymers [29] and conjugated polymers with lasing operation in the visible range [30].

4.2.1 Cavity parameters

Three crucial parameters of an optical microcavity are the Q factor, FSR and Finesse.

(a) Q Factor

The most common and important parameter of the cavity is the quality factor (Q factor). The definition of the quality factor for any resonant element can be simply given by equation [31];

$$\boldsymbol{Q = W_0 \frac{P_{stored}}{P_{lost}}} \qquad \textbf{4.1}$$

where $W_0 = 2\pi f_0$, which is the angular frequency at which the stored energy and dissipated power are measured. P_{stored} is the stored energy in the resonator and P_{lost} is the power dissipated by the cavity. Also the photon life time in the cavity is

$$\boldsymbol{\tau_{ph} = \frac{Q}{\nu}} \qquad \textbf{4.2}$$

Generally cavity Q factor can be measured through the spectrum rather than by using ring down time

$$\boldsymbol{Q = \frac{\lambda_0}{\delta\lambda}} \qquad \textbf{4.3}$$

where $\delta\lambda$ is the full width half maximum of the resonant peak.

(b) Mode volume

Another parameter to characterize microresonators is the mode volume, which is used to describe electric field energy density of optical mode within a cavity. A small mode volume cavity can confine a photon to the smallest possible volume. Hence the reduction of mode volume can enhance the

circulating intensity within a cavity [14]. The parameter $V_{mode,}$ can be defined as:

$$\mathbf{V_{mode}} \approx \frac{\int V_Q\, \varepsilon(\vec{r})|E^2|d^3r}{max\, \varepsilon(\vec{r})|E^2|} \qquad \mathbf{4.4}$$

where $\varepsilon(\vec{r})$ the dielectric constant of the material, E is the cavity field, and V_Q is the integration volume. The circulating intensity of the light in a cavity is a function of the mode volume and the input power, P_{in}. For a given input power the circulating intensity, I, within the resonator is given by

$$I = P_{in} \frac{\lambda}{2\pi n_g} \frac{Q}{V_{mode}} \qquad \mathbf{4.5}$$

where n_g is the group index. For mW pump powers and mode volumes of 1000 μm^3, it is possible to achieve electric field gradients of the order of GW/cm^2.

(c) Free spectral range

The free spectrum range is defined as the frequency spacing or wavelength spacing between two adjacent modes. If we define the two adjacent modes with resonant wavelength at λ_m and $\lambda_{m-1,}$ then the free spectral range (FSR):

$$FSR\ (\Delta\lambda) = \lambda_m - \lambda_{m-1} = \frac{\lambda^2}{\pi D n_{eff}} \qquad \mathbf{4.6}$$

where λ is the peak wavelength, D is the diameter of the cavity and n_{eff} is the effective refractive index of the medium.

(d) Finesse (F)

The finesse of the resonator is defined as the ratio of the FSR to the resonant line width.

$$\mathcal{F} = \frac{FSR}{\delta\lambda} \qquad \mathbf{4.7}$$

A physical explanation of finesse is the round trip number of the photon in the cavity. A suitable parameter taking both the photon storage time (Q factor)

and the resonator size (mode volume) into account, is the finesse, $\mathcal{F}$.

4.3 History of WGM Resonators

The Whispering Gallery in St. Paul's Cathedral in London, UK (figure 4.2) fascinated Lord Rayleigh a century ago. As in other round structures, such as City Hall in San Francisco and St. Peter's Basilica in the Vatican City, the curved walls have the ability to guide seemingly quiet sounds along the circumference, thus allowing a listener at the opposite end to vividly hear the whispers (figure 4.3). This effect does not work if one speaks at center of the dome or normally to the edge of the dome. Lord Rayleigh's famous paper detailed the physics of it in 1910 [32]. The answer to this strange effect is that the sound bounces along the smooth curved wall of the gallery with very little loss, and so it can be heard at a very long distance. The reason that it does not work if you speak at center on normally to the edge of the dome is that the increased amplitude of the noise allows it to circulate the gallery multiple times, and so the sounds all get mixed up and can no longer be heard properly. It can be viewed that there is a narrow region near the edge of the dome where the sound waves propagate with very low loss, and this is known as "whispering gallery modes" (WGM).

Figure 4.2 Whispering gallery in St. Paul's Cathedrel, London, UK

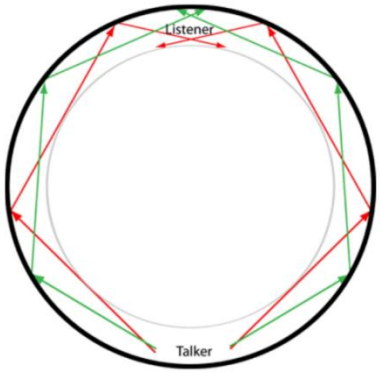

Figure 4.3 Acoustical reflection from the surface

This phenomenon which was first observed by sound wave bouncing around the edge of wall can also be applied to the optical wave by assuming that the inside and the outside of gallery region are filled with high refractive index material and low refractive index optical transparent material, respectively. Light inside a circular resonator can impinge on the surface and be totally internally reflected and trapped inside the resonator with minimum loss. It is very difficult to get light into a resonator from which it cannot escape, but in fact there is an evanescent field outside of the medium due to the total internal reflection [33] which can be used to couple into the structure. Recently, this phenomenon has been found in optical wave region in micro-circular cavity such as micro-disk, micro-ring, microsphere and micro-tube.

In fact, around the same time that Lord Rayleigh was describing the Whispering Gallery in London, Gustav Mie was investigating solutions for the reason for the sharp resonances when light passed through them [33]. In the meantime the observation of light scattering from sphere was described by Debye [34]. Those observations lead to the emergence of a new field of study of scattering of electromagnetic waves in different wavelength ranges [35-37].

This type of microcavities has rotational symmetric boundary, for instance, microspheres, microdisks, microcylinders and microtoroids, as shown in figure 4.4 (a) as taken from the reference [31]. Viewed in ray optics,

optical whispering gallery modes in the circular dielectric cavities can be easily understood with the concept of total internal reflection as shown in figure 4.4 (b). As shown in Figure 4.4(b), a ray is emited from the point A with an output angle χ (sin χ >1/n, where n is the refraction index of the cavity material). Then, it will be continually totally reflected on the cavity boundary due to the rotational symmetry. After finite reflections, the ray returns to the point A, and it gets a propagation phase θ. When $\theta = 2k\pi$ (k = 1,2,3,...), the propagating field undergoes constructive interference with itself. This means that only whole numbers of wavelengths of light can "fit" around the edge of the circular dielectric cavity. This selectivity causes discrete modes to exist in the cavity, known as whispering gallery modes. The electromagnetic field distribution of WGM was shown in figure 4.4 (c) using COMSOL Multiphysics software package.

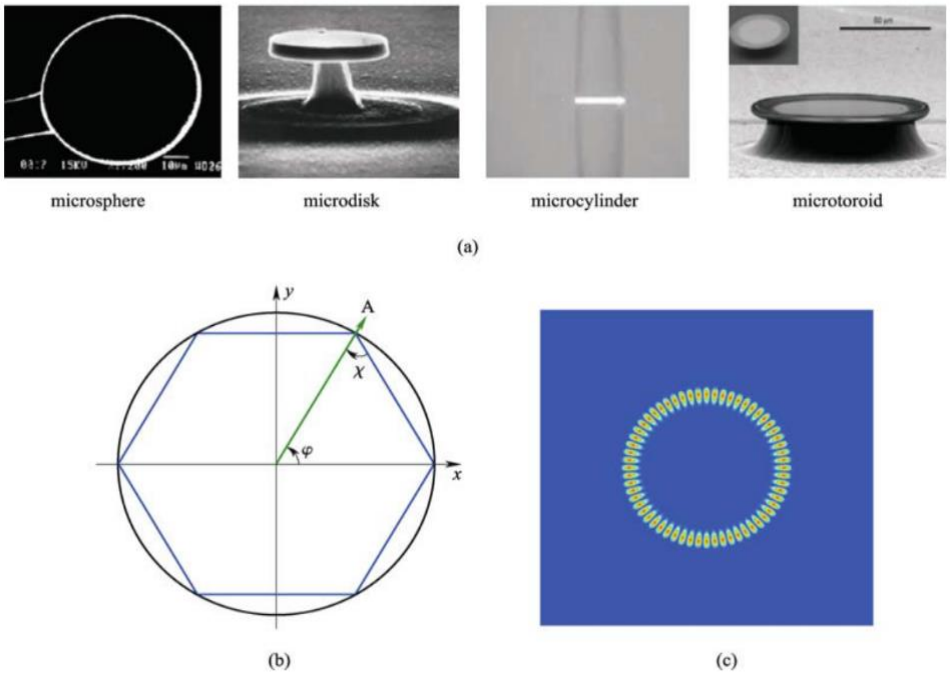

Figure 4.4 (a) Four typical whispering gallery microcavity; microsphere, micro disk, microcylinder, and microtoroid. (b) Geometrical optics of the WGM resonance; (c) wave optics representation of a WGM [31]

4.4 Resonance

Light that propagates through a dense material may polarize that medium, depending on how the molecules interact with the time-varying electric and magnetic fields. The permittivity of a material, ε_m, describes the time delay in the molecular response to the optical fields, and can be expressed in terms of the permittivity of a wave propagating through vacuum (ε_0) and a material-dependent relative permittivity (ε_r)i.e., $\varepsilon_m = \varepsilon_r\, \varepsilon_0$. It is often more convenient to work in terms of the refractive index, whose real part can be expressed as the ratio of the speed of light in a material $\nu_m(\lambda,T)$ to that in vacuum c. The complex refractive index at temperature T and wavelength λ is defined as

$$\boldsymbol{n(\lambda,T) = N(\lambda,T) + ik(\lambda,T) = \frac{c}{\nu_m(\lambda,T)} + ik(\lambda,T)} \qquad \textbf{4.8}$$

The imaginary part is related to the loss mechanisms in the material, like absorption or scattering. The speed of light in the medium is the product of the frequency of the electromagnetic wave, ν, which is independent of the material, and the wavelength in the medium, λ_m. This relationship may be expressed in terms of the speed of light in vacuum, λ_0, as

$$\boldsymbol{\lambda_m = \lambda_0 \frac{\nu_m}{c} = \frac{\nu_m}{\nu} = \frac{\lambda_0}{n}} \qquad \textbf{4.9}$$

WGM resonators typically have circular cross sections that enable light to be trapped as it propagates near the periphery. This circulating light is confined via total internal reflection at the interface between the resonator and the surrounding medium. Light for which a round trip is equal to an integer number of wavelengths (M) returns to the point it was coupled into the resonator in phase with itself, as illustrated in figure 4.4 (b). Constructive intereference occurs under these conditions, allowing the circulating intensity to grow until the rate at which light is coupled into the cavity is balanced by the rate at which it is lost. This phenomenon is referred to as resonance and the

3-dimensional electromagnetic field profile that describes the path of the resonant light takes is called the mode. For a given resonator, many modes are accessible. A particular mode is characterized by its mode number, which can be approximated as the number of wavelengths within the cavity (M) and by the wavelength required to excite that mode, λ_R.

$$2\pi n_{mode} R_{mode} \approx M\lambda_R \qquad 4.10$$

It is apparent from the criteria for resonance that the resonant wavelength is a function of the refractive index encountered by the mode as well as the radius of the mode, where $R_{mode} \approx R_{res}$ and R_{res} is the radius of the resonator. The free spectral range (FSR) is the wavelength interval that separates a mode of order M and its next-highest order mode (M+1). This quantity may be expressed by equation 4.4.

4.5 Theoretical analysis

The geometry of a hollow cylindrical dielectric waveguide is shown in figure 4.5. A hollow core of relative permittivity $\varepsilon_1 = 1$ is surrounded by a concentric layer of material having relative permittivity ε_2. The region exterior to the layer is free-space ($\varepsilon_3 = 1$). The axial fields in regions 1, 2, and 3 for TM mode [38] are:

$$E_z^{(1)}(r, \theta) = A_m J_m(p_1 r)\, e^{\pm jm\theta} \qquad 4.11$$

$$E_z^{(2)}(r, \theta) = (B_m J_m(p_2 r) + C_m Y_m(p_2 r))\, e^{\pm jm\theta} \qquad 4.12$$

$$E_z^{(3)}(r, \theta) = D_m K_m(q r)\, e^{\pm jm\theta} \qquad 4.13$$

where A_m , B_m , C_m , and D_m are arbitrary constants

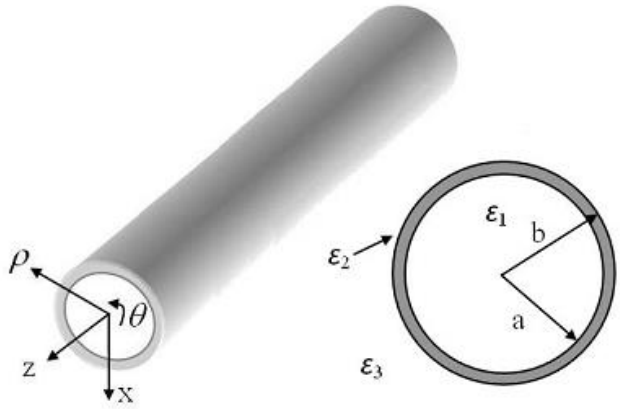

Figure 4.5 (a) Schematic of the cylindrical dielectric waveguide and cross section of the waveguide with inner radius b and outer radius a. Relative permittivity of each medium are labelled as ε1, ε2 and ε3.

The functions J_m, Y_m, and K_m are the Bessel functions of the first kind, second kind, and the modified Bessel function of the second kind respectively. $p_1^2 = \omega^2 \varepsilon_1\mu_0 - \beta^2 = k_1^2 - \beta^2$, $p_2^2 = \omega^2 \varepsilon_2\mu_0 - \beta^2 = k_2^2 - \beta^2$, and $q^2 = \beta^2 - \omega^2 \varepsilon_3\mu_0 = \beta^2 = k_3^2$, where $k_1 = \frac{\omega n_1}{c}$, $k_2 = \frac{\omega n_2}{c}$, $k_3 = \frac{\omega n_3}{c}$ are respectively the wave number of region 1, 2, 3, while n_1, n_2, n_3 are the corresponding refractive indices, β is the propagation constant, and m is the angular order. For an infinite hollow cylindrical dielectric waveguide with negligible absorption and no axial component of the propagation constant (β= 0), TM mode degenerates to WGM [39-41], then the equation becomes:

$$\mathbf{E_z^{(1)}(r, \theta) = A_m J_m(k_1 r)}\ e^{\pm jm\theta} \qquad \textbf{4.14}$$

$$\mathbf{E_z^{(2)}(r, \theta) = (B_m J_m(k_2 r) + C_m Y_m(k_2 r))}\ e^{\pm jm\theta} \qquad \textbf{4.15}$$

$$\mathbf{E_z^{(3)}(r, \theta) = D'_m H_m^{(1)}(k_3 r)}\ e^{\pm jm\theta} \qquad \textbf{4.16}$$

where $D'_m = (i\pi/2)\ e^{im\pi/2}\ D_m$, $H_m^{(1)}$ is the Hankal function of the first kind . The relation between $H_m^{(1)}$ and K_m is $K_m(-iz) = (i\pi/2)\ e^{im\pi/2}\ H_m^{(1)}(z)$.

Finally, the radial and azimuthal electric fields are derived from the axial electric field using Maxwell's equations. For TM mode in the cylindrical dielectric waveguide, transverse magnetic fields can be obtained as:

$$\mathbf{H_r(r,\theta)} = \frac{1}{p^2}\left[\frac{i\omega\varepsilon}{r}\frac{\partial E_z(r,\theta)}{\partial\theta}\right] \quad \textbf{4.17}$$

$$\mathbf{H_\theta(r,\theta)} = \frac{1}{p^2}\left[i\omega\varepsilon\frac{\partial E_z(r,\theta)}{\partial r}\right] \quad \textbf{4.18}$$

For WGM in the cylindrical dielectric waveguide, the above equations become:

$$\mathbf{H_r(r,\theta)} = \frac{i}{z_0k_0}\frac{1}{r}\frac{\partial E_z(r,\theta)}{\partial\theta} \quad \textbf{4.19}$$

$$\mathbf{H_\theta(r,\theta)} = \frac{-i}{z_0k_0}\frac{1}{r}\frac{\partial E_z(r,\theta)}{\partial r} \quad \textbf{4.20}$$

The field matching equations at the boundary surface r=a and r=b are expressed as: $E_z^{(1)}(a,\theta) = E_z^{(2)}(a,\theta)$, $H_\theta^{(1)}(a,\theta) = H_\theta^{(2)}(a,\theta)$, $E_z^{(2)}(b,\theta) = E_z^{(3)}(b,\theta)$, $H_\theta^{(2)}(a,\theta) = H_\theta^{(3)}(b,\theta)$. Satisfying these conditions gives: $[M]\,[A_m, B_m, C_m, D'_m]^T = 0$

where

$$\mathbf{[M]} = \begin{bmatrix} J_m(k_1 a) & -J_m(k_2 a) & -Y_m(k_2 a) & 0 \\ k_1 J'_m(k_2 a) & -k_2 J'_m(k_2 a) & k_2 Y'_m(k_2 a) & 0 \\ 0 & J_m(k_2 a) & Y_m(k_2 b) & -H_m^{(1)}(k_3 b) \\ 0 & k_2 J'_m(k_2 b) & k_2 Y'_m(k_2 b) & -k_3 H'^{(1)}_m(k_3 b) \end{bmatrix} \quad \textbf{4.21}$$

J'_m , Y'_m , $H'^{(1)}_m$ are the derivatives of J_m , Y_m and $H_m^{(1)}$. The dispersion equation can be obtained by setting $|M| = 0$

4.6 Simulation Model

Simulation model of the WGM resonator with waveguide coupling is illustrated in Figure 4.6. Geometrical parameters of the resonator and waveguide are as follows: outer ring radius 2.5 μm, ring width 0.3 μm, waveguide width 0.3 μm and distance from waveguide to the ring was set to 0.232 μm. Coupling to the microring resonator was simulated in 2D spatial

domain with RI of 3.2 both for ring and waveguide using COMSOL Multiphysics. The above dimensions were selected in order to overcome the computational limitations.

COMSOL was used to solve Helmholtz equation in 2D spatial domain for the structure shown in figure 4.6. Excitation source having spatial distribution of fundamental waveguide mode was set at left side of the waveguide. Transmitted power was monitored at the right side of the waveguide. To get transmission spectra, wavelength of the excitation source was set as a parameter and parametric sweep for different wavelengths was performed. To suppress any reflection from boundaries of computation window, perfectly matched layers were used.

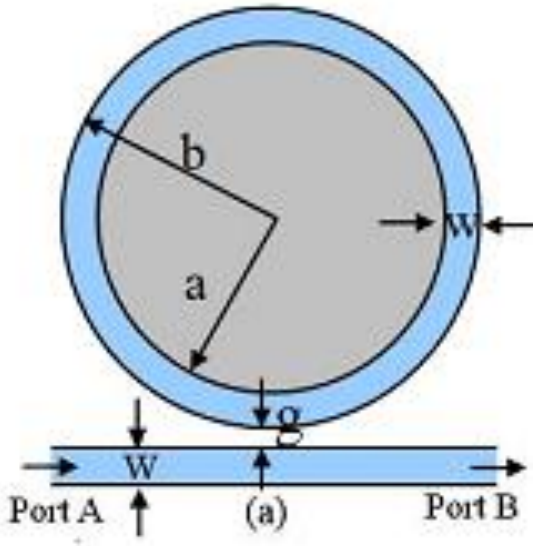

Figure 4.6 Simulation model of the WGM resonator with waveguide coupling.

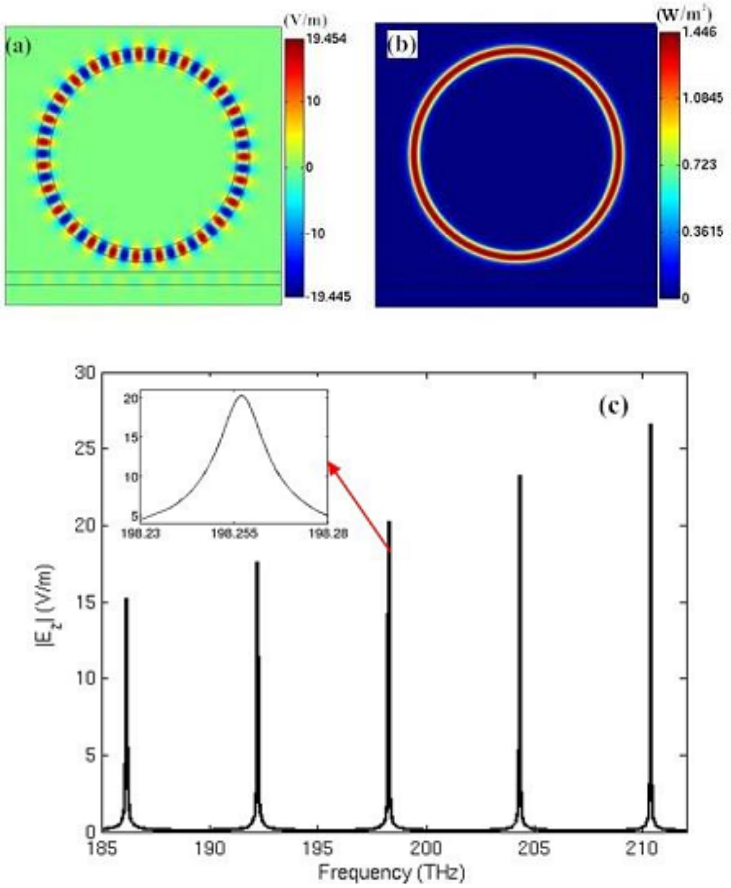

Figure 4.7 (a) Visualization of the steady-state electric field pattern in the air-core microring resonator at the frequency of fr = 198.257 THz (m = 27). (b) Power flow distribution. (c) Resonant frequency spectrum of the microresonator.

The electric field intensity $E_z^{(2)}$ is depending on the azimuthal mode number 'm' and wave number k_2. The simulation is done purely by solving the equation 4.15. From the simulation results we can see an increase in the field peak with the increase in the value of 'm' and 'k'. In order to avoid the computational complexities a small diameter resonator (2.5 μm) has been used in our study. Five resonance peaks have been identified with 'm' value 25,26,27,28 and 29 for this structure. Similar computational results have been already reported [42].

The asymptotic solutions for mode order p and mode number m are following [43]:

$$\boldsymbol{\lambda^{-1}(R, n_1, n_r, p, m) = \frac{1}{2\pi R n_1}\left[m+\frac{1}{2} + 2^{\frac{-1}{3}}\alpha(p)\left(m+\frac{1}{2}\right)^{\frac{1}{3}} - \frac{L}{(n_r^2-1)^{\frac{1}{2}}} + \frac{3}{10}2^{\frac{-2}{3}}\alpha^2(p)\left(m+\frac{1}{2}\right)^{\frac{-1}{3}} - 2^{\frac{-1}{3}} L\left(n_r^2 - \frac{2}{3}L^2\right)\frac{\alpha(p)\left(m+\frac{1}{2}\right)^{\frac{-2}{3}}}{(n_r^2-1)^{\frac{3}{2}}}\right]} \quad \textbf{4.22}$$

where $n_r = n_1/n_2$, $L = n_r^{-1}$ for TM modes, and $L = n_r$ for TE modes $\alpha(p)$ are the roots of the Airy function.

4.7 DDHPOF as a microcavity resonator

There has been a growing interest in exploiting organic and polymeric material showing high optical gain and stimulated emission properties for laser applications [44]. Wide tunability and high efficiency of laser dyes coupled with the high power density that can be easily achieved in waveguide structures make the devices based on dye doped polymer waveguides and fibers very promising [45]. Microring laser cavity offers a low resonance structure that has been utilized to demonstrate lasing with organic gain media [46]. Over the past several years, optically pumped microring laser emissions have been observed from different polymer gain materials. Cylindrical polymer microcavity provides excellent coupling of spontaneous emission into lasing modes and a high cavity Q-value which consequently leads to low lasing thresholds [47-48]. Due to their high Q-value and small mode volume, which leads to unprecedented narrow linewidth, these resonators are used in Microlasers, Biosensing applications [49-50], Optical switches, Add or Drop filters [8,9], etc. This technique may be applicable to a wide range of material systems because low optical cavity loss is obtained from a simple curved surface instead of multiple layer dielectric mirrors [53].

A micron sized polymer waveguide can confine light to its interior volume. The trapped light describes an orbital trajectory circum-navigating just below the cylindrical waveguide surface. The light in such cavities is

confined inside the gain medium by practically lossless total internal reflections [46]. Loss is due to the cavity surface curvature and light scattering from imperfections. When the waves come in-phase at a point after every revolution, constructive interference takes place. Resonance occurs when the guided wave drives itself coherently by returning in-phase after every revolution, thereby requiring an integer number of waves in one circum-navigation. The wave nature of the light allows the photon to penetrate beyond the dielectric boundary and into the surroundings as an evanescent field as explained in the Goos-Haschen shift in case of optical fibers.

The low threshold lasing characteristics of microcavity lasers, their relatively simple formation from polymers and their ability to be integrated directly into other optical components offer good opportunities for their commercial application [54]. Laser dye doped poly (methyl methacrylate) is found to be a highly efficient gain medium for laser source with narrow pulse width, wide tunable range as well as high gain, high power conversion and broad spectral bandwidth for optical amplifier [53]. Furthermore, theoretical studies have been reported on the resonance modes in a concentric or eccentric ring-type cavity [55]. Experimental studies on the ring-type cavity were also reported but not widely due to the difficulty in the fabrication and realization of ring-type cavity systems [56]. In thicker microring cavity ($d/D \geq 0.2$), where D is the outer diameter of micro-cavity and d is the thickness of ring (dye doped region), resonant modes are no longer guided [57]. In fact these optical modes never reach the inner /outer interface and therefore, are dubbed Whispering Gallery Modes (WGMs) [47,58]. The light in this case is confined by total internal reflections at the interface between air and dye doped region, and the mode intensity distribution is concentrated on the outer edge of the fiber and hence it can be easily collected from outer surface area of Dye Doped Hollow Polymer Optical fiber (DDHPOFs). The hollow fiber acts as a

waveguide forming a ring resonator similar to a polymer film on an optical fiber. An optical resonance will occur when the optical path length travelling inside the resonator is an integer multiple of wavelength. Here the path length is the circumference of the fiber. So WGM frequencies in an optical fiber or indeed in any cylindrical resonator, are reasonably well approximated by matching an integral number of wavelengths to the resonator circumference. In the present case, the DDDHPOFs can be modelled as a number of serially connected micro-disc type cavities as shown in figure 4.8.

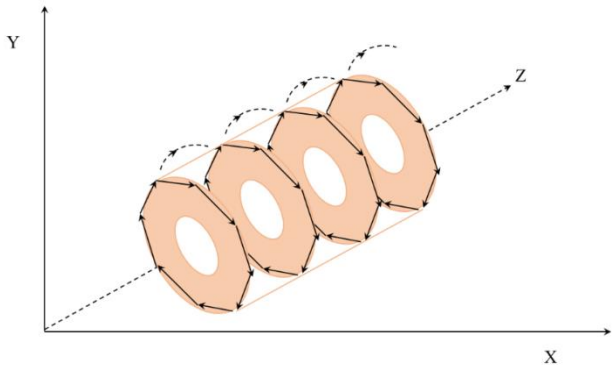

Figure 4.8 Schematic representation of micro disk cavity resonator model of dye doped hollow POF (DDHPOF).

In this section, we discuss the multimode laser emission characteristics at room temperature from different diameter hollow cylindrical microcavities made up of rhodamine 6G (10^{-4} mol/l) doped hollow PMMA optical fibers pumped by a frequency doubled Q-switched Nd:YAG laser. The typical procedure for the fabrication of DDHPOF was already described in chapter 3. A variety of microrings with different outer (OD) and inner (ID) diameters, such as 310 & 160, 400 & 210, 550 & 280 and 660 & 340 μm respectively were fabricated by utilizing the same technique. The variation in the OD measured for the different DDHPOFs is around 2 μm. In our case, d/D ratio for the different diameter DDHPOF is ~ 0.25. In the experimental setup, the DDHPOF is transversely pumped at 532 nm with a frequency doubled Q-

switched Nd:YAG laser (Spectra Physics) with 8 ns pulses at 10 Hz repetition rate as shown in figure 4.9. A set of calibrated neutral density filters was used to vary the pump power. The pump beam was focused onto the sample with the help of a convex lens of focal length 75 mm. The laser emission in the radial direction from the cylindrical microcavity was collected using a collecting fiber. The laser emission was directed to a spectrograph (SpectraPro-500i) coupled with a cooled CCD array with a resolution of 0.03 nm.

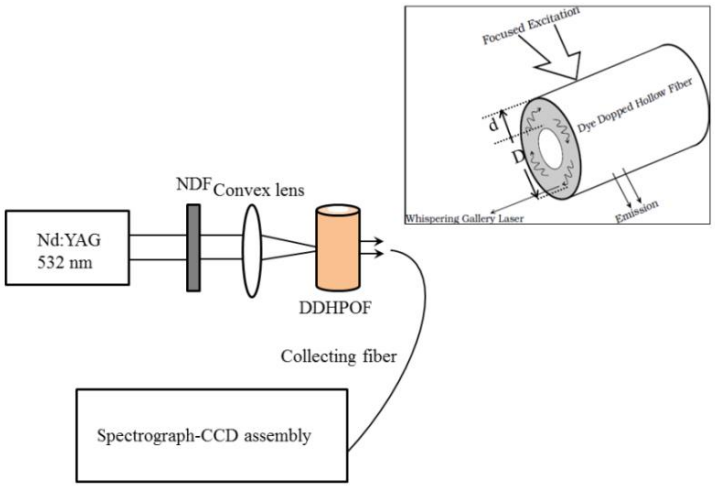

Figure 4.9 Schematic of experimental setup.

4.7.1 ASE to Lasing emission from DDHPOFs

At low pump intensities, the emission spectrum from the 400 μm DDHPOF exhibit a broad luminescence with a peak at 565 nm. By increasing the pump power we observe an increase in the output. When a certain threshold is reached, narrow lines begin to grow out of this broad luminescence, indicative of microring lasing [59] as depicted in figure 4.10. Above the clear threshold pump power, P_{th} (~20 mW) at which sharp spectral peaks and bright emission appeared, the emission intensity increased much

more rapidly with the excitation intensity. This sharp spectral peak is considered as resonant modes in a cylindrical microcavity.

The free spectral range (FSR) of the WGM is inversely proportional to the diameter of the resonator by the equation 4.5.

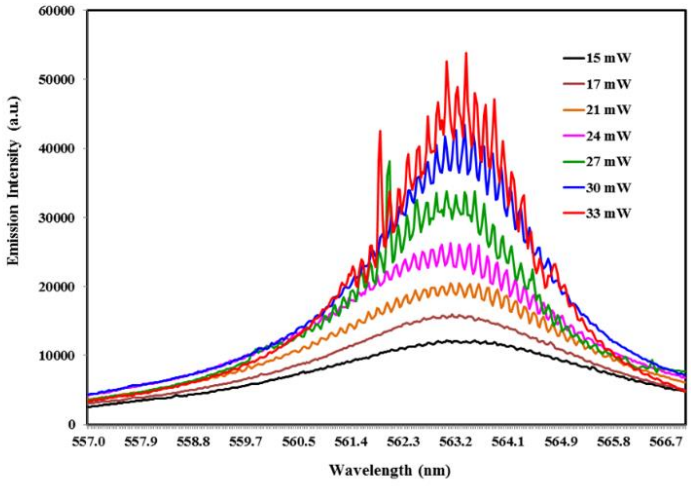

Figure 4.10 Emission spectra from 400 micron DDHPOF at different pump power.

4.7.2 WGM Lasing from different diameter DDHPOFs

The output power (numerically integrated output intensity) versus the pump power for different diameter DDHPOF is shown in figure 4.11. The observed change of slope in the curves is considered as laser threshold pump power; P_{th}, which is a clear signature of the onset of lasing. The linear dependence and change in slope reveal the laser action [60]. Due to the large thickness of the microring cavity, the cavity supports only WGMs, thus the variation of P_{th} should be less dependent on the diameter [61]. To obtain the output laser power the optical output spectra have been numerically integrated from 557-562 nm, 561-566 nm and 563-568 nm for 310 µm, 400 µm and 550 µm respectively.

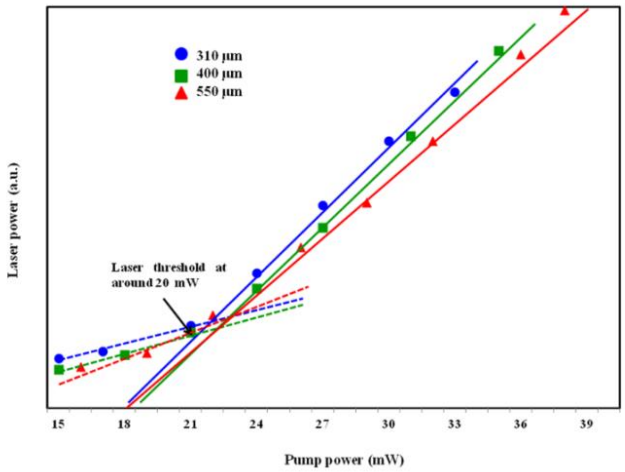

Figure 4.11 The output laser power versus the pump power for different diameter DDHPOFs. The linear dependence and change in slope reveal laser action. The lasing threshold is at about 20 mW.

4.7.3 Dye bleaching threshold

When the pump power is again increased, at a certain pump power the laser modes start to disappear, which is a clear evidence of degradation of laser dye as depicted in figure 4.12.

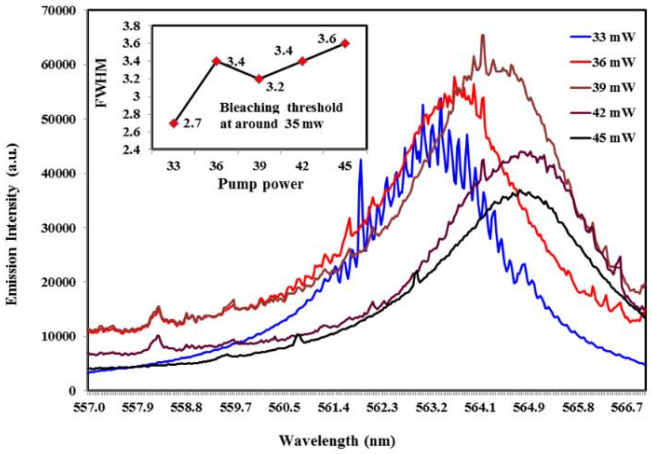

Figure 4.12 The emission spectra from a 400 micron diameter DDHPOF after bleaching of the dye.

This degradation leads to the bleaching of dye and the dye no longer gives stimulated emission which results in the vanishing of laser modes. The dye bleaching threshold is at about 35 mW in our study for 400 µm DDHPOF. From the inset, it is clear that FWHM of emission spectrum increased with pump power, and also a red-shift in the peak emission was observed after the bleaching of laser dye.

The observed FSR of the WGM spectra varied from 0.09 to 0.23 nm, when the diameter of the DDHPOF decreases from 660 to 310 µm. The emitted photon has a longer round trip distance for higher diameter fiber. Thus the cavity can support large number of longitudinal modes. The emission spectrum from the different diameter DDHPOFs for a given pump power (above P_{th}) is shown in figure 4.13. From the figure it is clearly observed that higher diameter DDHPOFs can support large number of longitudinal modes and also a red-shift in WGM envelope was observed.

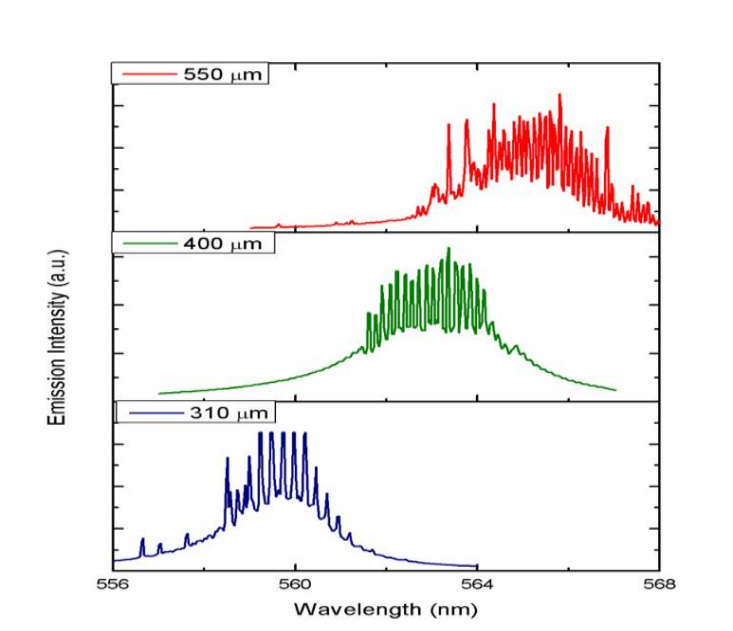

Figure 4.13 The spectra shows the typical WGM laser emission from different diameter DDHPOF as 310, 400 and 500 micron with pump power maintained at around 1.5 – 2 X P_{th}

The red-shift is due to stokes shift, which arises because of the overlap of absorption and emission spectra of Rh6G. The red-shift in the emission spectra shows an increase with dye concentration. Increasing diameter of the DDHPOF was somewhat similar to an increment in dye concentration. The variation of red-shift in WGM envelope of the cylindrical microcavities with different values of D is plotted in figure 4.14.

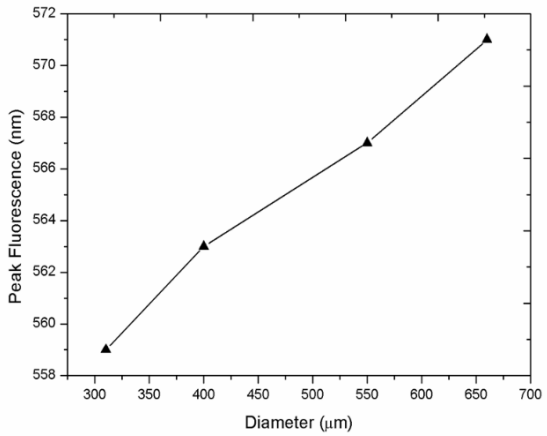

Figure 4.14 Peak fluorescence versus diameter, D of the cylindrical microcavity laser

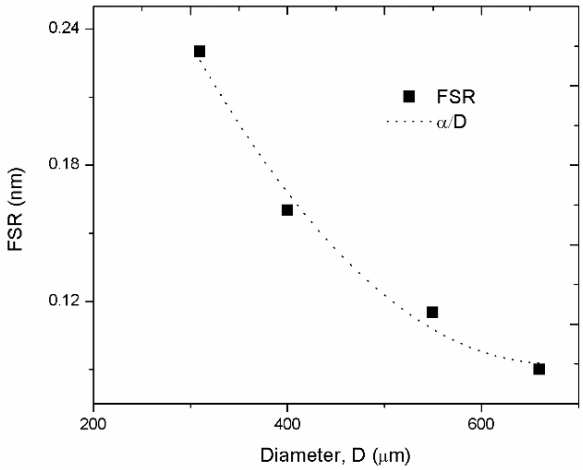

Figure 4.15 Relation between FSR and diameter

Figure 4.15 shows the relationship between the FSR value (experimentally determined by analysing the lasing spectrum) and the diameter of hollow fiber. It is well fitted by a α/D function, where α is a constant. The observed and calculated FSR of WGM spectrum for different diameter DDHPOFs are shown in table 4.1. The calculated value of FSRs can be estimated using Eqn 4.6. From the table a close agreement between the observed FSR and calculated values is observed. This observation is a clear evidence for the observed fine structures in the emission spectra which are resonant modes of the cavity formed by the cylindrical surfaces of the dye doped polymer optical fiber [62]. From the table it is also observed that the FWHM of the WGMs decreased from 0.09 to 0.05 nm with an increase in the diameter of DDHPOFs, but the magnitude of decrease become smaller. These results indicate that the presence of cylindrical microcavity, suppresses the excitation of random modes and the resonant conditions of lasing modes are mostly dependent on the geometry of the cylindrical microcavity [56].

Table 4.1 The total number of modes, FWHM of modes, Observed and calculated FSR of WGMs for different diameter DDHPOFs

Diameter (D) (μm)	Calculated FSR (nm)	Observed FSR(nm)	Number of modes	FWHM of modes (nm)
310 ± 2	0.23	0.23 ± .03	15	0.09
400 ± 2	0.16	0.16 ± .02	20	0.07
550 ± 2	0.12	0.12 ± .01	32	0.06
660 ± 2	0.09	0.09 ± .01	36	0.05

A measure of an optical resonator or cavity's ability to confine light of a given wavelength, λ_0 is usually expressed in terms of a Q-value which can be measured using equation 4.3. We have estimated the microlaser Q-value to be about 1×10^4 for 400 μm DDHPOF. The high Q-value in addition to the low

threshold, results in narrow laser emission lines. The evaluated Q-value from different diameter DDHPOFs shows strong wavelength dependence.

4.8 Pumping scheme dependent WGM emission

In this section, we have analysed pumping scheme dependent laser emission from Rh6G dye doped DDHPOF, with an outer diameter of 280 μm, inner diameter of 120 μm and a length of 5 cm. For this analysis, the pump beam was focussed onto the DDHPOFs either by a convex lens (figure 4.16 left inset) or by a cylindrical lens (figure 4.17 left inset). The pumping scheme is very much significant in practical applications, especially for optimizing the life of solid state dye gain media [63].

4.8.1 Spot Illumination Technique

When the pump beam is focussed into the DDHPOF with the help of a convex lens, the entire light is concentrated on a single point (~0.1 mm). Hence the power density at the focused point is very high. This leads to the excitation of only a few dye molecules to higher energy bands which can de-excite with an emission. The emitted light from this point gets propagated to other regions of the fiber. As a result, the short wavelength emission from dye molecules gets absorbed by itself and is re-emitted at longer wavelength due to stokes shift. When the pump power is increased the emission spectrum shows a line narrowing (due to amplified spontaneous emission (ASE)) [64]. With an increase in pump power, the molecules absorb more energy and hence the emission from these molecules can excite more of the neighbouring molecules which leads to a shift in the peak emission wavelength from 561 to 565 nm. That is, the red-shift is attributed to the absorption of shorter wavelength and emission from the neighbouring dye molecules at longer wavelengths. The red-shift and line narrowing as a function of pump power are depicted in figure 4.16. A clear line narrowing from 30 nm to 4 nm is observed when the

pump power is increased to 10 mW, above which no further line narrowing is observed due to gain saturation effect [64].

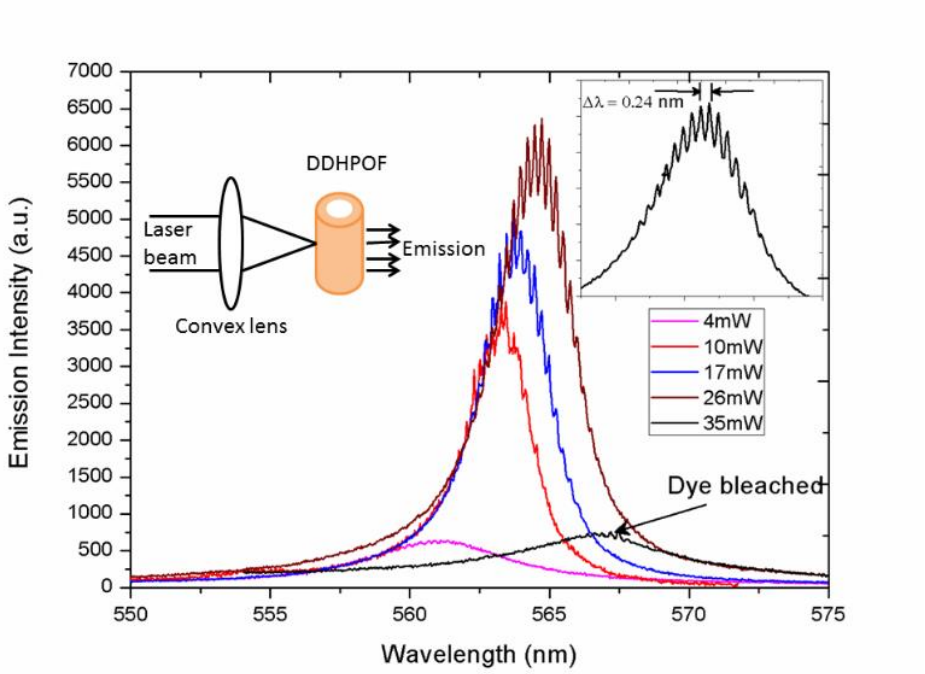

Figure 4.16 Emission spectrum from DDHPOF as a function of pump power by spot illumination technique and right inset shows the expanded modes at 26 mW.

At a threshold pump power, P_{th}, laser emission with multimode structures emerges as depicted in figure 4.16. This threshold behaviour of the laser peak intensity provides a clear signature of lasing. The expanded mode structure is clearly shown in figure 4.16 (right inset). From the equation 4.5, we get the mode spacing as 0.24 nm, which is the same as the observed mode spacing (figure 4.16). The strongest mode at 564.9 nm has an FWHM of 0.1 nm.

By focussing the pump power with a convex lens, the pump power density on the focussed point is very much higher. Hence, when the pump power is increased beyond a certain threshold (bleaching threshold), the dye molecules start to degrade, leading to bleaching of dye as depicted in figure 4.16. After bleaching of dye molecules, the emission shows a random behaviour, in terms

of observed emission intensity (figure 4.16 and 4.20), peak wavelength (figure 4.18) and FWHM (figure 4.19).

4.8.2 Stripe illumination

By using cylindrical lens, the pump power is focussed as a stripe of length 10 mm and approximately 0.5 mm width. Here the power density of focussed beam is very much smaller as compared to focussing by a convex lens. i.e. the interaction area between the pump radiation and dye molecules is very much larger. Hence large number of dye molecules could be excited simultaneously to higher energy bands and de-excite with an emission. However, the average power absorbed by each dye molecule is very small as compared to spot illumination (with the same pump power). Due to this, each molecule will de-excite at a longer wavelength. When the pump power is increased, the radiative transition probability gets enhanced at shorter wavelength side of the spectrum creating a shift in the spectrum towards the blue side [65]. As the pump power increases from 5 to 34 mW, it can be seen that the emission spectrum get shifted from 568 to 564 nm. The blue-shift and line narrowing as a function of pump power are presented in figure 4.14, 4.15 and 4.16. As the pump power is increased, a clear spectral narrowing is observed coupled with this blue shift. At a certain threshold pump power, narrow lines begin to emerge out of this emission spectrum, indicative of microring lasing [65-66]. The line narrowing is due to the fact that the number of modes for which the intensity above the threshold decreases because of the energy transfer from low power modes (longer wavelengths) to those lying nears the emission peak [64].

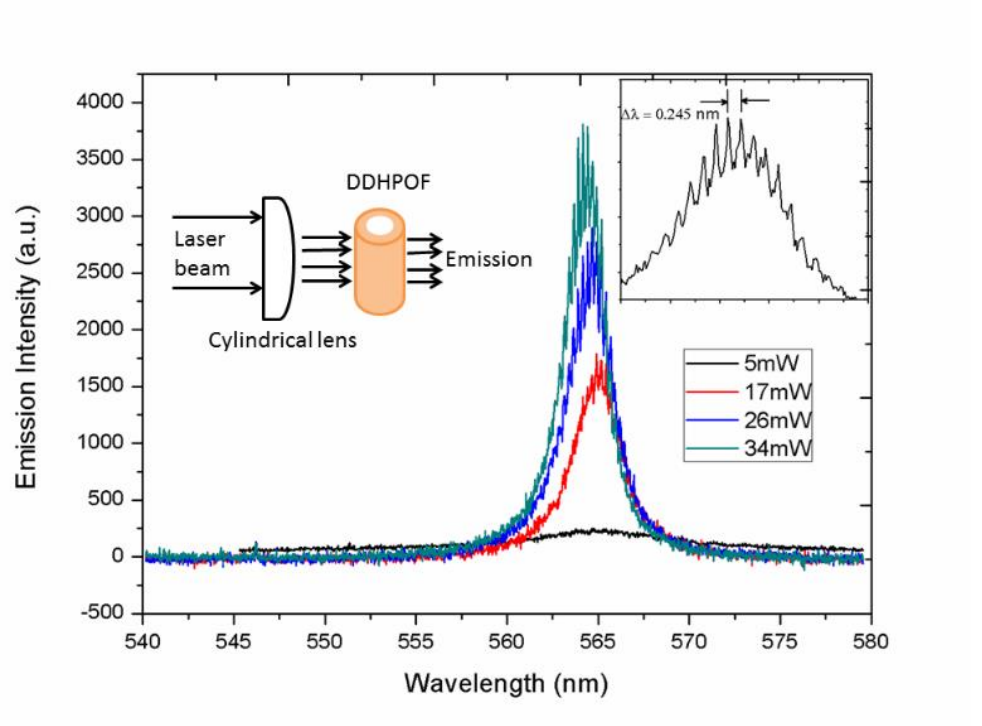

Figure 4.17 Emission spectrum from DDHPOF as a function of pump power by stripe illumination technique and right inset shows the expanded modes at 26 mW.

In other words, when the pump power is increased above the threshold (P_{th}), there can be a decrease in the average wavelength of the spectrum (λ_{av}). The average wavelength is defined as [66],

$$\boldsymbol{\lambda_{av}} = \frac{\int_{-\infty}^{\infty} \boldsymbol{\lambda}\, \boldsymbol{P(\lambda) d\lambda}}{\int_{-\infty}^{\infty} \boldsymbol{P(\lambda) d\lambda}} \qquad \textbf{4.23}$$

i.e. as the pump power is increased, the gain in the proximity of the peak wavelength of the emission cross section is larger, which produce a relative blue shift towards the maximum of the emission cross section. In the case of an inhomogeneous medium (dye), the gain at any wavelength is equal to the product of stimulated emission cross section and population density difference, i.e,

$$\boldsymbol{g_{\lambda}^{D}} = \boldsymbol{\Delta N_{ul}\, \sigma_{ul\,(\lambda)}^{D}} \qquad \textbf{4.24}$$

where g_{λ}^{D} is the gain at any wavelength, $\sigma_{ul\,(\lambda)}^{D}$ is the stimulated emission cross section and ΔN_{ul} is the population density difference. In the case of stripe illumination, a large number of dye molecules are involved in the emission process, hence the population density difference is higher for higher pump power. This will enhance the gain in the proximity of the peak wavelength of the emission cross section, which in turn leads to a relative blue shift (from 568 to 564 nm) in the emission spectrum towards the maximum of emission cross section (in our case ~564 nm). Further increase in pump power does not show any blue shift in the emission spectrum and this can be attributed due to gain saturation. Similar types of relative blue shift towards the peak of emission cross section have been observed with an increase in pump power in various other studies [64,66-68] also.

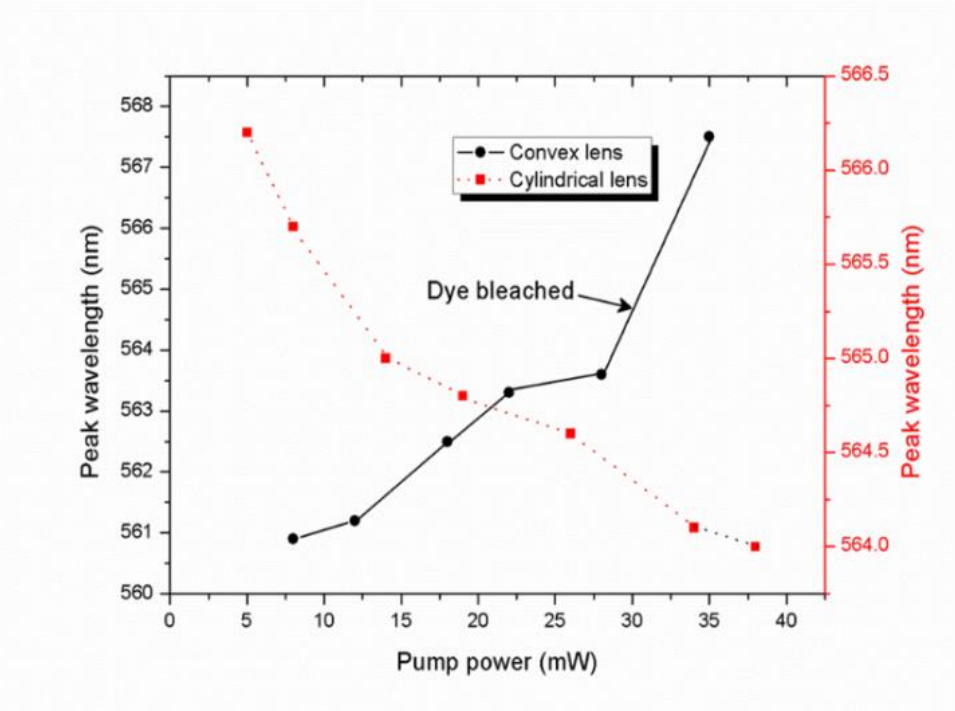

Figure 4.18 Shift in peak wavelength as a function of pump power.

To confirm the laser action in DDHPOF, the dependence of emission intensity on pump power is also studied. As shown in figure 4.20, clear

threshold behaviour can be observed. When the pump power is below the threshold, the output intensity increases very slowly (small dotted line in figure 4.20) and the emission spectrum is broad. Once the pump power is above threshold, output intensity changes dramatically (solid line in figure 4.20).

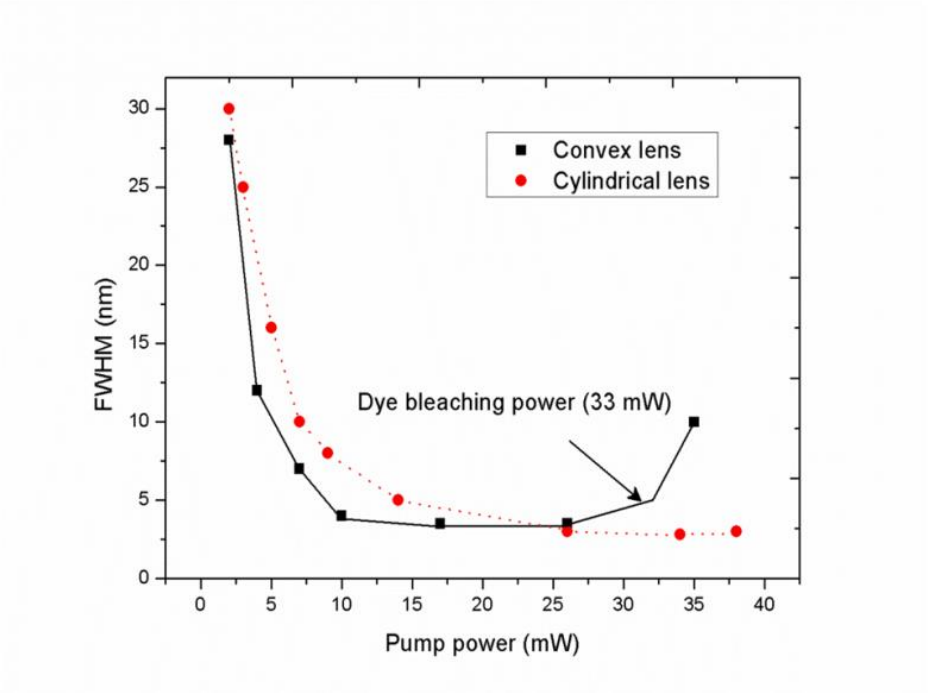

Figure 4.19 Line narrowing as a function of pump power (when the pump beam is focussed with convex and cylindrical lens

When pumping beam is focussed with a convex lens, the emission intensity shows much more pronounced threshold behaviour than in the case of cylindrical lens focussing. The pump threshold power, P_{th}, can be estimated from the corresponding light-light curves (figure 4.20). In the case of pumping beam focused with the convex lens the threshold is 10 mW in the place of 15 mW for cylindrical lens focusing and also the slope efficiency of the curve is enhanced by more than 3 times. This is also evident from the enhanced line narrowing for the convex lens focussing for any given pump power as shown

in figure 4.16. For a constant pump power, the power densities available for the two geometries are different. Higher power densities available using convex lens leads to emission at shorter wavelengths which subsequently shifts to larger wavelengths resulting in a red shift due to reabsorption as the pump power is increased. In the case of stripe illumination, lower power densities results in the emission at longer wavelengths which shifts to smaller wavelengths (blue shift) with increase in pump power. Hence in the present studies, at a particular pump power the peak emission wavelength in the two geometries coincide with one another.

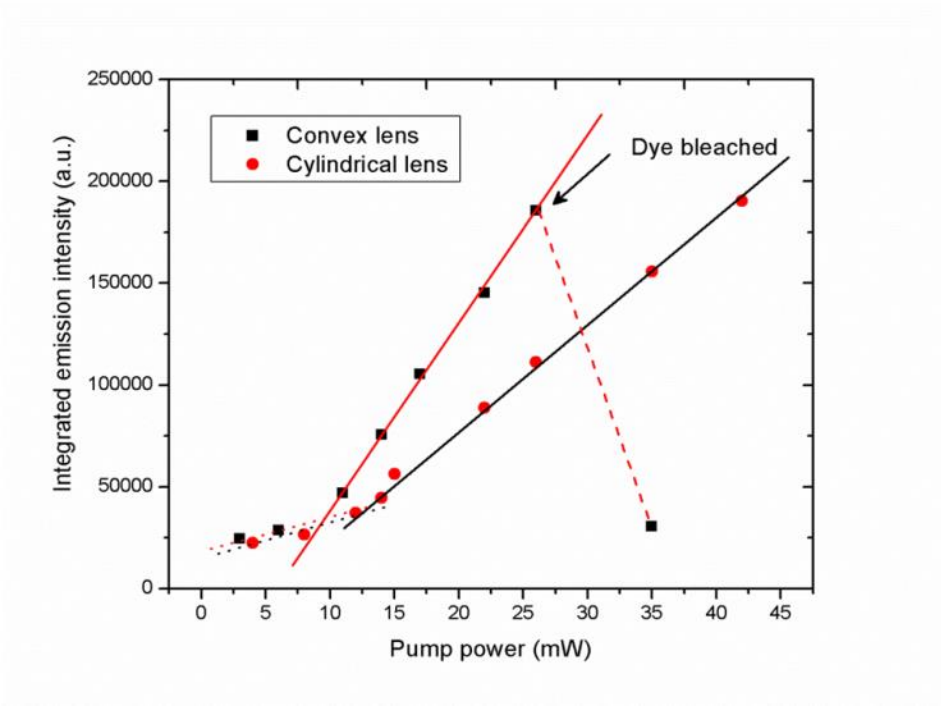

Figure 4.20 Integrated emission intensity from DDHPOF as a function of pump power for cylindrical and convex lens focussing

From the figure 4.16 and 4.17 inset, the measured mode spacing is ~0.24 nm. i.e. the mode spacing of the WGM laser emission from the DDHPOFs does not depend on the pumping scheme, but it depends on the type of dye doped in the fiber, refractive index of the fiber material and fiber diameter.

Photostability of DDHPOFs mainly depends on the pumping scheme and pump power. Due to higher power density, spot illumination will lead to quicker degradation of dye molecules as compared to stripe illumination. Hence pumping scheme plays a significant role in solid-state dye laser systems.

4.9 Conclusions

In this chapter we discuss a well resolved whispering gallery mode (WGM) laser emission from a free standing microring cavity based on dye doped hollow polymer optical fiber (DDHPOF), which is transversely pumped by a pulsed Nd:YAG laser. Different diameter cylindrical microcavity lasers have been fabricated and their performances have been evaluated. We observed that the resonant modes from cavities are well resolved WGMs. The microring laser was characterized by a well-defined, low threshold pump power at which the emission spectrum dramatically changes and collapses into several dominant microcavity laser modes with reduced mode spacing and high Q - value. Resonant modes are excited inside the gain medium which is strongly confined along the radial direction so that the spacing of lasing modes is controlled by the diameter of the cylindrical microcavity. A variation in the FSR from 0.23 to 0.09 nm is observed with an increase in the diameter of DDHPOF from 310 to 660 μm. It is also found that whispering gallery lasing envelope is shifted from 559 to 571 nm (Stokes shift) with the diameter. Two different pumping schemes have also been used for the characterization of WGM laser emission from DDHPOF. By spot illumination technique, the slope efficiency of the microcavity is enhanced by more than three times than the stripe illumination technique.

References

1 A. Einstein, “Zur Quantentheorie der Strahlung,” Physikal. Z. 18, 121–128 (1917).

2 R. Ladenburg, “Untersuchungen über die anomale Dispersion angeregter Gase,” Z. Phys. 48, 17–25 (1928).

3 N. G. Basov and A. M. Prokhorov, “3-level gas oscillator,” Zh. Eksp. Teor. Fiz. 27, 431–438 (1954).

4 J. P. Gordon, H. J. Zeiger, and C. H. Townes, “Molecular microwave oscillator and new hyperfine structure in the microwave spectrum of NH3,” Phys. Rev. 95, 282 (1954).

5 A. L. Schawlow and C. H. Townes, “Infrared and Optical Masers,” Phys. Rev. 112, 1940 (1958).

6 T. H. Maiman, “Stimulated Optical Radiation in Ruby,” Nature 187, 493–494 (1960).

7 A. Javan,W. R. Bennett, and D. R. Herriott, “Population Inversion and Continuous Optical Maser Oscillation in a Gas Discharge Containing a He-Ne Mixture,” Phys. Rev. Lett. 6, 106 (1961).

8 H. Kroemer, “A proposed class of hetero-junction injection lasers,” In Proc. IEEE, 51, 1782 – 1783 (1963).

9 C. K. N. Patel, “Continuous-Wave Laser Action on Vibrational-Rotational Transitions of CO2,” Phys. Rev. 136, A1187 (1964).

10 F. P. Sorokin and J. R. Lankard, “Stimulated Emission Observed from an Organic Dye, Chloro-aluminum Phthalocyanine,” IBM J. Res. Dev. 10, 162 (1966).

11 F. P. Schäfer, “Organic Dye Solution Laser,” Appl. Phys. Lett. 9, 306 (1966).

12 N. G. Basov, V. A. Danilychev, Y. Popov, and D. D. Khodkevich, “Laser Operating in the Vacuum Region of the Spectrum by Excitation of Liquid Xenon with an Electron Beam,” Zh. Eksp. Fiz. i Tekh. Pis’ma. Red. 12, 473–474 (1970).

13 Vahala K J. Optical Microcavities. Singapore: World Scientific, 2004.

14 Vahala K J. Optical microcavities. Nature, 2003, 424(6950): 839– 846.

15 P. Rabiei, W. H. Steier, C. Zhang and L. R. Dalton, “ Polymer micro-ring filters and modulators”, J. Lightwave Technol 20, 1968-1975 (2002).

16 H. C. Tapalian, J. P. Laine and P. A. Lane, “Thermo optical switches using coated microsphere resonators”, IEEE Photonic Tech L, 14, 1118-1120 (2002).

17 Q. Xu and M. Lipson, “All-optical logic based on silicon micro-ring resonators”, Opt. Express 15, 924-929 (2007).

18 F. Vollmer and S. Arnold, “Whispering-gallery-mode biosensing: label-free detection down to single molecules”, Nat. Methods 5,591-596 (2008).

19 T. J. Kippenberg and K. J. Vahala, “Cavity Opto-Mechanics,” Opt. Express 15,17172-17205 (2007).

20 F. Marquardt, “Optomechanics: Push towards the quantum limit,” Nat. Phys. 4, 513-514 (2008).

21 I. Wilson-Rae, N. Nooshi, W. Zwerger, and T. J. Kippenberg, “Theory of Ground State Cooling of a Mechanical Oscillator Using Dynamical Backaction,” Phys. Rev. Lett. 99, 093901(2007).

22 D. W. Vernooy, A. furusawa, N. P. Georgiades, V. S. Ilchenko, and H. J. Kimble, “Cavity QED with high whispering gallery modes,” Phys. Rev. A 57, R2293 (1998).

23 M. Pollinger and A. Rauschenbeutel, “All-optical signal processing at ultra-low powers in bottle microresonators using the Kerr effect,” Opt. Express 18, 17764-17775 (2010).

24 J. Schafer, J. P. Mondia, R. Sharma, Z. H. Lu, A. S. Susha, A. L. Rogach, and L. J. Wang, “Quantum dot microdrop laser,” Nano Lett. 8, 1709-1712 (2008).

25 R. Sharma, J. P. Mondia, J. Schafer, Z. H. Lu, and L. J. Wang, “Effect of evaporation on blinking properties of the glycerol microdrop Raman Laser,” J. Appl. Phys.105, 113104 (2009).

26 M. Pelton and Y. Yamamoto, “Ultralow threshold laser using a single quantum dot and a microsphere cavity,” Phys. Rev. A 59, 2418 (1999).

27 P. Del’ Haye, A. Schliesser, O. Arcizet, T. Wilken, R. Holzwarth, and T. J. Kippenberg, “Optical frequency comb generation from a monolithic microresonator,” Nature 450, 1214-1217 (2007).

28 A. A. Savchenkov, A. B. Matsko. V. S. I1chenko, and L. Maleki, “Optical resonators with ten million finesse,” Opt. Express 15, 6768-6773 (2007).

29 J. C. Knight, H. S. T. Driver, and G. N. Robertson, “Morphology dependent resonances in a cylindrical dye microlaser: Mode assignments, cavity Q values and critical dye concentrations”, J. Opt. Soc. Am. B 11, 2046 (1994).

30 N. Tessler, G. J. Denton, and R. H. Friend, “Lasing from conjugated-polymer microcavities; Nature 383, 695-697 (1996).

31 V. B. Braginsky, M. L. Gorodetsky and V. S. Ilchenko, “Quality-factor and nonlinear properties of optical whispering gallery modes”, Phys Lett A, 137, 393-397 (1989).

32 J. Ward and O. Benson: WGM microresonators: sensing, lasing and fundamental optics with microspheres, Laser Photonics Rev. 5, No. 4, 553–570 (2011) / DOI 10.1002/lpor.201000025.

33 Lord Rayleigh, “The problem of whispering gallery”, Phil. Mag. 20, 1001 (1910).

34 G. Mie, “Beitrage Zur Optik truber Medium, speziell Kolloidaler Metallosungen”, Ann. Phys. 330, 377-445 (1908).

35 H. C. Vande Hulst, “Light scattering by small particles” (Peter Smith Pub Ins, 1982).

36 P. W. Barber and R. K. Chang, Optical effects associated with small particles (World Scientific, 1988).

37 C. F. Bohren and D. R. Huffman, "Absorption and scattering of light by small particles (Wiley-VCH, 1988).

38 C. Yeh, F. Shimabukuro, "The Essence of Dielectric Waveguides", Springer: New York, NY, USA, pp. 165-167 (2008).

39 J. Heebner, R. Grover, T. Ibrahim, "Optical Microresonators: Theory, Fabrication, and Applications", Springer: New York, NY, USA, pp. 39-41(2008).

40 Wei Tan, Lei Shi and Xianfeng Chen, "Modeling of an Optical Sensor Based on Whispering Gallery Modes (WGMs) on the Surface Guiding Layer of Glass Filaments", Sensors 8, 6761-6768 (2008); DOI: 10.3390/s8106761.

41 Ming Huang, Jingjing Yang , Sun Jun , Shujuan Mu and Yaozhong Lan, "Simulation and Analysis of a Metamaterial Sensor Based on a Microring Resonator", Sensors 11, 5886-5899 (2011); doi:10.3390/s110605886.

42 J. J. Yang, M. Huang, and J. Sun, "Double negative metamaterial sensor based microring resonator", IEEE Sensors Journal, Vol. 11, No. 10, October 2011.

43 Sindy K. Y. Tang, Ratmir Derda, Qimin Quan, Marko Lončar, and George M. Whitesides "Continuously tunable microdroplet-laser in a microfluidic channel" , OPTICS EXPRESS Vol. 19, No. 3 / 2215 (2011).

44 S. Yokoyama, T. Nakahama, and S. Mashiko, "Amplified spontaneous emission and laser emission from a high optical-gain medium of dye-doped dendrimer", J. Luminecsence, 111, 285-290 (2005).

45 K. Geetha, M. Rajesh, V.P.N. Nampoori, C.P.G. Vallabhan and P. Radhakrishnan, "Laser emission from transversely pumped dye-doped free-standing polymer film", J. Opt. A: Pure Appl. Opt. 8, 189-193. (2006).

46 M. Kuwata-Gonokami, R. H. Jordan, A. Dodabalapur, H. E. Katz, M. L. Schilling, and R. E. Slusher, "Polymer microdisk and microring lasers", Opt. Lett. 20, 2093 (1995).

47 Y. Yamamoto and R. Slusher, "Optical processes in microcavities", Phys. Today 46, 66 (1993).

48 T. Grossmann, S. Scheleede, M. Hauser, M. B. Christiansen, C. Vannahme, C. Eschenbaum, S. Klinkhammer, T. Beck, J. Fuchs, G. U. Neinhhaus, U. Lemmer, A. Kristensen, T. Mappes, ans H. Kalt, "Low-threshold conical microcavity dye lasers", Appl. Phys. Lett. 97, 063304 (2010).

49 S. I. Shopova, R. Rajmangal, S. Holler, and S. Arnold, "Plasmonic enhancement of a whispering-gallery-mode biosensor for single nanoparticle detection", Appl. Phys. Lett. 98, 243104 (2011).

50 J. Silverstone, S. McFarlane, C. Manchee, and A. Meldrum, “Ultimate resolution for refractometric sensing with whispering gallery mode microcavities”, Opt. Lett. 20, 8284 (2012).

51 G. S. Murugan, J. S. Wilkinson, and M. N. Zervas, “Optical excitation and probing of whispering gallery modes in bottle microresonators: potential for all-fiber add–drop filters”, Opt. Lett. 35, 1893 (2010).

52 F. Monifi, J. Friedlein, S. K. Ozdemir, and L. Yang, “A robust and tunable add–drop filter using whispering gallery mode microtoroid resonator”, J. Lightwave Technol. 30, 3306 (2012).

53 M. Kailasnath, V.P.N. Nampoori and P. Radhakrishnan, “A microring multimode laser using hollow polymer optical fibre”, PRAMANA Vol. 75, 5 (2010).

54 K. Vahala, “Optical microcavities” Nature (London) 424, 839 (2003).

55 M. Sheeba, K.J. Thomas, M. Rajesh, V.P.N. Nampoori, C.P.G. Vallabhan, and P. Radhakrishnan, “Multimode laser emission from dye doped polymer optical fiber”, Applied Optics 46, 33 (2007).

56 C. L. Linslal, S. Mathews, P. Radhakrishnan, V. P. N. Nampoori, C. P. Girijavallabhan and M. Kailasnath, “Laser emission from the whispering gallery modes of a graded index fiber ”, Optics Letter 38, 18 (2013).

57 M. Heiblum and J. H. Harris, I "Analysis of curved optical waveguides by conformal transformation", IEEE J. Quantum Electron. QE-11, 75 (1975).

58 J. C. Knight, H. S. T. Driver, and G. N. Robertson, “Morphology-dependent resonances in a cylindrical dye microlaser: mode assignments, cavity Q values, and critical dye concentrations”, J. Opt. Soc. Am. B 11, 2046 (1994).

59 S. V. Frolov, M. Shkunov, Z. V. Vardeney, K. Yoshino, “Ring microlasers from conducting polymers”, Phys. Rev. B, 56, 4363, (1997).

60 Qinghai Song, Liying Liu, and Lei Xu, “Lasing action in dye doped polymer nanofiber knot resonator”, Journal of Light Wave Technology, 27 19 (2009).

61 H. Zhu, S. F. Yu, and W.F. Zhang, “Quasi-guiding Modes in Microfibers on a High Refractive Index Substrate”, Appl. Phys Lett 99, 043102 (2011).

62 Jaison Peter, C. P. G. Vallabhan, P. Radhakrishnan, V. P. N. Nampoori, and M. Kailasnath, “Microring lasing from a dye-doped polymer-coated silica fiber”, Laser Phys. 23, 115104 (2013).

63 E. De. La Rosa-Cruz, C. W. Dirk, O. Rodriguez and V. M. Castano. Fiber and Integrated Optics 20 (5), 457-464, (2001).

64 M. Rajesh, M. Sheeba, K. Geetha, C. P. G. Vallabhan, P. Radhakrishnan, and V. P. N. Nampoori. “Fabrication and characterization of dye-doped polymer optical fiber as a light amplifier”, Appl. Optics 46 (1), (2007).

65 Gernot Wirnsberger and G. D. Stucky, “Microring lasing from dye-doped silica/block coplymer nanocomposites”, Chem. Mater 12, 2525-2527, (2000).

66 Jon Arrue, Felipe Jimenzes, Igor Ayesta, M. Asuncion Illarramendi and Joseba Zubia, Polymer-optical-fiber lasers and amplifiers doped with organic dyes", Polymers 3, 1162-1180, (2011).

67 H. Z. Wang, F. L. Zhao, Y. J. He, X. G. Zheng, X. G. Huang, M. M. Wu, "Low-threshold lasing of a Rhodamine dye solution embedded with nanoparticle fractal aggregates", Opt. Lett. 23, 777-779, (1998).

68 S. Y. Lam, M. J. Damzen, "Characterisation of solid-state dyes and their use as tunable laser amplifiers", Appl. Phys. B, 77, 577-584, (2004).

Chapter 5
Unidirectional laser emission from a deformed annular cylindrical microcavity

"The science of today is the technology of tomorrow"
Edward Teller

Abstract

We report multimode laser emission from symmetric (SRC) as well as asymmetric resonant cylindrical (ARC) microcavity based on a rhodamine B dye doped hollow polymer optical fiber by transverse pumping. An SRC can provide a circularly symmetric whispering gallery mode (WGM)-like laser emission from its surface with a quality factor (Q) of ~1.2×10^4, while an ARC supports a strongly chaotic internal ray dynamics, which will in turn lead to an anisotropic emission with a lower Q of ~8×10^2 with a far field divergence of about 20˚ in the plane of the cavity.

We also observed two different sets of resonant laser modes: namely, fundamental whispering gallery high Q modes (HQMs) and leaky unidirectional low Q modes (LQMs) from asymmetric hollow polymer optical fibers.

The major content of this chapter has been communicated to "Journal of Luminescence" and "Optics Letter".

5.1 Introduction

Optical microcavities have attracted extensive research interest [1-3], not only for fundamental physics investigations [4] such as cavity quantum electrodynamics (c-QeD) and non-linear optics but also for potential applications in novel light sources, active filters in optics communication [2], photonic sensing devices for label free detection [5] and so on. A symmetric resonant cylindrical (SRC) polymer microcavity provides excellent coupling of spontaneous emission into lasing modes, and a high Q which consequently leads to low lasing thresholds [6]. Polymer materials have been found to be very attractive both from the technical and economical point of view with their low cost, ease of engineering, high optical quality and good chemical/biological compatibility. In general, almost all the microcavities have rotational symmetric boundary. Owing to the rotational symmetry, circulating light is confined via total internal reflection at the interface between the cavity wall and surrounding medium and only possible way of light loss from such cavity is through the evanescent leakage. Constructive interference occurs under these conditions, allowing the circulating intensity to grow until the rate at which it is lost. This phenomenon is referred to as resonance, and the path resonant light takes is called the mode. The resonant modes in such a circular/cylindrical shaped microcavities are termed as whispering gallery modes (WGMs). The high quality factor available plays the central role in various applications of such microcavities. There could be a variety of applications of microcavity lasers that have a few modes if they are stable and controllable [7]. However, the laser emissions from these types of microcavities are isotropic due to the rotational symmetry, which seriously limits their applications in a number of areas. For instance, an SRC cannot provide a controlled and stable directional emission or adequate output power

in the desired direction, thereby resulting in an unavoidable low efficiency of output couplings.

The above problem can effectively be overcome by selectively breaking the rotational symmetry of microcavities. In principle, any microcavity with broken rotational symmetry has directional emission. Nockel and Stone [8] have initially pointed out that a deformation of the cavity lead to partially chaotic ray dynamics and highly anisotropic emission. They also describe that, any deformation of the microcavity will leading to a significant modification of the evanescent leakage orientation from WGMs and appear as strongly directional distribution of output fields instead of the isotropic emissions, though the Q-factors are significantly spoiled. These types of the broken symmetry microcavity are generally known as deformed cavity or asymmetric resonant cavity (ARC). Also the deformed microcavities have rich physics related to quantum chaos-assisted tunneling, dynamical localization etc. The combination of the tunability and high efficiency of laser dyes [9] along with a unidirectional laser emission and high power density under certain deformation would be much desirable for integrated organic optoelectronic devices.

A small deformation on the cavity will generate a chaotic ray motion, but it is not fully chaotic, and will still have stable periodic orbits. However, breaking of symmetry allows the creation of favorable coupling points (leaky region) along the perimeters of the resonators [10-11]. These coupling points act as directional emission points for a deformed cavity, where the condition of total internal reflection is not fulfilled any longer. The far field profile of such cavity is determined by the path in phase space that the rays take to escape from the cavity through such coupling points. Hence the boundary shape and degree of deformation have significant role on the emission characteristics of such microcavities.

5.2 Experimental setup

In this work we have used 10 cm length of Rh B dye doped symmetric (SRC) as well as asymmetric (ARC) hollow polymer (PMMA) optical fiber with an outer diameter (D) of 660 μm and inner diameter (d) of 290 μm, which is having a refractive index of 1.49. In the previous paper [12], we reported a detailed explanation for the fabrication of the dye doped hollow polymer optical fiber. To realize an ARC, we have been used a bend Teflon rod instead of a straight one.

Right inset of figure 5.1 illustrates a schematic diagram of the experimental setup. Both polymer microcavities were transversely pumped individually using 10 ns pulses from a frequency doubled Nd: YAG laser (532 nm, 10 Hz). A set of calibrated neutral density filters were used for varying the pump power. The beam was focused onto the sample with the help of a convex lens with a focal length of 7.5 cm. The laser emission in the radial direction was collected using a collecting fiber, which was kept on a translator so as to enable the movement of the collecting fiber from the microcavity in the X-direction as well as along the microcavity in the Z-direction. The laser emission collected by the receiving fiber was directed to a 0.5m spectrograph (SpectraPro-500i) coupled with a cooled CCD array with a resolution of 0.03 nm. It was possible to detect the laser emission due to the whispering gallery modes (WGM) from the microcavities [12-14] using this arrangement.

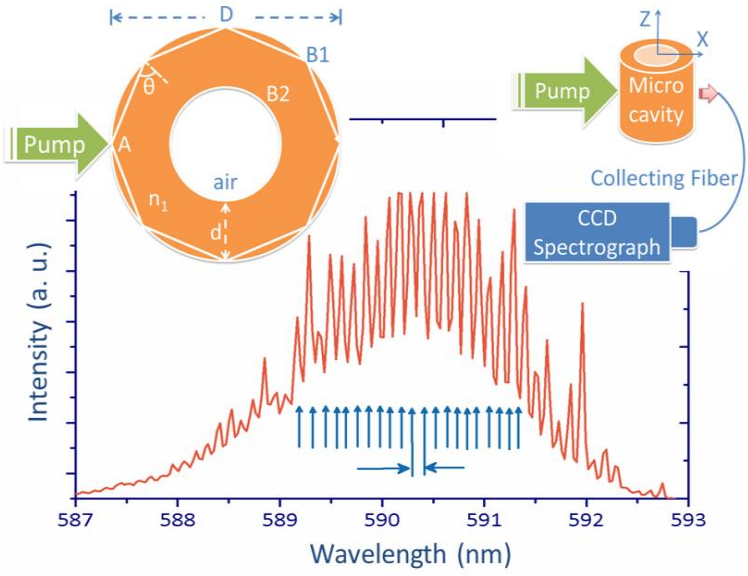

Figure 5.1 Typical output spectrum for a symmetric resonant (SRC) cylindrical microcavity having D = 660 µm and d = 290 µm. Left inset: schematic diagram of different regions in an SRC cavity with WGM resonance. Right inset: shows the schematic of experimental setup.

5.3 Section I:

5.3.1 Ray dynamics of SRC cavity

Viewed in ray optics, optical whispering gallery modes (WGMs) in the circular dielectric cavities can be easily understood with the concept of total internal reflection. The left inset of figure 5.1 shows that a ray emits from the point A with an incident angle θ ($\sin\theta > 1/n_1$, where n_1 is the refractive index of the cavity material) will be continually totally reflected on the cavity boundary due to rotational symmetry. After finite reflections, the ray returns to the point A without any change in phase, and the propagating field undergoes constructive interference with itself. In a microcavity, only a few numbers of wavelengths of light can fit around the edges of the circular dielectric cavity which leads to discrete modes in the cavity, known as WGMs. That is, lasing occurs at those frequencies that meet circumferential resonance conditions [13]. The Free-spectral range (FSR) of WGMs in cavities with rotational

symmetry can be theoretically estimated by equation 4.5. From the equation the evaluated value is 0.112 nm and our measurement gives an average value of $\Delta\lambda$ to be 0.11 nm which is in good agreement with theory.

The outer boundary diameter, D is much higher than inner boundary diameter, d and the structure of resonance mode is the same as that of the single boundary circular cavity. That is, WGMs are the only possible resonance modes.

Basically, strong light confinement of the WGMs in the dielectric microcavities is given by the total internal reflection and only a small evanescent leakage due to boundary curvature is a possible way of light loss. In SRC, the angle of incidence 'θ' is conserved at each collision and escape occurs isotropically by the exponentially slow process of evanescent leakage. While these WGMs reside mostly inside the cavity, a small portion extends to the outside in the form of evanescent wave (EW) [15]. The WGM emission from such cavity is mainly through surface and the usable power from surface emitting laser is small due to power is spreading to 360˚. Efficiently couple light out from such cavity generally requires an external evanescent wave elements, such as prisms [16], side polished fibers [17], and tapped fibers [18].

5.3.2 Simulations of SRC

Numerical simulation of SRC can be done by using COMSOL Multiphysics software package. A simulation model of the SRC is illustrated in figure 5.2 (a) and 5.2 (b) shows visualization of normal electric field distribution at the resonant frequency of f_r = 2.55534 e^{14} Hz and corresponding mode is considered as transverse magnetic (TM) mode. The resonant frequency spectrum and far-field profile is shown in figure 5.2 (c) and 5.2 (d) respectively.

For the sake of simplicity, the size of the proposed model is a much miniaturized version of the original microcavity. This model has an inner

hollow diameter (D_1) of 1 µm and outer ring material (D_2) of 2 µm with refractive index 1.5 as shown in figure 5.2 (a), with a far-field calculation boundary as shown in figure 5.2 (b). The PML (Perfect Matched Layer) boundary is set in the computational domain so as to avoid unwanted reflections in the calculation. The surface integration of the normal electric field along the ring provides the frequency versus normal electric field (shown in figure 5.2 (c)), which also represents the resonance spectrum of the ring. The input power is polarized perpendicular to the ring axis; the emission polarization of the electric field is oriented along a plane parallel to the fiber ring axis. From the resonance spectrum, one could observe that the FSR of resonance modes are almost periodical for SRC. The far field emission pattern of resonance condition in figure 5.2 (d) shows that the emission is anisotropic.

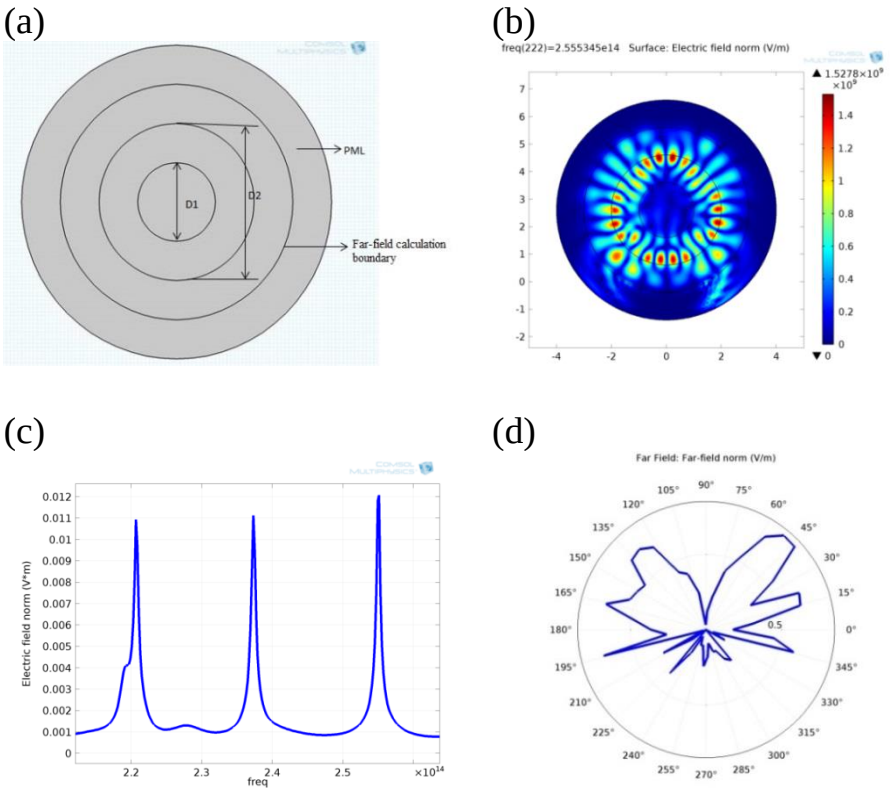

Figure 5.2 (a) Simulation modal (b) Electric field distribution (c) Resonance spectrum and (d) Far-field emission at resonant frequency from SRC.

5.4 Section II:

5.4.1 ARC cavity

To get a preferred directional (anisotropic) emission from a microcavity, the idea of breaking the rotational symmetry of WGM cavity was proposed by Nockel *et al.* [8]. Directional emission from asymmetric as well as elliptical whispering gallery resonators (WGRs) was also discussed by many researchers [19-21] in the beginning of 21st century. By breaking the symmetry in the shape of a microcavity provides control of both direction and intensity of light output without dramatically increase the laser threshold [22]. The deformed microcavity is also provides a significant modification of the evanescent leakage orientation for WGMs and provides a strongly directional distribution of output fields instead of the isotropic emission. Due to such anisotropic emission from an ARC cavity, the emission can easily be collected without the help of any external evanescent wave element. However, due to the deformation the evanescent leakage orientation from WGMs is very much high and consequently this will lead to escape of the photons that circulate within the cavity [23]. Those loss mechanisms broaden the resonance line-width and reduce the amount of light circulating inside the cavity, which in turn reduces the Q of WGMs with respect to SRCs. Therefore, the anisotropic optical modes in ARCs are rather leaky. Recently, many studies demonstrated that the emission directionality of deformed microcavities can be predicted theoretically by a ray dynamical calculation [20, 24-28]. With the increase of the deformation, the Q-factor exponentially decreases. This is due to the fact that the chaotic region increases with the deformation, and larger chaotic region will lead to easier escape from WGMs to the chaotic region by dynamical tunneling [29].

5.4.2 Ray optics analysis of ARC

Analyses of classical ray dynamics will lead to a better understand in the optical mode properties of a deformed microcavity, such as internal field pattern and emission directionality [30]. Ray model analysis in a deformed cavity is a sequential tunneling model in which optical power loss will occurs at each reflection due to Fresnal transmission and curvature of interface. This model could be improved by non-specular reflection as Goos-Hanchen effect (G-H) and Fresnel filtering (FF) [31-32]. According to ray picture of geometric optics, a light ray hits on a cavity boundary at an angle greater than critical angle will totally reflected on the interface. But in reality, the incident ray will be a beam, a bundle of rays with an angle of incidence 'θ_a' centered on a mean angle 'θ_i'. When θ_i is close to critical angle, the larger 'θ_i' experience total internal reflection, whereas the smaller 'θ_i' are refracted and hence the angle of reflected ray 'θ_r' is larger than original angle of incidence as shown in figure 5.3. This effect has been termed as FF [33].

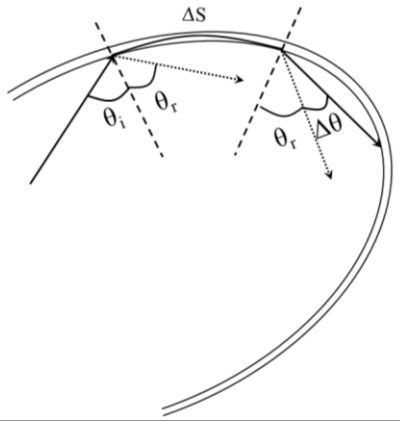

Figure 5.3 Shows generalized reflection law includes Goos-Hanchen (G-H) shift (ΔS) and an increase in the angle of the reflected ray from θr to 'θ+Δθ' (FF).

The shift in the starting position of the reflected ray along the surface is mainly due to the G-H effect. The shift in range of incident angle due to G-H effects will modify the average transmission coefficient for the ray. That is, the

G-H effect adds a small kick or lateral shift (ΔS) to the position variable of each bounce in phase space. Each kick contribute to small changes in 'sin θ' upon subsequent iterations of the deformed surface. Hence several cycle average of 'sin θ' will slowly vary with time, so that the cycle-average power loss rate of the trajectory is not constant.

5.4.3 Simulations of ARC

The Simulation model of the hollow asymmetric (elliptical) resonator (ARC) is illustrated in figure 5.4 (a), while figure 5.4 (b) shows the visualization of normal electric field distribution at the resonant frequency of f_r = 2.55534 e^{14} Hz. Figure 5.4 (c) shows the resonant frequency spectrum and 5.4 (d) shows its corresponding far-field profile.

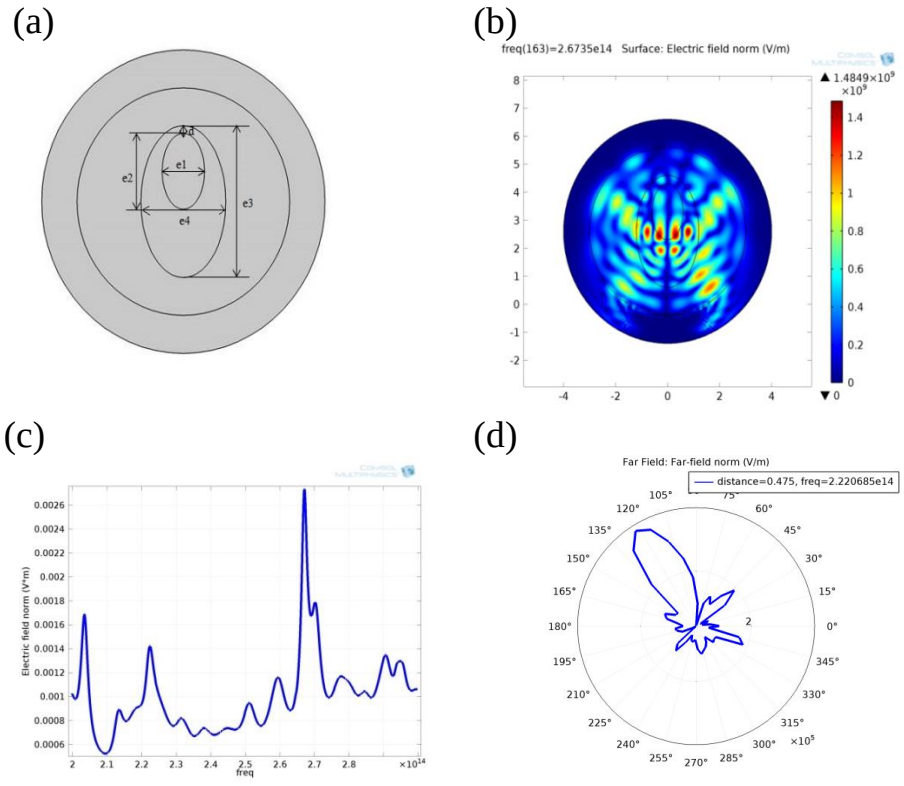

Figure 5.4 (a) Simulation modal (b) Electric field distribution (c) Resonance spectrum and (d) Directional far-field emission at resonant frequency from ARC.

The semi elliptical axis of the hollow resonator shown in figure 5.4(a) has the following dimensions. The inner hollow semi axis e_1 is 0.6 μm and e_2 is 1μm, and the dimensions of the outer hollow semi axis e_3 is 1.2 μm and e_4 equals 2 μm.

From the comparison of the fig 5.2 (d) and 5.4 (d) one could observe that the SRC cavity provide almost uniform emission in a plane, but ARC provide an enhanced directional emission in a plane. However both cavities do not provide an isotropic emission. From the electric field distribution pattern, one could observe that the field distribution is concentrated in some particular area of the ARC. This area can be found as bright scattering region due to highest curvature of the boundary. Far-field emission pattern in figure 5.4(d) shows that the emission is highly directional with a divergence angle less than 30˚.

5.5 Experimental results

In general, cylindrical microcavity resonance can drastically change the spontaneous emission spectrum of the active gain medium owing to the quantum electro-dynamic effect [34]. The left inset of figure 5.5 shows an enlarged view of the photograph of an ARC. The degree of deformation of such ARCs can be controlled during the fabrication of dye doped hollow polymer preform.

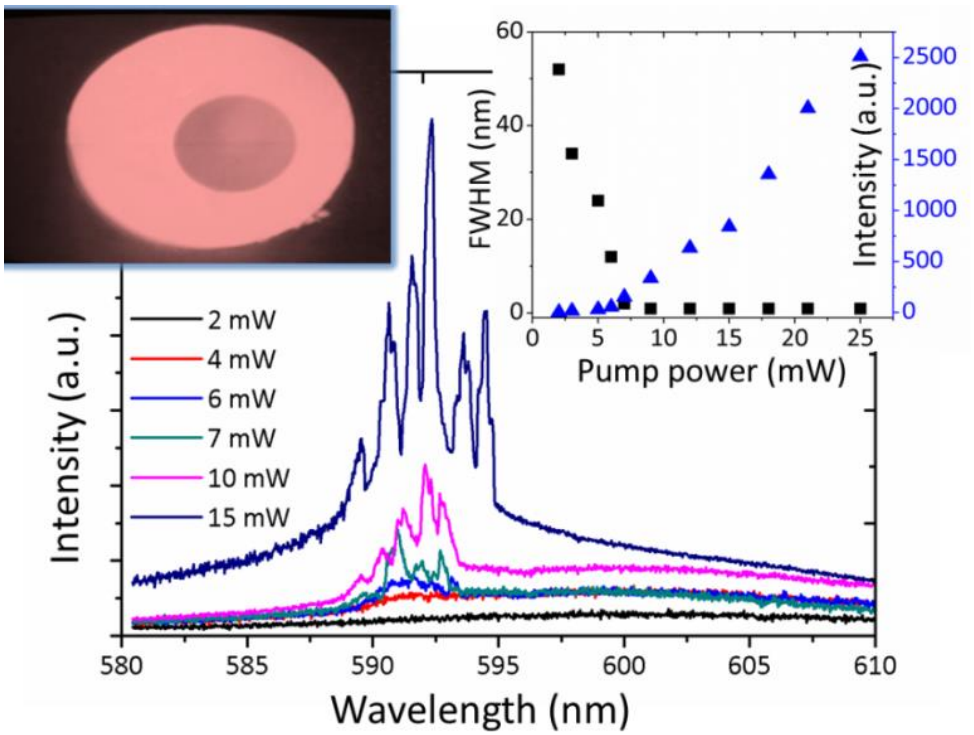

Figure 5.5 Emission spectra from an ARC at different pump power. Right inset shows the output intensity and FWHM of emission as a function of pump power (Laser threshold is indicated with arrow mark). Left inset shows the enlarged view of photograph of ARC taken in a CCD camera.

Dramatic change occurs in the ARC emission spectrum when excitation pump power, P exceeds the laser threshold pump power, P_{th}. At low P, only fluorescence spectrum was observed. As P increases, laser modes start to evolve from the broad spectrum. Further increase in pump power results in laser modes with most of the power confining itself into the modes having higher peak intensities. In this case the emission spectrum gets transformed into several dominant microcavity laser modes [11] as shown in figure 5.5. The guidance through the gain medium gave rise to intense narrow emission lines. Figure 5.5 right inset gives the full width half maximum and integrated emission intensity as a function of pump power. The laser threshold pump power was approximately 7 mW, at which drastic spectral narrowing and a sudden rising of output intensity are observed. The width of the highest peak

laser mode was about 0.8 nm; the corresponding Q was ~ 8×10^2, which is much smaller as compared to that of SRC (1.2×10^4) with same measuring conditions. Such broadening of laser modes is mainly attributed to the overlapping of multiple peaks with small mode spacing. However, the coherent radiation at cavity resonance dominates when the pump power level was above the lasing threshold and the spacing was essentially dictated by cavity resonance [35].

Breaking of rotational symmetry of the cavity boundary will breaks the uniform field distribution along the cavity boundary and may enables the position dependence of the resonant properties. Hence the adjacent modes may interfere either constructively or destructively within the limited mode lifetime. Because of the mode coupling effect and poor light confinement of such cavity the spacing between the WGMs was not at all uniform throughout the spectrum and intensity of all the dominant modes was very high as compared to ordinary WGMs from a SRC. Such WGMs are also referred as chaotic WGMs [23].

Emission directionality was one of the salient characteristics of ARC cavities. For a very slight deformation, the emission was the result of tunneling process, and the emission comes out tangentially at the boundary points with the highest curvature. To study the far-field directionality of laser emission from an ARC, we measure the intensity distribution of the laser output as a function of viewing angle with a fixed pump power of 22 mW. The tunneling of laser emission rate would be maximum at the boundary points with the highest curvature in the outer boundary, which can be ascribed to the increased tunneling emission of Q-spoiled high-order WGMs [36]. That is, in the highest curvature area, evanescent wave is transformed into a propagative wave at a certain distance to the surrounding form the boundary. A 1 mm pin hole was positioned in front of a collecting fiber kept in a rotational stage and attached

to a high speed photo-detector [34]. The distance between the collecting fiber and the microcavity was 3 mm. The intensity distribution of the lasing emission at 591 nm (highest intensity mode) was measured by varying the angle with reference to the transverse direction of the ARC. Initially collecting fiber was aligned parallel to the microcavity axis and which was referred as angle $\theta = 0^{o}$, where angle 0° refers to the highest curvature area. Then the output intensity of emission spectra was measured by gradually increase/decrease angle θ ($\pm\theta$) between -60º to 60º as shown in figure 5.6(c). It can be seen that the lasing intensity from 0 degree was much stronger than those measured from other angles, showing that the intensity distribution pattern of the microcavity possesses a good unidirectional laser emission property with a far field divergence of about 20°. Anisotropy of the photon escape rate on the highest curvature area will leads to the highly directional emission to a preferred direction. From these studies, one could conclude that the ARC cavity will provide a highly directional emission as compared to SRC cavity.

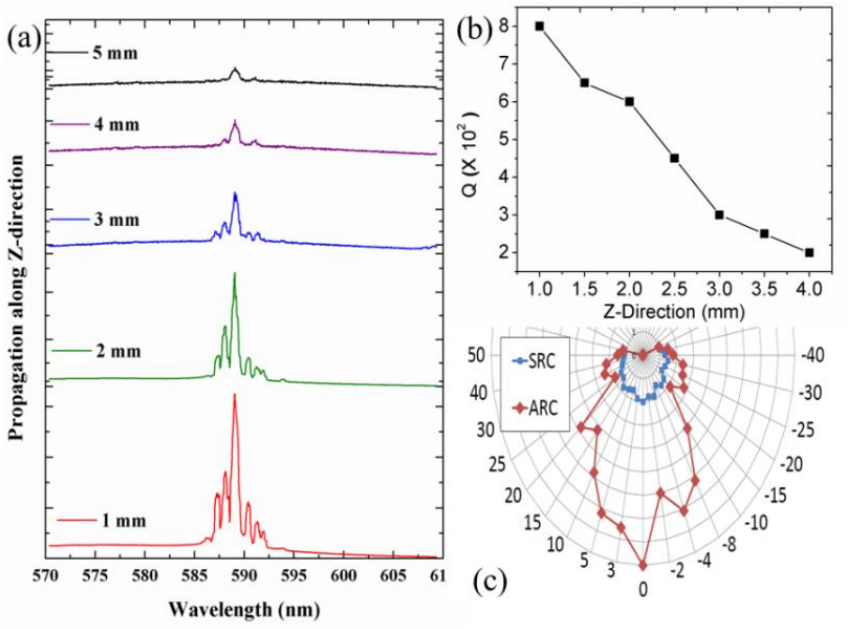

Figure 5.6 (a) Emission from ARC, when collecting fiber moves in Z-direction (b) Variation of Q factor of the highest intensity lasing mode with different propagation length. (c) Far-field angular distributions of emission intensities of all lasing modes from an ARC and SRC cavity.

The dependence of peak intensity of the lasing mode with respect to the distance along the Z-direction from the point of excitation was also measured in our studies. When the collecting fiber moves along the Z-direction of the doped fiber (1 mm to 4 mm) the intensity of the whole emission together with the mode structure diminishes as shown in figure 5.6(a). The variation of the Q factor of the highest lasing mode with different propagation length (Z-direction) was shown in the right top inset of figure 5.6(b). As the propagation length increases from 1 to 4 mm, the loss in the microcavity increases, as a result the Q factor reduces from 8×10^2 to 2×10^2. For larger Z, the modes which get propagated through the whole length of un-pumped region undergo self-absorption and remission in the microcavity. Above 5 mm, the emission losses its lasing behavior due to breaking of lasing condition that "net gain < different loss mechanism within the ARC".

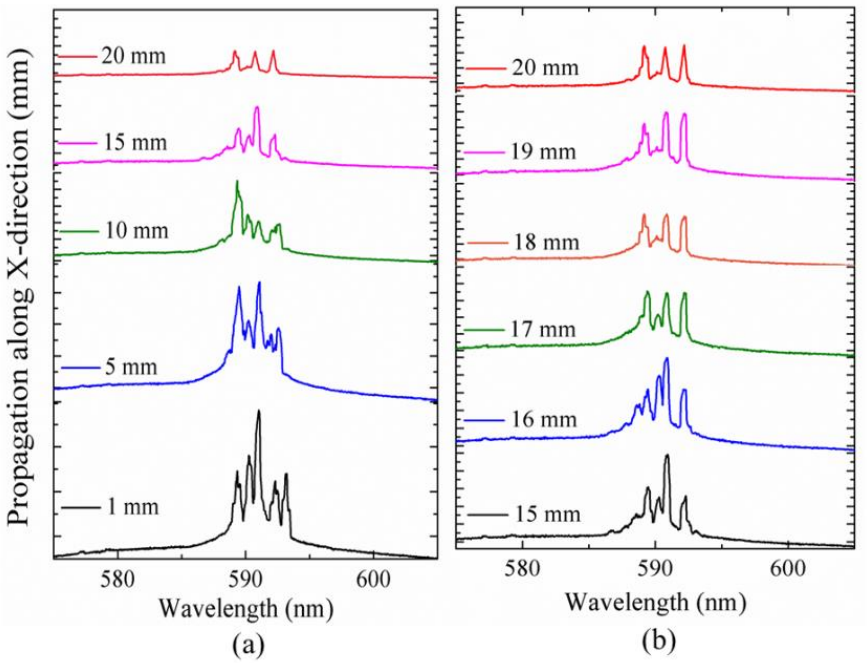

Figure 5.7(a) Emission spectra from ARC, when the collecting fiber moves in X-direction (1 to 20 mm). (b) Three laser modes with almost equal intensities were sustained and stable after a propagation distance from 16 to 20 mm in X-direction.

When the collecting fiber moves away from the ARC in the X-direction from 1 mm to 20 mm, the intensity of whole mode structure starts to decrease as shown in figure 5.7(a). Unlike the case of SRC, the emission from the ARC was highly directional and hence the laser emission can detected even after a propagation distance of 20 mm. Also in our study, beyond a propagation distance of 16 mm from the ARC, some modes are vanished from the spectrum and only three dominant laser modes were sustained with wavelengths 589.2 nm, 591 nm and 592.2 nm having equal intensities as shown in figure 5.7(b). The reduction in the number of lasing modes and the stabilization of such modes are keys to many organic opto-electronic device applications.

5.6 Section III:

In this section, we report controlling the emission directionality of an annular structured cylindrical microcavity by suitably positioned the air hole.

5.6.1 Asymmetric hollow microcavity

An annular structured asymmetric resonant (ARC) microcavity can support WGM like high-Q modes (HQMs) and leaky directional low-Q modes (LQMs) as shown in the figure 5.8. From this ray optics picture, a ray emanating at an angle much greater than critical angle ($\chi > \chi_c$) may travel along the circumference of the cavity with minimum loss. A ray with such a large angle of incidence never encounters the hollow region of the cavity. Hence it circulates as whispering gallery trajectory with high Q, also referred as HQM and is expected to emit without any preferred direction [37].

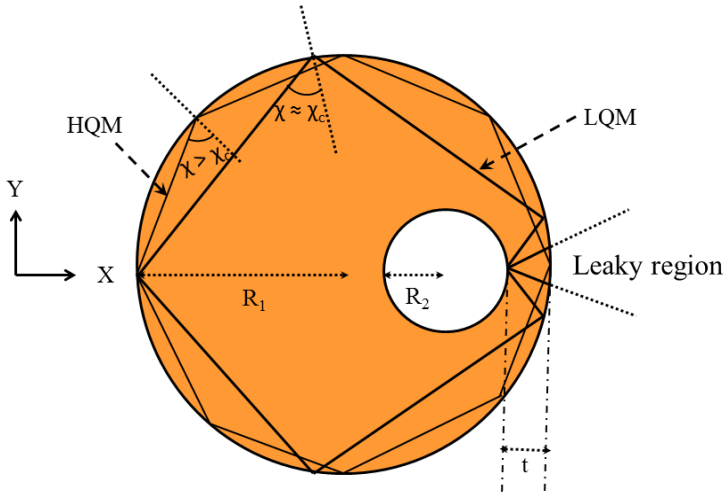

Figure 5.8 Schematic of an asymmetric annular microcavity with radius R_1. The radius of hole is R_2, the distance to cavity surface is t.

Consider a ray striking the outer boundary interface at an angle closer to the critical angle ($\chi \approx \chi_c$) that reaches the inner boundary. In the case of minimal distance of the hole, 't' to the outer boundary, the ray will hit the hole several times and form a chaotic trajectory. This region is considered as a leaky region

(see figure 5.8), where the light rays will refract out quickly after few reflections. Due to high loss (escape rate) such modes have a low Q, hence referred as LQM.

5.6.2 Emission directionality

To investigate individual mode distribution in ARC, near-field images and far-field emission patterns are simulated using COMSOL Multiphysics.

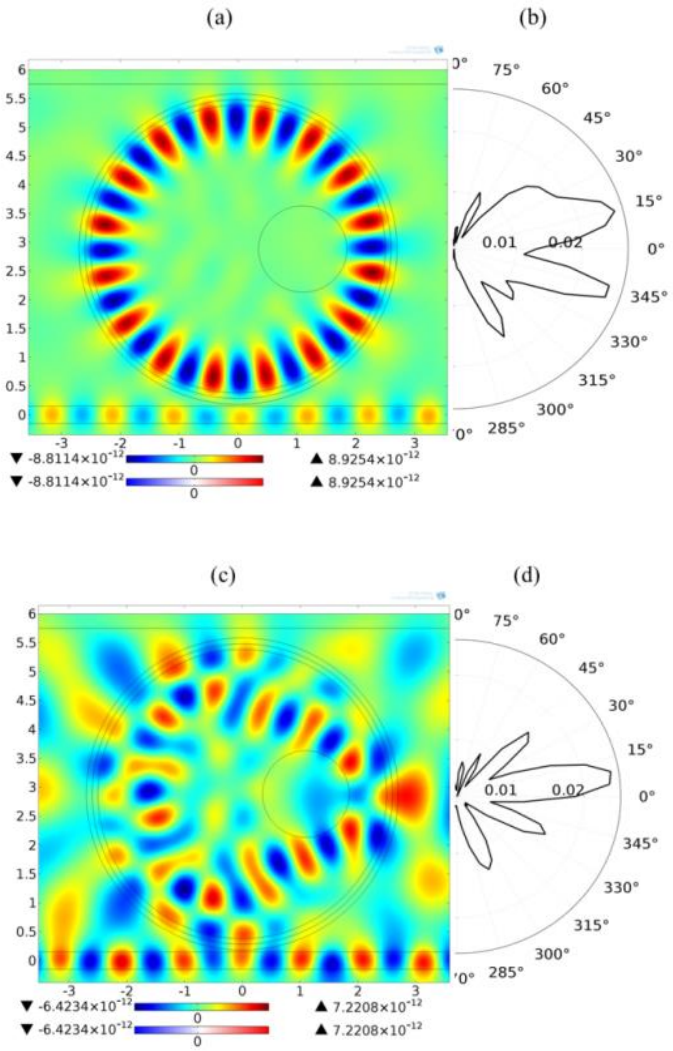

Figure 5.9 (a) Electric field distribution of HQM (b) far-field emission pattern on-resonance condition (c) Electric field distribution of LQM and (d) corresponding far-field emission pattern

The intensity distribution of the lower order radial modes in an annular structured ARC is localized just beneath the outer boundary of the cavity and is not affected by the existence of inner boundary. The radiation Q of such modes is high (HQM) due to minimum loss, in which surface scattering is the dominant mechanism for total loss. Figure 5.9 (a) shows the electric field distribution (near-field image) and (b) its corresponding far-field emission pattern of HQM from an ARC. When the wavelength is tuned on-resonance with HQM, the light is scattered from the entire boundary and hence, the HQM shows an isotropic far-field emission pattern with a divergence angle about 105˚. Figure 5.9 (c) and (d) shows the near-field images and its corresponding far-field emission pattern of LQM, when tuned on resonance. From the near-field images, the bright scattering is mainly observed in the leaky region. Far-field emission pattern shows that the emission could have a good directionality with a narrow divergence angle about 15˚.

5.6.3 Controlling directional emission

The radiation Q of LQM is mainly attributed to radiation loss due to refractive escape by suitably positioned air-hole within the ARC. Leaky region can be tuned by controlling the deformation (t/R_1) of ARC. The effect of the hole position can be measured by varying the t/R_1 value of ARC. Figure 5.10 shows the far-field divergence angle of LQM with varying t/R_1 on resonance condition.

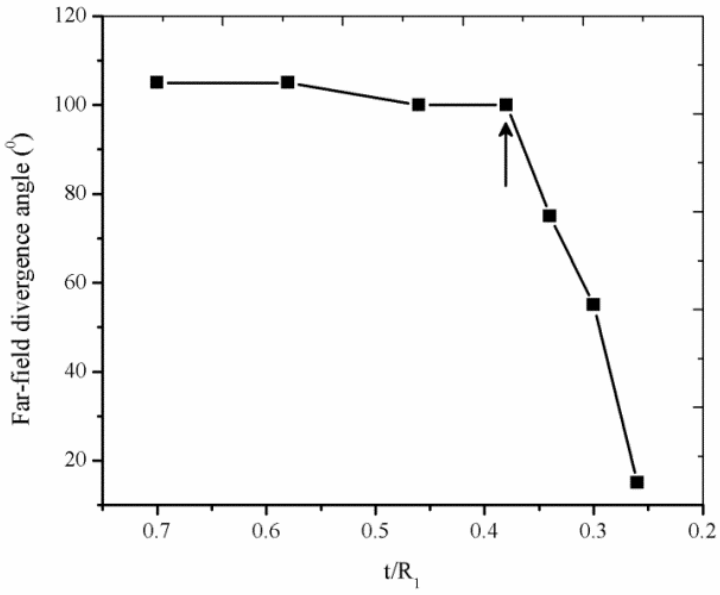

Figure 5.10 Effect of hole position (t/R1) on the far-field profile of an ARC

Figure 5.10 shows that the far-field emission pattern of LQM is strongly modified by the position of hole. From the figure, one could observe that the emission directionality increase with decreasing the value of t/R_1. At a particular value of $t/R_1 \approx 0.34$ (see the arrow mark in figure 5.10), the far-field emission pattern shows a directional emission. This is due to the fact that the LQM may interact with the hollow region of the ARC and radiate out through the leaky region. The best emission directionality we found for LQM with $t/R_1 \approx 0.26$. At this value, the emission is highly directional with a far-field divergence of 15˚. From the simulation study, we observed that the emission directionality is mainly determined by the nature of chaotic trajectories in the leaky region due to the asymmetric shape of the cavity.

Figure 5.11 shows the typical lasing spectrum from asymmetric annular structured cylindrical microcavity with t/R1 ≈0.27. The emission spectrum shows a number of sharp peaks centered around 592 nm. This emission spectrum can be separated into two groups. The sharp single peaks with no

fixed spacing are due to LQM, whereas the low intensity peaks in clustered form arise from LQM. The free spectral range (FSR) of HQM is found to be 0.085 nm, which corresponds to the fundamental WGMs of the 870 μm cylindrical microcavity. This value is in good agreement with the theoretically estimated value by equation 4.5 of 0.086 nm, where n is the refractive index of the PMMA and λ is the lasing wavelength. The Q value of HQMs and LQMs is found to be 1.2 $\times 10^4$ and 5×10^3 respectively. The lower Q of LQM is mainly attributed to the radiation loss due to refractive escape by intentionally constructed asymmetric shape of the cavity.

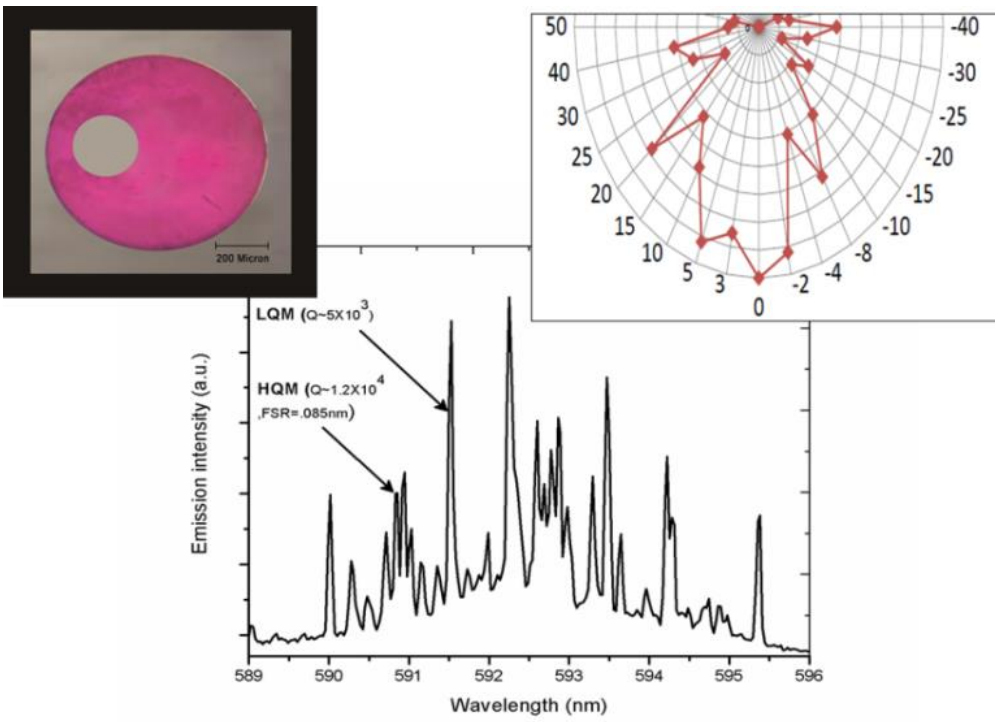

Figure 5.11 Typical laser emission spectrum of deformed RhB-doped hollow polymer optical fiber. The left inset shows the cross-sectional view of the deformed hollow polymer fiber. The right inset shows the far-field emission pattern.

Emission directionality is one of the salient characteristics of ARC cavities. A 1 mm pin hole was positioned in front of a collecting fiber kept in a rotational

stage and attached to a high speed photo-detector. The distance between the collecting fiber and the microcavity was 1 mm. The intensity distribution of the highest intensity mode was measured by varying the angle with reference to the transverse direction of the ARC. Initially collecting fiber was aligned transverse to the microcavity axis (x-axis) (see figure 5.8) and which was referred as angle $\theta=0^{o}$, where angle 0° refers to the highest curvature area. Then the output intensity of emission spectra was measured by gradually varying the angle θ ($\pm\theta$) between -60^{o} to 60^{o} as shown in inset of figure 5.11. It can be seen that the lasing intensity from 0 degree was much stronger than those measured from other angles, showing that the intensity distribution pattern of the microcavity possesses a good unidirectional laser emission with a far-field divergence of about 20°.

5.7 Conclusion

We have developed a symmetric (SRC) and asymmetric (ARC) cylindrical photo-pumped microcavity laser based on a free standing PMMA hollow fiber doped with rhodamine B laser dye. An SRC cavity provides laser emission with a quality factor, Q of $\sim 1.2 \times 10^{4}$. Owing to the deformation of an ARC, the value of Q could be spoiled during the lifetime of a given resonance. Such anisotropy of the photon escape rate then leads to the highly directional emission to a preferred direction. This feature can be effectively utilized in designing efficient microlasers and light emitting diodes. Benefiting from the low cost and good chemical compatibility of polymer materials, the fabrication of such annular structured cylindrical shaped polymer microcavity lasers with unidirectional emission holds great potentials for use of elements of integrated organic opto-electronic devices. We demonstrated an efficient way to control the emission directionality by a suitably positioned the air hole within the microcavity. It is found that the far-field emission pattern of LQM shows a good directionality with a narrow divergence angle when compared with

HQM. It is also found that the emission directionality can be tuned by adjusting the value t/R_1. Further studies being carried out with different degree of deformations in annular structured cylindrical microcavities to achieve high Q-unidirectional laser emission.

References

1. K. J. Vahala. (2003, August). "Optical microcavities". Nature 424. pp. 839-846. Available: doi:10.1038/nature01939.
2. Y. S. Park, A. K. Cook, and H. Wang, (2006, August). "Cavity QED with diamond nanocrystals and silica microspheres". Nano Lett. 6 (9), pp. 2075–2079. Available: DOI: 10.1021/nl061342r.
3. M. Humor and I. Musevic, (2010). "3D microlasers from self-assembled cholesteric liquid-crystal microdroplets" Opt. Express 18 (26), pp. 26995-27003. Available: doi: 10.1364/OE.18.026995
4. H. M. Gibbs, G. Khitrova, and S. W. Koch, (2011). "Exciton-polariton light-semiconductor coupling effects", Nat. Photonics 5, 273. Available: doi:10.1038/nphoton.2011.15
5. M. Humar, M. Ravnik, S. Pajk, and I. Musevic, (2009). "Electrically tunable liquid crystal optical microresonators", Nat. Photonics 3, 595. pp. 595 – 600. Available: doi:10.1038/nphoton.2009.170.
6. J.C. Knight, H. S. T. Driver, and G. N. Robertson, (1994). "Morphology-dependent resonances in a cylindrical dye microlaser: mode assignments, cavity Q values, and critical dye concentrations", J. Opt. Soc. Am. B, 11 (10), 2046. Available: doi: 10.1364/JOSAB.11.002046.
7. Hyo Seng Kim, Seung Kwan Kim, and Byoung Yoon Kim, (1996). Longitudinal mode control in few-mode erbium-doped fiber lasers", Optics Letters, Vol 21 (15), No. 15. Available: 10.1364/OL.21.001144.
8. J. U. Nockel and A. D. Stone, (1997). "Ray and wave chaos in asymmetric resonant optical cavities", Nature 385,pp. 45-47. Available: 10.1038/385045a0.
9. Jaison Peter, Mahesh Kumar, V. R. Ananad, Rasool Saleem, Ananthu Sebastian, P. Radhakrishnan, V. P. N. Nampoori, C. P. G. Vallabhan, Radhakrishna Prabhu, and M. Kailasnath, (2016, January). "Solvent effects on lasing characteristics for Rh B laser dye", J. Lumin., Volume 169, Part A, pp. 227–232. Available: doi:10.1016/j.jlumin.2015.09.002.
10. V. A. Podolskiy, E. E. Narimanov, (2005). "Chaos-assisted tunneling in dielectric microcavities", Opt. Lett., 30 (5), pp. 474-476. Available: doi: 10.1364/OL.30.000474.
11. Q. F. Yang, X. F. Jiang, Y. L. Cui, L. Shao, Y. F. Xiao, (2013, August). "Dynamical tunneling-assisted coupling of high-Q deformed microcavities using

a free-space beam" Phys. Rev. A., 88 (2), 023810 Available: DOI:http://dx.doi.org/10.1103/PhysRevA.88.023810.

12. Jaison Peter, Radhakrishnan P., Nampoori V. P. N., Kailasnath M., (2014, May). "Multimode laser emission from free-standing cylindrical microcavities", J. Lumin. 149, pp. 204-207. Available: doi:10.1016/j.jlumin.2014.01.003.

13. Jaison Peter, Vallabhan C. P. G., Radhakrishnan P., Nampoori V. P. N. and Kailasnath M., (2013, October). "Microring lasing from a dye-doped polymer-coated silica fiber", Laser Phys. 23 (11), 115104 Available: http://iopscience.iop.org/article/10.1088/1054.

14. Jaison Peter, Rasool Saleem, Ananthu Sebastian, Radhakrishnan P., Nampoori V. P. N., Girijavallabhan C. P., and Kailasnath M., (2014, June). "Pumping scheme dependent multimode laser emission from free-standing cylindrical microcavity", Optics Communications, 320, pp. 125-128. Available: doi:10.1016/j.optcom.2014.01.054

15. J. C. Knight and H. S. T. Driver, (1995). "Mapping whispering-gallery modes in microspheres with a near-field probe", Opt. Lett. 20, pp.1515-1517. Available: doi: 10.1364/OL.20.001515.

16. Mohammad Ahmad and Larry L. Hench, (2005, January). "Effect of taper geometries and launch angle on evanescent wave penetration depth in optical fibers", Biosensor and Bioelectronics 20 (7), pp. 1312-1319. Available: doi:10.1016/j.bios.2004.04.026.

17. M. L. Gorodetsky and V. S. Ilchenko, (1994, December). "High-Q optical whispering-gallery microresonators: precession approach for spherical mode analysis and emission patterns with prism couplers", Opt. Communications, 113 (1-3), pp. 133-143. Available: doi:10.1016/0030-4018(94)90603-3.

18. N. Debreuil, J. C. Knight D. Leventhal, V. Sandoghdar, J. Hare, V. Lefer-Suguin, J. M. Raimond, S. Haroche, (1995). "Eroded monomode optical fiber for whispering-gallery mode excitation in fused-silica microspheres", Opt. Lett. 20 (8), pp. 1515-1517. Available: doi: 10.1364/OL.20.000813.

19. F. Hide, M. A. Diaz-Garcia, B. J. Schwartz, M. R. Andersson, Q. Pei, and A. J. Heeger, (1996, September). "Semiconducting polymers: a new class of solid-state laser materials", Science 273, pp. 1833. Available: http://search.proquest.com/openview/7d03e046180187a929908bb3245bceb5/1?pq-origsite=gscholar.

20. M. Cai, O. Painter, K. J. Vahala, (2000, July). "Observation of critical coupling in a fiber taper to a silica-microsphere whispering-gallery mode system", Phys. Rev. Lett 85 (74), pp. 74-77. Available: DOI:http://dx.doi.org/10.1103/PhysRevLett.85.74.

21. S. Lacey, H. Wang, (2001). "Directional emission from whispering-gallery modes in deformed fused-silica microspheres", Opt. Lett. 26 (24), pp. 1943-1945. Available: doi: 10.1364/OL.26.001943

22. S. Lacey, H. Wang, D. H. Foster, and J. U. Nockel, (2003, July). "Directional tunneling escape from nearly spherical optical resonators", Phys. Rev. Lett. 91, 033902. Available: DOI:http://dx.doi.org/10.1103/PhysRevLett.91.033902

23. S. K. Kim, S. H. Kim, G. H. Kim, H. G. Park, D. J. Shin, and Y. H. Lee, (2004). "Highly directional emission from few-micron-size elliptical microdisks", Appl. Phys. Lett. 84 (6), pp. 861-863. Available: http://dx.doi.org/10.1063/1.1646459.

24. Narimanov E. E., Podolskiy V. A., (2006). "Chaos-assisted tunneling and dynamical localization in dielectric microdisk resonators", IEEE Journal of Selected Topics in Quantum Electronics, 12, pp. 40-51 Available: http://cat.inist.fr/?aModele=afficheN&cpsidt=17501820.

25. Yun-Feng XIAO, Chang-Ling ZOU, Yan LI, Chun-Hua DONG, Zheng-Fu HAN and Qihaung GONG, (2010, June). "Asymmetric resonant cavities and their applications in optics and photonics: a review", Front. Optoelectron. China 3 (2), pp. 109-124. Available: DOI 10.1007/s12200-010-0003-2.

26. D. K. Armani, T. J. Kippenberg, S. M. Spillane, K. J. Vahala, (2003, February). "Ultra-high-Q toroid microcavity on a chip", Nature 421, pp. 925-928. Available: doi:10.1038/nature01371.

27. T. J. Kippenberg, H. Rokshari, T. Carmon, A. Scherer and K. J. Vahala, (2005, July). "Analysis of radiation-pressure induced mechanical oscillation of an optical microcavity", Phy. Rev. Lett. 95, 033901 Available: DOI:http://dx.doi.org/10.1103/PhysRevLett.95.033901.

28. B. Dayan, A. S. Parkins, T. Aoki, E. P. Ostby, K. J. Vahala and H. J. Kimble, (2008, February). "A photon turnstile dynamically regulated by one atom", Science 319, pp. 1062-1065. Available: DOI: 10.1126/science.1152261

29. C. L. Zou, F.W. Sun, C. H. Dong, F. J. Shu, X. W. Wu, J. M. Cui, Y. Yang, Z. F. Han, and G. C. Guo, (2013, October). "High-Q and unidirectional emission whispering gallery modes: Principles and design", IEEE journal of selected topics in quantum electronics, Vol. 19, No. 5 Available: DOI:10.1109/JSTQE.2012.2220896.

30. Soo-Young Lee, "Optical Mode Properties of 2-D Deformed Microcavities", (2010). Advances in optical and photonic devices, Book edited by K. Young Kim, ISBN, 978-953-7619-76-3, pp. 352.

31. F. Goos and H. Hanchen, (1947). "A new and fundamental experiment on total reflection", Ann. Phys. (Leipzig) 1, 333.

32. H. Schomerus and M. Hentschen, (2006, June). "Correcting ray optics at curved dielectric microresonator interfaces: phase-space unification of Fresnel filtering and the Goos-Hänchen shift", Phys. Rev. Lett., 96, 243903. Available: DOI:http://dx.doi.org/10.1103/PhysRevLett.96.243903

33. E. G. Altmann, G. Del magno and M. Hentschel, (2008, September). "Non-Hamiltonian dynamics in optical microcavities resulting from wave-inspired

corrections to geometric optics", EPL (Europhysics Letters), 84, 10008, Available: doi: 10.1209/0295-5075/84/10008.

34. C. Gmachl, F. Capasso, E. E. Narimanov, J. U. Nockel, A. D. Stone, J. Faist, D. L. Sivco, and A. Y. Co, (1998, June). "High-power directional emission from microlasers with chaotic resonators", Science 280 (5369), pp. 1556-1564. Available: DOI: 10.1126/science.280.5369.1556.

35. H. J. Brouwer, V. V. Krasnikov, A. Hilberer, G. Hadziioannou, (1996, November) "Blue superradiance from neat semiconducting alternating copolymer films" Adv. Mater. 8 (11), pp. 935–937. Available: DOI: 10.1002/adma.19960081116.

36. Jaison Peter, Radhakrishna Prabhu, P. Radhkrishnan, C. P. G. Vallabhan, V. P. N. Nampoori, and M. Kaialsnath, "Angular dependent light emission from planar waveguides", J. Appl. Phys. 117, 015301. Available: http://dx.doi.org/10.1063/1.4905011.

37. V. M. Apalkov and M. E. Raikh, "Directional emission from a microdisk resonator with a linear defect", Phys. Rev. B, 70, 195317 (2004).

Chapter 6
Dye doped polymer coated microcavities

"If we know what we were doing it wouldn't be research."

Albert Einstein

Abstract

A detailed study of amplified spontaneous emission from a polymer thin film doped with rhodamine 6G is presented. The emission spectrum of the dye-doped polymer thin film on a glass substrate exhibits high directionality, narrow linewidth and presence of soft threshold behavior. Performance of a compact solid-state laser based on leaky mode propagation from dye-doped polymer free-standing film waveguide is also discussed.

The second part of this chapter demonstrates pulsed, photo-pumped multimode laser emission in the visible spectral range from cylindrical microcavities of dye doped thin polymer film deposited on silica core optical fiber. The laser emission is characterised by two different sets of resonant modes viz; waveguided modes (WMs) and whispering gallery modes (WGMs). Simultaneous occurrence of the WGM and WMs will lead to a resonant modulation in the laser emission spectrum.

---

*The major content of this chapter has been published in the journal "**Laser Physics,** 23(11), 115104(2013) and **Journal of Applied Physics.** 117, 015301 (2015).*

6.1 Introduction

The design of a microcavity provides one possibility for a compact light-emitting device structure. The microcavity devices consist of the luminescent material placed within a Fabry–Perot resonator with a length of the order of the wavelength of emitted light. In this way the light emission is coupled to the cavity mode(s) and characteristically the light output is spectrally narrowed and directed. Microcavities provide excellent coupling of spontaneous emission into lasing modes, as well as high Q-value which consequently leads to low lasing thresholds [1]. Lasing, in addition requires an optical cavity to produce optical feedback, which subsequently forms resonant laser modes [2]. These necessary feedback features can be achieved by patterning the material in disc or ring form. We are interested to achieve microlasers on solid supports (either cylindrical or planar) that are easy to handle and might be integrated, for example in sensing devices [3]. A microring laser cavity offers a low loss resonance structure that has been utilized to demonstrate lasing with organic gain media [4]. Planar microcavities [5], however, are prone to losses due to imperfect reflection and emission leakages to the sides of the microcavity plane. Cylindrical microcavities may support waveguide and whispering gallery modes [1], both of which are due to total internal reflections inside the active volume and this can be practically lossless.

Organic luminescent materials have been widely studied in light emitting devices and solid-state lasers because of their light weight, ease of processing, low cost, flexibility, and spectral range coverage from the blue to far IR [15]. Laser devices of various structures have been achieved by a variety of resonator designs, including microcavities [16], micro-disks [17], micro-rings [18] and hollow fibers [19-20]. Polymer materials have been found to be very attractive both from the technical and economical point of view with its high optical quality, better chemical compatibility with organic dyes and

inexpensive processing techniques [21]. The combination of the tunability and high efficiency of laser dyes with the high power density that can be easily achieved in waveguide structures makes devices based on dye-doped polymer waveguides and fibers very promising [22-24].

Light amplification and spectral narrowing have been studied earlier in various systems both in the liquid and solid forms, where the spectral linewidth is reduced to a value less than 10 nm [25-27]. Spectral narrowing in most such systems is explained in terms of amplified spontaneous emission (ASE), where the spontaneously emitted luminescence is amplified by the gain medium as it propagates along the path of the maximum optical gain [20]. Reflections from the internal surfaces can increase the path length or allow multiple passes inside the gain medium which in turn build up the ASE at a faster rate [28]. Recently, laser emission from conjugated polymers and dendrimer doped polymers have also been reported [26,29]. There have been numerous investigations on laser emission from polymer planar microcavities [24,30] and polymer microring lasers [19,31].

6.2 Section I:

6.2.1 Fabrication of microring resonator

Dip-coating technique works very well for producing thin films on supporting structures such as silica core fiber [6]. In the present study, the polymer gain layer is formed on the surface of an unclad silica optical fiber [7]. Cylindrical shaped thin polymer films were prepared by dipping commercially available multimode silica optical fiber (from which the cladding was removed) into precursor solution [3]. The precursor solution had a molar composition of poly methyl methacrylate (PMMA)/Ethanol/Rh B = 5gms/15ml/1×10^{-4} mol/litre. Thin polymer rings were consequently formed around the glass cylindrical core following fast drying in the air [8]. The self-assembled polymer microstructure in the form of cylindrical microrings are

similar to those previously reported in ref [9], with deposited films of laser dyes blended in transparent polymers.

6.2.2 Laser emission from microring resonator

Since the refractive index of the silica fiber is lower than that of the polymer gain layer, there could exist laser resonances, which are confined to the polymer layer, and provide the optical feedback required for lasing. To support the polymer gain layer a silica optical fiber was used, and its refractive index has a bulk value of n_s = 1.46, which is less than that of PMMA (n_p = 1.49). The coated polymer gain layer is sufficiently thin, so that the whispering gallery modes (WGMs) of high Q factors exist in the core support facilitating the low threshold laser oscillations [10]. The polymer layer thickness is important, as it determines the fraction of the light in the core that gets extracted evanescently from the gain medium. Cylindrical microcavities may support waveguided modes (WMs) and WGMs [1], both of which arise due to total internal reflections inside the composite structure of the active volume and thus can be practically lossless [11].

6.2.3 Experimental setup

The laser emission was characterized with the optical setup presented in chapter 3 (see figure 3.10). The spectral peak intensity of the polymer ring laser is positioned at the maximum of optical gain which in turn corresponds to the photo-luminescent spectrum peak [12] around 590 nm. A large number of sharp lines can see within the fluorescent emission profile. The lasing modes are spectrally narrow with an FWHM of 0.05 nm with a pump power of P_{th}×8, where P_{th} is the lasing threshold pump power. Due to the fairly large thickness of the optical fiber (420 μm), there are large number of longitudinal modes that can be supported by the microcavity[13].

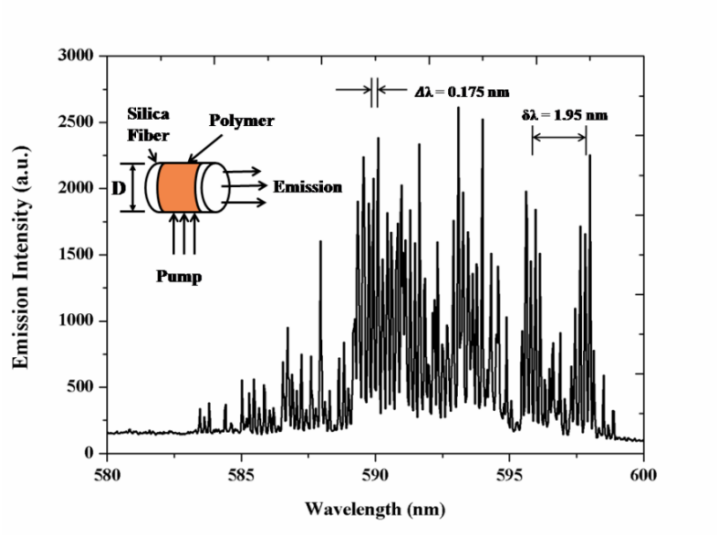

Figure 6.1 Emission spectrum of dye coated on glass fiber with diameter D = 420 µm and pump power of 24 mW (P_{th}×8). The inset depicts the measurement geometry

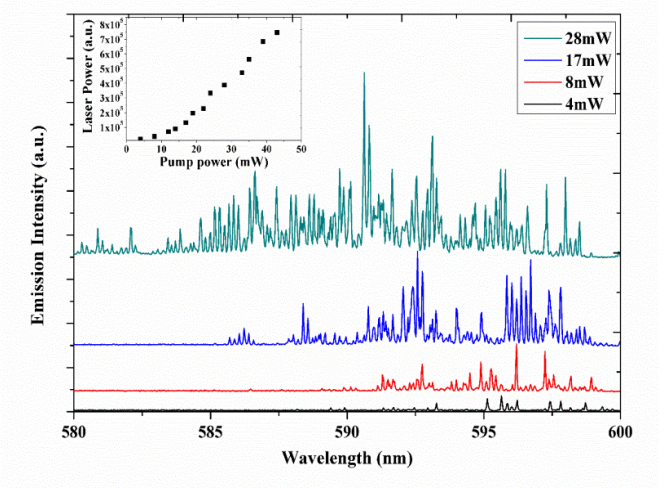

Figure 6.2. Typical emission spectra recorded. From the bottom to top, P = P_{th}×1.33, P = P_{th}×2.67, P= P_{th}×5.67 and P = P_{th}×9.33 respectively. Inset shows the output laser power (numerically integrated output intensity) versus the pump power.

When the pump power is higher than the lasing threshold (P_{th}×1.33) microring lasing modes appear in the longer wavelength range (595-600 nm) of the photoluminescence spectra of the gain medium. When the pump power

was further increased, the lasing modes with high intensities start to develop on the shorter wavelength region of the spectra. The number of lasing modes and the resonant mode intensities increase with pump power as can be clearly seen in the figure 6.2. Inset shows the output laser power (numerically integrated output intensity) versus the pump power.

At a pump power of P_{th}×9, the lasing modes are found to cover the entire photo-luminescence emission band of the gain medium .i.e 580-600 nm. When the polymer layer thickness, 'd' is very small, the film acts as a curved two-dimensional waveguide [11] and the resonant wavelengths for the waveguided lasing modes are given by the following equation [9]

$$m\lambda_m = \pi D n_{eff} \qquad 6.1$$

where m is an integer, λ_m is the resonant wavelength, D is the silica fiber diameter and n_{eff} is the effective index of refraction in the cylindrical polymer waveguide.

The wavelength of each WGM mode is determined by,

$$\Delta\lambda = \lambda_m - \lambda_{m-1} = \frac{\lambda^2}{\pi D n_{eff}} = 0.177 \text{ nm} \qquad 6.2$$

which is in good agreement with experimentally observed Δλ (figure 6.1) of 0.175 nm.

6.2.4 Modulation of laser modes

The observed variations in the mode intensities as shown in the figure 6.3 can be explained on the basis of the simultaneous occurrence of WGM and WG modes. This leads to lasing output with the modulated Q_{cav} with wavelength separation

$$\delta\lambda = \Delta\lambda \frac{n_{eff}}{\Delta n_{eff}} \qquad 6.3$$

where Δn_{eff} is the difference between n_{eff} of the WG and WGM [8] with the parameters of the waveguide structure explained in our present study. We

have calculated the wavelength separation δλ=1.965 nm, which agrees well with the observed value (1.95 nm) as shown in figure 6.1.

The thin ring resonator which is formed around the silica fiber can support whispering gallery modes propagating along their cylindrical edges. Whispers are able to produce a low Q feedback mechanism to modify Q_{cav} of the waveguided modes in the polymer ring [12]. The laser emission spectra are modulated by the superposition of the WGMs on the WMs as shown in figure 6.3. Q_{cav} is increased if waveguided and whispering modes are in resonance, and Q_{cav} decreases if the corresponding resonant wavelengths are detuned from each other [8]. We therefore attribute the appearance of the emission spectra to a resonant modulation of the waveguided modes by whispering gallery modes [3].

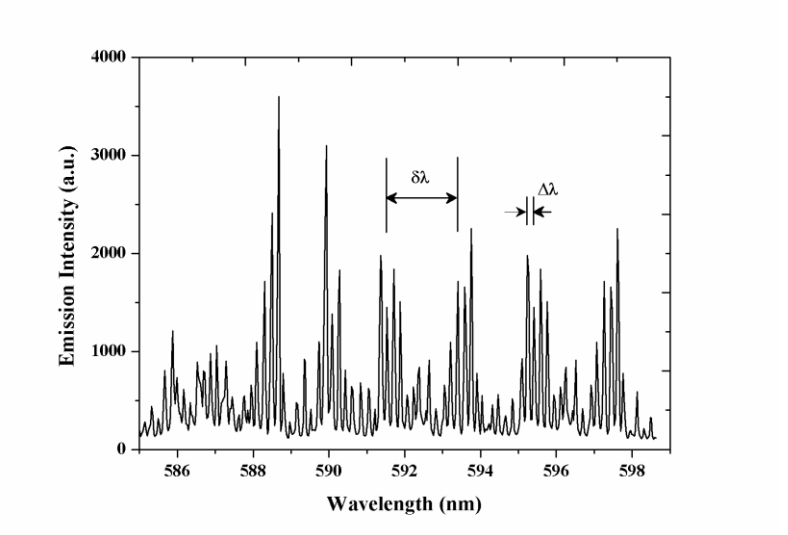

Figure 6.3. Resonant modulation of the waveguided modes and whispering gallery modes

In the present study, we estimate the microlasers Q value to be about 1.2×10^4, which in addition to the low laser threshold, results in narrow laser emission lines with width of about 0.05 nm.

6.3 Section II:

6.3.1 Fabrication of Asymmetric planar waveguides

To fabricate the rectangular waveguide, rhodamine 6G doped poly methyl methacrylate (PMMA) thin films with an average thickness of ~ 3 μm were deposited by spin coating technique onto a glass substrate. The precursor solution had a molar composition of PMMA/Anisole/Rh6G = 2gms/15ml/1×10^{-4} mol/l. Thin polymer films were formed on the glass substrate following fast drying in air. The refractive index of the doped polymer film (n_p = 1.49) is higher than the refractive index of the glass substrate (n_s = 1.46). A semi-leaky waveguide or a quasi-waveguide is obtained, where the light is confined by the film/air interface while at the film/substrate interface, a portion of light will reflect back into the film (guided mode) and the remaining refracted to the substrate, which is shown in the inset of fig. 6.4. This light will propagate through the substrate is termed as cutoff mode [32-34]. Hence some of the light will be leaked into the glass substrate and propagate through the glass substrate, which is referred as the leaky region of the waveguide and on the top side light will more tightly confined in the polymer film. So we can consider that this type of waveguide has a semi-leaky structure. The different guided modes propagating within the gain layer have different reflectivity losses due to Fresnel law. Thus the glass-doped polymer-air structures formed an asymmetric slab optical waveguide, which supports only the transverse mode as the guided mode within the emission band of the doped polymer [15]. Because of the extremely small thickness of the polymer film (3 μm), we assume that the mode propagated through the film is fundamental transverse mode. As a result, a quasi-waveguide provides a much stronger mode restriction capability than conventional total internal reflection waveguides. However, if the incident angle is slightly smaller than the critical angle, some of the light will refract

(leak) into the substrate and propagate in a direction nearly parallel to the interface between the film and substrate as shown in figure 6.4 inset.

6.3.2 Experimental setup

Investigations on the ASE properties of these films were carried out by optical pumping of the films by the second harmonic output of a Q-switched Nd:YAG laser with 8 ns pulses at 10 Hz repetition rate. The experimental setup is shown in figure 6.4. The pump power was adjusted with neutral density filters, and focused into the polymer-coated film by a cylindrical lens into a 1 mm × 0.4 mm stripe. A slit was incorporated in the path of the beam between cylindrical lens and the sample so as to vary the stripe length onto the sample surface. The emission from the sample was collected by a multimode fiber and guided to a 0.5 m spectrograph coupled with a cooled CCD array. The distance between the collecting fiber and the waveguide edge was 1 cm.

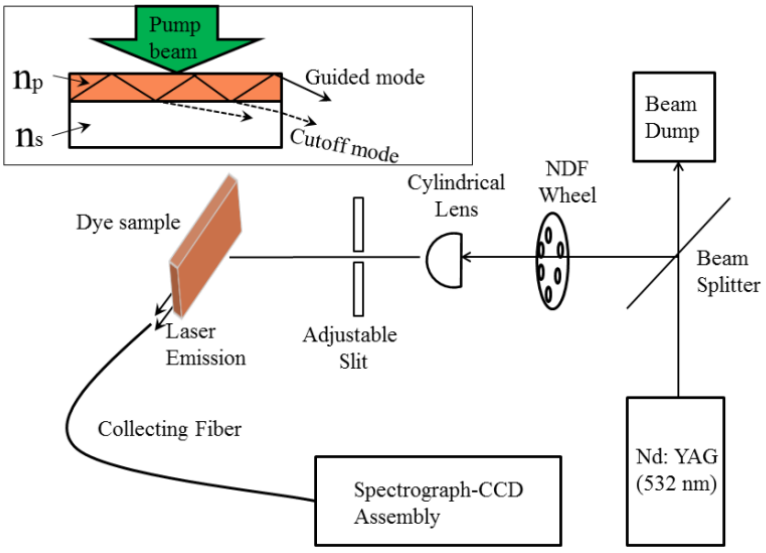

Figure 6.4. Schematic representation of the experimental setup. Inset shows the Ray-tracing description of light propagating in a planar waveguide.

6.3.3 Amplified spontaneous emission (ASE)

Figure 6.5 shows the absorption and photoluminescence spectra of the Rh6G doped PMMA film. The doped polymer film exhibits a featureless absorption band that peaks at 530 nm and emission with a peak of 570 nm, which is the characteristic emission of the Rh6G dye molecule. When the optically dense dye doped thin film is excited such that it forms a cylindrically shaped active gain medium, the fluorescence emitted by the molecules at one end is strongly amplified by the active medium and it preferentially emits the optical power along the direction of excitation, giving a highly directional output beam [35]. As a result, a large portion of the dye-doped polymer emission was optically confined within the film by internal reflections. Using the refractive index of the substrate, ns = 1.46, and that of the PMMA film, np = 1.49, we estimate the fraction of emission which is waveguided or "trapped" inside the film as

$$f = \sqrt{1 - \left(\frac{n_s}{n_p}\right)^2} = 0.2 \qquad 6.4$$

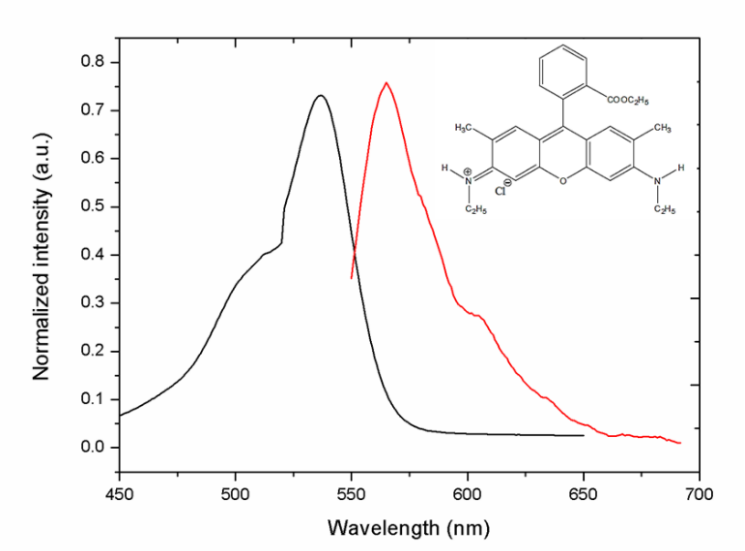

Figure 6.5. The absorption and photoluminescence spectra of Rh6G doped in a PMMA film. Inset, chemical structure of Rh6G

If the incident angle of the propagating light is larger than the critical angle of the interface between the film and glass substrate, the light can propagate inside the film without leakage. The spectrally narrow emission (~5 nm) from such films is observed only along the plane of the film (A in figure 6.6), whereas the emission perpendicular to the film surface remained spectrally broad (~40 nm) (B). This is due to the fact that at low grazing angles, it has low loss normal to the plane of the film and thus the polymer-air interface has almost zero transmission due to total internal reflection. This indicates that ASE is due to waveguided polymer emission which propagates alongside the film and thus experiences the largest gain. For our measurements of ASE we used an excitation region in the shape of a narrow stripe. As a result, ASE was predominantly emitted along the axis of stripe.

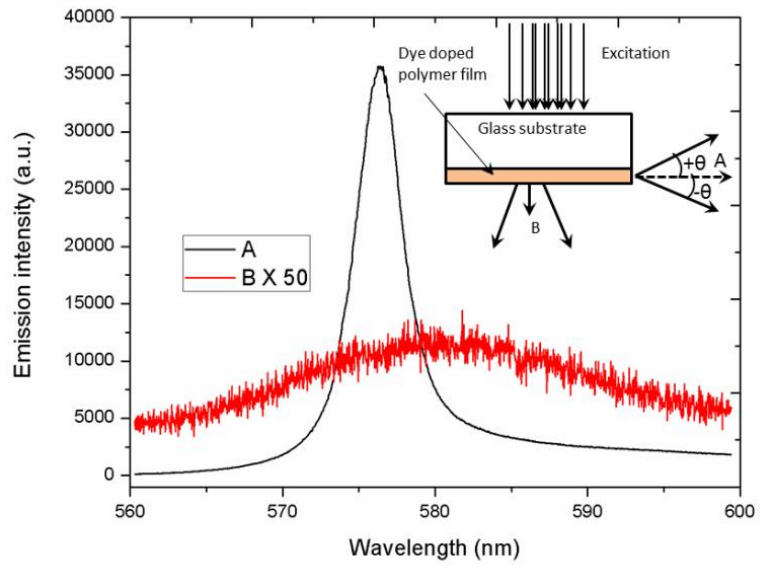

Figure 6.6. The emission spectra from the dye-doped polymer film measured in the direction parallel (A) and perpendicular (B) to the film surface at the same excitation intensity (20 mW); emission intensity B is magnified by 50. The inset illustrate the experimental setup

6.3.4 Line narrowing and blue-shift

Due to stripe illumination a large number of Rh6G dye molecules undergo population inversion when it is optically pumped by the second-harmonic output of an Nd:YAG laser. At low pump powers the emission spectrum from the film exhibit broad fluorescence. To understand the nature of ASE in detail, the dependence of emission intensity on incident pump power is studied. As pump power is increased, the emission spectra shows a line narrowing effect coupled with blue-shift as shown in figures 6.7 and 6.8. With an increase in pump power, the radiative transition probability gets enhanced at shorter wavelength side of the spectrum creating a shift in the spectrum towards the blue side [19]. Figure 6.8 inset shows the blue-shift of the emission spectrum as a function of pump power. As the pump power increases from 8 to 20 mW, it can be seen that the emission spectrum gets shifted from 584 to 576 nm. Spectral line narrowing as a function of pump power is the signature of light amplification [36-37]. The collapses of the FWHM in the emission spectrum and the change in the slope in the output emission intensity are the indication of the onset of ASE above a certain threshold (P_{th} = 12 mW). Also, spectral narrowing from 52 to 5 nm is observed, when the pump power is increased to 15 mW above which no further line narrowing is observed due to gain saturation effect. On a detailed study of the emission spectrum of the dye-doped polymer thin film, it is found that the emission spectrum exhibits all the features of ASE, namely the property of directionality, narrow linewidth and presence of soft threshold behavior [38]. Directionality of the output beam is so obvious that no focusing is required to collect the beam.

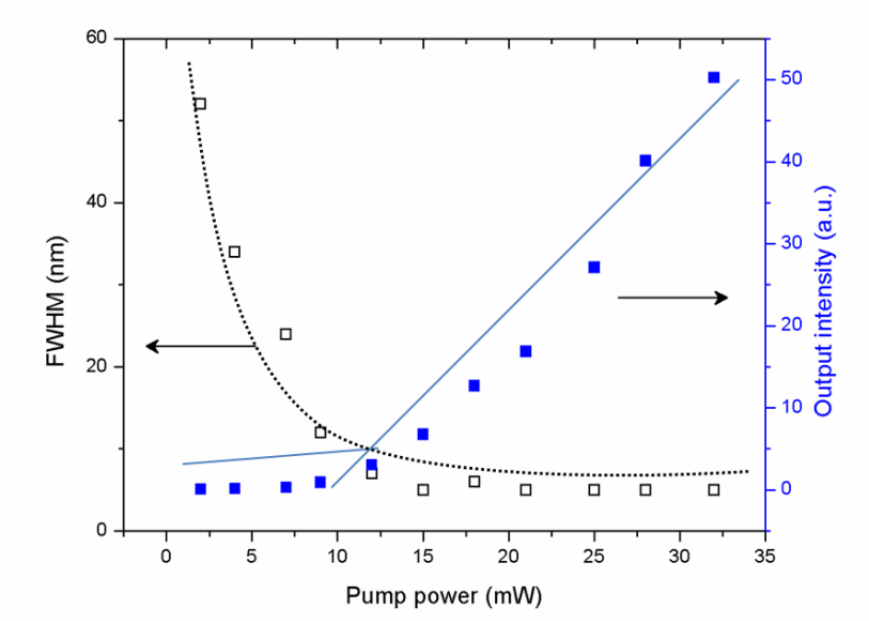

Figure 6.7. Output emission intensity integrated over all wavelengths as a function of pump power (filled square) and dependence of the FWHM on the pump power (open squares).

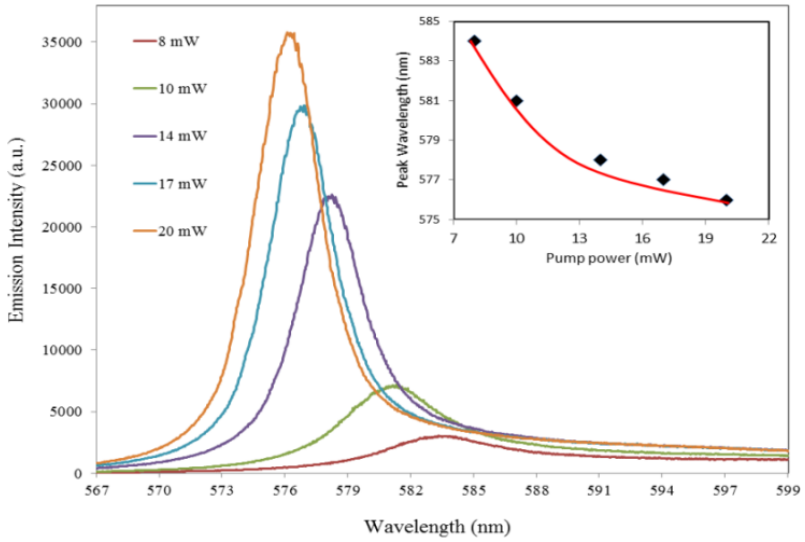

Figure 6.8. The emission spectra from planar waveguide at various pump power. Inset : Blue-shift in peak wavelength as a function of pump power.

6.3.5 Characteristics of Cut-off and Waveguide mode

To study the directionality of the ASE from the asymmetric planar waveguide, we measured the output intensity and Full-Width-Half-Maximum (FWHM) of emission spectra as a function of viewing angle from the plane parallel to film axis. To measure the FWHM and output intensity as a function of viewing angle θ, the collecting fiber is kept in a rotational stage. The output intensity and FWHM of emission spectra as a function of viewing angle are measured as shown in figure 6.9. Initially, collecting fiber is aligned parallel to the waveguide axis and which is referred as angle $\theta = 0^{o}$. Then the FWHM and output intensity of emission spectra is measured by gradually increasing/decreasing angle θ (±θ) between -40 to 40°. The detailed examination of the output emission spectra is measured at different angles. The FWHM of emission is almost constant with an angle θ between -7˚ to 10˚ and gradually increase the FWHM at larger θ. This indicates that the guided mode is only observed in small ranges of angle due to confinement of light in the film. The increase in emission intensity at angle higher than 10˚ (exactly 10˚ to 16˚) is due to cutoff mode. This additional peak in output intensity is a clear indication of coexistence of the cutoff mode in our asymmetric planar waveguide structure.

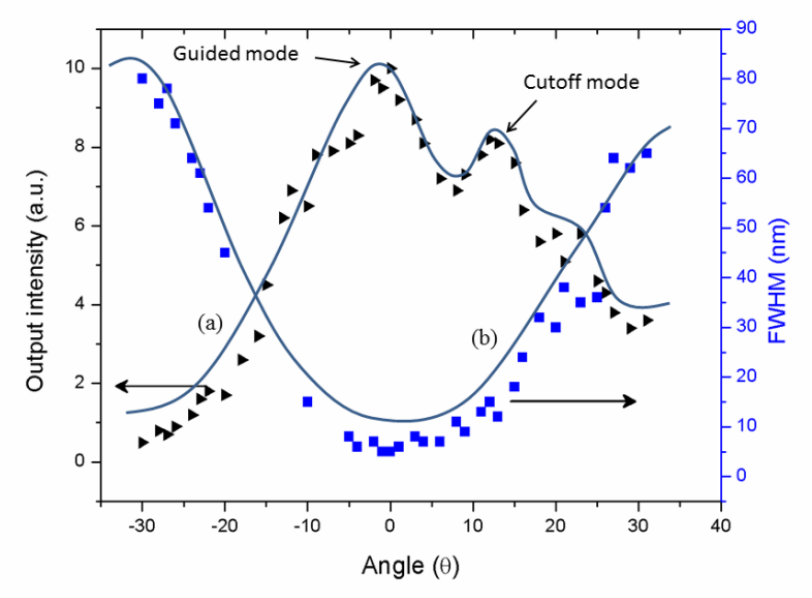

Figure 6.9. The output intensity (a) and FWHM (b) of the emission spectra from the planar waveguide as a function of viewing angle by keeping a constant pump power of 25 mW

6.4 Section III:

6.4.1 Fabrication of free-standing planar waveguides

In this section we describe the observation of multimode laser emission from a transversely pumped free-standing polymer film. Solid-state free-standing thin films were prepared by incorporating Rh6G dye with PMMA. Commercially available PMMA of 5 gms was dissolved in 15 ml of anisole. The weight percentage was chosen to get optimum viscosity for the formation of good quality films. The dye was dissolved in this solution at a concentration of 1×10^{-4} mol/l. Films of 50 μm thickness were tape cast on glass sheets from this solution. When solvent was fully evaporated, high-quality free-standing films could be peeled off from the glass sheet. The lateral faces of the films obtained were of good optical finish and as such no further polishing was required.

6.4.2 Multimode laser emission

The same experimental setup (explained in section 6.3.2) was employed to study the emission characteristics from the dye-doped free-standing polymer film as well. Laser emission requires an external feedback. In the present case no feedback is provided with external mirrors. Since the pumped polymer film was a free-standing one, the lateral faces of the film acted as mirrors, thus giving rise to a Fabry-Perot-type optical cavity for which length corresponds to the film thickness [38]. The excited active medium can be considered as a number of serially connected Fabry-Perot optical cavities. In the case of a thin stripe excitation, the stimulated emission occurs in a direction along the stripe [39]. The multiple passes between the film surfaces directly increase the gain. When the gain of the active medium compensates the losses in the medium, laser emission occurs. According to laser theory the gain in the active medium is $\exp \sigma (N_2 - (g_2/g_1)N_1)l$, where σ is the stimulated emission cross section and l is the length of active medium [38]. Owing to the sample geometry and pumping scheme, the longitudinal modes of the cavity are analogous to the transverse modes of the waveguides [10]. When the pump power is increased beyond the lasing threshold (in our sample 15 mW), the emission spectrum collapsed into multiple narrow lines as shown in figure 6.10. This evenly spaced peaks clearly indicates the existence of resonant modes. Above the threshold, the total emission intensity increased much more rapidly with the pump power.

The existence of a Fabry-Perot optical cavity between the lateral faces of the free-standing film is thus confirmed by the occurrence of well-resolved discrete peaks in the emission spectrum. The mode spacing at λ can be calculated using the equation which describes Fabry-Perot cavities, namely,

$$\Delta\lambda = \frac{\lambda^2}{2nL} \qquad 6.5$$

where λ is the wavelength of the strongest emission line, n is the refractive index and L is the length of the resonator cavity. In the present case, the length of the Fabry-Perot cavity corresponds to the thickness of the polymer films. The observed mode spacing (0.9 nm) (as shown in figure 6.10) agrees well with the calculated value (0.86 nm). These values confirm that the observed equally spaced fine structures in the emission spectra are Fabry-Perot-type modes of the optical cavity formed by the lateral faces of the waveguide [10].

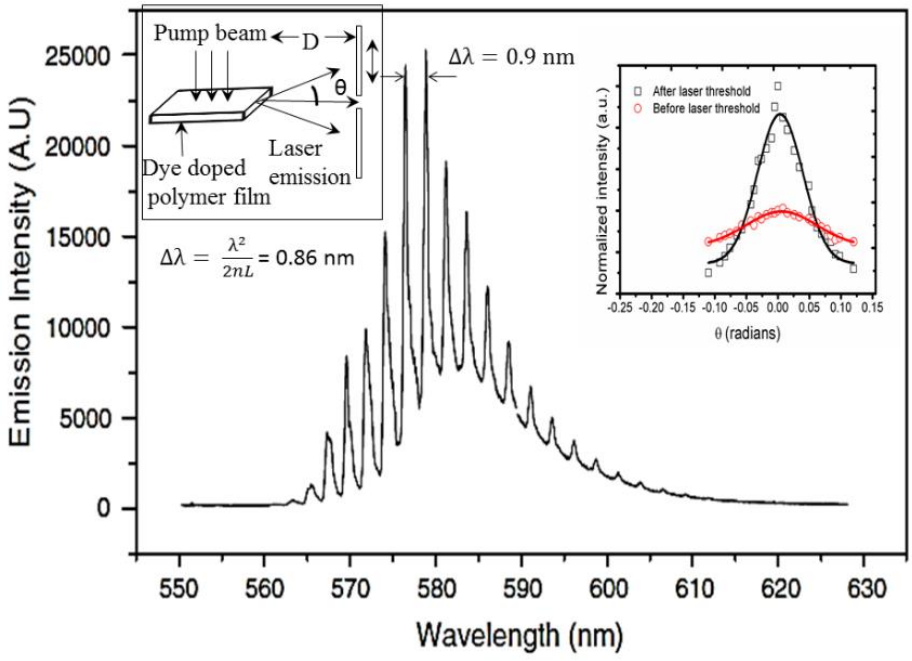

Figure 6.10 Multimode laser emission from 50 μm thick rhodamine 6G doped PMMA films at a pump power of 22 mW. Left inset, schematic diagram of the setup for intensity distribution measurement. Right inset, intensity distribution of the output of a planar microcavity (data points were well-fitted with a Gaussian curve (before and after laser threshold))

6.4.3 Directionality of laser emission

Another salient characteristic of laser emission is its increased directionality. The measurement geometry of the intensity distribution of the output from a planar microcavity has been shown in the figure 6.10 left inset.

A 1 mm pinhole was positioned in front a collecting fiber, which was kept in a translational stage and attached to a high-speed photo-detector. The distance between collecting fiber and free-standing film was 50 mm. By varying the height of the pinhole and collecting fiber simultaneously parallel to the fiber axis, we monitored the emission intensity at a given angle θ. Below lasing threshold, the intensity distribution of emission is broad. As the pump power is increased above the lasing threshold, the lasing action occurred in the direction of the highest gain parallel to the excitation stripe (θ = 0º). To confirm the spatial light confinement during the gain guiding, we measured the beam profile of the emission near the film as shown in figure 6.10 right inset. The intensity distribution is measured and the Gaussian curve is fitted on the data points from the output emission intensity above and below lasing threshold. Below lasing threshold, the regular photoluminescence emission from the planar microcavity is not highly directional, concentrated in the plane of the illuminated area of the microcavity within an angle Δθ of a few hundredths of a radian. Also, the emission anisotropic pattern abruptly changes above the laser threshold to Δθ = 0.1 radian, showing increased directionality of the laser modes.

The ability of an optical resonator or cavity to confine light of a given wavelength range around λ_0 is usually measured in terms of quality factor or Q factor. In the present study, we estimate the Q value of the microlasers to be $> 3 \times 10^3$,which results in narrow laser emission lines with a width < 0.2 nm. Further improvements in the film quality may lead to enhanced directionality and high Q value of the planar microcavity laser emission.

6.5 Conclusions

In summary, we have achieved an efficient photopumped multimode lasing in cylindrical microcavity formed by dye doped thin polymer film deposited on silica core optical fiber. The laser emission is characterised by

narrow emission lines (~ 0.05 nm), a well-defined excitation threshold and high Q (1.2×10^4), which can be very useful in sensor application. The thin ring resonator which is formed around the silica fiber can support whispering gallery modes as well as waveguided modes. By adjusting the waveguide parameters like polymer film thickness and n_{eff} , the number of modes within the gain profile can be controlled.

We also presented a detailed study of the amplified spontaneous emission and laser emission from an asymmetric and free-standing planar waveguide based on a rhodamine 6G doped PMMA film. The spectrally narrow emission (~5 nm) from an asymmetric planar waveguide was observed only in the plane of the film, whereas the emission perpendicular to the film surface remained spectrally broad (~40 nm). ASE spectrum from the film exhibits high directionality, narrow linewidth and presence of soft threshold behavior. A blue-shift in ASE has been also observed when the pump power was increased from 8 to 20 mW allowing a limited range of tuning of emission wavelength. From the study of directionality of ASE, the light amplification in an asymmetric planar waveguide is found to be due to two different propagation modes; namely, waveguide mode and cutoff mode. Well-resolved laser modes with equal spacing were observed from a free-standing planar waveguide, which confirm the optical feedback from the Fabry-Perot-like optical cavity formed between the lateral surfaces of the thin film. The multimode laser emission from free-standing planar microcavity was characterized by narrow emission lines (<0.2 nm) with high Q (>3×10^3) and increased directionality (0.1 radian).

References

1. J. C. Knight, H. S. T. Driver and G. N. Robertson, “Morphology-dependent resonances in a cylindrical dye microlaser: mode assignments, cavity Q values, and critical dye concentrations”, J. Opt. Soc. Am. B 11, 2046 (1994).

2. S. V. Frolov and Z. V. Vardeny, “Plastic microring lasers on fibers and wires”,Appl. Phys. Lett. 72, 15 (1998).
3. Gernot Wirnsberger and Galan D. Stucky, “Microring lasing from dye-doped silica/block copolymer nanocomposites”, Chem Mater 12, 2525-2527 (2000).
4. M. Kuwata-Gonokami, R. H. Jordan, A. Dodabalapur, H. E. Katz, M. L. Schilling and R. E. Slusher, “Polymer microdisk and microring lasers”, Opt. Lett. 20, 2093 (1995).
5. N. Tessler, G. J. Denton and R. H. Friend, “Lasing from conjugated-polymer microcavities”, Nature (London) 382, 695 (1996).
6. D. Zhao, P. Yang, N. Melosh, J. Feng, B. F. Chmelka, G. D. Stucky, “Continuous mesoporous silica films with highly ordered large pore structures”, Adv Mater 10, 1380 (1998).
7. Takeyuki Kobayashi and Nuala Byrne, “Plastic evanescent microlaser”, Appl. Phys. Lett. 99, 153307 (2011).
8. S. V. Frolov, M. Shkunov and Z. V. Vardeny, “Ring microlasers from conducting polymers”, Phys. Rev. B 56, 8 (1997).
9. H. P. Weber and R. Ulrich, “A Thin-Film Ring Laser”, Appl. Phys. Lett. 19, 38 (1971).
10. Siyaka I. Shopova, Hongying Zhou, and Xudong Fan, “Optofluidic ring resonator based dye laser” Appl. Phys. Lett 90, 221101 (2007).
11. S. V. Frolov, A. Fujii, D. Chinn and z. V. Vardeny, “Cylindrical microlasers and light emitting devices from conducting polymers”, Appl. Phys. Lett 72, 22 (1998).
12. S. V. Frolov, M. Shkunov and Z. V. Vardeny, M. Ozaki and K. Yoshino, “Laser action in conducting polymers”, Invited paper SPIE Vol 3145.
13. Jaison Peter, P. Radhakrishnan, V. P. N. Nampoori and M. Kailasnath, “Multimode laser emission from free-standing cylindrical microcavities”, Journal of Lumin. 149, 204-207 (2014).
14. O. Svelto, Principle of Lasers (Plenum, New York, 1989).
15. Wu Lu, Bo Zhong, and Dongge Ma, “Amplified Spontaneous Emission and Gain from Optically Pumped Films of Dye-Doped Polymers”, Applied Optics. 43, 26 (2004).
16. J. C. Knight, H. S. T. Driver, and G. N. Robertson, “Morphology dependent resonances in a cylindrical dye microlaser: mode assignments, cavity Q values and critical dye concentrations”, J. Opt. Soc. Am. B. 11, 10 (1994).
17. R. E. Slusher, "Optical processes in microcavities”, Semicond. Sci. Technol. 9, 2025-2030 (1994).

18. Jaison Peter, C. P. G. Vallabhan, P. Radhakrishnan, V. P. N. Nampoori and M. Kailasnath, “Microring lasing from a dye-doped polymer-coated silica fiber”, Laser Phys. 23, 115104 (2013).

19. Jaison Peter, C. P. G. Vallabhan, P. Radhakrishnan, V. P. N. Nampoori and M. Kailasnath, “Pumping Scheme Dependent Multimode Laser Emission from Free-standing Cylindrical Microcavity”, Optics Comm. 320,.125-128 (2014).

20. Jaison Peter, P. Radhakrishnan, V. P. N. Nampoori and M. Kailasnath, “Multimode laser emission from free-standing cylindrical microcavities”, J. Lumin 149, 204-207 (2014).

21. Ritty J. Nedumpara, K. Geetha, V. J. Dann, C. P. G. Vallabhan, V. P. N. Nampoori and P. Radhakrishnan,“Light amplification in dye doped polymer films” J. Opt. A: Pure Appl. Opt. 9, 174-179 (2007).

22. G. D. Peng, P. L. Chu, Z. Xiong, T. W. Whitbread and R. P. Chaplin, “Dye-doped step-index polymer optical fiber for broadband optical amplification,” J. Lightwave Technol. 14, 2215-2223 (1996).

23. M. Karimi, N. Granpayeh and M. K. Morraveg Farshi, “Analysis and design of a dye-doped polymer optical fiber amplifier,” Appl. Phys. B, 78, 387-396 (2004).

24. K. Geetha, M. Rajesh, V. P. N. Nampoori, C. P. G. Vallabhan and P. Radhakrishnan, "Laser emission from transversely pumped dye-doped free-standing polymer film" J. Opt. A: Pure Appl. Opt. 8, 189-193 (2006).

25. M. Kailasnath, V. P. N. Nampoori and P. Radhakrishnan, “A microring multimode laser using hollow polymer optical fibre”, PRAMANA journal of physics, 75, 5 (2010).

26. A. Otomo, S. Yokoyama, T. Nakahama and S. Mashiko, “Supernarrowing mirrorless laser emission in dendrimer-doped polymer waveguides”, Appl. Phys. Lett. 77, 3881-3 (2000).

27. S. A. Berg, R. H. Schoonderwoerd, H. F. M. Schoo, G. W. Hooft, and E. R. Eliel, “From amplified spontaneous emission to laser oscillation: dynamics in a short-cavity polymer laser”, Opt. Lett. 24, 1847-9 (1999).

28. K. Walter. Solid State Laser Engineering (Berlin: Springer) 182-5 (1972).

29. M. Fahis, I. Polyzos, G. Tsigaridas, V. Giannetas, P. Persiphonis, I. SpilioPoulos, and J. Mikroyannidis, Phys. Rev. B, 65, 195-203 (2002).

30. N. Tessler, G. J. Denton, and R. H. Friend, “Lasing from conjugated-polymer microcavities”, Nature 382, 695-7 (1996).

31. M. Kuwata- Gonokami, R. H. Jordan, A. Dobalapur, H. E. Katz, M. L. Schilling and R. E. Slusher, “Polymer microdisk and microring lasers”, Opt. Lett. 20, 2093-5 (1995).

32. M. Pauchard, J. Swensen, D. Moses, A. J. Heeger, E. Perzon, and M. R. Anderson, “Optical amplification of the cutoff mode in planar asymmetric polymer waveguides”, Appl. Phys. Lett. 83(22), 4488-4490 (2003).

33. D. Yokoyama, M. Moriwake, and C. Adachi, “Spectrally narrow emission at cutoff wavelength from edges of optically and electrically pumped anisotropic organic films”, J. Appl. Phys. 103(12), 123104 (2008).

34. Xianjie Li, Suijun Liu, Feng Li, and Yuguang Ma, “Optical amplification of two different propagation modes in organic small molecular waveguide structure”, Opt. Express, 19, 17691-17696 (2011).

35. M. D. McGehee, R. Gupta, S. Veenstra, E. K. Miller, M. A. Diaz-Garcia and A. J. Heeger, “Semiconducting polymer distributed feedback lasers,” Phys. Rev. B. 58, 7035-7039 (1998).

36. M. Rajesh, M. Sheeba, K. Geetha, C. P. G. Vallabhan, P. Radhakrishnan, V. P. N. Nampoori, Appl. Opt. 46 (1) (2007) 824.

37. Jaison Peter, C. P. G. Vallabhan, P. Radhakrishnan, V. P. N. Nampoori, M. Kailasnath, Opt. and Laser Techn. 63 (2014) 34-38.

38. O. Svelto and D. C. Hanna, Springer. Principles of Laser 4th edn, pp 71-3 (1998).

39. S. V. Frolov, Z. V. Vardeny, K. Yoshino and R. H. Baughman, “Stimulated emission in high-gain organic media”, Phys. Rev. B. 59, R5284-7 (1999).

Chapter 7
Microring embedded cylindrical microcavities

"Dreams is not what you sleep in sleep, is the thing which doesn't let you sleep"

A P J Abdul Kalam

Abstract

Optical microcavity resonators are the potential candidates for microlasers as well as fundamental studies in cavity quantum electrodynamics. Strongly modulated multimode laser emission has been observed from rhodamine B (Rh B) doped microring resonator embedded in the inner walls of the silica capillary by transverse pumping. We have studied the lasing behavior of different thickness microring cavities with enhanced mode selection. Particularly almost single mode lasing with a side mode suppression ratio of up to 10.2 dB is obtained from a very small microring cavity. The lasing modes inside such cavities can be easily collected from one end due to its very good propagation characteristics.

---

*The major content of this chapter has been communicated in journal "**Laser Physics Letter**".*

7.1 Introduction

In the last few decades, optical microcavity resonators are of an extensive research interest [1], not only due to their small mode volumes, ease of fabrication and high quality (Q) factor, but also for the potential applications such as low cost laser sources, active add-drop filters and photonic sensing devices [2]. High Q optical microresonators with strong optical confinement to the gain region can be obtained using the whispering gallery modes (WGMs) propagating around the edges of a sphere, disk, cylinder or ring [3]. Once the confinement of light on the scale of photon wavelength is achieved, the coupling strength is greatly enhanced due to cavity quantum electrodynamics effect. Cylindrical microcavity lasing have been investigated from different types of polymer and polymer coated optical fibers such as step index [4], graded index [5], hollow [6] and coated fiber [7]. The main disadvantage of WGM microcavity is that its surface emission and the absence of proper directional output coupling method. This is due to the fact that the WGMs come from the total internal reflections at the circular boundary and a small portion extends to the outside in the form of evanescent filed.

A layered circular microcavity will provide additional boundaries that introduce interference or guiding effects so as to modify the cavity modes significantly. Such evanescent wave coupled microcavity laser can not only provide an axial (end) laser emission but also convey its output power to long distance with minimum loss. Various studies on the layered microcavity have been conducted with spherical shells, ring microdisks and capillary tubes. The layered cavity itself has attracted much interest due to its complex mode structure and interferential modulation effect [8]. The first observation of interference modulation of lasing modes due to the coupling of electromagnetic fields between the layers was reported by Knight *et al.* [9]. These types of interference modulation effect on the lasing spectrum are of

practical importance because it can provide a scheme for mode selection in a broad–gain microcavity laser. Later a modified version of an efficient mode selection scheme was reported by Moon *et al.* [10]. This type of microcavity can generate nearly single mode lasing within the emission spectral width due to the strong coupling between the optical field and the gain medium.

7.2 Resonance modes in a microring embedded cavities

The usual method of fabrication of a microring cylindrical polymer microcavity is by making a coating of few microns thick conducting polymers [11] or a dye doped transparent polymer of high refractive index over a glass or quartz unclad fiber. In our study, the microring is formed by a thin coating of a polymer gain layer inside a silica capillary. Figure 7.1 shows the schematic of a thin ring-type microcavity with inner radius 'a', ring radius 'b' and outer radius 'c'. The refractive index of the outer silica region, ring-polymer layer and inner region are m_1, m_2, and m_3 respectively ($m_1 < m_2$, $m_3=1$). The microring cavity can be defined as the outer boundary B_0 (air-silica interface), ring-boundary B_1 (silica-polymer interface) and inner boundary B_2 (polymer-air interface). The ray optics picture in figure 7.1 shows all the possible categories of resonance modes in the proposed microring cavity. The notable resonance modes in a thin ring-type cavity are the waveguide modes (WMs), which are originated by total internal reflections of light between the boundaries B_1 and B_2. Circulating light trapped in the polymer ring region at resonant frequency will slowly refract (leak) tangentially from the region at a rate determined by the value m (relative refractive index, $m = m_1 / m_2$). If the silica capillary radius (outer), $c < m_1 b$, the angle of incidence upon the boundary B_0 is greater than the critical angle, the two cavities formed by the internal (B_1) and external (B_0) refractive index discontinuities will be strongly coupled. This will lead to generate another mode in the microcavity, which is termed as modified WGMs.

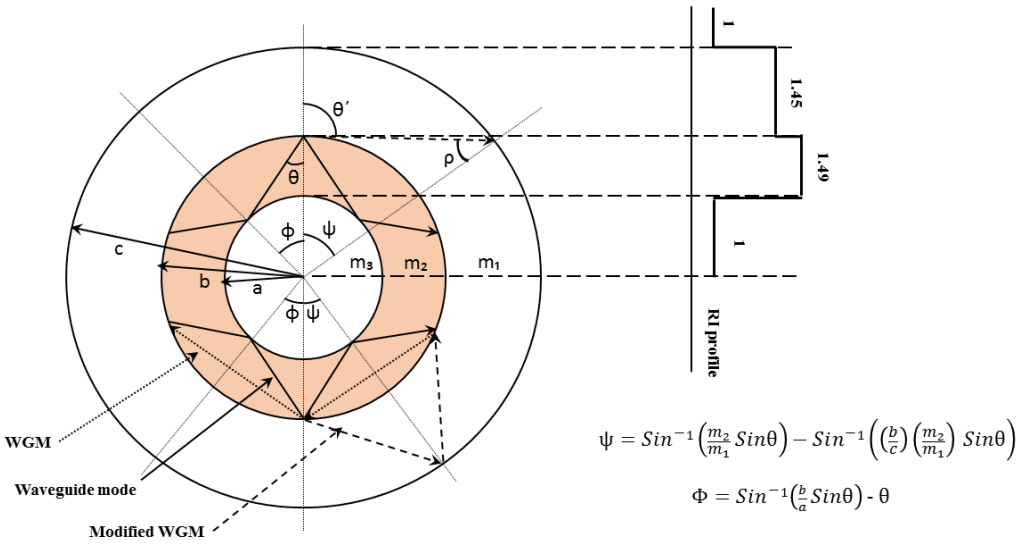

Figure 7.1 Schematic of a thin ring-type microcavity with its refractive index profile

The half-angle of the refracted ray is denoted as ψ and the half-angle of the reflected ray (waveguided ray) is denoted as Φ and are determined by m_1, m_2, a, b, c and the incident angle. From the ray optics model the value of the ψ and Φ can be derived as,

$$\psi = Sin^{-1}\left(\frac{m_2}{m_1}Sin\theta\right) - Sin^{-1}\left(\left(\frac{b}{c}\right)\left(\frac{m_2}{m_1}\right)Sin\theta\right)$$

$$\Phi = Sin^{-1}\left(\frac{b}{a}Sin\theta\right) - \theta$$

If Φ and ψ are not equal, as illustrated in the upper part of figure 7.1, the refracted ray experiences reflection loss upon each reflection at the boundary B_1, resulting in an accumulated loss sufficient to suppress laser oscillation [10]. Under the condition Φ=ψ, the total internally reflected waves will interfere constructively or destructively depending on the path-length difference $\Delta L = 2(m_1pq - m_2pr)$.

7.3 Preparation of microring embedded cavities

To demonstrate the proposed microring laser, we conducted a lasing experiment for which setup is similar to that of section 6.2.3. In the present study, the polymer gain layer is coated on the inner wall of a fused silica hollow capillary tube with an outer diameter of 320 µm, inner diameter of 250µm and a refractive index (m_1) of 1.458. To fabricate a thin ring resonator, we filled a precursor solution into the silica capillary. The precursor solution had a molar composition of polymethyl methacrylate (PMMA)/ Anisole / Rh6G = 2 gms / 15 ml/ 1×10^{-4} mol l^{-1}. By evaporating the polymer solution with forced air flow, we could obtain a thin polymer gain layer coating whose refractive index, m_2 (1.49) was larger than that of silica. This coating process was repeated to achieve the desired coating thickness. The flow rate of air and viscosity of the solution, which in turn depends on the concentration of PMMA was very important to form a thin uniform coating on the inner wall. Thickness of the coating was measured with a high resolution microscope image of the cross section of the capillary. Since the multiple layer coatings were manually conducted the thickness of the polymer layer fluctuated slightly.

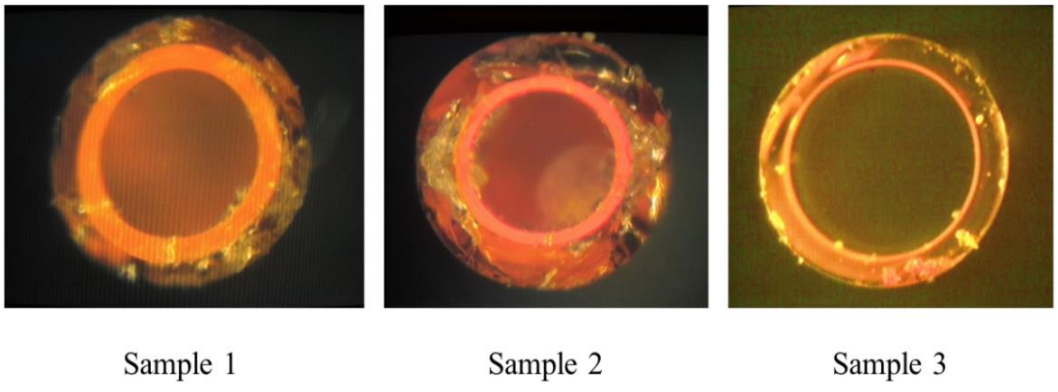

Figure 7.2 Cross-sectional view of different size micro-ring cavity using microscopic camera.

7.4 Experimental setup

To observe lasing from the proposed microring cavity, the polymer-film coated capillary was optically pumped by the second harmonics output of a Q-switched Nd:YAG laser (Spectra Physics) with 8 ns pulses at 10 Hz repetition rate. The pump power was adjusted with neutral density filters, and focused by a cylindrical lens into a 1 mm × 4 mm stripe transverse to the polymer coated capillary, as shown in figure 7.2. The emission from the microcavity was collected using an optical fiber and the spectrum was analyzed with a spectrograph (SpectraPro-0.5m) attached to a charge coupled device camera. In general, microcavity resonances can drastically change the spontaneous emission spectrum of the active gain medium via the quantum electrodynamics effects [12].

7.5 Laser emission characteristics

Under low Pump pulse energy (PPE) < 50 μJ, the sample 1 displays a weak and broad emission spectrum. Dramatic changes occur in the microcavity emission spectrum when the PPE exceeds the laser threshold PPE (P_{th}). As PPE increases above P_{th}, multiple sharp peaks with a linewidth as narrow as 0.06 nm emerge from the broad spectrum, the intensity of whole emission increase rapidly with the further increase of PPE. A plot of integrated intensity of emission peaks with respect to the PPE is shown in the bottom inset of figure 7.3. The observed non-linear increase of emission intensity is an indication of lasing phenomena from the microcavity and the lasing threshold is determined to be ~ 100 μJ. The cavity Q factor can be calculated from the emission linewidth, and it is found to be ~1.2×10^4. The Q factor of the microcavity tends to remain constant over a wide range of pump intensities. This result justified that the Q factor of a WGM laser emission from an organic microring laser tends to remain constant and independent of the PPE.

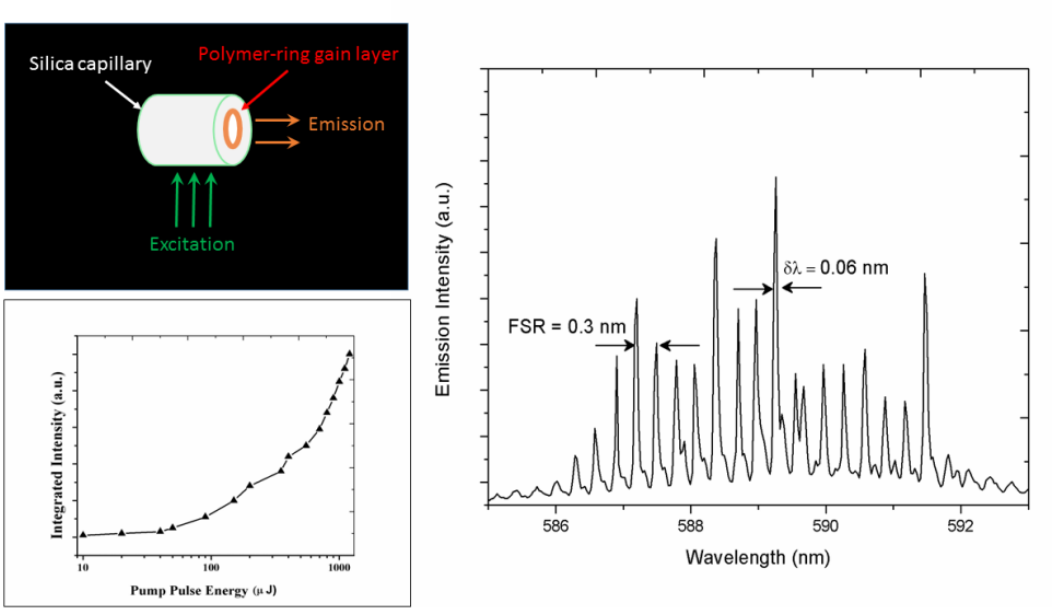

Figure 7.3 WGM lasing spectrum from a thick micro-ring cavity. Top inset shows the schematic of experimental setup and bottom inset shows the integrated emission intensity of the peaks as a function of pump pulse energy.

7.6 Modulation of resonance modes

In sample1, the width of gain layer is fairly large (~ 35 μm), the structure of resonance modes is same as the single boundary cavity: that is WGM is the only possible resonance mode in this condition. Since the outer size (~ 320 μm) of the silica capillary was very large compared to the inner size (~ 250 μm), the outer boundary B_0 can be neglected, even though slight feedback from the capillary outer boundary might induce some modulation effect in the inner layer mode structure. The resonant wavelength λ_m, separated by $\Delta\lambda = \lambda_m - \lambda_{m+1}$, is given by [7] $\Delta\lambda = \lambda^2/\pi nD = 0.31\ nm$, which is in good agreement with the experimentally observed Δλ (figure 7.3) of 0.3 nm. Resonant modes are no longer waveguided in thicker polymer ring microcavities [13]. In such cavities, optical modes never reach inner boundary B_2 and the mode intensity

distribution is concentrated on the ring-boundary B_1, and they do not realize the existence of B_2 [14].

On the other hand, the resonance mode structure becomes more complex as the width of the gain layer (ring) is small. When the width of the ring is of the order of wavelength of light, there might exist another type of resonance mode, so called waveguide modes (WMs). In sample 2, the ring-thickness is moderate (~15 μm). In these types of layered microcavity, the pumping efficiency of laser can be substantially enhanced due to the high overlapping ratio between the waveguide modes and gain region. Hence the ring type microcavity can provide additional functionalities such as coupling of different sets of modes by controlling the thickness of the ring. We also observe that the lasing peaks are considerably modulated as a clustered pattern. Strong peaks appeared nearly periodically and the interference period can be defined by the equation $\delta\lambda \approx \lambda^2/\Delta L$. The wavelength seperation between two locally strong peaks was measured to be ~1.5 nm as shown in figure 7.4.

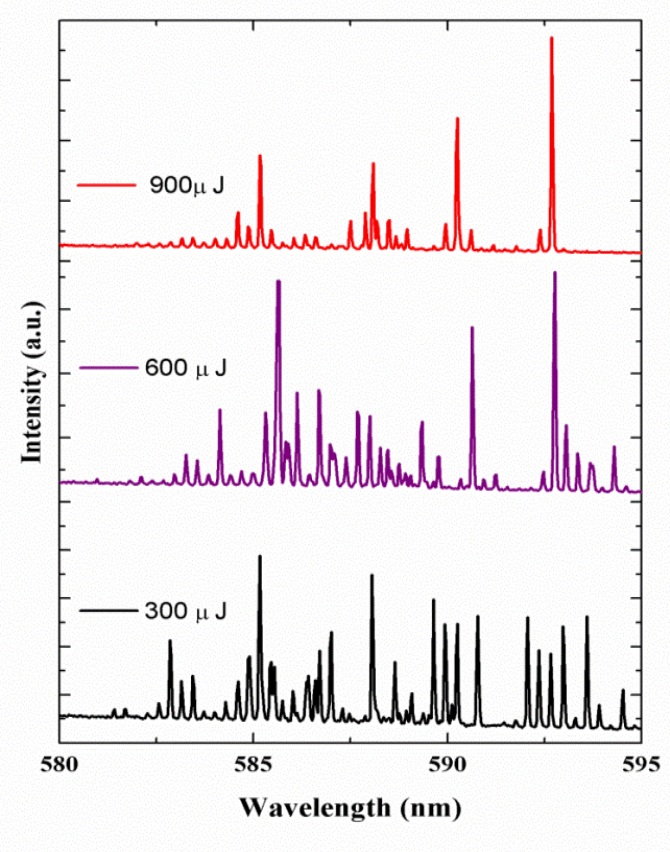

Figure 7.4 Modulated WGM lasing spectrum from sample 2 with increasing PPEs.

Strongly modulated spectra have been observed from a moderately thin-ring microcavity (sample 2) with ring-thickness of ~15 μm. Because the RI difference (Δn) between m_1 and m_2 layer is small, a fraction of light rays at B_1 interface will reflected back into polymer region. The interference effect is originated by the recombination of refracted (leaked) lasing light from boundary B_1 and reflects back into B_1 from B_0. Hence the two subcavities formed by the internal and external RI discontinuity will be strongly coupled. The profile of lasing spectrum also changes as the PPE increases. The observed lasing peaks showed a periodic spectral profile with improved characteristics of mode selection and interference period well matched with

the prediction by a ray-optics model. Consider the two half-angles (Φ and Ψ) are equal, then the path-length difference (ΔL) of the two rays is about 230 μm at θ=59.2˚. The calculated interference period ($\approx \lambda^2/\Delta L$) of 1.5 nm is consistent with the measured value of ~1.56 nm within the experimental error. We strongly believe that this effect is due to the interaction of more than one set of modes. Such efficient mode selection results from the strong constructive or destructive interference caused by the relevant coupling between the waveguided rays, refracted and reflected rays. The refracted ray is enhanced with increasing PPE and the width of the mode clusters decrease due to different non-linear interaction with microcavity [15]. Due to this effect, the side modes due to WGM lasings are found to be suppressed from spectra. At higher PPE, enhanced laser peaks are observed at periodic interval with a good side mode suppression ratio (SMSR). In sample 2 we could obtain a SMSR value of 6.2 dB from the strongly modulated spectrum at 1.1 mJ PPE. In our case the periodicity of the modulations are not perfectly matched due to small surface irregularities of the coated layer.

7.7 Single mode laser emission

In the sample 3, the thickness of micro-ring is very small (~8 μm). In such cavities the intensities of WGM lasing is very small as compared to the lasing peaks due to the constructive interference effect, which is originated by the recombination of three resonant modes viz WGM, WM and modified WGM as shown in figure 7.1.

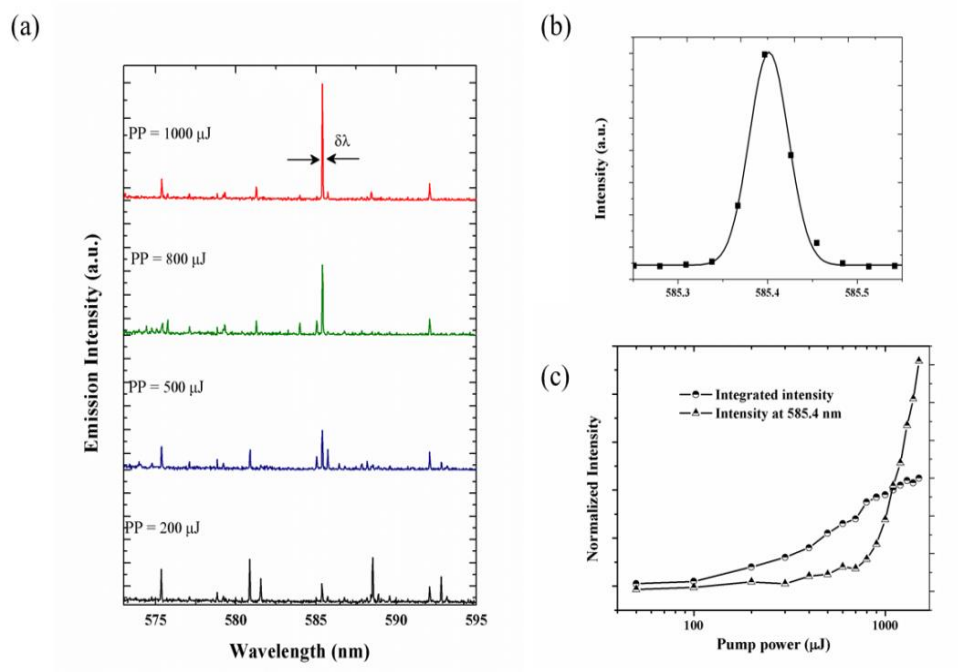

Figure 7.5 (a) Strongly modulated lasing mode spectra from a sample 3 at different PPE. Almost single mode emission is observed at a PPE of 1000 µJ. (b) shows the magnified version of the highest intensity lasing line at 585.4 nm with Gaussian fit and (c) shows emission intensity of 585.4 nm mode and integrated emission intensity versus pump power.

Figure 7.5 (a) shows the laser emission spectra from sample 3. From the emission spectra one could observe that the emission intensity at 585.4 nm mode has a very sharp line-width of 0.04 nm and its power increase nonlinearly with PPE as compared to other lasing modes. At high PPE > 800 µJ, some of the modes do not appear and those that appear have a much lower level. This type of quenching might be due to the non-linear interactions between the different modes that are supported within the cavity. Nearly single mode lasing with SMSR of 10.2 dB is obtained from the modulated spectrum. In this sample, over 70% of the observed emissions are from the single mode at a PPE of 1000 µJ. Figure 7.5 (b) shows the magnified version of the highest intensity lasing line at 585.4 nm with Gaussian fit. Figure 7.5 (c) plots the emission intensity of 585.4 nm lasing mode and spectrally integrated intensity

of other lasing modes as a function of PPE. Table 7.1 details of the sample, lasing threshold and modulation parameters of the different ring-thickness microcavities.

Table 7.1 Details of the sample, lasing threshold and modulation parameters of the different ring-thickness microcavities.

Sample	Micro-ring thickness	Lasing threshold (PPE)	FWHM (λ_{FWHM}) and Q-Factor	Modulation period ($\delta\lambda$), SMSR (dB)
Sample 1	35 µm	100 µJ	λ_{FWHM} = 0.06 nm Q = 9.8×10^3	NA
Sample 2	15 µm	150 µJ	λ_{FWHM} = 0.05 nm Q = 1.2×10^4	1.2 nm 6.2 dB
Sample 3	8 µm	200 µJ	λ_{FWHM} = 0.04 nm Q = 1.4×10^4	2.5nm 10.2 dB

The details of all the parameters of the different ring-thickness microcavity are listed in table 7.1. It can be seen that the laser threshold increases with decreasing ring thickness of the microring resonators. Since the dye molecules are restricted to the inner wall of the capillary, lasing threshold increase with decrease in thickness of the gain layer. The larger thickness results in longer gain path length and hence show lower threshold values [16].

7.8 Conclusions

Rh B dye doped polymer microring cavities have been fabricated on the inner wall of the hollow silica capillary. The laser emission characteristics of different ring-thickness cavities have been studied. Thin layered cavity can have a strong mode selection through an enhanced interferential coupling

effect. Almost single mode lasing with a SMSR of 10.2 dB is obtained from the thin-layered microcavity. We also observe that the lasing threshold is inversely proportional to the microring thickness. Such microring cavities can have potential applications in sensors, tunable laser source, low-threshold laser device to generate single mode emission in simple and cost-effective manner.

References

1. Rui Chem, Van Duong Ta and Han Dong Sun, "Single mode lasing from hybrid hemispherical microresonators", Scientific Reports 2, 244 (2011), DOI: 10.1038/srep00244.
2. A. Polman, B. Min, J. Kalkman, T. J. Kippenberg and K. J. Vahala, "Ultralow-threshold erbium-implanted toroidal microlaser on silicon" Appl. Phys. Lett. 84,1037 (2004).
3. M. Kuwata Gonokami, R. H. Jordan, A. Dodabalapur, H. E. Katz, M. L. Schilling, R. E. Slusher and S. Ozawa, "Polymer microdisk and microring lasers", Opt. Lett. 20, 20, pp. 2093-2095, (1995).
4. V. D. Ta, R. Chen, L. Ma, Y. J. Ying, and H. D. Sun, "Whispering gallery mode microlasers and refractive index sensing based on single polymer fiber", Laser and Photon. Rev. 7, 1, pp. 133-139 (2013).
5. C. L. Linslal, S. Mathew, P. Radhakrishnan, V. P. N. Nampoori, C. P. Girijavallabhan and M. Kailasnath, "Laser emission from the whispering gallery modes of a graded index fiber", Opt. Lett. 38, 17, pp. 3261-3263 (2013).
6. Jaison Peter, P. Radhakrishnan, V. P. N. Nampoori, and M. Kailasnath, "Multimode laser emission from free-standing cylindrical microcavities", J. Lumin., 149, pp. 204-207 (2014).
7. Jaison Peter, C. P. G. Vallabhan, P. Radhakrishnan, V. P. N. Nampoori, and M. Kailasnath, "Microring lasing from a dye-doped polymer-coated silica fiber", Laser Phys. 23, 17 (2013).
8. H. J. Moon, "Photon tunneling behavior in a coated cylindrical microcavity laser", J. Opt. Soc. Am. B., Vol 27, No. 3 (2010).
9. J. C. Knight, H. S. T. Driver, R. J. Hutcheon, and G. N. Robertson, "Core-resonance capillary-fiber whispering-gallery-mode laser", Opt. Lett. 17, 18, pp. 1280-1282 (1992).
10. H. J. Moon and K. An, "Interferential coupling effect on the whispering-gallery mode lasing in a double-layered microcylinder", Appl. Phys. Lett. 80, 3250 (2002).

11. S. V. Frolov, M. Shkunov, and Z. V. Vardeny, “Ring microlasers from conducting polymers”, Phys. Rev. B., Vol 56, No.8 (1997).

12. A. J. Campillo, J. D. Eversole, and H. B. Lin, “Cavity quantum electrodynamic enhancement of stimulated emission in microdroplets”, Phys. Rev. Lett 67, 437 (1991).

13. M. Heiblum and J. H. Harris, “Accurate numerical method for the calculation of bending loss in optical waveguides using a matrix approach”, IEEE J. Quantum Electron QE-11, 75 (1975).

14. J. C. Knight, H. S. T. Driver and G. N. Robertson, “Morphology-dependent resonances in a cylindrical dye microlaser: mode assignments, cavity Q values, and critical dye concentrations”, J. Opt. Soc. Am. B, 11, 10, pp. 2046-2053 (1994).

15. C. L. Linslal, S. Sebastian, S. Mathew, P. Radhakrishnan, V. P. N. Nampoori, C. P. Girijavallabhan, and M. Kailasnath, “Microring embedded hollow polymer fiber laser”, Applied Physics Letters 106, 131101 (2015).

16. Martin Djiango, Takeyuki Kobayashi, Estella Bouron, Werner J. Blau, Yasuhiro Suzuki and Toshikuni Kaino, “Operating characteristics of near-infrared self-assembled polymer microlasers”, Opt. Lett. Vol. 32, No. 11 (2007).

Chapter 8
Conclusion and future research prospects

"Impossible is not a scientific term"

Vanna Bonta

Abstract

This chapter deals with the main conclusions of the work presented in this thesis. A brief sketch of future research prospects is also mentioned in this chapter.

8.1 Major conclusions

- Polymer optical waveguide systems are gaining much interest in the recent years due to their potential advantages such as low weight, low processing temperature, economic viability, geometrical versatility and so on.
- Poly methyl-methacrylate (PMMA) is found to be an ideal polymer material for the fabrication of polymer waveguides due to their low loss in the visible region and their ability to incorporate very high concentration of optical gain media like organic dyes and rare-earth components.
- Organic dyes of Xanthene (Rhodamine) family have been extensively used as gain medium for dye doped polymer waveguides because of its large absorption and emission cross-sections, high internal quantum efficiency and wide spectral range of their emission.
- Photophysical and lasing characterization of Rhodamine laser dyes are carried out in different solvents, mainly focusing on Rh B, a highly fluorescent dye in the orange-red region. The emission characteristics were successfully compared with computational data.
- Different types of dye doped PMMA based optical fibers were fabricated successfully by the *preform method* using the fiber drawing workstation. Detailed measurements were made to understand the amplified spontaneous emission (ASE) and photo-degradation phenomena in those POF systems.
- Multimode laser emission corresponding to whispering gallery mode (WGM) from dye (Rh 6G) doped hollow polymer (PMMA) fiber (DDHPOF) is observed when excited with second harmonics of Nd:YAG laser.
- Numerical analysis of the WGM microresonator using COMSOL Multiphysics was performed.

- Tunability of WGM laser emission and variation in free spectral range (FSR) is obtained by varying the diameter of DDHPOFs.
- Two different pumping scheme viz. spot and stripe illumination is employed to study slope efficiency, laser threshold and tuning of laser emission from DDHPOFs.
- In order to get a stable and directional emission an asymmetric resonant cavity (ARC) is realized by the controlled deformation of DDHPOFs. Comparison of emission characteristics of an SRC and ARC is performed by simulation and experiment.
- Fabrication and emission characteristics of asymmetric and free-standing planar waveguide are discussed. The light amplification in an asymmetric planar waveguide is due to two different modes; namely, waveguide mode and cutoff mode.
- Interferential modulation of laser emission due to simultaneous occurrence of two different sets of resonant modes viz waveguide mode (WG) and WGM was observed from Rh 6G dye doped PMMA coated unclad silica fiber.
- Rh 6G dye doped microring embedded silica tube exhibit sharp lasing lines with strong mode selection. Nearly single mode laser emission with a high SMSR value is observed from these microcavities.

8.2 Future research prospects

- Photostability, is one of the major problem associated with the dye doped polymer waveguide systems. Instead of dye, rare-earth and nanoparticle doped polymer waveguides may provide an enhanced photostability and nonlinear optical properties.

- Studies using femtosecond pump source will be useful to understand fast optical nonlinear processes taking place in the different dye doped waveguides.
- Nanoparticles doped POFs has lots of potential applications in developing random lasing and sensing devices, especially surface plasmon response (SPR) based sensors.
- Further improvements in the polymer waveguide quality will reduce the laser threshold and increase the Q factor of device.
- Realization of different degree of deformations in annular structured cylindrical microcavities to achieve high Q-unidirectional laser emission.
- Microring resonators have several attractive features for sensing applications. One of the most important applications for hollow WGRs is in the area of Biosensing. It's high quality factor and multiple pass interaction nature allows resolving small shifts in resonance wavelength induced by any sensing object near the resonator.
- Development of novel polymer waveguide structures such as microstructured polymer optical fibers (m-POFs) opens up new possibilities for technologies and applications. Work in this direction has already started in our lab.

Appendix

Appendix

Appendix

IOP PUBLISHING LASER PHYSICS
Laser Phys. **23** (2013) 115104 (3pp) doi:10.1088/1054-660X/23/11/115104

Microring lasing from a dye-doped polymer-coated silica fiber

Jaison Peter, C P G Vallabhan, P Radhakrishnan, V P N Nampoori and M Kailasnath

International School of Photonics, Cochin University of Science and Technology, Cochin-682022, India

E-mail: jaison.peter@gmail.com

Received 16 August 2013
Accepted for publication 11 September 2013
Published 7 October 2013
Online at stacks.iop.org/LP/23/115104

Abstract
We demonstrate pulsed, photopumped multimode laser emission in the visible spectral range from cylindrical microcavities of dye-doped thin polymer film deposited on silica core optical fiber. The laser emission is characterized by narrow emission lines (∼0.05 nm), a well-defined excitation threshold and high $Q \sim 1.2 \times 10^4$. We observed two different sets of resonant laser modes: namely, waveguided ring modes in the polymer film and whispering gallery modes close to the optical fiber surface.

(Some figures may appear in colour only in the online journal)

Polymer and polymer-coated microcavities have attracted increasing interest in recent years due to their many advantages (e.g., low cost, diversity, flexible mechanical properties, rich surface functionalities, and ease of fabrication and incorporation of functional materials) over inorganic materials. The design of a microcavity provides one possibility for a compact light-emitting device structure. The microcavity devices consist of luminescent material placed within a Fabry–Perot resonator with a length of the order of the wavelength of emitted light. In this way the light emission is coupled to the cavity mode(s) and characteristically the light output is spectrally narrowed and directed. Microcavities provide excellent coupling of spontaneous emission into lasing modes, as well as high Q-value which consequently leads to low lasing thresholds [1]. Lasing, in addition requires an optical cavity to produce optical feedback, which subsequently forms resonant laser modes [2]. These necessary feedback features can be achieved by patterning the material in disc or ring form. We are interested in achieving microlasers on solid supports (either cylindrical or planar) that are easy to handle and might be integrated, for example in sensing devices [3]. A microring laser cavity offers a low loss resonance structure that has been utilized to demonstrate lasing with organic gain media [4]. Planar microcavities [5], however, are prone to losses due to imperfect reflection and emission leakages to the sides of the microcavity plane. Cylindrical microcavities may support waveguide and whispering gallery modes [1], both of which are due to total internal reflections inside the active volume and thus can be practically lossless.

The dip-coating technique works very well for producing thin films on supporting structures such as silica core fiber [6]. In the present study, the polymer gain layer is formed on the surface of an unclad silica optical fiber [7]. Cylindrically shaped thin polymer films were prepared by dipping commercially available multimode silica optical fiber (from which the cladding was removed) into precursor solution [3]. The precursor solution had a molar composition of polymethyl methacrylate (PMMA)/ethanol/Rh6G = 5 gms/15 ml/1 $\times$ 10^{-4} mol l^{-1}. Thin polymer rings were consequently formed around the glass cylindrical core following fast drying in air [8]. The self-assembled polymer microstructure in the form of cylindrical microrings is similar to those previously reported in [4, 9], with deposited films of laser dyes blended in transparent polymers.

Since the refractive index of the silica fiber is lower than that of the polymer gain layer, there can exist laser resonances, which are confined to the polymer layer, and provide the optical feedback required for lasing. To support the polymer gain layer a silica optical fiber was used. Its refractive index has a bulk value of $n_s = 1.46$, which is less than that of PMMA ($n_p = 1.49$). The coated polymer gain layer is sufficiently thin that the whispering gallery modes (WGMs) of high Q factors exist in the core support facilitating

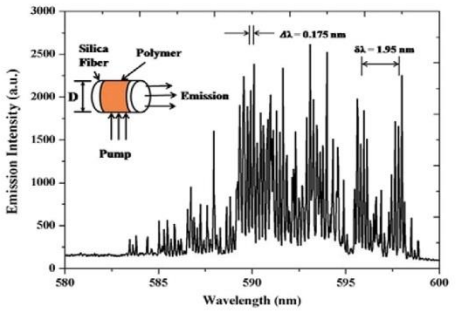

Figure 1. Emission spectrum of dye coated on glass fiber with diameter $D = 420\ \mu$m and pump power of 24 mW ($P_{th} \times 8$). The inset depicts the measurement geometry.

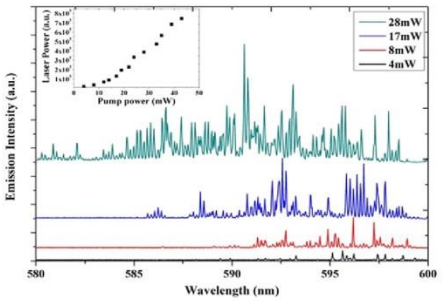

Figure 2. Typical emission spectra taken at (from bottom to top) $P = P_{th} \times 1.33$, $P = P_{th} \times 2.67$, $P = P_{th} \times 5.67$ and $P = P_{th} \times 9.33$. The inset shows the output laser power (numerically integrated output intensity) versus the pump power.

the low threshold laser oscillations [10]. The polymer layer thickness is important, as it determines the fraction of the light in the core that gets extracted evanescently from the gain medium. Cylindrical microcavities may support waveguided modes (WMs) and WGMs [1], both of which arise due to total internal reflections inside the composite structure of the active volume and thus can be practically lossless [11].

To observe lasing from the ring configuration as described above, the polymer-film-coated fibers were optically pumped by the second harmonic output of a Q-switched Nd:YAG laser (532 nm, 10 Hz). The pump power was adjusted with neutral density filters, and focused by a cylindrical lens into a 1 mm × 0.4 mm stripe transverse to the polymer-coated fiber (figure 1 inset). The emission from the microcavity was collected by use of another optical fiber and the spectrum was analyzed with a spectrograph attached to a charge-coupled device camera. The spectral peak intensity of the polymer ring laser is positioned at the maximum of optical gain which in turn corresponds to the photo-luminescent spectrum peak [12] around 590 nm. A large number of sharp lines can be seen within the fluorescent emission profile. The lasing modes are spectrally narrow with a FWHM of 0.05 nm with a pump power of $P_{th} \times 8$, where P_{th} is the lasing threshold pump power. Due to the fairly large thickness of the optical fiber (420 μm), there are large number of longitudinal modes that can be supported by the microcavity [3] (figure 1).

When the pump power is higher than the lasing threshold ($P_{th} \times 1.33$) microring lasing modes appear in the longer wavelength range (595–600 nm) of the photo-luminescence spectra of the gain medium. When the pump power is further increased, the lasing modes with high intensities start to develop on the shorter wavelength region of the spectra. The number of lasing modes and the resonant mode intensities increase with pump power as can be clearly seen in figure 2. The inset shows the output laser power (numerically integrated output intensity) versus the pump power.

At a pump power of $P_{th} \times 9$, the lasing modes are found to cover the entire photo-luminescence emission band of the gain medium i.e. 580–600 nm. When the polymer layer thickness 'd' is very small, the film acts as a curved two-dimensional waveguide [11] and the resonant wavelengths for the waveguided lasing modes are given by the following equation [4, 9]:

$$m\lambda_m = \pi D n_{\text{eff}}, \tag{1}$$

where m is an integer, λ_m is the resonant wavelength, D is the silica fiber diameter and n_{eff} is the effective index of refraction in the cylindrical polymer waveguide.

In addition to the waveguided modes in the polymer film, the cylindrical glass fiber may support WGM propagating close to the fiber surface [13]. The wavelength of each WGM mode is determined by

$$\Delta\lambda = \lambda_m - \lambda_{m-1} = \lambda^2/\pi D n_{\text{eff}} = 0.177\ \text{nm}, \tag{2}$$

which is in good agreement with the experimentally observed $\Delta\lambda$ (figure 3) of 0.175 nm. The observed variations in the mode intensities as shown in figure 3 can be explained on the basis of the simultaneous occurrence of WGM and WG modes. This leads to lasing output with the modulated Q_{cav} with wavelength separation

$$\delta\lambda = \Delta\lambda \frac{n_{\text{eff}}}{\Delta n_{\text{eff}}}, \tag{3}$$

where Δn_{eff} is the difference between n_{eff} of the WG and WGM [8] with the parameters of the waveguide structure explained in our present study. We have calculated the wavelength separation $\delta\lambda = 1.965$ nm, which agrees well with the observed value (1.95 nm) as shown in figure 1.

The thin ring resonator which is formed around the silica fiber can support whispering gallery modes propagating along their cylindrical edges [1]. Whispers are able to produce a low Q feedback mechanism to modify Q_{cav} of the waveguided modes in the polymer ring [12]. The laser emission spectra are modulated by the superposition of the WGMs on the WMs as shown in figure 3. Q_{cav} is increased if waveguided and whispering modes are in resonance, and Q_{cav} decreases if the corresponding resonant wavelengths are detuned from each other [8]. We therefore attribute the appearance of the

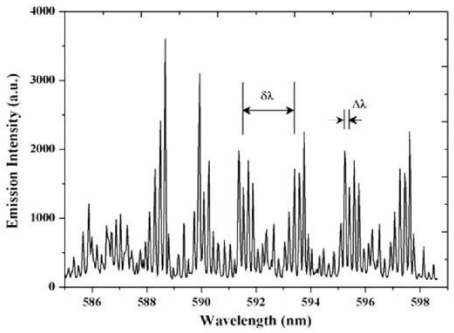

Figure 3. Resonant modulation of the waveguided modes and whispering gallery modes.

emission spectra to a resonant modulation of the waveguided modes by whispering gallery modes [3].

The ability of an optical resonator or cavity to confine light of a given wavelength range around λ_0 is usually measured in terms of quality factor or Q factor, which is given as

$$Q = 2\pi\nu_0 \frac{P_{\text{stored}}}{P_{\text{lost}}} = \frac{\nu_0}{\delta\nu}, \tag{4}$$

where P_{stored} and P_{lost} are the power stored within the cavity and lost from the cavity, respectively, while $\delta\nu$ is the spectral line-width of the cavity mode at frequency ν_0. In the present study, we estimate the microlaser's Q value to be about 1.2×10^4, which in addition to the low laser threshold, results in narrow laser emission lines with width of about 0.05 nm.

In summary, we have achieved an efficient photopumped multimode lasing in cylindrical microcavity formed by dye-doped thin polymer film deposited on silica core optical fiber. The laser emission is characterized by narrow emission lines (∼0.05 nm), a well-defined excitation threshold and high Q (1.2×10^4), which can be very useful in sensor application. The thin ring resonator which is formed around the silica fiber can support whispering gallery modes as well as waveguided modes. By adjusting the waveguide parameters like polymer film thickness and n_{eff}, the number of modes within the gain profile can be controlled.

Acknowledgments

The authors acknowledge the financial support from Kerala State Council for Science, Technology and Environment (KSCSTE) and the Department of Science and Technology (DST). Jaison Peter is grateful to the University Grant Commission (UGC) for the research fellowship.

References

[1] Yamamoto Y and Slusher R 1993 *Phys. Today* **46** 66
Knight J C, Driver H S T and Robertson G N 1994 *J. Opt. Soc. Am.* B **11** 2046
[2] Frolov S V and Vardeny Z V 1998 *Appl. Phys. Lett.* **72** 15
[3] Wirnsberger G and Stucky G D 2000 *Chem. Mater.* **12** 2525–7
[4] Kuwata-Gonokami M, Jordan R H, Dodabalapur A, Katz H E, Schilling M L and Slusher R E 1995 *Opt. Lett.* **20** 2093
[5] Tessler N, Denton G J and Friend R H 1996 *Nature* **382** 695
[6] Zhao D, Yang P, Melosh N, Feng J, Chmelka B F and Stucky G D 1998 *Adv. Mater.* **10** 1380
[7] Kobayashi T and Byrne N 2011 *Appl. Phys. Lett.* **99** 153307
[8] Frolov S V, Shkunov M and Vardeny Z V 1997 *Phys. Rev.* B **56** 8
[9] Weber H P and Ulrich R 1971 *Appl. Phys. Lett.* **19** 38
[10] Shopova S I, Zhou H and Fan X 2007 *Appl. Phys. Lett.* **90** 221101
[11] Frolov S V, Fujii A, Chinn D and Vardeny Z V 1998 *Appl. Phys. Lett.* **72** 22
[12] Frolov S V, Shkunov M, Vardeny Z V, Ozaki M and Yoshino K *Proc. SPIE* **3145** 2
[13] Svelto O 1989 *Principle of Lasers* (New York: Plenum)

Appendix

Journal of Luminescence 169 (2016) 227–232

Contents lists available at ScienceDirect

Journal of Luminescence

journal homepage: www.elsevier.com/locate/jlumin

Solvent effects on lasing characteristics for Rh B laser dye

Jaison Peter [a,*], Mahesh Kumar [b], V.R. Ananad [a], Rasool Saleem [a], Ananthu Sebastian [a], P. Radhakrishnan [a], V.P.N. Nampoori [a], C.P.G. Vallabhan [a], Radhakrishna Prabhu [c], M. Kailasnath [a]

[a] International School of Photonics, Cochin University of Science and Technology, Cochin 682022, India
[b] Department of Applied Chemistry, Cochin University of Science and Technology, Cochin 682022, India
[c] School of Engineering, Robert Gordon University, Aberdeen AB10 1FR, Scotland, UK

ARTICLE INFO

Article history:
Received 17 December 2014
Received in revised form
19 August 2015
Accepted 2 September 2015
Available online 25 September 2015

Keywords:
Dye laser
Stokes shift
Solvent tuning
Resonant modulation

ABSTRACT

We demonstrate pulsed, photopumped multimode laser emission in the visible spectral range from rhodamine B dye dissolved in various solvents. The laser emission is characterized by a well-defined, low threshold pump power at which the emission spectral intensity dramatically increases and collapsed into several dominant laser modes with reduced mode spacing and spectral width. The modes were found to originate from the subcavities formed by the plane-parallel walls of the cuvette containing the gain medium. The cavity lasing spectral structure and the numbers of longitudinal modes were easily controlled by changing the solvents. A shift in the emission spectra has been also observed by changing the solvents will allow a limited range of tuning of laser emission wavelength. We also determined the gain coefficient and stimulated emission cross-section for the Rh B dye dissolved liquid laser system. A detailed discussion of the solvent effect in the lasing characteristics of Rh B in different solution is explained along with the computational data.

1. Introduction

The first laser was built in 1960 by Maiman [1], 44 years after Einstein's discovery of stimulated emission. Six years after, the first dye laser was realized by Sorokin and Lankard [2].The ultra-wide wavelength tuning range and the ability to generate both narrow linewidth continuous wave output and ultra-short pulses make dye lasers an ideal coherent source for spectroscopy [3]. Generally, laser dyes are complex organic molecules containing long chains of conjugated double bonds. The complex molecular structure will leads to many vibrational and rotational energy levels within a single electronic state. Therefore, laser dyes often have strong and wide absorption bands in the UV and visible region [4,5]. Liquid dye lasers are the first material systems used to study the laser action and other optical processes in microcavities. In liquid dye lasers, tuning of the laser wavelength is performed either by changing the concentration of the dye, *concentration tuning* or by changing the optical path length in the cavity. To change the optical path of the cavity, the solvent of the dye can be changed, thereby changing the refractive index in the cavity. This method is so called *solvent tuning*. One should keep in mind that by changing the solvent, other properties of the fluid which can affect the laser wavelength may be changed due to the interaction between dye molecules and solvent molecules.

The solvent plays an important role in photophysical properties of laser dye. In this paper, we analyze the solvent effects on the laser emission characteristics for Rhodamine B (Rh B) laser dye. In our study, Rh B dye is dissolved in different solvents such as ethanol, methanol, butanol, ethylene glycol and glycerol, which are pumped longitudinally with short light pulses of several energies [6,7]. Apart from its particularly large cross section, it has high photochemical stability, which is important in practice to withstand multiple excitation cycles with a pulsed pump laser. Organic laser dyes typically show a large fluorescence yield ranging from about 0.6 to near the optimum 1.0. Fig. 1 shows the absorption spectra of Rh B with a concentration of 5×10^{-4} mol/dm^3, which is dissolved in ethanol, butanol and glycerol respectively. These spectra were measured in a cuvette of diameter 0.1 cm using a UV–vis spectrophotometer (Jasco V-570). The absorption spectra exhibit a solvatochromic shifts after exchange between one solvent to another. Due to the electron redistribution within the solvent molecules, the energy difference between ground state and excited states will vary.

Fig. 2 shows the tuning of emission wavelength peak with variation in the dye concentration in methanol. The peak emission wavelength of Rh B dye with 1×10^{-4} mol/dm^3 concentration is

* Corresponding author.
E-mail address: jaison.peter@gmail.com (J. Peter).

http://dx.doi.org/10.1016/j.jlumin.2015.09.002
0022-2313/

found to be at 589 nm. By increasing the concentration of Rh B, the peak wavelength shows a clear redshift and at 5×10^{-3} mol/dm^3 concentration the emission peak is at 624 nm. Due to Stokes shift, the shorter wavelength of emission spectrum is absorbed by Rh B molecule and re-emit to the higher wavelength. The increase in concentration will increase the interaction between the dye molecules and the fluorescence light will result the shifting of the emitted fluorescence peak towards the longer wavelength region. This type of concentration dependent red-shift was also reported by Schafer [3]. These types of tuning of the emission wavelength by changing the concentration of the dye are generally known as *concentration tuning*. The inset of Fig. 2 shows the redshift of emission spectra as a function of dye concentration. From this, it is clear that the lasing wavelength is tunable over a wide range (589–624 nm) due to the overlap of absorption and emission spectra of Rh B dye. However, after a particular dye concentration, the shift tends to exhibit saturation behavior.

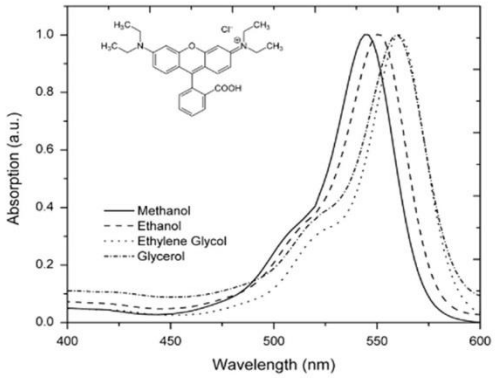

Fig. 1. Absorption spectra of Rh B dye (5×10^{-4} mol/dm^3) dissolved in various solvent. Inset shows the molecular formula of Rh B.

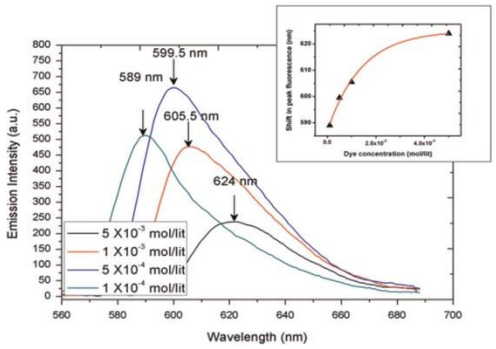

Fig. 2. Florescence spectra of Rh B dye dissolved in methanol with different concentration. Inset shows red-shift of peak fluorescence with the concentration of Rh B.

2. Experimental setup

To observe lasing from the different dye solution, we used the second harmonic output of a Q-switched Nd:YAG laser that emits pulses of 8 ns duration at a repetition rate of 10 Hz as the excitation source. The pump power was adjusted with neutral density filters, and focused by a cylindrical lens into a 0.2 mm × 4 mm stripe transverse to a quartz cuvette of 1 cm inner length that contained dye solution. The schematic of the experimental setup is shown in the left inset of Fig. 3. This optical setup induces amplified spontaneous emission (ASE) along with the gain guiding and laser emission. The parallel windows of the quartz cuvette will provide the optical feedback, which is necessary for laser action. The emissions guided along the excitation stripe were collected from the side of the cuvette using a collecting fiber, and were then spectrally analyzed using a spectrometer and a charge coupled device. All the investigations were done in Rh B dye solutions with a constant dye concentration of 5×10^{-4} mol/dm^3 in different solvents, while all the experimental conditions such as pump power, ambient temperature, excitation length of the gain medium and mode of collection remained the same.

3. Photophysical properties of dye

The unique features of dye lasers are directly linked to the molecular structure and the photophysical properties of organic dye molecules. The complex molecular structure also leads to many vibrational and rotational levels within the single electronic state. The effective homogeneous line-broadening mechanism due to the

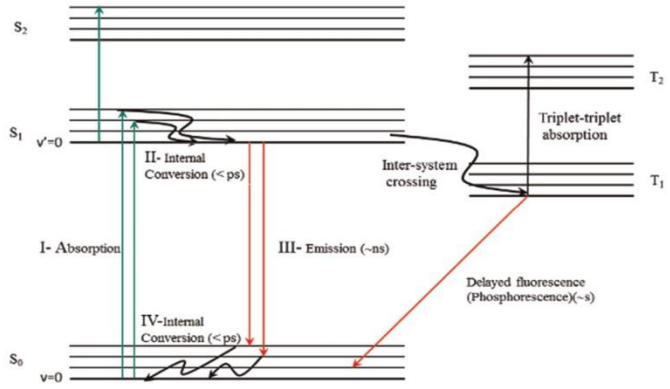

Fig. 3. Typical energy level diagram of dye molecule.

Appendix

collision with solvent molecules smears these sublevels into unresolved overlapping bands. The homogeneous broadened spectra of dye molecules enable very efficient channeling of pump power into narrow band laser emission. Dye laser can be considered as a classical four level system (for simplicity, just neglect the triplet state). Under optical excitation, dye molecules are pumped from ground state S_0 ($\nu=0$) to some vibrational–rotational sublevels in the first excited singlet state S_1 ($\nu \neq 0$) as marked I in Fig. 3 (this vertical line represent the absorption line of dye molecule). The dye molecules in this level will quickly relax to the bottom of S_1 ($\nu=0$) (the lowest rotational–vibrational sublevel). This non-radiative decay process happens on the time scale of a few pico-seconds or less (this is represented by II). This energy lost in the process contribute to the heating of solvents. From the upper laser level, dye molecules can undergo either spontaneous emission or stimulated emission into some rotational–vibrational sublevel in S_0 ($\nu \neq 0$) marked as III. This vertical line represents the emission line of dye molecules. Due to fast non-radiative decay, the molecules are quickly relax into the bottom of the ground state S_0 ($\nu=0$) within a few pico-seconds marked as IV.

When the properties of the solvent changes such as refractive index (n) and dielectric constants (ε), the ground and excited state of the dye to be stabilized instantaneously by movements of electron within the solvent molecules. This electron redistribution results a change in energy difference between ground and excited states. The stokes shift is related to the orientation polarizability term Δf, which is also known as solvent polarity function. The value of Δf can be measured by,

$$\Delta f = \left(\frac{\varepsilon-1}{2\varepsilon+1} - \frac{n^2-1}{2n^2+1}\right) \quad (1)$$

The difference in two terms (first term is depends on the polarizability and second term depends on the RI) accounts for the spectral shifts due to re-orientation of the solvent molecules. Hence the energy state difference between excited state and ground state of the dye is sensitive to the different properties of the solvents.

4. Computational data

The geometry of Rhodamine B was optimized with Density Functional Theory (DFT) and the highest occupied molecular orbital (HOMO) and lowest unoccupied molecular orbital (LUMO) of the molecule in gas phase was calculated using B3LYP exchange correlation functional [8,9] and 6-31+G(d) basis set implemented in Gaussian 09 suite of codes [10]. The stationary points are characterized by frequency analysis. The solvent effects were included by Conductor-like Polarizable Continuum Model (CPCM) [11,12] solvation model. The vertical excitation energy and oscillator strength of Rhodamine B in different solvent are listed in Table 1 and have been broadened with Gaussian function ($\Delta\lambda=40$ nm). On comparing the TDDFT/PCM calculated data with experimental results we demonstrate the accuracy of the TDDFT/PCM approach for calculating vertical transition energy.

However, the experimental and theoretically calculated energy gap shows a difference. This is because the calculation was done in gas phase while the absorption spectrum is taken in liquid phase. (More details are given in Supporting information). The vertical excitation results using the computational method will give some accurate data of the photophysical properties in different environments.

5. Result and discussions

To study the emission characteristics from the dye dissolved in butanol, the emission spectra were recorded for various pump power.

Table 1
Vertical excitation data of Rhodamine B in different solvent.

Solvent	State	Main character	Wavelength (nm)	Oscillator strength (f)
Ethanol	State 1	H→L	538.65	1.1666
	State 2	H-1→L	426.94	0.0466
	State 3	H-2→L	373.58	0.0165
Methanol	State 1	H→L	539.84	1.1725
	State 2	H-1→L	427.24	0.0464
	State 3	H-2→L	369.54	0.0623
Butanol	State 1	H→L	536.54	1.1558
	State 2	H-1→L	426.44	0.0469
	State 3	H-2→L	381.60	0.0048

When the pump power was increased, the amplified spontaneous emission spectrum collapsed into multiple narrow lines as shown in Fig. 4. In the laser spectrum, each emission line had a linewidth less than 0.1 nm. Such a spectral narrowing cannot be found in ordinal ASE in which the linewidth gradually decreases to several nanometers [13]. A clear threshold behavior in the emission versus excitation intensities plot and a second decrease in the linewidth at higher excitation intensity indicated the onset of laser action (right inset of Fig. 4). The strongly modulated laser spectrum with numerous evenly spaced peaks clearly indicates the resonant modes. Above the threshold, the total emission intensity increased much more rapidly with the excitation pump power. As the pump power increased, the lasing action occurred in the direction of the highest gain parallel to the excitation stripe. For increasing pump powers, the absorption decreases and the fluorescence grows due to the increased population inversion, thus the gain grows. Due to Stokes shift, the gain maximum grows and moves towards the higher energy side (smaller wavelengths). The gain maximum is very important since it has a big influence on the spectral position of the laser mode. Ideally, if all cavity modes have the same loss, the laser mode is the cavity mode which is positioned closest to the gain maximum. Similar blue-shift with the pump power has been also observed in various dye lasers systems [14,15].

The spectral peak intensity of the polymer ring laser is positioned at the maximum of optical gain which in turn corresponds to the photo-luminescent spectrum peak [15] around 590 nm. A large number of sharp lines can be seen within the fluorescent emission profile. The lasing modes are spectrally narrow with a FWHM of 0.05 nm with a pump power of $P_{th} \times 4$ ($\sim$15 mW), where P_{th} is the lasing threshold pump power. When the pump power is higher than the lasing threshold ($P_{th} \times 1.2$) lasing modes appear in the longer wavelength range (593–596 nm) of the photo-luminescence spectra of the gain medium. When the pump power is further increased, the lasing modes with high intensities start to develop on the shorter wavelength region of the spectra. The number of lasing modes and the resonant mode intensities increase with pump power as can be clearly seen in Fig. 5. The blue-shift as a function of pump power is attributable to the transfer of mode energy to that of the shorter wavelength side, which has gotten a large gain coefficient. However, the magnitude of this transition of energy gets saturated after a particular pump power.

The net gain of the dye doped laser system was generally measured by the variable stripe length (VSL) method. An adjustable slit was used to select the central portion and vary the width of the pump beam. The output intensity has been measured by,

$$I(\lambda) = \frac{\eta g'(\lambda)}{g(\lambda)}\left(e^{g(\lambda)l} - 1\right), \quad (2)$$

where $g(\lambda)(=g'(\lambda)-\alpha$, α is the loss coefficient) is the net gain coefficient, $g'(\lambda)$ is the internal gain coefficient due to stimulated emission process and l is the length of the pumped stripe. The value of the gain can be determined by plotting the emission intensity as a

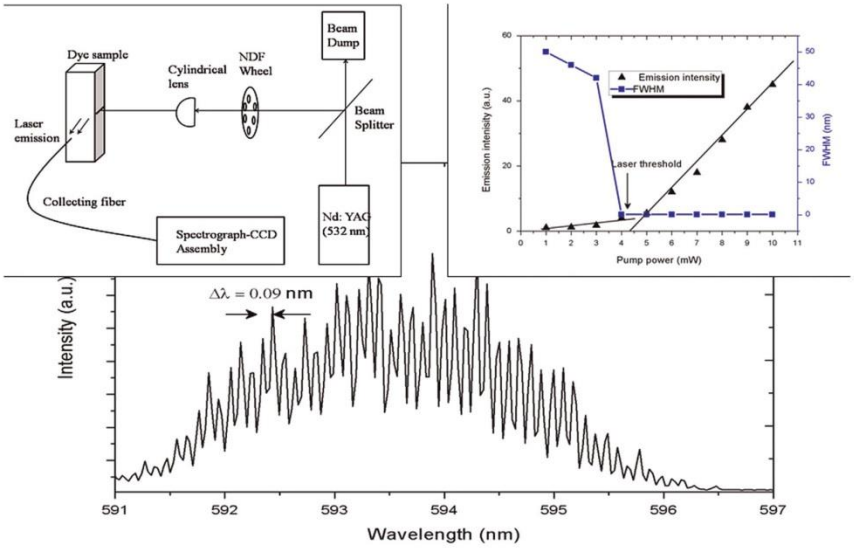

Fig. 4. Lasing spectrum of Rh B solution in Butanol at a pump power of 15 mW. Left inset shows the schematic of experimental setup and right inset shows the emission intensity and FWHM of emission band versus pump power.

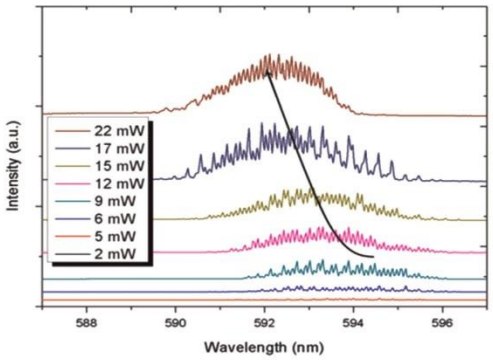

Fig. 5. The graph illustrates the lasing output intensities of Rh B dye (5×10^{-4} mol/dm^3) dissolved in butanol at different pump power. The spectrum moves towards shorter wavelengths with growing pump power.

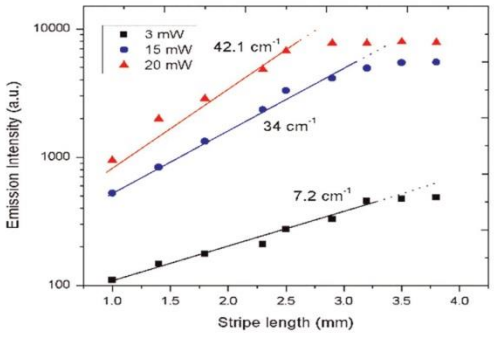

Fig. 6. Dependence of the emission intensity on stripe length at three different pump power for dye dissolved in butanol as 3, 15 and 20 mW respectively. The solid lines are fits to the data using Eq. (2). (For interpretation of the references to color in this figure, the reader is referred to the web version of this article.)

function of pumped stripe length and fitting the resulting curve to the expected dependence given by Eq. (2). The systematic measurements of the intensity of the emitted light as a function of stripe length for three different pump power at 3 mW, 15 mW and 20 mW respectively have been shown in Fig. 6.

The black line in Fig. 6 is a fit of the data to Eq. (2), which yields a net gain of 7.2 cm^{-1} at a pump power of 3 mW ($< P_{th}$). Above P_{th}, the measured gain is 34 cm^{-1} and 42.1 cm^{-1} by fitting the data using blue and red line for 15 and 20 mW respectively. In Eq. (2), we are not considered the gain saturation effect and thus the net gain coefficient is applicable only for those subsets of data before gain saturation.

One of the other important optical quantity used to characterize a laser medium is stimulated emission cross-section (σ_e). The value of σ_e can be derived from the emission spectrum $E(\lambda)$ (which was not shown for the simplicity) by using [md11]

$$\sigma_e = \lambda^4 E(\lambda)/8\pi c\tau m^4, \quad (3)$$

where c is the speed of light in free space, m is the refractive index of the medium (solvent), τ is the fluorescent life time and it is assumed to be 2 ns. From Eq. (3), we could obtained the value of $\sigma_e \sim 8 \times 10^{-18}$ cm^{-1}.

In our lasing experiment, external feedback at the cuvette sides might have encouraged the lasing action. It was expected that both the stimulated emission along with the gain guiding and the external feedback at the cuvette sides would induce a high gain for the laser action [16]. The occurrence of mode structure from dye solution was also reported by Guang et al. where the laser emission was attributed to the Fresnel reflection feedback from the two parallel optical windows of the cuvette [17]. Thus the partial reflectance from the window of the cuvette produces the effect of a Fabry–Perot etalon and provides

Appendix

the optical feedback necessary for laser emission. In this case four subcavities are involved for cavity lasing; the cavity lasing wavelength should fulfill the following resonant conditions [18]:

$$\left.\begin{array}{c} 2[nL+ n'(l_1+l_2)] = K_1\lambda, \\ 2nL = K_2\lambda, \\ 2(nL+ n'l_2) = K_3\lambda, \\ (nL+ n'l_1) = K_4\lambda, \end{array}\right\} \quad (4)$$

where L is the length of the medium, n' is the refractive index (RI) of quartz, l_1 and l_2 are the thickness of the cuvette, n is the RI of the gain medium and K_1, K_2, K_3 and K_4 are arbitrary integers [17]. The resonance condition providing the shortest spectral periodicity is obtained by the subtraction of the conditions 1 and 3, which results

$$2n'l_1 = K\lambda, \quad (5)$$

where $K=K_1-K_3$. The above equation is equivalent to the maximum transmission condition of the Fabry–Perot etalon with an equivalent optical thickness of $n'l_1$. This implies that the cavity lasing spectrum will be modulated by this equivalent Fabry–Perot etalon provide the optical feedback necessary for laser emission. For the lasing spectrum the wavelength spacing between two adjacent modes is given by

$$\Delta\lambda = \frac{\lambda^2}{2n'l_1}, \quad (6)$$

where λ is the average lasing wavelength. Substituting for refractive index of quartz, n' as 1.46, the average lasing wavelength λ as 593 nm and the $\Delta\lambda$ obtained from our studies with a cuvette of 1 cm path length as 0.09 nm. The thickness of the first parallel window is measured as $\sim 1.1 \pm .03$ mm. The estimated value of l_1 is found to be 1.15 mm at different position of the cuvette, which is in close agreement with the observed value.

The dye medium is found to be sensitive to the polarity and refractive index (RI) of the solvent in its nature of laser emission. The interaction between the solvents and the dye molecules affects the energy difference between ground state and excited states. This energy difference is described by the Lippert equation. Most of the laser dyes are polar in nature and excitation into their low lying excited singlet state will be accompanied by an increase in the dipole moment. Hence the solvent polarity has a decisive role in shifting the laser wavelengths. In most of the cases, increasing the solvent polarity will shift the gain curve towards the longer wavelength side which is known as Stokes shift [19]. The emission spectra are recorded for different solvents such as ethanol, butanol, and glycerol with fixed dye concentration of 5×10^{-4} mol/dm^3 as shown in Fig. 7. All the experimental conditions remained the same throughout the investigations with an ambient temperature of 21 °C. The result shows a correlation between the physical characteristics such as RI, polarity of the different solvents and the multimode laser emission from the cavity. From the figure one could observe that the change in solvents introduces a corresponding shift in emission spectra. From ethanol to butanol the shift is approximately 4 nm, and from ethanol to glycerol the shift is approximately 6 nm. These types of shift in the emission spectrum with change in the solvent will allow a limited range of tuning of emission wavelengths. However, the spectral width and spacing between the adjacent lasing modes does not depends on the nature of the solvents but it mainly depends on structure of the cavity.

For a detailed analysis of the effect of solvent in the lasing characteristics of Rh B laser dye, the dye is also dissolved in different solvents such as methanol, toluene and ethylene glycol with the fixed dye concentration of 5×10^{-4} mol/dm^3. Interesting results were obtained and showed that the shift in emission spectrum not only depends upon the value of RI and polarity of solvents but also the lower threshold population inversion [5] given by the solvents molecules. For the non-polar solvents like toluene, a deviation is observed from the polar and dipole aprotic solvents. This is due to the fact that toluene has a comparatively lower quantum yield and high RI, which is almost higher than the quartz cuvette. Hence the reflection coefficient of the surface is also important for the lasing characteristics. Table 2 summarizes RI of the different solvents, polarity, peak wavelength, and number of lasing modes of Rh B dye dissolved in various solvents. From the table the laser emission is observed to be red-shifted in ethylene glycol solution which is less polar and RI as compared to glycerol. This may be attributed to the more viscous nature of glycerol, which may reduce the molecules interaction between dye and solvent molecules. The increased interaction between the dye molecules and the fluorescent light will result in the shifting of emission wavelength toward the longer wavelength region. From this we can also conclude that the laser emission from the dye solution not only depends on the RI and polarity of the solvent but also depends on the other nature of solvents such as viscosity and higher quantum efficiency or lower cavity loss of the solvents.

Fig. 7 shows a typical lasing spectrum from Rh B dissolved in methanol. The lasing peaks were considerably modulated as a clustered pattern. The resonance condition providing the widest spectral periodicity is obtained by the subtraction of the last two condition of Eq. (3), which results,

$$2n'(l_2-l_1) = K\lambda, \quad (7)$$

where $K=(K_3-K_4)$. From Eq. (4) the modulation period can be determined by,

$$\delta\lambda = \frac{\lambda^2}{2n'(l_2-l_1)}, \quad (8)$$

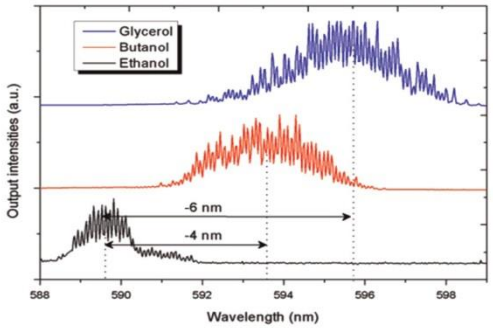

Fig. 7. Three measured laser spectra using Rh B dissolved (5×10^{-4} mol/dm^3) in ethanol, butanol and glycerol as the active gain medium, respectively with a pump power of 15 mW. The change of solvent introduces an over-all shift of the output spectra due to a shift of the gain-spectrum of the dissolved laser dye.

Table 2
Comparison of RI, polarity, emission peak, number of modes for different solvents [20–24].

Solvent name	RI	Polarity	Emission peak (nm)	Number of lasing modes	Dielectric constant (ϵ)
Methanol	1.33	5.1	590	26	32.7
Ethanol	1.36	5.2	591	24	24.5
Butanol	1.39	3.9	594	42	–
Ethylene glycol	1.43	5.4	598	46	37
Glycerol	1.47	5.8	596	62	42.5
Toluene	1.49	2.4	585	(Only ASE)	2.38

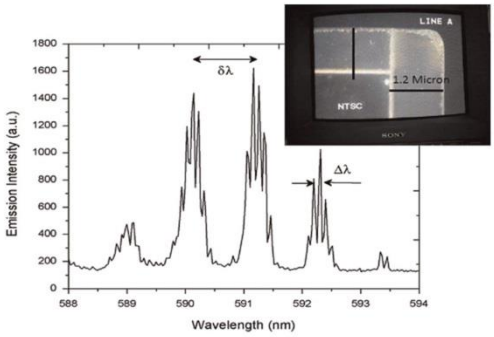

Fig. 8. Resonant modulation of laser modes of Rh B dye dissolved in methanol at a pump power of 15 mW. Inset shows the enlarged view of the variation in the thickness of the two walls of the cuvette.

From the equation we can observed that the modulation period is inversely proportional to the difference in the wall thickness (l_2-l_1) of the cuvette. The measured mode spacing $\delta\lambda$ is $\sim$1.2 nm which is in good agreement with the calculated value of mode spacing ($\sim$1.19 nm), where (l_2-l_1) is estimated as 100 μm.

The photograph of the CCD image taken for two walls of a cuvette is given in Fig. 8 inset, which clearly indicates the change in thickness of the different walls of the cuvette. The obtained laser emission spectra are modulated by the superposition of the laser modes due to optical thickness of $n'l_1$ and difference in the wall thickness $n'(l_2-l_1)$ as shown in Fig. 8. We therefore attribute the appearance of emission spectra to a resonant modulation of the two type's laser resonant modes within the cavity.

6. Conclusion

Multimode laser emissions from Rh B laser dye in different solvents are investigated. The features of the mode structure in the emission spectra are employed to study the effects of solvents on the laser emission of the dye. The laser modes are found to originate from the subcavities formed by the plane parallel walls of the cuvette containing the gain medium. Changing solvent will allow a shift in the emission wavelength, which will allow a limited range of tuning of emission wavelength. The amount of shift in emission wavelength depends on the different physical property of the solvents, such as polarity, refractive index, viscosity etc. The solvatochromic and Stokes-shift of Rh B in various solvents were successfully compared to experimental data with computational data. In our study we also determined the gain coefficient and stimulated emission cross-section of the Rh B dye laser system. The dye dissolved methanol solution will also provide a modulated laser emission due to two set of laser resonance achieved by the difference in the wall thickness of the cuvette.

Acknowledgment

The authors acknowledge University Grant Commission (UGC) (grant no. F.No.184-2/2013 (IC)) and Department of Science and Technology (DST) (grant no. INT/FINLAND/P-9) for the financial support. Jaison Peter is grateful to UGC for the research fellowship. The theoretical calculations have been performed in Gaussian suite of codes installed at Department of Applied Chemistry for which the authors gratefully acknowledge the support from Prof. K. Sreekumar.

Appendix A. Supplementary material

Supplementary data associated with this article can be found in the online version at http://dx.doi.org/10.1016/j.jlumin.2015.09.002.

References

[1] Frank L. Pedrotti, Leno S. Pedrotti, Introduction to Optics, second second edition, 1996, Patience Hall International; (bearing dates of 1993), 1987; Prentice-Hall, Inc; ISBN: 0-13-501545-6.
[2] F.P. Schafer (Ed.), Dye Lasers, Springer-Verlag, Berlin-Heidelberg, New York, 1973.
[3] F.P. Schäfer, Dye Lasers, Topics in Applied Physics, vol. 1, Springer, Berlin, Heidelberg, New York, 1978.
[4] M. Gersborg-Hansen, S. Balslev, N.A. Mortensen, A. Kristensen, Microelectron. Eng. 78–79 (2005) 185.
[5] O.G. Pereson, J.P. Webb, W.C.J. Mcclolgin, Appl. Phys. 42 (5) (1971) 1917.
[6] G.D. Peng, Z. Xiong, P.L. Chu, J. Lightwave Technol. 16 (1998) 2365.
[7] A. Tagaya, Y. Koike, E. Nichei, S. Teramoto, K. Fujii, T. Yamamoto, K. Sasaki, Appl. Opt. 34 (1995) 988.
[8] R.G. Parr, W. Yang, Density-Functional Theory of Atoms and Molecules, Oxford University Press, Oxford, 1989.
[9] A.D.J. Becke, Chem. Phys. 98 (1993) 5648.
[10] M.J. Frisch, G.W. Trucks, H.B. Schlegel, G.E. Scuseria, M.A. Robb, J.R. Cheeseman, G. Scalmani, V. Barone, B. Mennucci, G.A. Petersson, H. Nakatsuji, M. Caricato, X. Li, H.P. Hratchian, A.F. Izmaylov, J. Bloino, G. Zheng, J.L. Sonnenberg, M. Hada, M. Ehara, K. Toyota, R. Fukuda, J. Hasegawa, M. Ishida, T. Nakajima, Y. Honda, O. Kitao, H. Nakai, T. Vreven, J.A. Montgomery Jr., J.E. Peralta, F. Ogliaro, M. Bearpark, J.J. Heyd, E. Brothers, K.N. Kudin, V.N. Staroverov, R. Kobayashi, J. Normand, K. Raghavachari, A. Rendell, J.C. Burant, S.S. Iyengar, J. Tomasi, M. Cossi, N. Rega, J.M. Millam, M. Klene, J.E. Knox, J.B. Cross, V. Bakken, C. Adamo, J. Jaramillo, R. Gomperts, R.E. Stratmann, O. Yazyev, A. J. Austin, R. Cammi, C. Pomelli, J.W. Ochterski, R.L. Martin, K. Morokuma, V. G. Zakrzewski, G.A. Voth, P. Salvador, J.J. Dannenberg, S. Dapprich, A.D. Daniels, Ö. Farkas, J.B. Foresman, J.V. Ortiz, J. Cioslowski, D.J. Fox, Gaussian 09, Revision D.01, Gaussian, Inc., Wallingford CT, 2009.
[11] P.J. Stephens, F.J. Devlin, C.F. Chabalowski, M.J. Frisch, J. Phys. Chem. 98 (1994) 11623.
[12] V. Barone, M. Cossi, J. Phys. Chem. A 102 (1998) 1995.
[13] D.S. Weirsma, M.P. Van Albada, A. Lagendijk, Nature 373 (1995) 203.
[14] Jaison Peter, Rasoo Saleem, Ananth Sebastia, P. Radhakrishnan, V.P. N. Nampoori, C.P. Girijavallabhan, M. Kailasnath, Opt. Commun. 320 (2014) 125.
[15] C.P.G. Jaison Peter, P. Vallabhan, V.P.N. Radhakrishnan, Nampoori, M. Kailasnath, Laser Phys. 23 (2013) 115104.
[16] Jaison Peter, P. Radhakrishnan, V.P.N. Nampoori, M. Kailasnath, J. Lumin. 149 (2014) 204.
[17] Yokoyama Shiyoshi, Otomo Akira, Shinro Mashiko, Appl. Phys. Lett. **80** (7-9) (2002).
[18] Guang S. He, Raffaella Signorini, Paras N. Prasad, Appl. Opt. **37** (24) (1998) 5720–5726.
[19] Nedumpara Ritty, K.J. Thomas, V.K. Jayasree, C.P. Girijavallabhan, V.P. N. Nampoori, P. Radhakrishnan, Appl. Opt. **46** (21) (2007) 4786–4792.
[20] J.R. Lakowicz, Principle of Fluorescence Spectroscopy, Plenum Press, New York, 1983 (Chapter 9).
[21] B. Bilenberg, B. Hebo, J.P. Kutter, A. Kristensen, Proceedings of the 12th International Conference on Solid-State Sensors, Actuators and Microsystems, Transducers 03, Boston, MA, USA, 2003, pp. 206–209.
[22] ⟨www.kabusa.com/Dielectric-constants.pdf⟩.
[23] ⟨www.engineeringtoolbox.com/refractive-index-d-1264.html⟩.
[24] ⟨Depts.washington.edu/eooptic/linkfiles/dielectric-chart%5B1%5D.pdf⟩.

JOURNAL OF APPLIED PHYSICS **117**, 015301 (2015)

Angular dependent light emission from planar waveguides

Jaison Peter,[1,2,a)] Radhakrishna Prabhu,[2] P. Radhakrishnan,[1] C. P. G. Vallabhan,[1] V. P. N. Nampoori,[1] and M. Kailasnath[1]
[1]*International School of Photonics, Cochin University of Science and Technology, Cochin 682022, India*
[2]*CRE$^+$E, IDEAS Research Institute, Robert Gordon University, Aberdeen AB10 7GJ, United Kingdom*

(Received 8 October 2014; accepted 4 December 2014; published online 5 January 2015)

We have investigated the angular dependence of amplified spontaneous emission (ASE) and laser emission from an asymmetric and free-standing polymer thin films doped with rhodamine 6G, which is transversely pumped by a pulsed Nd:YAG laser. A semi-leaky waveguide or quasi-waveguide structure has been developed by spin coating technique. In these waveguides, the light was confined by the film/air-film/glass substrate interfaces. At the film/substrate interface, a portion of light will reflect back into the film (guided mode) and the remaining refracted to the substrate resulting in cutoff modes. A blue-shift in ASE has been observed when the pump power was increased from 8 to 20 mW allowing a limited range of tuning of emission wavelength. To study the directionality of the ASE from the waveguide, we have measured the output intensity and FWHM of emission spectra as a function of viewing angle (θ) from the plane parallel to film. From the detailed examination of the output emission spectra, as $+\theta$ increases from 0° there has been an initial decrease in output intensity, but at a particular angle $\approx$10° an increase in output intensity was observed. This additional peak in output intensity as $+\theta$ is a clear indication of coexistence of the cutoff mode. We also present a compact solid-state laser based on leaky mode propagation from the dye-doped polymer free-standing film ($\sim$50 μm thickness) waveguide. The partial reflections from the broad lateral surfaces of the free-standing films provided the optical feedback for the laser emission with high directionality. For a pump power of 22 mW, an intense line with FWHM <0.2 nm was observed at 578 nm. © *2015 AIP Publishing LLC*.
[http://dx.doi.org/10.1063/1.4905011]

INTRODUCTION

Organic luminescent materials have been widely studied in light emitting devices and solid-state lasers because of their light weight, ease of processing, low cost, flexibility, and spectral range coverage from the blue to far IR.[1] Laser devices of various structures have been achieved by a variety of resonator designs, including microcavities,[2] micro-disks,[3] micro-rings,[4] and hollow fibers.[5,6] Polymer materials have been found to be very attractive both from the technical and economical point of view with its high optical quality, better chemical compatibility with organic dyes, and inexpensive processing techniques.[7] The combination of the tunability and high efficiency of laser dyes with the high power density that can be easily achieved in waveguide structures makes devices based on dye-doped polymer waveguides and fibers very promising.[8–10]

Light amplification and spectral narrowing have been studied earlier in various systems both in the liquid and solid forms, where the spectral linewidth is reduced to a value less than 10 nm.[11–13] Spectral narrowing in most such systems is explained in terms of amplified spontaneous emission (ASE), where the spontaneously emitted luminescence is amplified by the gain medium as it propagates along the path of the maximum optical gain.[6] Reflections from the internal surfaces can increase the path length or allow multiple passes inside the gain medium which in turn build up the ASE at a faster rate.[14] Recently, laser emission from conjugated polymers and dendrimer doped polymers has also been reported.[12,15] There have been numerous investigations on laser emission from polymer planar microcavities[10,16] and polymer microring lasers.[5,17]

EXPERIMENTAL METHODS

In this section, we report a detailed study of ASE spectra observed in a thin dye-doped polymer film. To fabricate the rectangular waveguide, rhodamine 6G doped poly methyl methacrylate (PMMA) thin films with an average thickness of $\sim$3 μm were deposited by spin coating technique onto a glass substrate. The precursor solution had a molar composition of PMMA/Anisole/Rh6G = 2 g/15 ml/1 $\times$ 10^{-4} mol/l. Thin polymer films were formed on the glass substrate following fast drying in air. The refractive index of the doped polymer film ($n_p = 1.49$) is higher than the refractive index of the glass substrate ($n_s = 1.46$). A semi-leaky waveguide or a quasi-waveguide is obtained, where the light is confined by the film/air interface while at the film/substrate interface, a portion of light will reflect back into the film (guided mode) and the remaining refracted to the substrate (cutoff mode).[18–20] The different guided modes propagating within the gain layer have different reflectivity losses due to Fresnel law. Thus, the glass-doped polymer-air structures formed an asymmetric slab optical waveguide, which supports only the fundamental transverse mode as the guided

a)Author to whom correspondence should be addressed. Electronic mail: jaison.peter@gmail.com

mode within the emission band of the doped polymer.[1] As a result, a quasi-waveguide provides a much stronger mode restriction capability than conventional total internal reflection waveguides. However, if the incident angle is slightly smaller than the critical angle, some of the light will refract (leak) into the substrate and propagate in a direction nearly parallel to the interface between the film and substrate as shown in Fig. 1 inset.

Investigations on the ASE properties of these films were carried out by optical pumping of the films by the second harmonic output of a Q-switched Nd:YAG laser with 8 ns pulses at 10 Hz repetition rate. The experimental setup is shown in Fig. 1. The pump power was adjusted with neutral density filters and focused into the polymer-coated film by a cylindrical lens into a 1 mm × 0.4 mm stripe. A slit was incorporated in the path of the beam between cylindrical lens and the sample so as to vary the stripe length onto the sample surface. The emission from the sample was collected by a multimode fiber and guided to a 0.5 m spectrograph coupled with a cooled CCD array. The distance between the collecting fiber and the waveguide edge was 1 cm.

RESULTS AND DISCUSSIONS

Amplified spontaneous emission

Figure 2 shows the absorption and photoluminescence spectra of the Rh6G doped PMMA film. The doped polymer film exhibits a featureless absorption band that peaks at 530 nm and emission with a peak of 570 nm, which is the characteristic emission of the Rh6G dye molecule. When the optically dense dye doped thin film is excited such that it forms a cylindrically shaped active gain medium, the fluorescence emitted by the molecules at one end is strongly amplified by the active medium and it preferentially emits the optical power along the direction of excitation, giving a highly directional output beam.[21] As a result, a large portion of the dye-doped polymer emission was optically confined within the film by internal reflections. Using the refractive index of the substrate, $n_s = 1.46$, and that of the PMMA film,

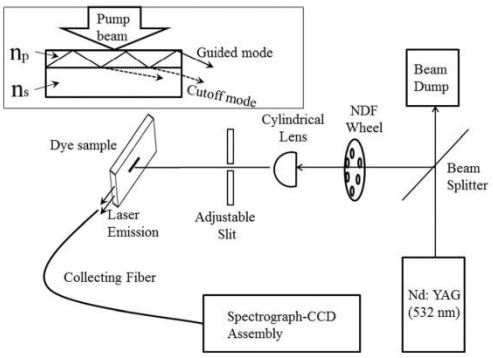

FIG. 1. Schematic representation of the experimental setup. Inset shows the Ray-tracing description of light propagating in a planar waveguide.

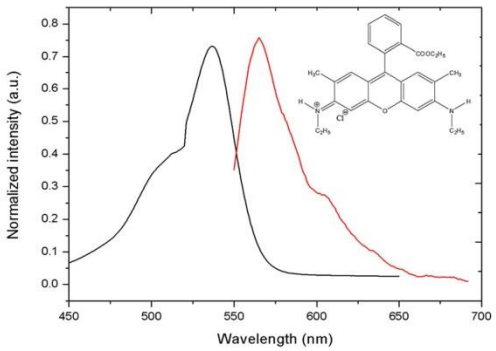

FIG. 2. The absorption and photoluminescence spectra of Rh6G doped in a PMMA film. Inset, chemical structure of Rh6G.

$n_p = 1.49$, we estimate the fraction of emission which is waveguided or "trapped" inside the film as

$$f = \sqrt{1 - \left(\frac{n_s}{n_p}\right)^2} = 0.2. \quad (1)$$

If the incident angle of the propagating light is larger than the critical angle of the interface between the film and glass substrate, the light can propagate inside the film without leakage. The spectrally narrow emission (~5 nm) from such films is observed only along the plane of the film (A in Fig. 3), whereas the emission perpendicular to the film surface remained spectrally broad (~40 nm) (B in Fig. 3). This is due to the fact that at low grazing angles, it has low loss normal to the plane of the film, and thus the polymer-air interface has almost zero transmission due to total internal reflection. This indicates that ASE is due to waveguided polymer emission, which propagates alongside the film and thus experiences the largest gain. For our measurements of ASE, we used an excitation region in the shape of a narrow stripe. As a result, ASE was predominantly emitted along the axis of stripe.

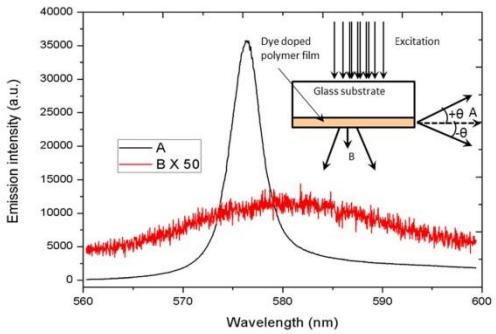

FIG. 3. The emission spectra from the dye-doped polymer film measured in the direction parallel (A) and perpendicular (B) to the film surface at the same excitation intensity (20 mW); emission intensity B is magnified by 50. The inset illustrates the experimental setup.

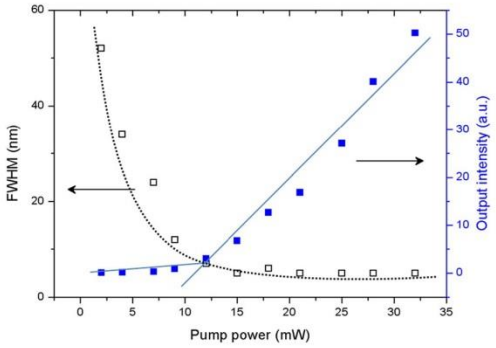

FIG. 4. Output emission intensity integrated over all wavelengths as a function of pump power (filled square) and dependence of the FWHM on the pump power (open square).

Due to stripe illumination, a large number of Rh6G dye molecules undergo population inversion when it is optically pumped by the second-harmonic output of an Nd:YAG laser. At low pump powers, the emission spectrum from the film exhibits broad fluorescence. To understand the nature of ASE in detail, the dependence of emission intensity on incident pump power is studied. As pump power is increased, the emission spectra show a line narrowing effect coupled with blue-shift as shown in Figs. 4 and 5. With an increase in pump power, the radiative transition probability gets enhanced at shorter wavelength side of the spectrum creating a shift in the spectrum towards the blue side.[5] Fig. 5 inset shows the blue-shift of the emission spectrum as a function of pump power. As the pump power increases from 8 to 20 mW, it can be seen that the emission spectrum gets shifted from 584 to 576 nm. Spectral line narrowing as a function of pump power is the signature of light amplification.[22,23] The collapses of the full-width-half-maximum (FWHM) in the emission spectrum and the change in the slope in the output emission intensity are the indication of the onset of ASE above a certain threshold ($P_{th} = 12$ mW). Also, spectral narrowing from 52 to 5 nm is observed, when the pump power is increased to 15 mW above which no further line narrowing is observed due to gain saturation effect. On a detailed study of the emission spectrum of the dye-doped polymer thin film, it is found that the emission spectrum exhibits all the features of ASE, namely, the property of directionality, narrow linewidth, and presence of soft threshold behavior.[24] Directionality of the output beam is so obvious that no focusing is required to collect the beam.

To study the directionality of the ASE from the asymmetric planar waveguide, we measure the output intensity and FWHM of emission spectra as a function of viewing angle from the plane parallel to film axis as shown in Fig. 3 inset. To measure the FWHM and output intensity as a function of viewing angle θ, the collecting fiber is kept in a rotational stage. The output intensity and FWHM of emission spectra as a function of viewing angle are measured as shown in Fig. 6. Initially, collecting fiber is aligned parallel to the waveguide axis and which is referred as angle $\theta = 0°$. Then, the FWHM and output intensity of emission spectra are measured by gradually increase/decrease angle θ ($\pm\theta$) between -40 and $40°$. From the detailed examination of the output emission spectra, as $+\theta$ increases from $0°$ there is an initial decrease in output intensity, but at a particular angle $\approx 10°$ an increase in output intensity is observed. This additional peak in output intensity as $+\theta$ is a clear indication of coexistence of the cutoff mode.

Laser emission

In this section, we describe the observation of multimode laser emission from a transversely pumped free-standing polymer film. Solid-state free-standing thin films were prepared by incorporating Rh6G dye with PMMA. Commercially available PMMA of 5 g was dissolved in

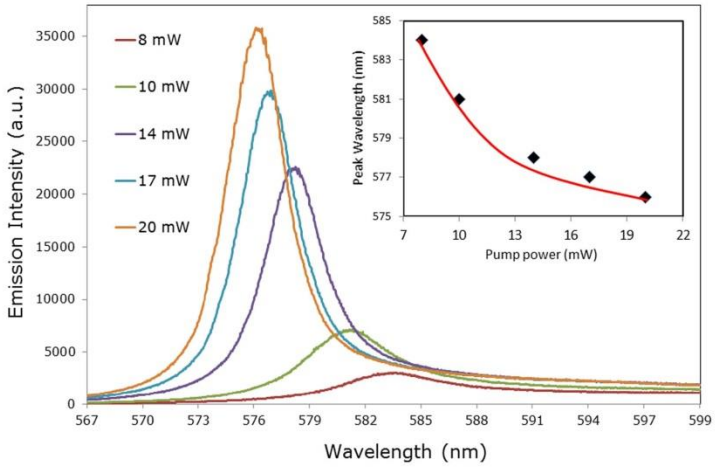

FIG. 5. The emission spectra from planar waveguide at various pump powers. Inset: Blue-shift in peak wavelength as a function of pump power.

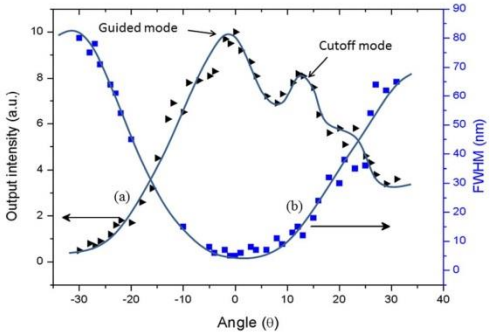

FIG. 6. The output intensity (a) and FWHM (b) of the emission spectra from planar waveguide as a function of viewing angle by keeping a constant pump power of 25 mW.

15 ml of anisole. The weight percentage was chosen to get optimum viscosity for the formation of good quality films. The dye was dissolved in this solution at a concentration of 1×10^{-4} mol/l. Films of 50 μm thickness were tape cast on glass sheets from this solution. When solvent was fully evaporated, high-quality free-standing films could be peeled off from the glass sheet. The lateral faces of the films obtained were of good optical finish and as such no further polishing was required.

The same experimental setup (explained in the Experimental Methods) was employed to study the emission characteristics from the dye-doped free-standing polymer film as well. Laser emission requires an external feedback. In the present case, no feedback is provided with external mirrors. Since the pumped polymer film was a free-standing one, the lateral faces of the film acted as mirrors, thus giving rise to a Fabry-Perot-type optical cavity for which length corresponds to the film thickness.[10] The excited active medium can be considered as a number of serially connected Fabry-Perot optical cavities. In the case of a thin stripe excitation, the stimulated emission occurs in a direction along the stripe.[25] The multiple passes between the film surfaces directly increase the gain. When the gain of the active medium compensates the losses in the medium, laser emission occurs. According to laser theory, the gain in the active medium is $\exp \sigma\,(N_2 - (g_2/g_1)N_1)l$, where σ is the stimulated emission cross section and l is the length of active medium.[24] Owing to the sample geometry and pumping scheme, the longitudinal modes of the cavity are analogous to the transverse modes of the waveguides.[10] When the pump power is increased beyond the lasing threshold (in our sample 15 mW), the emission spectrum collapsed into multiple narrow lines as shown in Fig. 7. This evenly spaced peaks clearly indicate the existence of resonant modes. Above the threshold, the total emission intensity increased much more rapidly with the pump power.

The existence of a Fabry-Perot optical cavity between the lateral faces of the free-standing film is thus confirmed by the occurrence of well-resolved discrete peaks in the emission spectrum. The mode spacing at λ can be calculated using the equation which describes Fabry-Perot cavities, namely,

$$\Delta\lambda = \frac{\lambda^2}{2nL}, \tag{2}$$

where λ is the wavelength of the strongest emission line, n is the refractive index, and L is the length of the resonator cavity. In the present case, the length of the Fabry-Perot cavity corresponds to the thickness of the polymer films. The observed mode spacing (0.9 nm) (as shown in Fig. 7) agrees well with the calculated value (0.86 nm). These observations confirm that the observed equally spaced fine structures in the emission spectra are Fabry-Perot-type modes of the optical cavity formed by the lateral faces of the waveguide.[10]

Another salient characteristic of laser emission is its increased directionality. The measurement geometry of the intensity distribution of the output from a planarmicrocavity has been shown in Fig. 7 left inset. A 1 mm pinhole was positioned in front of a collecting fiber, which was kept in a translational stage and attached to a high-speed

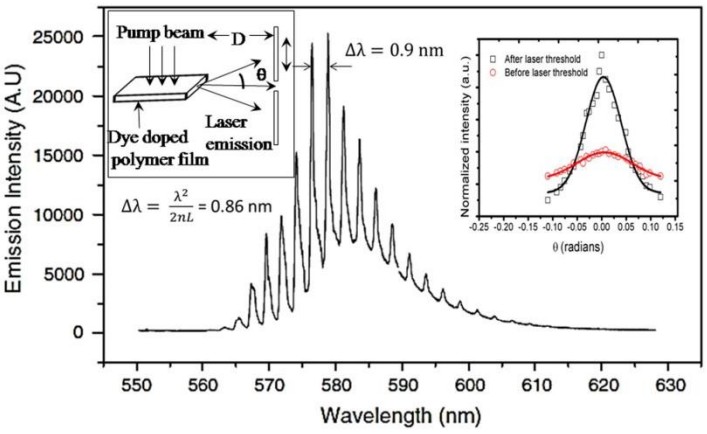

FIG. 7. Multimode laser emission from 50 μm thick rhodamine 6G doped PMMA films at a pump power of 22 mW. Left inset, schematic diagram of the setup for intensity distribution measurement. Right inset, intensity distribution of the output of a planar microcavity (data points were well-fitted with a Gaussian curve (before and after lasing threshold)).

photo-detector. The distance between collecting fiber and free-standing film was 50 mm. By varying the height of the pinhole and collecting fiber simultaneously parallel to the fiber axis, we monitored the emission intensity at a given angle θ. Below lasing threshold, the intensity distribution of emission is broad. As the pump power is increased above the lasing threshold, the lasing action occurred in the direction of the highest gain parallel to the excitation stripe ($\theta = 0°$). To confirm the spatial light confinement during the gain guiding, we measure the beam profile of the emission near the film as shown in Fig. 7 right inset. The intensity distribution is measured and the Gaussian curve is fitted on the data points from the output emission intensity above and below lasing threshold. Below lasing threshold, the regular photoluminescence emission from the planar microcavity is not highly directional, concentrated in the plane of the illuminated area of the microcavity within an angle $\Delta\theta$ of a few hundredths of a radian. Also, the emission anisotropic pattern abruptly changes above the laser threshold to $\Delta\theta = 0.1$ rad, showing excess directionality of the laser modes.

The ability of an optical resonator or cavity to confine light of a given wavelength range around λ_0 is usually measured in terms of quality factor or Q factor, which is given as

$$Q = 2\pi\nu \frac{P_{stored}}{P_{lost}} = \frac{\lambda_0}{\delta\lambda}, \quad (3)$$

where P_{stored} and P_{lost} are the power stored within the cavity and lost from the cavity, respectively, while $\delta\lambda$ is the spectral line-width of the cavity modes at wavelengths λ_0. In the present study, we estimate the Q value of the microlasers to be $>3 \times 10^3$, which results in narrow laser emission lines with a width <0.2 nm. Further improvements in the film quality may lead to enhanced directionality and high Q value of the planar microcavity laser emission.

CONCLUSION

In summary, we have presented a detailed study of the amplified spontaneous emission and laser emission from an asymmetric and free-standing planar waveguide based on a rhodamine 6G doped PMMA film. The spectrally narrow emission ($\sim$5 nm) from an asymmetric planar waveguide was observed only in the plane of the film, whereas the emission perpendicular to the film surface remained spectrally broad ($\sim$40 nm). ASE spectrum from the film exhibits high directionality, narrow linewidth, and presence of soft threshold behavior. A blue-shift in ASE has been also observed when the pump power was increased from 8 to 20 mW allowing a limited range of tuning of emission wavelength. From the study of directionality of ASE, the light amplification in an asymmetric planar waveguide is due to two different propagation modes; namely, waveguide mode and cutoff mode. Well-resolved laser modes with equal spacing were observed from a free-standing planar waveguide, which confirm the optical feedback from the Fabry-Perot-like optical cavity formed between the lateral surfaces of the thin film. The multimode laser emission from free-standing planar microcavity was characterized by narrow emission lines (<0.2 nm) with high Q ($>3 \times 10^3$) and increased directionality (0.1 rad).

ACKNOWLEDGMENTS

The authors acknowledge University Grants Commission (UGC) and DST (Department of Science and Technology) for the financial support. Jaison Peter is grateful to Dr. Virginia Dawod for the support given during the work at IDEAS Research Institute, Robert Gordon University. He is also thankful to UGC, New Delhi, India for his research fellowship.

[1]W. Lu, B. Zhong, and D. Ma, "Amplified spontaneous emission and gain from optically pumped films of dye-doped polymers," Appl. Opt. **43**, 5074 (2004).
[2]J. C. Knight, H. S. T. Driver, and G. N. Robertson, "Morphology dependent resonances in a cylindrical dye microlaser: Mode assignments, cavity Q values and critical dye concentrations," J. Opt. Soc. Am. B **11**, 2046 (1994).
[3]R. E. Slusher, "Optical processes in microcavities," Semicond. Sci. Technol. **9**, 2025–2030 (1994).
[4]J. Peter, C. P. G. Vallabhan, P. Radhakrishnan, V. P. N. Nampoori, and M. Kailasnath, "Microring lasing from a dye-doped polymer-coated silica fiber," Laser Phys. **23**, 115104 (2013).
[5]J. Peter, C. P. G. Vallabhan, P. Radhakrishnan, V. P. N. Nampoori, and M. Kailasnath, "Pumping scheme dependent multimode laser emission from free-standing cylindrical microcavity," Opt. Commun. **320**, 125–128 (2014).
[6]J. Peter, P. Radhakrishnan, V. P. N. Nampoori, and M. Kailasnath, "Multimode laser emission from free-standing cylindrical microcavities," J. Lumin. **149**, 204–207 (2014).
[7]R. J. Nedumpara, K. Geetha, V. J. Dann, C. P. G. Vallabhan, V. P. N. Nampoori, and P. Radhakrishnan, "Light amplification in dye doped polymer films," J. Opt. A: Pure Appl. Opt. **9**, 174–179 (2007).
[8]G. D. Peng, P. L. Chu, Z. Xiong, T. W. Whitbread, and R. P. Chaplin, "Dye-doped step-index polymer optical fiber for broadband optical amplification," J. Lightwave Technol. **14**, 2215–2223 (1996).
[9]M. Karimi, N. Granpayeh, and M. K. MorravegFarshi, "Analysis and design of a dye-doped polymer optical fiber amplifier," Appl. Phys. B **78**, 387–396 (2004).
[10]K. Geetha, M. Rajesh, V. P. N. Nampoori, C. P. G. Vallabhan, and P. Radhakrishnan, "Laser emission from transversely pumped dye-doped free-standing polymer film," J. Opt. A: Pure Appl. Opt. **8**, 189–193 (2006).
[11]M. Kailasnath, V. P. N. Nampoori, and P. Radhakrishnan, "A microring multimode laser using hollow polymer optical fibre," Pramana J. Phys. **75**(5), 923–927 (2010).
[12]A. Otomo, S. Yokoyama, T. Nakahama, and S. Mashiko, "Supernarrowingmirrorless laser emission in dendrimer-doped polymer waveguides," Appl. Phys. Lett. **77**, 3881–3883 (2000).
[13]S. A. Berg, R. H. Schoonderwoerd, H. F. M. Schoo, G. W. Hooft, and E. R. Eliel, "From amplified spontaneous emission to laser oscillation: Dynamics in a short-cavity polymer laser," Opt. Lett. **24**, 1847–1849 (1999).
[14]K. Walter, *Solid State Laser Engineering* (Springer, Berlin, 1972), pp. 182–185.
[15]M. Fahis, I. Polyzos, G. Tsigaridas, V. Giannetas, P. Persiphonis, I. SpilioPoulos, and J. Mikroyannidis, Phys. Rev. B **65**, 195–203 (2002).
[16]N. Tessler, G. J. Denton, and R. H. Friend, "Lasing from conjugated-polymer microcavities," Nature **382**, 695–697 (1996).
[17]M. Kuwata-Gonokami, R. H. Jordan, A. Dobalapur, H. E. Katz, M. L. Schilling, and R. E. Slusher, "Polymer microdisk and microring lasers," Opt. Lett. **20**, 2093–2095 (1995).
[18]M. Pauchard, J. Swensen, D. Moses, A. J. Heeger, E. Perzon, and M. R. Anderson, "Optical amplification of the cutoff mode in planar asymmetric polymer waveguides," Appl. Phys. Lett. **83**(22), 4488–4490 (2003).

Appendix

[19]D. Yokoyama, M. Moriwake, and C. Adachi, "Spectrally narrow emission at cutoff wavelength from edges of optically and electrically pumped anisotropic organic films," J. Appl. Phys. **103**(12), 123104 (2008).
[20]X. Li, S. Liu, F. Li, and Y. Ma, "Optical amplification of two different propagation modes in organic small molecular waveguide structure," Opt. Express **19**, 17691–17696 (2011).
[21]M. D. McGehee, R. Gupta, S. Veenstra, E. K. Miller, M. A. Diaz-Garcia, and A. J. Heeger, "Semiconducting polymer distributed feedback lasers," Phys. Rev. B **58**, 7035–7039 (1998).
[22]M. Rajesh, M. Sheeba, K. Geetha, C. P. G. Vallabhan, P. Radhakrishnan, and V. P. N. Nampoori, Appl. Opt. **46**(1), 106 (2007).
[23]J. Peter, C. P. G. Vallabhan, P. Radhakrishnan, V. P. N. Nampoori, and M. Kailasnath, Opt. Laser Technol. **63**, 34–38 (2014).
[24]O. Svelto and D. C. Hanna, *Principles of Laser*, 4th ed. (Springer, 1998), pp. 71–73.
[25]S. V. Frolov, Z. V. Vardeny, K. Yoshino, and R. H. Baughman, "Stimulated emission in high-gain organic media," Phys. Rev. B **59**, R5284–R5287 (1999).

Optics & Laser Technology 63 (2014) 34–38

Contents lists available at ScienceDirect

Optics & Laser Technology

journal homepage: www.elsevier.com/locate/optlastec

ASE and photostability measurements in dye doped step index, graded index and hollow polymer optical fiber

Jaison Peter*, C.P.G. Vallabhan, P. Radhakrishnan, V.P.N. Nampoori, M. Kailasnath

International School of Photonics, Cochin University of Science and Technology, Cochin 682022, India

ARTICLE INFO

Article history:
Received 19 November 2013
Received in revised form
7 February 2014
Accepted 19 March 2014
Available online 12 April 2014

Keywords:
Polymer optical fiber
Line-narrowing
Red-shift

ABSTRACT

Three categories of polymer optical fibers viz., step index (SI), graded index (GI) and hollow types doped with Rhodamine 6G (Rh6G) at specific concentrations were fabricated to study their optical properties. Detailed measurements were made to understand the amplified spontaneous emission (ASE) and photodegradation phenomena in these polymer optic fiber (POF) systems. Rh6G doped hollow POF shows maximum line narrowing for a given pump power at 532 nm when side illumination technique is employed. A redshift in ASE has been observed when propagation length is increased allowing a limited range of tuning of emission wavelength. Photostability studies show that GI POF has the maximum endurance at a given pump power.

1. Introduction

From early days of development of dye lasers, attempts were made to overcome problems posed by organic solvents by incorporating dye molecules into solid matrices [1,2]. Solid-state dye materials avoid the problems of toxicity, volatility and flammability, providing a low cost gain medium, and are compact and easy to operate and maintain [3]. Their applications range over a number of areas like spectroscopy, communications, atmospheric sensing, medical treatment and so on. The first solid-state dye laser was reported by Soffer and Mcfarland [1] and then by Peterson and Snavely [2] in the late 1960s. Various classes of materials like porous glasses, organically modified silicates, sol–gel materials and polymers were extensively studied as host materials for laser dyes, in terms of their optical properties and commercial viability [4]. In addition to low cost and tunability, the configurability and potential for minimal size of solid-state dye doped material would be advantageous in integrated optics application [5].

Polymer optical fibers (POFs) have attracted considerable attention during the past two decades for short distance communication because of their unique characteristics, such as flexibility, ease of handling, and relative low cost [6]. POFs have the potential to be used in optical logic-devices such as optical switches and amplifiers because of the fiber waveguide geometry, which is compatible with silica glass fibers, low production cost and wide range of available materials that can be incorporated into the fiber core [7]. Properties like attenuation due to microbends, sensitivity to temperature and humidity of POFs can be effectively utilized for sensor applications [8].

Polymeric matrices have some advantages over other host materials because they have better chemical compatibility with organic dyes, and are inexpensive and easy to fabricate. However they suffer from relatively poor thermal conductivities as well as lower laser radiation damage thresholds [5]. Polymethyl-Methacrylite (PMMA) is one of the most commonly used polymeric hosts [9], which shows higher optical homogeneity and transparency in the visible region of electromagnetic spectrum [3]. Most of the work on solid-state dye lasers has been elaborated with dyes' emission in the yellow and red regions of the spectrum, using the well-known rhodamine 6G (Rh6G). Rh6G is the best known of all laser dyes and has been frequently investigated in solid-state dye lasers in a variety of solid hosts, on account of its high fluorescence quantum yield, low intersystem crossing rate and low excited state absorption at both pump and lasing wavelengths [10]. Fluorescence in a fiber can be enhanced to the effect of transverse confinement, making it possible to build efficient optical amplifiers, light sources and lasers.

Organic luminescent dyes dissolved in polymers as potential sources of light amplifying media are still very attractive for fabrication of tunable lasers with high gain and dye-life due to easy processing, low cost and wide spectral range [11]. In this paper we report side illumination fluorescence (SIF) technique [12–15] to study the emission characteristics and dye-life of different types of dye doped POFs. In a hollow POF, major portion of the optical power propagates through the solid fiber material (fiber ring) and only a minor portion of the optical power propagates through the hollow region. Due to holes in the middle, the hollow POF has a good thermal relaxation as compared to step

* Corresponding author.
E-mail addresses: jaison.peter@gmail.com, jaisonpeter@cusat.ac.in (J. Peter).

http://dx.doi.org/10.1016/j.optlastec.2014.03.013
0030-3992/

index fiber. Therefore, the hollow fiber has a better photostability compared with step index fiber.

2. Experimental

PMMA preform was fabricated by the controlled polymerization of Methyl-Methacrylite (MMA). The typical procedure for the fabrication of dye doped SI preforms was furnished by Rajesh et al. [14]. In our study, we use Rh6G dye with a concentration of 10^{-5} M/l which was added during the polymerization process. We have used a Teflon based technique for the PMMA tube (hollow preform) fabrication [16–18]. Kailasnath et al. reported a detailed explanation for the fabrication of dye doped GI preforms [17]. For the fabrication of GI preform, initially a hollow PMMA tube (without dye) with desired inner and outer diameters was prepared. This PMMA tube was then filled with a mixture of MMA, 0.4 wt% benzoyl peroxide (BPO), 0.1 wt% of *n*-butyl mercaptan (CTA), 5 wt% of diphenyl phthalate (DPP), and 10^{-5} m/l Rh6G. The filled tube was placed in an oven at 80 °C for 24 h and 90 °C for another 10 h for the complete polymerization process. Finally the different preforms were heat-drawn into fiber at a stable temperature of 180 °C. By adjusting the feed rate of the preform and draw rate of the fiber, different types of dye doped fibers with an outer diameter of about 500 μm have been fabricated. The inner diameter of dye doped hollow fiber was measured as 220 μm. The refractive indices (RI) of the different types of dye doped fibers are shown in Fig. 1. In the case of GI fiber, the refractive index (RI) along the axis was measured ≈1.52 and the RI at the surface of the fiber was ≈1.49. The GI fiber has a parabolic RI profile [17]. Due to undoped cladding region, the effective volume of dye in GI fiber was much smaller than the hollow and SI fiber.

3. Results and discussions

Optical emissions from different types of dye doped fibers (SI, GI and hollow) were excited using 532 nm radiation from a frequency doubled pulsed Nd:YAG laser (Quanta Ray DCRII) with 8 ns pulses at 10 Hz repetition rate as shown in Fig. 2. Each fiber sample with a length of 10 cm has been used in our study. The transverse pumping was done with the pump beam profile as a stripe (of length 10 mm and approximately 0.5 mm width) by employing a cylindrical lens of appropriate focal length [19,20]. Spectral emission characteristics and gain studies were carried out by collecting the emission from the doped fiber using a multimode silica fiber as a detector which is coupled to a monochromator-CCD system.

Fluorescence of dye doped POF is due to the absorption and re-emission mechanism taking place in the dye molecules [21]. The emission spectra from Rh6G doped hollow POFs at various pump powers are depicted in Fig. 3. At a low pump power (< 10 mW), only a broad fluorescence spectrum is observed. There is a narrowing coupled with a blueshift in the emission spectra as pump power is increased as shown in Fig. 3. This blueshift widening is due to the selective excitation of those modes which have sufficient gain for amplification [10]. Comparison of emission spectra from dye doped SI, hollow and GI POFs at a given pump power (30 mW) is shown in Fig. 4. From SI to GI doped POFs the shift in peak fluorescence is ~10 nm and from SI to hollow doped POFs the shift is ~6 nm. The shift in peak fluorescence is attributed to the variation of the effective volume of dye in different types of POFs.

Fig. 5 shows the FWHM of spectral emission from different types of dye doped POFs as a function of pump power. The amplified spontaneous emission (ASE) begins at 10 mW and the FWHM decreases continuously from 42 to 5 nm up to 35 mW. At higher pump power, the emission peak grows and narrows until most of the energy from the sample is emitted within the emission peak. From Fig. 5 the maximum line narrowing is observed in the hollow POFs. This is due to the fact that the number of modes for which the intensity is above the threshold decreases, as a result of the energy transfer from the low power modes to those lying near the emission peaks [14]. Hence above threshold there are less modes in hollow POFs as compared to SI and GI POFs. Spectral line narrowing as a function of pump power is a clear sign of light amplification. Above a certain pump power, the number of modes with an output intensity above the threshold is unchanged, leading to saturation of the line-width.

The output emission is measured from one end of the fiber, by varying the pumping region with the help of a 3D translation stage. Optical loss coefficients for shorter and longer distances of

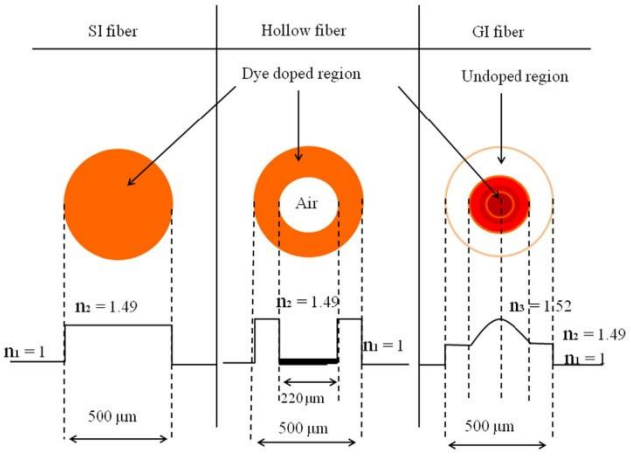

Fig. 1. Refractive indices of the different types of dye doped fibers.

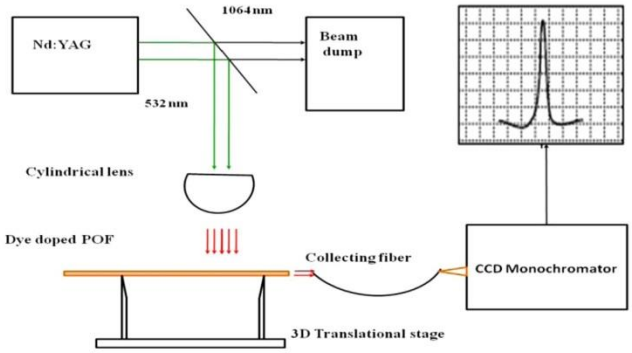

Fig. 2. Schematic illustration of experimental setup.

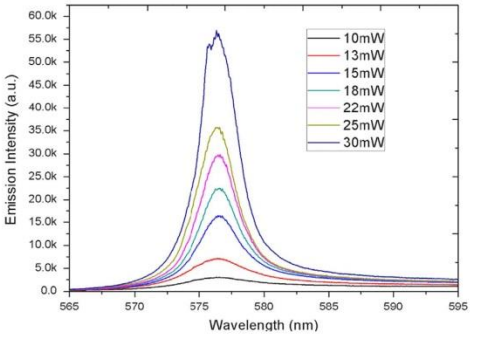

Fig. 3. Emission spectrum from Rh6G doped hollow POF at different pump powers.

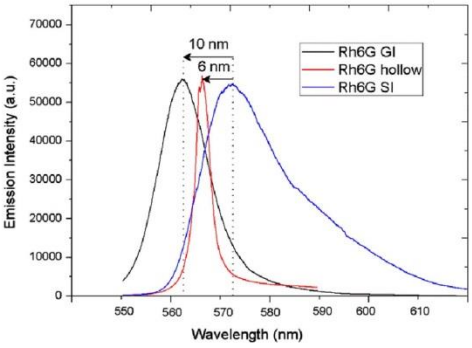

Fig. 4. Comparison of emission spectra from Rh6G doped hollow, GI and SI POFs at a pump power of 30 mW.

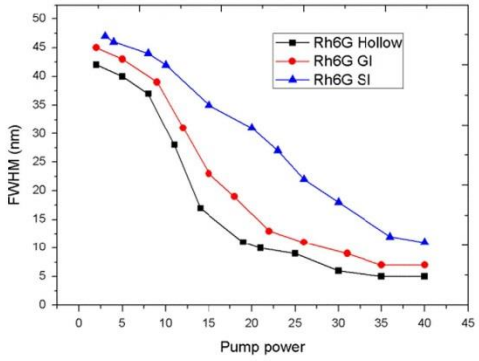

Fig. 5. FWHM of the spectral emission from Rh6G doped hollow, GI and SI POF as a function of pump power.

propagation through the dye doped fiber are different. Fig. 6 shows the variation of output intensity and shift in peak wavelength with the length of Rh6G doped SI, GI and hollow POF at a pump power of 30 mW. The optimum length for maximum output intensity from different types of fiber is different. As the propagation distance increases, the magnitude of the output intensity increases up to a length of 2 cm for SI, 4 cm for hollow and 7 cm for GI POF. Further increase in length will reduce the intensity due to various loss mechanisms such as absorption and scattering of fluorescence. Optimum length of fiber samples also depends on the dye concentration and input pump power because a larger effective length of inverted medium can be achieved by a higher pump power [22].

The redshift of the fluorescent signal is fiber length dependent, and is produced by the self-absorption and re-emission effects of the laser dye. Due to this self-absorption and re-emission process, the peak emission wavelength shows a red-shift with an increase in concentration [23]. Increasing the path length through the dye doped sample is somewhat similar to an increment in dye concentration. The experimental result of the redshift in the fluorescence peak when the fiber length is increased for different types of doped fiber is shown in Fig. 6. The redshift in fluorescence can be attributed to the gain achieved as the radiation is propagated through the amplifying medium as well as due to the re-emission from the interacting dye molecules at longer wavelengths. These types of red-shift in peak fluorescence with propagation length will allow a limited range of tuning of emission wavelength from the different types dye doped fibers.

An important parameter, determining potential application of the solid-state dye laser system in which the ASE phenomenon can be observed, is the rate of photo-degradation of the dye during the prolonged exposure to pulsed excitation of laser light. Hence

Appendix

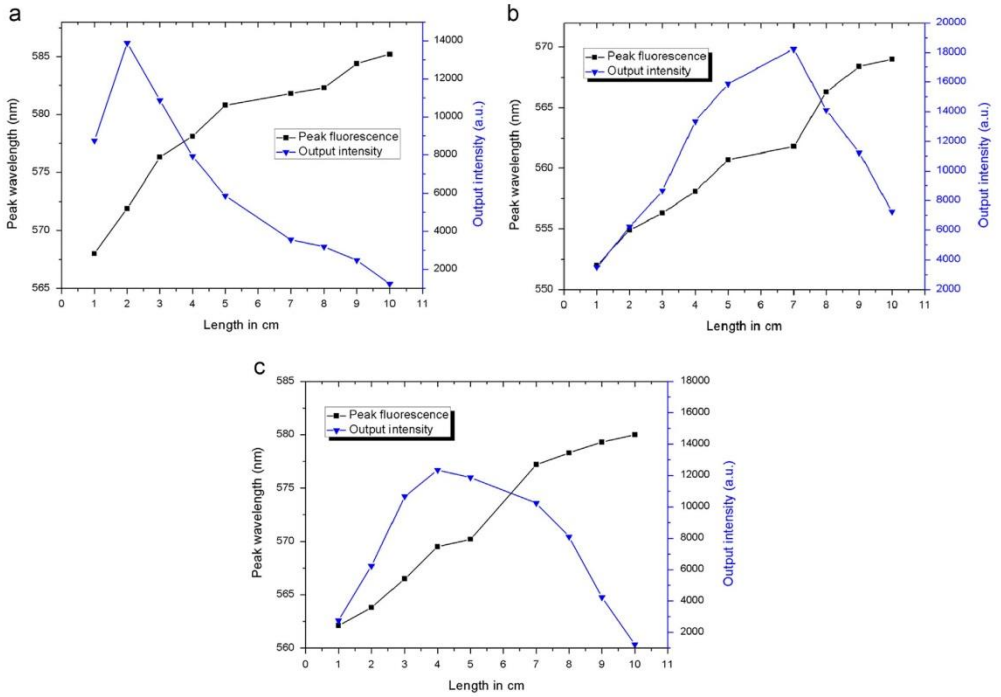

Fig. 6. Variation of emission peak and output intensity with length of Rh6G doped SI-POF (a), GI-POF (b) and hollow POF at a pump power of 30 mW.

photostability is one of the main concerns in solid-state gain media. In most organic laser dye systems, luminescence efficiency decreases after a few thousands of excitation pulses and a photo-bleaching effect is observed [11].

Optical amplifiers and lasers made of dye doped fiber require a much less pump power than the bulk material, because of the effective confinement and long interaction length available in fiber geometry [18]. Since photo-bleaching increases with exposure intensity, low pump power would increase the life time of gain medium. Also, the thin and long geometry of the fiber is ideal for good thermal relaxation to minimize the thermally induced photo-bleaching as well [24]. Therefore solid-state dye doped gain media usually have limited dye-life. Optical bleaching of organic dyes also results due to thermal effect from optically absorbing impurities. Fig. 7 shows an evolution of normalized output intensity as a function of number of pump pulses for above 3 types of fibers under the condition described above. The half-life for bleaching of different types of dye doped POFs has been compared. From the figure it is observed that Rh6G doped GI-POF has the highest dye-life as compared to other types of dye doped POFs. For a pump power of 30 mW, the output intensity becomes 50% of initial value after 150,000 excitation pulses. From the study, we also concluded that the photo-degradation is particularly fast in step index fiber, moderate in hollow fiber and slower in graded index fiber for a given pump power. In the case of higher average power and low intensity, the bleaching of dye molecules could be assumed mainly due to thermal effect. But in the low average power and high intensity case, the bleaching could be assumed to be mainly induced by the excited state absorption [25].

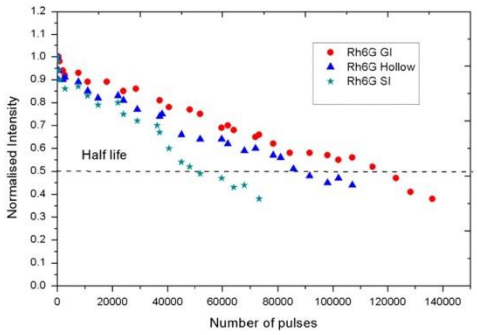

Fig. 7. Normalized output intensity as a function of number of pump pulses for Rh6G doped different types of POFs at a pump power of 30 mW.

Fig. 8 shows the normalized output intensity as a function of exposure time for Rh6G doped hollow POF at different pump powers. The higher pump intensity could cause quicker degradation of dye molecules. From the figure it is observed that the photo-bleaching increases with the increase of the exposure intensity while low pump intensity would increase the life of the gain medium [24].

Table 1 summarizes peak wavelength, optimum length, line-width and half-life of Rh6G doped hollow, GI and SI POFs

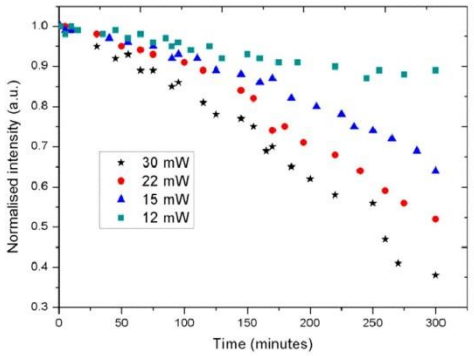

Fig. 8. Normalized emission intensity (for Rh6G hollow at different pump powers) versus the exposure time.

Table 1
Emission characteristics of Rh6G doped hollow, GI and SI POFs

Fiber type	Peak wavelength (nm)	Optimum length (cm)	FWHM (nm)	Half-life (shot)
Rh6G hollow	562	4	5	95,000
Rh6G GI	565	7	7	120,000
Rh6G SI	572	2	10	50,000

investigated in the present study. The experiment was carried out at 10 Hz repetition rate with a pump power of 30 mW.

4. Conclusion

Laser pump power dependence of fluorescence emitted from Rh6G doped SI and GI and hollow POFs was studied. Rh6G doped hollow POF shows the highest spectral narrowing for a given pump power compared to GI and SI POFs. With the increase in propagation length through the fiber, the emission peak shows a redshift due to self-absorption and re-emission by the dye molecules. Thus we could tune the ASE wavelength by adjusting the propogation distance through the fiber. The capability to tune the emission peak position gives the possibility to tune the spectral output of the doped POFs. The peak wavelength, optimum length, line-width and half-life of Rh6G hollow, GI, and SI POFs were compared. From our study, we also concluded that the photodegradation is particularly fast in step index, moderate in hollow and slower in graded index fiber for a given pump power.

Acknowledgment

The authors acknowledge the financial support from Department of Science and Technology (DST), Govt. of India. Jaison Peter is grateful to the University Grant Commission (UGC) for the research fellowship.

References

[1] Soffer BH, McFarland BB. Appl Phys Lett 1967;10:266–7.
[2] Peterson OG, Snavely BB. Appl Phys Lett 1968;12:238–40.
[3] Chen DY, Jiang YG, Fan RW, Jia EB, Xia YQ, Yao Y. Laser Phys 2009;19:1877–81.
[4] Rahn Mark D, King Terence A. Appl Opt 1995;34(36):8260–71.
[5] Costela A, Garcia-Moreno I, Tian H, Su J, Chen K, Amat-Guerri F, et al. Chem Phys Lett 1997;277:392–8.
[6] Jiang Changhong, Kuzyk Mark G, Ding Jow-Lian, Johns William E, Welker David J. J Appl Phys 2002;92:1.
[7] Chiron, B, In: Proceedings of SPIE on plastic optical fibers, 1991, Boston, MA, Vol. 1592, p. 86–95.
[8] Muto, S, Sato, H and Hosaka, T, In: Proceedings of the third international conference on plastic optical fibers and applications – POF, 1994, Yokohama, Japan,p. 46–48.
[9] Peter Jaison, Radhakrishnan P, Nampoori VP N, Kailasnath M. J Lumin 2014;149:204–7.
[10] Geetha K, Rajesh M, Nampoori VP N, Vallabhan CP G, Radhakrishnan P. J Opt A: Pure Appl Opt 2006;8:189–93.
[11] Sznitko L, Mysliwiec J, Parafinuik K, Szukalski A, Palewska K, Bartkiewicz S, et al. Chem Phys Lett 2011;512:247–50.
[12] Zhigang Zang, Takahiro Minato, Paolo Navaretti, Yasuhiro Hinokuma, Marcus Duelk, Christian Velez, et al. IEEE Photonics Technol Lett 2010;22(10):721–3.
[13] Zang Zhigang, Mukai Keisuke, Navaretti Paolo, DUELK Marcus, Velez Christian, Hamamoto Kiichi. IEICE Trans Electron 2011;E94-C(5):862–4.
[14] Rajesh M, Geetha K, Sheeba M, Vallabhan CP G, Radhakrishnan P, Nampoori VP N. Opt Eng 2006;45(7):820–3.
[15] De La Rosa-Cruz E, Dirk CW, Rodriguez O, Castano VM. Fiber Integr Opt 2001;20(5):457–64.
[16] Kailasnath M, Nampoori VP N, Radhakrishnan P. Pramana – J Phys 2010;75:923–7.
[17] Peng GD, Chu PL, Lou X, Chaplin RA. J Electron Eng 1995;15:289.
[18] Kailasnath M, Sreejaya TS, Kumar R, Vallabhan CPG, Nampoori VPN, Radhakrishnan P. Opt Laser Technol 2008;40:687–91.
[19] Kruhlak RJ, Kuzyk MG. J Opt Soc Am B 1999:161756–67.
[20] Peter Jaison, Vallabhan CP G, Radhakrishnan P, Nampoori VP N, Kailasnath M. Laser Phys 2013;23:115104.
[21] Shank CV. Physics of dye lasers. Rev Mod Phys 1975;47:649.
[22] Sheeba M, Rajesh M, Nampoori VP N, Radhakrishnan P. Appl Opt 2008;47:1907–12.
[23] Schafer FP. Dye laser (topics in applied physics) 1990;1 ([chapter 1]).
[24] Vrentas JS, et al. Macromolecules 1994;27:5570.
[25] Peng GD, Chu PL, Xiong Z, Whitbread TW, Chaplin RP. J Lightwave Technol 1996;14:2215–23.

Appendix

Optics Communications 320 (2014) 125–128

Contents lists available at ScienceDirect

Optics Communications

journal homepage: www.elsevier.com/locate/optcom

Pumping scheme dependent multimode laser emission from free-standing cylindrical microcavity

Jaison Peter *, Rasool Saleem, Ananthu Sebastian, P. Radhakkrishnan, V.P.N. Nampoori, C.P. Girijavallabhan, M. Kailasnath

International School of Photonics, Cochin University of Science and Technology, Cochin 682022, India

ARTICLE INFO

Article history:
Received 29 October 2013
Received in revised form
7 January 2014
Accepted 21 January 2014
Available online 30 January 2014

Keywords:
Microring cavity
Red-shift
Blue-shift
WGMs

ABSTRACT

We report the observation of multimode laser emission from a free-standing microring cavity based on rhodamine 6G dye doped hollow poly(methyl methacrylate) optical fiber (DDHPOF) obtained by pulsed photo-excitation. Two different pumping schemes were employed to characterize DDHPOF; the stripe illumination and the spot illumination. By using spot illumination, the slope efficiency of system is enhanced by more than 3 times than that of the stripe illumination and also a red-shift in emission spectrum is observed with the pump power. When the pump power is increased beyond the threshold value, laser emission occurs with a multimode structure. From the relation between mode spacing and diameter of cylindrical cavity, the lasing action is considered to be formed by whispering gallery modes (WGMs).

1. Introduction

In the last decades, solid state dye gain media has attracted considerable research interest [1]. Solid state dye lasers have many advantages than their counterpart in liquid form, such as, reduced toxicity, easier and safer to handle, etc. PMMA (poly methyl mathacrylate), the most frequently used polymer host for dye lasers, shows best optical transparency in the visible spectral range [2] and is compatible with most of the organic dyes used as dopants [3]. Laser dye doped PMMA is found to be a highly efficient medium for laser source with narrow pulse width and wide tunable range as well as for optical amplifier with high gain, high power conversion and broad spectral bandwidth [4–6]. Rhodamine 6G (Rh6G), the best known of all laser dyes, has high quantum yield and a low intersystem crossing rate [2]. For Rh6G, there is also a spectral region of overlap between the absorption and emission bands.

Optical amplifiers and lasers made of dye doped fiber require much less pump power than in bulk material, because of the effective confinement and long interaction length available in the fiber [7]. These microcavities confine light into an interior region close to the surface of the resonator by resonant circulation due to the total internal reflection at the boundary [8]. Resonators having a diameter s from a few tens to several hundreds of micrometers can have a very large free spectral range of several nanometers. Generally, a microring cavity is realised by making a coating of a few micron thick conducting polymers [9] or dye doped transparent polymer over a glass fiber. The most important parameter for a solid-state dye laser system is the rate of dye photo-degradation. In all applications of a laser dye, the main concern is the photostability of the dye under irradiation by the pump light [10]. The bleaching of dye molecules could be assumed mainly due to the thermal effect. Also, the thin and long geometry of the fiber is ideal for good thermal relaxation to minimize the thermally induced photo-bleaching as well [11].

2. Experimental

In this paper, we are presenting the effect of pumping scheme on the multimode laser emission from a cylindrical microcavity structure fabricated by Rhodamine 6G dye (10^{-4} mol/l) doped hollow poly (methyl methacrylate (PMMA)) optical fiber (DDHPOF). The detailed fabrication process of DDHPOFs was already reported by kailasnath et al. [5]. In our study we used Rh6G doped DDHPOF, which is having a dye concentration of 10^{-4} mol/l, with an outer diameter of 280 μm, inner diameter of 120 μm and a length of 5 cm. DDHPOFs samples were transversely pumped using 8 ns pulses from a frequency doubled Nd:YAG laser (532 nm, 10 Hz). A set of calibrated neutral density filters were used for varying the pump power. The average pump power was varied from 2 mW to 40 mW and the emission from the sample was collected using a collecting fiber coupled to a monochromator-CCD system (SpectraPro) with a resolution of 0.03 nm.

* Corresponding author.
E-mail addresses: jaison.peter@gmail.com, jaisonpeter@cusat.ac.in (J. Peter).

0030-4018/$ - see front matter © 2014 Elsevier B.V. All rights reserved.
http://dx.doi.org/10.1016/j.optcom.2014.01.054

The pump beam was focused onto the DDHPOFs either by a convex lens (Fig. 1 left inset) or by a cylindrical lens (Fig. 2 left inset). Pumping scheme is very much significant in practical applications, especially for optimizing the life of solid state dye gain media [1].

3. Results and discussions

3.1. Spot illumination technique

When the pump beam is focused into the DDHPOF with the help of a convex lens, the entire light is concentrated on a single point (~0.1 mm). Hence the power density at the focused point is very high. This leads to the excitation of only a few dye molecules to higher energy bands which can de-excite with an emission. The emitted light from this point gets propagated to other regions of the fiber. As a result, the short wavelength emission from dye molecules gets absorbed by itself and is re-emitted at longer wavelength due to stokes shift. When the pump power is increased the emission spectrum shows a line narrowing (due to amplified spontaneous emission (ASE)) [12]. With an increase in pump power, the excited molecules absorb more energy and hence the emission from these molecules can excite more neighboring

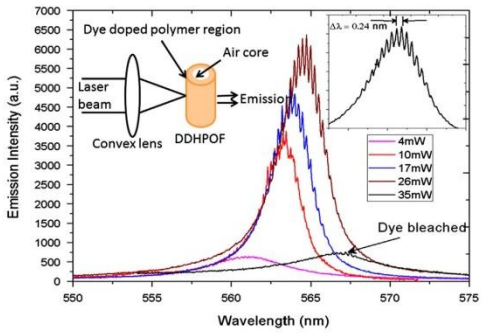

Fig. 1. Emission spectrum from DDHPOF as a function of pump power. Left inset shows the pumping scheme and right inset shows the expanded modes at 26 mW.

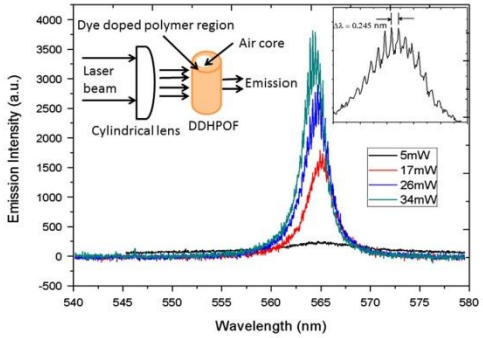

Fig. 2. Emission spectrum from DDHPOF as a function of pump power. Left inset shows the pumping scheme and right inset shows the expanded modes at 26 mW.

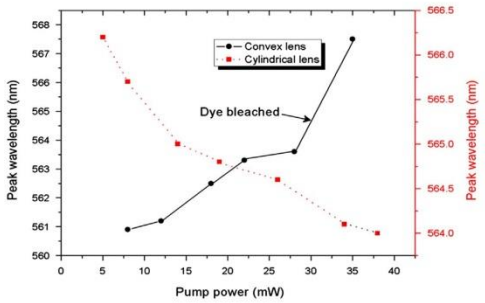

Fig. 3. Shift in peak wavelength as a function of pump power (when pump power is focused with convex and cylindrical lens).

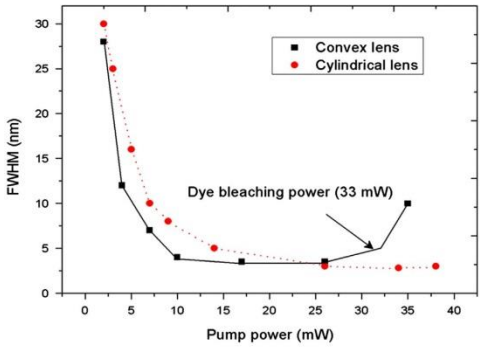

Fig. 4. Line narrowing as a function of pump power (when the pump beam is focussed with convex and cylindrical lens).

molecules which leads to a shift in the peak emission wavelength from 561 to 565 nm with pump power. That is, the red-shift is attributed to the absorption of shorter wavelength and emission from the neighboring dye molecules at longer wavelengths. The red-shift and line narrowing as a function of pump power are depicted in Figs. 3 and 4. A clear line narrowing from 30 nm to 4 nm is observed when the pump power is increased to 10 mW, above which no further line narrowing is observed due to gain saturation effect [12].

At higher pump powers a change in the spectral shape was observed. Fig. 5 shows the evolution of spectrally integrated emission intensity as a function of pump power for the multimode lasing from the DDHPOF. At a threshold pump power, P_{th} (~10 mW), laser emission with multimode structures emerges as depicted in Fig. 1. This threshold behavior of the laser peak intensity provides a clear signature of lasing. The expanded mode structure is clearly shown in Fig. 1 (right inset).

The DDHPOFs can be modeled as a number of serially connected microring cavities [3]. Thus the expected mode spacing $\Delta\lambda$ is given by

$$\Delta\lambda = \lambda_m - \lambda_{m-1} = \lambda^2/\pi D n_{eff}$$

where λ is the wavelength of strongest emission line, n is the refractive index of the fiber material, and D is the diameter of the fiber. From the equation we get the mode spacing as 0.24 nm,

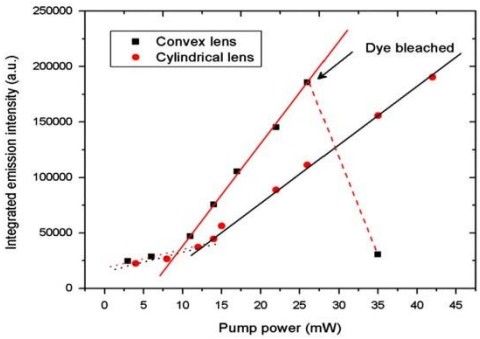

Fig. 5. Integrated emission intensity from DDHPOF as a function of pump power for cylindrical and convex lens focusing.

which is the same as the observed mode spacing (Fig. 1). The strongest mode at 564.9 nm has an FWHM of 0.1 nm.

By focusing the pump power with a convex lens, the pump power density on the focused point is very much higher and hence when the pump power is increased beyond a certain threshold (bleaching threshold); the dye molecules start to degrade, this will leads to bleaching of dye as depicted in Fig. 1. After bleaching of dye molecules, the emission shows a random behavior, in terms of observed emission intensity (Figs. 1 and 5), peak wavelength (Fig. 3) and FWHM (Fig. 4).

3.2. Stripe illumination

By using cylindrical lens, the pump power is focused as a stripe of length 10 mm and approximately 0.5 mm width. Here the power density of focused beam is very much smaller as compared to focusing by a convex lens. i.e. the interaction area between the pump radiation and dye molecules is very much larger. Hence large number of dye molecules could be excited simultaneously to higher energy bands and de-excite with an emission. However, the average power absorbed by each dye molecule is very small as compared to spot illumination (with the same pump power). Due to this, each molecule will de-excite at a longer wavelength. When the pump power is increased, the radiative transition probability gets enhanced at shorter wavelength side of the spectrum creating a shift in the spectrum towards the blue side [13]. As the pump power increases from 5 to 34 mW, it can be seen that the emission spectrum gets shifted from 568 to 564 nm. The blue-shift and line narrowing as a function of pump power are presented in Figs. 2, 3 and 4. As the pump power is increased, a clear spectral narrowing is observed coupled with this blue shift. At a certain threshold pump power, narrow lines begin to emerge out of this emission spectrum, indicative of microring lasing [13,14]. The line narrowing is due to the fact that the number of modes for which the intensity above the threshold decreases because of the energy transfer from low power modes (longer wavelengths) to those lying nears the emission peak [12].

In other words, when the pump power is increased above the threshold (P_{th}), there can be a decrease in the average wavelength of the spectrum (λ_{av}). The average wavelength is defined as

$$\lambda_{av} = \int_{-\infty}^{\infty} \lambda\, P(\lambda)d\lambda \,/\, \int_{-\infty}^{\infty} P(\lambda)d\lambda,$$

i.e. as the pump power is increased, the gain in the proximity of the peak wavelength of the emission cross section is larger, which produce a relative blue shift towards the maximum of the emission cross section. In the case of an inhomogeneous medium (dye), the gain at any wavelength is equal to the product of stimulated emission cross section and population density difference, i.e.,

$$g_{\lambda}^{D} = \Delta N_{ul}\, \sigma_{ul(\lambda)}^{D},$$

where g_{λ}^{D} is the gain at any wavelength, $\sigma_{ul(\lambda)}^{D}$ is the stimulated emission cross section and ΔN_{ul} is the population density difference. In the case of stripe illumination, a large number of dye molecules are involved in the emission process, hence the population density difference is higher for higher pump power. This will enhance the gain in the proximity of the peak wavelength of the emission cross section, which in turn leads to a relative blue shift (from 568 to 564 nm) in the emission spectrum towards the maximum of emission cross section (in our case ~564 nm). Further increase in pump power does not show any blue shift in the emission spectrum and this can be attributed due to gain saturation. Similar types of relative blue shift towards the peak of emission cross section have been observed with an increase in pump power in various studies [12,15–17].

To confirm the laser action in DDHPOF, the dependence of emission intensity on pump power is also studied. As shown in Fig. 5, clear threshold behavior can be observed. When the pump power is below the threshold, the output intensity increases very slowly (small dotted line in Fig. 3) and the emission spectrum is broad. Once the pump power is above threshold, output intensity changes dramatically (solid line in Fig. 5).

When pumping beam is focused with a convex lens, the emission intensity shows much more pronounced threshold behavior than in the case of cylindrical lens focusing. The pump threshold power, P_{th}, can be estimated from the corresponding light–light curves (Fig. 5). In the case of pumping beam focused with the convex lens the threshold is 10 mW in the place of 15 mW for cylindrical lens focusing and also the slope efficiency of the curve is enhanced by more than 3 times. This is also evident from the enhanced line narrowing for the convex lens focussing for any given pump power as shown in Fig. 4. For a constant pump power, the power densities available for the two geometries are different. Higher power densities available using convex lens leads to emission at shorter wavelengths which subsequently shifts to larger wavelengths resulting in a red shift due to reabsorption as the pump power increased. In the case of stripe illumination, lower power densities results in the emission at longer wavelengths (blue shift) with increase in pump power. Hence in the present studies, at a particular pump power the peak emission wavelength in the two geometries coincide with one another.

From Figs. 1 and 2 inset, the measured mode spacing is ~0.24 nm. i.e. the mode spacing of the WGM laser emission from the DDHPOFs does not depend on the pumping scheme, but it depends on the type of dye doped in the fiber, refractive index of the fiber material and fiber diameter. Photostability of DDHPOFs mainly depends on the pumping scheme and pump power. Due to higher power density, spot illumination will lead to quicker degradation of dye molecules as compared to stripe illumination. Hence pumping scheme plays a significant role in solid-state dye laser systems.

4. Conclusion

Pumping scheme dependent multimode laser emission from a cylindrical microcavity formed by rhodamine 6G dye doped hollow polymer optical fiber is observed. As the pump power is increased, stripe illumination shows a blue-shift (from 565 to 561 nm) and spot illumination shows a red-shift (from 562 to 566 nm) for the emission spectra. The spectra also show a line

narrowing due to amplified spontaneous emission and at a threshold power, laser emission with multimode structure emerges. By spot illumination technique, the slope efficiency of the microcavity is enhanced by more than 3 times than the stripe illumination technique. From the mode spacing, we can confirm that the lasing action is formed by whispering gallery modes.

Acknowledgment

The authors acknowledge the financial support from Department of Science and Technology (DST), Govt. of India. Jaison Peter is grateful to the University Grant Commission (UGC) for the research fellowship. The author also wishes to thank P.S. Sreekumari and Bejoy Varghese for their valuable discussion during the work.

References

[1] E.De. La Rosa-Cruz, C.W. Dirk, O.Rodriguez, V.M. Castano, Fiber Integr. Opt. 20 (5) (2001) 457.
[2] K. Geetha, M. Rajesh, V.P.N. Nampoori, C.P.G. Vallabhan, P. Radhakrishnan, J. Opt. A: Pure Appl. Opt. 8 (2006) 189.
[3] M. Sheeba, K.J. Thomas, M. Rajesh, V.P.N. Nampoori, C.P.G. Vallabhan, P. Radhakrishnan, Appl. Opt. 46 (2007) 33.
[4] G.D. Peng, Pak L. Chu, Zhengjun Xiong, Trevor W. Whitebread, Rod P. Chaplin, J. Light Wave Technol. 14 (1996) 10.
[5] M. Kailasnath, V.P.N. Nampoori, P. Radhakrishnan., Pramana J. Phys. 75 (5) (2010).
[6] P. Jaison Peter, V.P. N. Radhakrishnan, Nampoori, M. Kailasnath, J. Lumin., http://dx.doi.org/10.1016/j.jlumin.2014.01.003, in press.
[7] M. Kailasnath, T.S. Sreejaya, C.P.G. Rajesh Kumar, V.P.N. Vallabhan, Nampoori, P. Radhakrishnan, Opt. Laser Technol. 40 (2008) 687.
[8] C.L. Linslal, S. Mathew, P. Radhakrishnan, V.P.N. Nampoori, C.P.G. Vallabhan, M. Kailasnath, Opt. Lett. 38 (2013) 18.
[9] S.V. Frolov, M. Shkunov, Z.V. Vardeny, Phys. Rev. B 56 (1997) 8.
[10] Ritty J. Nedumpara, Binoy Paul, A. Santhi, P. Radhakrishnan, V.P.N. Nampoori, Spectrochem. Acta Part A 60 (2004) 435.
[11] Y. Koike, T. Ishigure, E.J. Nihei, Light Technol. 13 (1995) 1475.
[12] M. Rajesh, M. Sheeba, K. Geetha, C.P.G. Vallabhan, P. Radhakrishnan, V.P. N. Nampoori., Appl. Opt. 46 (1) (2007) 824.
[13] C.P.G. Jaison Peter, P. Vallabhan, V.P.N. Radhakrishnan, Nampoori, M. Kailasnath, Laser Phys. 23 (2013).
[14] Gernot Wirnsberger, G.D. Stucky, Chem. Mater. 12 (2000) 2525.
[15] Jon Arrue, Felipe Jimenzes, Igor Ayesta, M. Asuncion Illarramendi, Joseba Zubia, Polymers 3 (2011) 1162.
[16] H.Z. Wang, F.L. Zhao, Y.J. He, X.G. Zheng, X.G. Huang, M.M. Wu, Opt. Lett. 23 (1998) 777.
[17] S.Y. Lam, M.J. Damzen, Appl. Phys. B 77 (2004) 577.